HIGH-RESOLUTION STABLE ISOTOPE ANALYSIS OF BIOGENIC CARBONATES AS PROXY EVIDENCE FOR HOLOCENE ENVIRONMENTAL CHANGE: EXAMPLES FROM AUTHIGENIC LAKE CARBONATE AND BIVALVE ISOTOPE PROFILES

A Thesis Submitted to the College of
Graduate Studies and Research
In Partial Fulfillment of the Requirements
For the Degree of Doctor of Philosophy
In the Department of Geological Sciences
University of Saskatchewan
Saskatoon

ANDREW WILLIAM KINGSTON

PERMISSION TO USE

In presenting this thesis/dissertation in partial fulfillment of the requirements for a Postgraduate degree from the University of Saskatchewan, I agree that the Libraries of this University may make it freely available for inspection. I further agree that permission for copying of this thesis/dissertation in any manner, in whole or in part, for scholarly purposes may be granted by the professor or professors who supervised my thesis/dissertation work or, in their absence, by the Head of the Department or the Dean of the College in which my thesis work was conducted. It is understood that any copying or publication or use of this thesis/dissertation or parts thereof for financial gain shall not be allowed without my written permission. It is also understood that due recognition shall be given to me and to the University of Saskatchewan in any scholarly use which may be made of any material in my thesis/dissertation.

DISCLAIMER

This dissertation was exclusively created to meet the thesis and/or exhibition requirements for the degree of Doctor of Philosophy at the University of Saskatchewan. References in this thesis/dissertation to any specific commercial products, process, or service by trade name, trademark, manufacturer, or otherwise, does not constitute or imply its endorsement, recommendation, or favoring by the University of Saskatchewan. The views and opinions of the author expressed herein do not state or reflect those of the University of Saskatchewan, and shall not be used for advertising or product endorsement purposes.

Requests for permission to copy or to make other uses of materials in this thesis/dissertation in whole or part should be addressed to:

Head of the Department of Geological Sciences
University of Saskatchewan
Saskatoon, Saskatchewan S7N 5E2
Canada

OR

Dean
College of Graduate Studies and Research
University of Saskatchewan
107 Administration Place
Saskatoon, Saskatchewan S7N 5A2
Canada

UNIVERSITY OF SASKATCHEWAN
College of Graduate Studies and Research

ABSTRACT

Submitted in partial fulfillment
Of the requirements of the

DEGREE OF DOCTOR OF PHILOSOPHY

By

Andrew William Kingston

Department of Geological Sciences
University of Saskatchewan
November, 2016

Examining Committee:

Dr. Samuel Butler	Department Chair, Department of Geological Sciences
Dr. William P. Patterson	Supervisor, Department of Geological Sciences
Dr. Chris Holmden	Department of Geological Sciences
Dr. Bruce Eglington	Department of Geological Sciences
Dr. Keith Hobson	Department of Biology, University of Western Ontario
Dr. Aaron Diefendorf	Department of Geology, University of Cincinnati

High-Resolution Stable Isotope Analysis of Biogenic Carbonates as Proxy Evidence for Holocene Environmental Change: Examples from Authigenic Lake Carbonate and Bivalve Isotope Profiles

Biogenic carbonates are valuable archives of paleoenvironmental information because they record chemical signatures of ambient environmental conditions during their formation. Therefore, long-term records of biogenic carbonates provide long-term records of environmental conditions that can be utilized to develop climate histories for specific regions to explore past climatic change. Traditionally, these studies have been conducted with low temporal resolution owing to analytical or economical restrictions. Although these records provide valuable information surrounding long-term climatic change, they lack the resolution to resolve the short-term climatic oscillations such as the Pacific Decadal Oscillation and El Niño Southern Oscillation that drive environmental change.

This dissertation focuses on using high-resolution stable isotope analysis of biogenic carbonates for paleoenvironmental reconstruction and associated applications. Three studies are presented herein, applying increasing sampling resolution from sub-centennial, to sub-decadal, to sub-seasonal, that illustrate the diversity of paleoenvironmental information gained with each increase in resolution. The first study uses sub-centennial oxygen isotope analysis of authigenic lake carbonate to assess how climate change has affected precipitation patterns in the southern Yukon Territory from the end of the last glacial to the present day. Large changes in atmospheric circulation patterns associated with changes in the strength of the North Pacific High and the Aleutian Low pressure systems lead to variations in the oxygen isotope value of precipitation in the southwest Yukon Territory recorded in the oxygen isotope values of lake carbonate. The degradation of a glacial anticyclone led to a reduction in strength of the Aleutian Low coupled with an increase in the strength of the North Pacific High resulting in an increase in summer precipitation to the southwest Yukon represented by an increase in effective moisture following the transition from the Late Pleistocene to the Early Holocene.

The second study is a sub-decadal oxygen isotope record of lacustrine carbonate stretching back 8,000 years to quantify the strength and state of the Pacific/North American (PNA) Index through time. This study relies on the relationship between the PNA Index and the oxygen isotope values of precipitation from central Canada (Birks and Edwards, 2009), and the ability of Sturgeon Lake to accurately represent $\delta^{18}O$ values of precipitation. Results show that the strength of the PNA varied through time. The Early to Mid-Holocene (8,000- 4,200 years BP) is characterized by large fluctuations between PNA^{+} and PNA^{-} phases; PNA^{-}-like conditions dominate the period after 4,200 years BP; and ~1,800 years BP PNA^{+}-like conditions resume. Changes in the Holocene PNA pattern are shown to be contemporaneous with similar changes in Holocene records of El Niño illustrating the intrinsic relationship between Pacific climate patterns.

The final study uses sub-seasonal oxygen isotope records from bivalves derived from an overwash deposit to define the seasonality of the deposit. Data indicate a late spring to early summer timing of deposition that presents an alternative interpretation to the previous late fall tsunami origin hypothesis.

In conclusion, this dissertation focused on improving our understanding of how paleoenvironmental information is archived in biogenic carbonates by focusing on the use of

high-resolution sampling strategies. Modifying the sampling resolution resulted in an enhanced understanding of how short-term climate oscillations drive climate and illustrates how the type of paleoenvironmental information generated varies with sampling resolution.

Keywords: Stable isotope, climate change, Holocene, bivalve, marl, Pacific/North American, El Niño Southern Oscillation, Pacific Decadal Oscillation, Aleutian Low, late glacial

ACKNOWLEDGEMENTS

In the end a PhD dissertation represents the culmination of many years of work including innumerable collaborations and help along the way. This thesis is no different and I wish to acknowledge some truly inspiring people who motivated and helped me along the way.

I would like to start off by acknowledging my supervisor Bill Patterson. Bill helped show me the many ways of the isotope geochemist. He provided direction when needed, but more importantly permitted me the freedom to pursue my own research directions allowing me to develop as a scientist. I will always remember the crazy stories and good times in the field.

I would also like to acknowledge my committee, Bruce Eglington, Chris Holmden, and Geoff Koehler for helping with sound advice along the road. Bruce Eglington deserves special mention for his advice and assistance with times series analysis; thanks for helping me get my head around it all. Tim Prokopuik was always around for a chat and always seemed to know what was wrong with the mass spec. Thanks for all the help Tim.

For all of my friends in grad school at the University of Saskatchewan, you guys made living in Saskatoon a great time. I will always remember all of the escapades we had together from our ventures into microbiology to learning about interesting uses of gas cylinders, I had a great time and learned a lot. My McMaster friends have been some of my longest and best friends. You guys provided much of the support when I needed it the most. Duncan, Fletcher, Cowie, Benson, Steph, Luke, and Brett -thanks. Pete van Hengstum has gone from student to professor in the time it took to write this. You have always been an inspiration and I am happy we were able to work together on side projects. I'm excited for our future collaborations and what they might discover.

I also would like to thank my family, including my parents David and Linda and my brother Dave. Our adventures around the world created the framework for my thirst for knowledge and I will be forever grateful for the inspiration and motivation that you all provided. Thank you for all of your help along the way, it was essential.

Finally, I would like to thank my wife Holly. You have provided never-ending love and support that made the final push possible. Thank you for all of the time spent editing and discussing isotope geochemistry. I appreciate all the energy you devoted to helping this through to the end.

DEDICATION

To my wife Holly, who always believed in me. She encouraged me through the good times and the hard times.

NOTE TO READER

The original version of this document contains many color figures that are necessary for an accurate understanding the content. The original dissertation is on file in the Department of Geosciences at the University of Saskatchewan.

TABLE OF CONTENTS

LIST OF TABLES

LIST OF FIGURES

LIST OF ABBREVIATIONS

AD – Anno Domini
AL – Aleutian Low
BP – Before Present
COHMAP – Cooperative Holocene Mapping Project
ENSO – El Niño Southern Oscillation
GCM – Global Climate Model
GISP – Greenland Ice Sheet Project
GMWL – Global Meteoric Water Line
GNIP – Global Network for Isotopes in Precipitation
IAEA – International Atomic Energy Agency
ITCZ – Inter Tropical Convergence Zone
LEL – Local Evaporation Line
LGM – Last Glacial Maximum
LMWL – Local Meteoric Water Line
HTM – Holocene Thermal Maximum
MTM – Multi Taper Method
NBS – National Bureau of Standards
NCAR – National Center for Atmospheric Research
NCEP – National Centers for Environmental Prediction
NGRIP – North Greenland Ice core Project
NIST – National Institute of Standards and Technology
NOAA – National Oceanic and Atmospheric Administration
NSERC – National Science and Engineering Research Council
PDO – Pacific Decadal Oscillation
PNA – Pacific/North American
SST – Sea Surface Temperatures
VPDB – Vienna Pee-Dee Belemnite
VSMOW – Vienna Standard Mean Ocean Water
YD – Younger Dryas

CHAPTER 1
OVERVIEW

1.1 Motivation

The Earth's climate is in a constant state of flux. This fact has always been a challenge for human civilizations that benefit from a narrow range of climatic variability. Climate modes such as the Pacific Decadal Oscillation and El Niño have considerable socioeconomic impacts (e.g. Changnon, 1999). For example, variations in North Pacific sea surface temperatures related to phase changes of the Pacific Decadal Oscillation result in disruptions to salmon fisheries on the western coast of Canada (Mantua et al., 1997); and El Niño events are associated with higher potential for extreme temperature events in Western Canada (Shabbar, 2006), and force flood and drought cycles in the heavily populated west coast of the USA (Cayan et al., 1999). As we advance our knowledge about Holocene climate change, it is becoming increasingly apparent that the connection between highly variable climate and cultural change is potentially causal (Sandweiss et al., 1999), indicating that climate change was an important influence on the development of human civilizations. In order to better understand the dynamic interactions of climate of the past, paleoclimate, we must have a firm understanding of the conditions and processes responsible for perturbations in the climate system.

A challenge in characterizing the effects of oscillatory climate phenomenon is that our instrumental record extends back a relatively short period of time. Lower-frequency climate patterns are not well resolved in the historical record and we must look to the geological record to extend climate records further back in time. Climate proxies such as ice cores (Grootes et al., 1993), tree-rings (Fritts et al., 1979), bivalves (Schöne et al., 2005), lake sediment (Kirby et al., 2002), and speleothems (Wang et al., 2005) have been used to extend this record.

The better we characterize and understand climates of the past, the better our ability to generate accurate current-day global climate models, which may help predict the effects of future climate change (e.g. Hargreaves and Annan, 2009). In summary, accurate characterization of past climate is essential to our understanding of future climate and climate change, however, we are limited to paleoclimate proxies that have complex relationships to past-climate conditions. Therefore, detailed analysis of a wide variety of paleoclimate proxies, especially those at high

resolution, is essential in order to further our understanding of the complex and dynamic climate system.

1.2 Stable Isotope Paleoclimatology

From the beginning of the field of isotope geochemistry, Harold Urey in his seminal paper described thermodynamically how oxygen isotope values of carbonate reflect environmental conditions during their formation (Urey, 1947). From this formative work McCrea (1950), Urey et al. (1951), and Epstein et al. (1951) developed the oxygen isotope paleotemperature scale in carbonates, calibrating it using synthetic and biogenic carbonates. Subsequent work has refined these initial relationships to reflect the different minerals of carbonate including, aragonite by Patterson et al. (1993) and calcite by Kim and O'Neil (1997). In this dissertation environmental records are drawn from authigenic lake carbonates composed of calcite; and marine bivalves composed of aragonite, thus drawing on the knowledgebase stretching back to the beginning of the field of isotope geochemistry.

1.3 Oxygen Isotope Records from Lake Carbonate

The first two chapters of this dissertation evaluate oxygen isotope values of authigenic lake carbonate to provide environmental information over the Holocene. Authigenic lake carbonate is precipitated *in situ,* recording environmental conditions of the lake during formation and, therefore, does not include allochthonous (or transported) forms of carbonate such as detrital carbonate or invertebrate shells that can have different isotope signals (*c.f.* Kelts and Talbot, 1989). Oxygen isotope values of lake carbonate were measured by Stuiver (1968) who was investigating changes in the oxygen isotope value of meteoric precipitation over the last 11,000 years. Since then much work has been done to understand the mechanism of carbonate precipitation (e.g. McConnaughey, 1991) and the environmental signals recorded (e.g. Kelts and Talbot, 1989; Leng and Marshall, 2004). The formation of authigenic lake carbonate in temperate lakes typically occurs during summer months when elevated temperatures combine with photosynthetic consumption of dissolved CO_2 results in supersaturation with respect to $CaCO_3$ in the microenvironment adjacent to plant cells (Kelts and Hsu, 1978). Therefore, carbonate production is normally restricted to lakes with underlying carbonate bedrock or sediment. Lake algae accrete extracellular carbonate crystals during photosynthesis

(McConnaughey, 1991), thus the majority of carbonate precipitation occurs during periods of maximum algal growth coinciding with a narrow range of temperatures (Drummond et al., 1995). This means that typically variations in oxygen isotope values of lake carbonate reflects changes in lake water oxygen isotope values with modest temperature effects. Figure 1.1 illustrates a model of the sources of oxygen isotope variability in lake carbonates, many of which are dependent on lake-specific limnological conditions. In general, the most important factors affecting authigenic carbonate oxygen isotope values are the ratio of evaporation to precipitation also known as effective moisture and the oxygen isotope value of precipitation (surface water flow and groundwater flow can also play a role but are also closely related to precipitation). The first two chapters describe oxygen isotope records of two lakes from different limnological conditions. The first from a lake situated in the rain shadow of the Coastal Mountains of the Yukon Territory where evaporation plays an important role and moisture is dominantly sourced from the adjacent coastal region (Chapter 2). The second lake is situated along the southern boundary of the boreal forest in Saskatchewan where changes in circulation patterns affect moisture sources, but shorter water residence times reduce the effects of evaporation (Chapter 3).

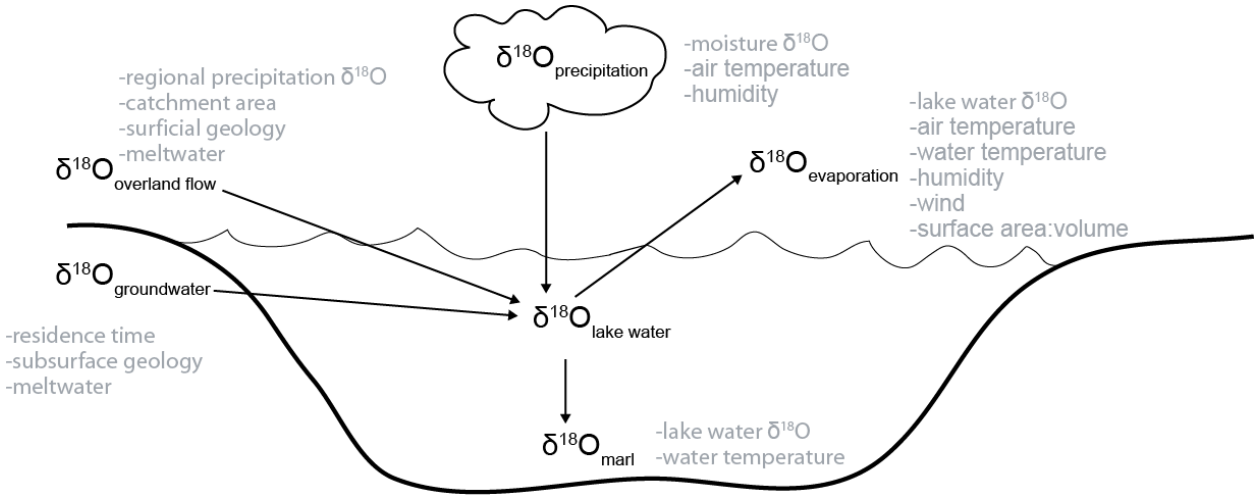

Figure 1.1 Oxygen isotope model of authigenic lake carbonates

1.4 Bivalve Isotope Sclerochronology

The final chapter of this dissertation investigates the use of stable isotope variability in the shells of marine bivalves as a tool to seasonally date overwash deposits. Sclerochronology is the

study of chemical variations in the accretionary hard parts of organisms. The term "sclerochronology" was coined by Buddemeier et al. (1974) in reference to the potential of coral exoskeletons to record environmental information analogous to tree-rings and dendrochronology. The term has now been applied to all sequentially deposited biogenic materials including bivalve shells. Bivalve isotope sclerochronology focuses on developing isotope profiles from cross-sections of bivalve shells in order to investigate seasonal changes in environmental conditions (e.g. Gröcke and Gillikin, 2008). In general, most bivalves are known to secrete shell carbonate in oxygen isotope equilibrium with seawater with very few exceptions (Schöne and Surge, 2012). Therefore, environmental conditions recorded as oxygen isotope values in shell carbonate can be used to track changes in environmental conditions over time. Oxygen isotope ratios in shell carbonate are controlled by the oxygen isotope value of ambient water and water temperature during shell formation. In marine species, where the oxygen isotope value of seawater remains fairly constant over time, oxygen isotope values of shell carbonate can be used to calculate seasonal variations in seawater temperature (Jones et al., 1989). These seasonal temperature variations recorded in the oxygen isotope values of shell carbonate can be used to determine the bivalve's season of death by comparison of the oxygen isotope values at the shell margin with seasonal water temperature variations. Shackleton (1973) first used this technique to determine the season of site occupation from archaeological shell midden deposits. A related technique is employed in the third chapter of this dissertation, that aims to determine the season that an overwash unit was deposited in order to attempt to match a historical record of storm and tsunami events with the geological record.

1.5 The Advantages of High-Resolution Datasets

Traditionally, many paleoclimate records have been sampled at low temporal resolution due to analytical or economic constraints and, therefore, are only able to assess general long-term trends in climate. Although this is valuable, many climatic patterns and oscillations occur on shorter time scales that are not elucidated in these long-term datasets; to explore them requires much higher resolution. For this reason, traditional studies are unable to resolve high-frequency climate oscillations that are important drivers of climate. For example, it is known that the El Niño Southern Oscillation is second only to the seasonal cycle in predicting interannual climate in Western Canada (Shabbar, 2006). However, the El Niño Southern Oscillation has a 3 to 5-year

period (Graham and White, 1988) requiring sub-decadal resolution in order to properly assess its influence on regional climate. In addition, changes in the seasonal cycle require sub-seasonal resolution in order to assess how seasonality has changed through time.

In this dissertation three case studies are presented that use stable isotope values of carbonates to assess (a) the influence of Pacific climate phenomenon on the hydrology of a subarctic lake in the southern Yukon Territory; (b) how paleoprecipitation patterns in central Saskatchewan have changed in relation to the Pacific/North American pattern; and (c) how high-resolution isotope analysis of bivalve shells can help distinguish the timing and thus, origin of overwash deposits. Though each study has a unique and independent research objective, there are marked similarities in the approach of all three chapters. All of these studies highlight the intrinsic value of generating high-resolution records. The bivalve study (Chapter 4) represents sub-seasonal sea surface temperature cycles, the central Saskatchewan record is sub-decadal (Chapter 3) and the Yukon Territory record is sub-centennial (Chapter 2). These records illustrate that despite previous suggestions that Holocene climate has been stable, it is indeed variable, and indicates the importance of exploring short-term climate cycles in order to better evaluate longer-term climate patterns.

1.6 Chapter Overview and Knowledge Gaps

In Chapter 2, subarctic climate change from the Pleistocene-Holocene boundary to the Late Holocene is evaluated based on authigenic lake carbonates from the southern Yukon Territory. In this region climate systems from the Pacific Ocean dominate with the strength and position of the Aleutian Low providing the strongest influence on winter precipitation to the region (Mock et al., 1998). Previous paleoclimate studies from this area suggest that Holocene variations in the Aleutian Low are responsible for changes in atmospheric circulation and precipitation patterns in the southern Yukon (Fisher et al., 2004; Anderson et al., 2005). However, precipitation patterns in this region are heterogeneous as a result of the Coast Mountains that impart an intense rain shadow to the interior of the Yukon and switch the season of maximum precipitation between coastal and interior sites (Cayan and Peterson, 1989). Despite these heterogeneities the majority of climate studies from the region still focus on wintertime precipitation patterns (e.g. the Aleutian Low), ignoring the potential effects of summertime precipitation patterns. In the first study, the gap in knowledge about the effects of North Pacific climate systems on the

summertime precipitation patterns is addressed in the context of site locality relative to the Coast Mountains along with a discussion of changes in paleoprecipitation patterns from the Pleistocene-Holocene boundary to present.

The second study (Chapter 3) focuses on Central Saskatchewan climate change and the influences of the Pacific/North American pattern on driving precipitation in the region. This area is more climatologically homogeneous than the Yukon Territory as there are no adjacent mountains. Modern records from the region show a strong relationship between precipitation oxygen isotope anomalies and the Pacific/North American (PNA) Index. A proxy for Holocene paleoprecipitation oxygen isotope values is produced from authigenic lake carbonate that extends back 8,000 years. It is known that variations in the state of the PNA pattern have climatological implications as PNA^+ periods are associated with warm dry conditions across the prairies, whereas PNA^- phases are associated with cooler conditions (Leathers et al., 1991). However, a gap in our knowledge of the evolution of PNA pattern through the Holocene exists, as there are no climate records from the node of the PNA that are sampled at a high enough resolution to resolve high frequency climate phenomenon such as the PNA. This second study presents an oxygen isotope record from a node of the PNA pattern (Sturgeon Lake, Saskatchewan) that identifies large temporal changes in the state and strength of the PNA, that is linked to regional climate change.

The third and final study (Chapter 4) uses sub-seasonal isotope records from bivalves in order to evaluate depositional processes behind overwash deposits. Distinguishing between tempestites, tsunamites, and lag deposits is difficult in the geological record (Sugawara et al., 2008). Therefore, the development of tools that could facilitate better characterization of these deposits in the geological record would be beneficial. Currently in this field, the employment of geochemical techniques is under-utilized (Chagué-Goff, 2010), suggesting a potential gap in knowledge that is addressed herein. In this study, isotope profiles from multiple specimens of several species are used to evaluate the timing of death of these bivalves. A comparison of these timings allows us to determine how closely related the timing of death was and thus postulate as to the cause of death. Tsunamis and storms should lead to similar time of death across all specimens whereas lag deposits will likely have variable timings. In addition, if these deposits are historical we can compare local environmental conditions with those recorded by the isotope

values of the bivalves that can link the timing of deposition with specific events in the historical record.

1.7 Structure of Dissertation

Each chapter of the dissertation is treated as an independent scientific contribution including relevant figures, tables and references. A concluding summary is provided at the end to reiterate the findings presented in each chapter and summarize the relationship of each study with the overarching theme of the thesis, while also introducing the subsequent chapter. Additional supplemental figures and data have been provided in the appendices. The data presented in this dissertation will also be uploaded to the NOAA World Data Center for Paleoclimatology after publication in peer-reviewed journals in order to make the data available for future research.

1.8 References

Anderson, L., Abbott, M. B., Finney, B. P., & Burns, S. J. (2005). Regional atmospheric circulation change in the North Pacific during the Holocene inferred from lacustrine carbonate oxygen isotopes, Yukon Territory, Canada. Quaternary Research, 64(1), 21-35.

Buddemeier, R. W., Maragos, J. E., & Knutson, D. W. (1974). Radiographic studies of reef coral exoskeletons: rates and patterns of coral growth. Journal of Experimental Marine Biology and Ecology, 14(2), 179-199.

Cayan, D. R., & Peterson, D. H. (1989). The influence of North Pacific atmospheric circulation on streamflow in the west. Geophysical Monograph, 55, 375-397.

Cayan, D. R., Redmond, K. T., & Riddle, L. G. (1999). ENSO and hydrologic extremes in the western United States*. Journal of Climate, 12(9), 2881-2893.

Chagué-Goff, C. (2010). Chemical signatures of palaeotsunamis: A forgotten proxy? Marine Geology, 271(1), 67-71.

Changnon, S. A. (1999). Impacts of 1997-98 El Niño generated weather in the United States. Bulletin of the American Meteorological Society, 80(9), 1819-1827.

Drummond, C. N., Patterson, W. P., & Walker, J. C. (1995). Climatic forcing of carbon-oxygen isotopic covariance in temperate-region marl lakes. Geology, 23(11), 1031-1034.

Epstein S., Buchsbaum R., Lowenstam HA., & Urey HC. 1953. Revised carbonate–water isotopic temperature scale. Bulletin of the Geological Society of America 64, 1315–1326.

Fisher, D. A., Wake, C., Kreutz, K., Yalcin, K., Steig, E., Mayewski, P., Andreson, L., Zheng, J., Rupper, S., Zdanowicz, C., Demuth, M., Waszkiewicz, M., Dahl-Jensen, D., Goto-Azuma, J., Bourgeois, J.B., Koerner, R.M., Sekerka, J., Osterberg, E., Abbott, M.B., Finney, B.P., & Burns, S. J. (2004). Stable isotope records from Mount Logan, Eclipse ice cores and nearby Jellybean Lake. Water cycle of the North Pacific over 2000 years and over five vertical kilometres: sudden shifts and tropical connections. Géographie Physique et Quaternaire, 58(2-3), 337-352.

Fritts, H. C., Lofgren, G. R., & Gordon, G. A. (1979). Variations in climate since 1602 as reconstructed from tree rings. Quaternary Research, 12(1), 18-46.

Graham, N.E., White, W.B., 1988. The El Niño cycle: a natural oscillator of the Pacific Ocean—atmosphere system. Science 240, p. 1293–1302.

Gröcke, D. R., & Gillikin, D. P. (2008). Advances in mollusc sclerochronology and sclerochemistry: tools for understanding climate and environment. Geo-Marine Letters, 28(5-6), 265-268.

Grootes, P. M., Stuiver, M., White, J. W. C., Johnsen, S., & Jouzel, J. (1993). Comparison of oxygen isotope records from the GISP2 and GRIP Greenland ice cores.

Hargreaves, J. C., & Annan, J. D. (2009). On the importance of paleoclimate modelling for improving predictions of future climate change. Climate of the Past, 5(4), 803-814.

Jones, D. S., Arthur, M. A., & Allard, D. J. (1989). Sclerochronological records of temperature and growth from shells of *Mercenaria mercenaria* from Narragansett Bay, Rhode Island. Marine Biology, 102(2), 225-234.

Kelts, K., & Hsü, K. J. (1978). Freshwater carbonate sedimentation. In Lakes (pp. 295-323). Springer New York.

Kelts, K., & Talbot, M. (1990). Lacustrine carbonates as geochemical archives of environmental change and biotic/abiotic interactions. In Large Lakes (pp. 288-315). Springer Berlin Heidelberg.

Kim, S. T., & O'Neil, J. R. (1997). Equilibrium and nonequilibrium oxygen isotope effects in synthetic carbonates. Geochimica et Cosmochimica Acta, 61(16), 3461-3475.

Kirby, M., Patterson, W. P., Mullins, H., & Burnett, A. (2002). Post-Younger Dryas climate interval linked to circumpolar vortex variability: isotopic evidence from Fayetteville Green Lake, New York. Climate Dynamics, 19(3-4), 321-330.

Leathers, D. J., Yarnal, B., & Palecki, M. A. (1991). The Pacific/North American teleconnection pattern and United States climate. Part I: Regional temperature and precipitation associations. Journal of Climate, 4(5), 517-528.

Leng, M.J., & Marshall, J.D., 2004. Palaeoclimate interpretation of stable isotope data from lake sediment archives. Quaternary Science Reviews 23, 811–831.

Mantua, N.J., Hare, S.R., Zhang, Y., Wallace, J.M., & Francis, R.C., (1997), A Pacific interdecadal climate oscillation with impacts on salmon production: Bulletin of the American Meteorological Society, v. 78, p. 1069–1079.

McConnaughey, T. (1991). Calcification in *Chara corallina*: CO2 hydroxylation generates protons for bicarbonate assimilation. Limnology and Oceanography, 36(4), 619-628.

McCrea, J.M., 1950. On the isotopic geochemistry of carbonates and a paleotemperature scale. Journal of Chemical Physics 18, 849−857.

Mock, C. J., Bartlein, P. J., & Anderson, P. M. (1998). Atmospheric circulation patterns and spatial climatic variations in Beringia. International Journal of Climatology, 18(10), 1085-1104.

Patterson, W. P., Smith, G. R., & Lohmann, K. C. (1993). Continental paleothermometry and seasonality using the isotopic composition of aragonitic otoliths of freshwater fishes. Climate change in continental isotopic records, 191-202.

Sandweiss, D. H., Maasch, K. A., & Anderson, D. G. (1999). Transitions in the mid-Holocene. Science, 283(5401), 499.

Schöne, B. R., Fiebig, J., Pfeiffer, M., Gleβ, R., Hickson, J., Johnson, A. L., Dreyer, W. & Oschmann, W. (2005). Climate records from a bivalved Methuselah (*Arctica islandica*, Mollusca; Iceland). Palaeogeography, Palaeoclimatology, Palaeoecology, 228(1), 130-148.

Schöne, B. R., & Surge, D. M. (2012). Part N, Revised, Volume 1, Chapter 14: Bivalve sclerochronology and geochemistry. Treatise Online, 46, 1-24.

Shabbar, A. (2006). The impact of El Niño-Southern oscillation on the Canadian climate. Advances in Geosciences, 6, 149-153.

Shackleton, N.J. (1973). Oxygen isotope analysis as a means of determining season of occupation of prehistoric midden sites. Archaeometry 15, 133–141.

Stuiver, M. (1968). Oxygen-18 content of atmospheric precipitation during last 11,000 years in the Great Lakes region. Science, 162(3857), 994-997.

Sugawara, D., Minoura, K., & Imamura, F. (2008). Tsunamis and tsunami sedimentology. Tsunamiites—Features and Implications, 9-49.

Urey, H. 1947. The thermodynamic properties of isotopic substances. Journal of the Chemical Society, 562−581.

Urey, H. C., Lowenstam, H. A., Epstein, S., & McKinney, C. R. (1951). Measurement of paleotemperatures and temperatures of the Upper Cretaceous of England, Denmark, and the southeastern United States. Geological Society of America Bulletin, 62(4), 399-416.

Wang, Y., Cheng, H., Edwards, R. L., He, Y., Kong, X., An, Z., Wu, J., Kelly, M.J., Dykoski, C.A., & Li, X. (2005). The Holocene Asian monsoon: links to solar changes and North Atlantic climate. Science, 308(5723), 854-857.

CHAPTER 2

LATE QUATERNARY CLIMATE CHANGE IN THE SOUTHWEST YUKON TERRITORY: EVIDENCE FROM AUTHIGENIC LAKE CARBONATE

2.1 Abstract

Oxygen isotope values ($\delta^{18}O_{carb}$) of authigenic lake carbonate from Spirit Lake in the southwest Yukon Territory provide a history of effective moisture and variability in atmospheric circulation patterns during the Holocene. A 10.6-meter core provides a record extending back to the Pleistocene-Holocene transition, yielding detailed chronological and climatic information about deglacial and later events in the southwest Yukon. $\delta^{18}O_{carb}$ values suggest that increased moisture advection to the region increases meteoric precipitation characterized by low $\delta^{18}O_{precipitation}$ values due to Rayleigh fractionation associated with rainout as it passes over the adjacent Coast Mountains. Decreasing $\delta^{18}O_{lakewater}$ values force lower $\delta^{18}O_{carb}$ values. This occurs when North Pacific sea surface temperatures are higher and/or during periods of intensified Aleutian Low and North Pacific High pressure centers. As moisture advection decreases, evaporation of lake water becomes more significant, increasing $\delta^{18}O_{lakewater}$ values leading to higher $\delta^{18}O_{carb}$ values. $\delta^{18}O_{carb}$ values decrease significantly at the end of the Younger Dryas indicative of a significant change in atmospheric circulation following the collapse of the Laurentide Ice Sheet. It is suggested that the removal of the glacial anticyclone led to a northward migration of the North Pacific high resulting in increased summer precipitation in the region, thus reducing lake evaporation, as exemplified by lower $\delta^{18}O_{carb}$ values during the Holocene. Lake $\delta^{18}O_{carb}$ values reach a minimum coincident with the Holocene Thermal Maximum, indicating warm moist conditions that are followed by modern-like conditions developing around 6,500 years BP.

2.2 Introduction

2.2.1 Background

Yukon marl lakes represent an exceptionally important archive of past climate because the high-latitude setting generates an amplified response to climatic change (Roots, 1989). Detailed and accurate assessments of past climate change and its effects on the environment are crucial for better predicting the effects of future climate change. Previous paleoclimate research in the southwestern Yukon has focused mainly on the Holocene due to a lack of climate records extending back continuously past 11,700 years because glacial erosion destroyed the older records. Therefore, records extending into the Pleistocene are rare but essential to our understanding of how (a) we got to the present climate state and (b) how the transition out of the glacial period occurred within a global context.

Past climate records from the Yukon Territory and surrounding region have shown considerable variability in climate through the Holocene. At the end of the Last Glacial Maximum (LGM) some areas of the Yukon were ice-free (e.g. Antifreeze Pond; Vermaire and Cwynar, 2010), while others were covered in hundreds of meters of glacial ice, epitomizing the heterogeneous nature of the climate in this region (Bond, 2004). Paleoclimate studies of the region support this notion with spatially complex responses to climate events such as the Younger Dryas (Kokorowski et al., 2008) and the Holocene Thermal Maximum (Kaufman et al., 2004). The highly variable physiography of the region is partially responsible for this heterogeneity as coastal mountains block maritime moisture from the interior regions. Therefore, it is essential to have a broad regional distribution of studies to create an accurate picture of climate dynamics.

In the Gulf of Alaska, the Aleutian Low (AL) atmospheric pressure system is the main "center of action" in the region during the winter (Rodionov et al., 2007) and as such it has been the focus of much research. The Aleutian Low is strongest in the winter when it represents the region where Pacific cyclones reach peak intensities (Rodionov et al., 2007). However, the strength and position of the AL varies greatly over time (Overland et al., 1999). During periods of deeper and eastward shifted ALs, coastal sea surface temperatures (SST) increase, leading to warmer and moister air advection onto coastal North America increasing terrestrial air temperatures (Trenberth and Hurrell, 1994). When this occurs there is also a southward shift of storm tracks as well as ecological effects (Trenberth and Hurrell, 1994). Periods of eastward

displaced and deeper AL have been suggested to be associated with increased maritime precipitation to in the study region (Spooner et al., 2003; Anderson et al., 2005c). During the summer the position and strength of the North Pacific High exerts some control on North Pacific circulation patterns (Sawada and Handa, 1998), and upwelling along the coast (Sabin and Pisias, 1996; Pisias et al., 2001). Considerably less research has been carried out on the North Pacific High and its effects on local climate, despite evidence suggesting a correlation with river discharge from sites on the leeward side of coastal mountain ranges in Alaska (Cayan and Peterson, 1989). In essence, we have an incomplete understanding of the relationship between coastal weather patterns and general atmospheric circulation patterns (Stabeno et al., 2004), including major climate variability such as the Pacific Decadal Oscillation (Mantua and Hare, 2002).

Terrestrial proxies from the Pacific Northwest suggest significant variability in the amount and source of moisture through the Holocene (e.g. Fisher et al., 2004; Anderson et al. 2005b, 2005c), however, the main causes of this variability are poorly understood. This suggests that longer, more detailed histories of climate change in the Yukon are required in order to develop a better understanding of the behaviour of North Pacific climate since the end of the last glacial.

Lake cores are invaluable archives of paleoclimatology information because their mineralogical and faunal components provide a wealth of information about past environmental/climate conditions (c.f. Leng and Marshall, 2004). Marl lakes are particularly useful because authigenic carbonate sediment records ambient environmental information during formation thereby yielding an important proxy for paleoclimate reconstruction (e.g. Stuiver, 1968; Talbot, 1990). Authigenic lake carbonate precipitated in isotopic equilibrium with lakewater provides a proxy for changes in the temperature and $\delta^{18}O_{lakewater}$ values through time. $\delta^{18}O_{lakewater}$ values can vary in complex ways, influenced by variability in seasonality of precipitation, the balance between precipitation and evaporation, moisture sources, and changes in local hydrology. $\delta^{18}O_{precipitation}$ values are typically related to air temperature, latitude, moisture source, and continentality of the air mass (Dansgaard, 1964). In the case of the Pacific Northwest the Holocene $\delta^{18}O_{lakewater}$ values are believed to be dominated by the source of moisture and the precipitation-evaporation balance (effective moisture), thereby providing information on variation in atmospheric circulation patterns (Anderson et al., 2005c) and aridity (Anderson et al., 2005b).

The objective of this study is to use high-resolution stable isotope analyses of authigenic lake carbonate to understand how climate in the Yukon has changed since the last glacial. This encompasses deglaciation of the region as well as Early to Mid-Holocene climate dynamics and their relationship to regional climate change. This study is the first to present a lake sediment isotope record that extends continuously back into the Pleistocene in the southwest Yukon, providing a unique data set for understanding Late Pleistocene-Holocene climate dynamics in the region. It is hoped that this will help elucidate the role that atmospheric teleconnections played in the development of Post-Glacial climate on both a regional and global scale.

2.2.2 Previous Paleoclimate Studies

The Spirit Lake region has been examined in several previous paleoclimate studies. Anderson et al. (2005a) conducted a study of Jellybean Lake; a smaller open lake located ~10 km to the north of Spirit Lake. This lake differs from Spirit Lake in that it is smaller and considered an open system with a short residence time, minimal evaporative effects, and hence lake carbonate $\delta^{18}O_{carb}$ values that are thought to accurately reflect local $\delta^{18}O_{precipitation}$ values (Anderson et al. 2005a). Marcella Lake (aka Kettlehole Pond), also studied by Anderson et al. (2005a; b), is a closed system lake located ~55 km east of Spirit Lake. This lake is notably smaller and has a higher $\delta^{18}O_{lakewater}$ value (–8.0‰) indicative of significant evaporation, suggesting that lake carbonate $\delta^{18}O_{carb}$ values reflect regional evaporative conditions (Anderson et al., 2005b). A record of Holocene palynology from Marcella Lake has also been described (Cwynar, 1988) as helping connect regional ecological changes with the paleoclimate interpretations from lake carbonate.

2.2.3 Site Locality

Spirit Lake is located in southwestern Yukon Territory at 60°15’0”N; 134°44’24”W (Fig. 2.1). It is a medium sized lake (~0.7 km^2) with a maximum depth of ~30 m at its northern end. The lake is elongated in the north-south direction with a broader, shallower (~1-2 m) southern end. The shallow southern end has a well-developed carbonate (marl) bench from which a Vibra-core was extracted in August 2009. There is no distinct surface inflow or outflow of water, although an abandoned outflow stream to the south suggests there was surficial outflow in the past. Inflow is likely dominated by groundwater and surface flow from melting snow from

adjacent Cariboo Mountain and its north-south trending ridge system that forms the eastern boundary of the lake. The lake is located in a valley once occupied by the large glacial Lake Watson following the melting of the Cassiar Lobe of the Cordilleran Ice Sheet (Bond, 2004). Average monthly precipitation and temperature data from nearby Whitehorse (50 km northwest) indicates that summer maximum temperatures average 14°C and winter minima average –18°C (Environment Canada, 2013). This region is positioned in the rain shadow of the Coastal Range, receiving an average of ~250 mm annual precipitation, in contrast to the ~4000 mm of precipitation that typically falls along the coast less than 250 km to the west (Climate Normals for Whitehorse, YK and Yakatut, AK respectively; Environment Canada, NOAA). Although the highest monthly precipitation occurs in the summer months, subzero temperatures from fall-spring mean that most of the annual precipitation is stored and then released during the spring freshet.

The IAEA's Global Network in Precipitation operated a station at Whitehorse from 1961-1966 and again from 1986-1989 providing average monthly $\delta^{18}O_{precipitation}$ values shown in Fig. 2.2. $\delta^{18}O_{precip}$ values generally track average air temperatures except in the spring and fall periods when there are positive departures from the air temperature trend. This is due to the diverse nature of the precipitation type (i.e. rain and snow) falling during this transition period, and is clearly visible in the bimodal distribution of $\delta^{18}O_{precipitation}$ values during these time periods (Fig. 2.2).

2.3 Methods

2.3.1 Vibra-coring

Lake cores were obtained using a Vibra-core rig mounted on a platform between two Bombard Commando 4 boats, used to lower aluminum tubing coupled to a concrete vibrator. The vibration produced by the vibrator liquefies the sediment around the casing allowing for maximum penetration. Two-meter lengths of aluminum tubing are added as needed until maximum core depth is reached. At Spirit Lake a depth of approximately 10.6 meters was reached after which a hand held winch was used to hoist the core tubes back to the surface where they were capped, labelled, and stored for processing in the lab. Difficulties in extracting the first tube caused approximately 5 cm of sediment loss from the bottom of the first core tube, shown as a gap in the beginning portion of the isotopic record. In addition, due to high water content and

the unconsolidated nature of the sediment-water interface coupled with the failure of our piston in the field, the top sediment closest to the sediment-water interface were mixed and thus not suitable for analysis.

2.3.2 Local Meteoric Water Sampling

Regional meteoric waters were sampled from several streams, lakes and rivers in July 2008 and August 2009. Water samples were collected in 100 mL Nalgene containers that were rinsed with the water sample before filling and capping with no headspace. Capped samples were taped and transported back to the Saskatchewan Isotope Laboratory where they were analyzed for $\delta^{18}O$ and δD values on a Picarro L1102-*i* Isotopic Liquid Water Analyzer based on wavelength-scanned cavity ring down spectroscopy (WS-CRDS)

2.3.3 Carbonate Isotopic Analyses

Aliquots of carbonate were extracted from the core such that only fine grain marl sediment was sampled, avoiding shell debris as well as non-carbonate materials, prior to placing samples into stainless steel sample boats. Sample boats were then heated to 200°C for one hour *in vacuo* in order to prevent potential contamination from organic matter and volatiles in the sediment that may interfere with isotope analyses. Carbonate samples were subsequently analyzed using a Kiel IV automated carbonate preparation device directly coupled to a ThermoFinnigan MAT 253 mass spectrometer and calibrated using NBS-19 at the University of Saskatchewan. All results are reported in standard per mil notation (‰) relative to VPDB. Standard deviation of NBS-19 analyses was better than 0.05‰ for $\delta^{13}C$ and 0.1‰ for $\delta^{18}O$.

To evaluate whether authigenic lake carbonate faithfully records environmental conditions during formation, Anderson et al. (2007) measured water temperature, $\delta^{18}O$ values of the lake water along with $\delta^{18}O$ values of carbonate derived from *Chara* encrustations (marl). Deviations from equilibrium $\delta^{18}O$ values were found to be generally less than 0.4‰ with the exception of Jackfish Lake. We can estimate disequilibrium at Spirit Lake with a lakewater temperature of 15°C (using the calcite-water fractionation equation of Kim and O'Neil, 1997), the youngest $\delta^{18}O_{carb}$ value (–15.3‰$_{VPDB}$) and measured lakewater $\delta^{18}O_{H_2O}$ value of –15.3‰$_{VSMOW}$ (converted to VPDB using Coplen et al., 1983) to calculate a predicted $\delta^{18}O_{carb}$ value of –15.6‰. The offset between measured and the predicted value is 0.3‰, therefore $\delta^{18}O_{carb}$ is assumed to be in close

isotopic equilibrium with lakewater at Spirit Lake. The small offset could easily result from some of the collected modern carbonate forming at a temperature other than that recorded on the day of collection.

2.3.4 Radiocarbon Analysis

Core chronology was determined using a combination of radiocarbon dating and seasonal couplet counting. Five different types of materials were sampled for radiocarbon analysis. These include aquatic mosses (bryophytes); carbonate sediment, mollusc shells, insect remains, and wood (charcoal and unburned wood). Co-occurring plant and carbonate sediment samples were taken at several intervals to assess how the reservoir effect in the dissolved inorganic carbon pool has changed through time. Samples were washed and then sent to Rafter Radiocarbon Laboratory for carbon-14 analysis. A total of 14 samples were submitted for radiocarbon analysis. Results are presented in Table 1. Radiocarbon ages were calibrated using CALIB 6.0 following the corrections of Reimer et al. (2009). Details of the dated materials along with radiocarbon and calibrated ages are shown in Table 1.

2.4 Results

2.4.1 Age Model

Fourteen samples of terrestrial and aquatic material were used to construct the age model and radiocarbon history of the lake. Descriptions of these samples are included with the ^{14}C ages in Table 2.1. Two of these dates, NZA-33643 and NZA-33998, were excluded from the age model because the first appeared to be a mix of terrestrial carbon and DIC sources and the second was spuriously old compared to closely situated adjacent dates.

Radiocarbon dating of material from Spirit Lake is complicated by high concentrations of dissolved inorganic carbon in the lake water associated with carbonate bedrock and alluvium. Local Triassic limestones and dolostones from the Hancock Member underlie Spirit Lake and have essentially no ^{14}C, therefore when dissolved and incorporated in river and lake water, they decrease the ^{14}C concentration in the dissolved inorganic carbon pool of the lake. The incorporation of old carbon leads to erroneously older dates and is known as the *hardwater effect* (Deevey et al., 1954). This hardwater effect may vary through time (Mott, 1975), further complicating the development of age models. In the case of Spirit Lake as with other subarctic

lakes, during deglaciation there was little terrestrial biomass in the watershed and hence little terrestrial-sourced dissolved organic matter or particulate organic matter. Thus, the lakewater carbon pool would have been dominated by dissolved calcium carbonate from the surrounding bedrock. A combination of increased incorporation of surrounding terrestrial biomass and atmospheric-CO_2 equilibration with lake water through the Holocene leads to the incorporation of more modern ^{14}C into the lake carbon pool resulting in a reduction of the hardwater effect over time. To compensate for this, dates were first separated into two groups (a) terrestrial- or atmospheric-based carbon dates, that have no hardwater effects; and (b) dissolved inorganic carbon-based dates, that have carbon sourced from lakewater and have hardwater effects. To determine the difference between the DIC-based dates and atmospheric based dates over time equivalent DIC-based dates had to be calculated for the depth equivalent of the atmospheric-based dates. To accomplish this a linear regression was fit through the two DIC-based dates bracketing the atmospheric-based date to calculate the DIC-based date corresponding with the terrestrial-based dates. The terrestrial dates were then subtracted from modeled DIC-based dates in order to determine the magnitude of the hardwater effect over time. We observe a large decrease in the hardwater effect in Spirit Lake (Table 1). The initial hardwater effect (at 503.8 cm depth) is large at ~7,730 years, similar in magnitude to the ~7,030 year hardwater effect determined by MacDonald et al. (1987) in an Alberta lake following deglaciation of that area. Over the Holocene, the hardwater effect decreases to 5,520 years at 407.6 cm depth and then 1,660 years at 22.5 cm depth. An exponential curve was fit to the hardwater effect values. The hardwater effect line was subtracted from the DIC-based dates to correct the DIC-based dates for the hardwater effect. These corrected ages were then combined with the terrestrial-based ages to construct the age model. The age model was constructed by fitting a linear regression between each of the dates including the varve counting dates discussed below.

Below ~5 m sediment mineralogy changes from carbonate- to siliciclastic-dominated and no organic matter was found below this depth that could be radiocarbon dated (Fig. 2.3). In this portion of the core, couplets of silt/sand and clay were assumed to represent seasonal changes in sedimentation, with lighter colored coarse sediment representing spring and summer inflows and dark colored clays deposited during cooler ice covered conditions. Seasonal couplets (i.e. varves) were visually counted, however, counting errors associated with non-distinct couplet boundaries, potential sediment loss associated with deformation features (e.g. slumping, erosion) suggests the

calculated age is likely to be slightly underestimated. The number of varves (equal to one year of deposition) for the first section of siliciclastic-dominated core was then added on to the age modeled (based on radiocarbon age model, see above) for the top of siliciclastic-dominated section (11,747 years BP). The number of varves for each sequential core section was then added onto this age, noting the depth related to section tops and bottoms. These ages were then used in the final age model as discussed above.

The sedimentation rate changed significantly throughout the record, varying between 0.3 mm/yr to 0.7 mm/yr in the upper portion and around 4 mm/yr in the lower 5 meters of the core. These differences relate to changes in the proximity to glacial outwash (lower section) and productivity in the lake (upper section).

2.4.2 *Regional Meteoric Water Isotope Data*

A compilation of isotope values of regional meteoric water is presented in Fig. 2.4. Isotopic analyses of precipitation conducted by the IAEA (GNIP, IAEA) for Whitehorse provide the basis for a Local Meteoric Water Line (LMWL). Water isotope data from Anderson (2005) and this study provide a detailed picture of the $\delta^{18}O_{H2O}$ and $\delta^{2}H_{H2O}$ values of rivers, lakes, and springs of the region. By separating lake and river samples we can develop a local evaporation line (LEL) that describes the evolution of water isotope values in evaporating water bodies. Lakes higher along the LEL undergo more intense evaporation than those closer to the LMWL that tends to include hydrologically closed lakes. The value at which the LEL intersects the LMWL typically represents the average isotope value of precipitation in the region (i.e. $\delta^{2}H = -161‰$ and $\delta^{18}O = -21.2‰_{VSMOW}$), similar to the average annual precipitation at Whitehorse ($\delta^{2}H = -168‰$; $\delta^{18}O = -21.6‰_{VSMOW}$). Jellybean Lake has a $\delta^{18}O_{lakewater}$ value of $-19.9‰_{VSMOW}$, very similar to the intersection of the LEL with the LMWL suggesting its $\delta^{18}O_{lakewater}$ value is indicative of the mean annual $\delta^{18}O_{precipitation}$ value. Spirit Lake has a $\delta^{18}O_{lakewater}$ value in the middle of the LEL whereas Marcella Lake exhibits very high evaporative conditions. Clegg and Hu (2010) observed that surface water evaporation during ice-free periods was important in controlling lake water $\delta^{18}O_{H2O}$ in the southern Brooks Range with $\delta^{18}O_{lakewater}$ values deviating from the LMWL. We see a similar deviation from the LMWL at Spirit Lake suggesting that $\delta^{18}O_{lakewater}$ values are

sensitive to both evaporation and the $\delta^{18}O_{precipitation}$ values of precipitation indicating the Spirit Lake $\delta^{18}O_{carb}$ record provides a proxy for effective moisture.

2.4.3 Sedimentological Evidence of Limnological Conditions

Core sedimentology and local glacial geomorphological evidence suggests that this area was initially beneath a large proglacial lake (Bond, 2004). During the post-glacial climate transition, core sedimentology changes from the glaciolacustrine silt and clay dominated lower sediment, to the more carbonate rich upper sediment, indicating increased productivity in the lake associated with post-glacial regional warming. This change in depositional characteristics occurs at ~5 meters depth in the core, representing a shift from allochthonous, glacially sourced sediment, to authigenic marl production (Fig. 2.3). X-ray diffraction of sediment indicates carbonates are dominantly composed of calcite (See Appendix A).

The upper carbonate-rich portion of the core is dominated by light grey to brownish marl with abundant ostracod, bivalve, and gastropod shells. The first meter also contains abundant bryophytes that decrease in abundance below 1.1 m. There is no evidence of sub-aerial exposure in the core such as the pelletized marl encountered at Jellybean Lake (Anderson et al., 2005c). Silt layers are apparent at ~3.5 m, becoming abundant below 3.7 m, dominating the record below 5.2 m. Below 5.2 m, sediment is composed of rhythmic couplets that likely represent annual changes in lake water energy as discussed above. Couplet size begins to increase slightly downcore with thicker light-colored silty units, with the lowest meter of core containing couplets as thick as 1 cm. This increase in silt content probably reflects increased glacial meltwater associated with a more glacio-proximal location at the coring site. The absence of poorly sorted coarse grain sediment suggests deposition in a large proglacial lake in an ice-distal location (Lamoureux and Gilbert, 2004). Strandlines at an elevation of 778 m along Bennett Lake (~5 km south of Spirit Lake) indicate that the modern Spirit Lake surface was under ~120 m of water during deglaciation (Bond, 2004), further supporting an ice-distal glacio-lacustrine origin of sediment in the lower 5 meters at Spirit Lake. X-ray diffraction analysis of the lowermost sediment indicates that feldspars (69.6%) and quartz (20.2%) dominate the mineralogy of the silts and clays with minor amounts of kaolinite (7.5%) and calcite (2.7%). Mineralogy of the lower sediment is reflective of the siliciclastics derived from various volcanic complexes surrounding the area in addition to small amounts of marl precipitation. Higher sediment loads

generated by regional deglaciation during the early Holocene dilutes the lacustrine carbonate record offering potential for a higher resolution climate record during this important period of turbulent climatic change.

2.4.4 $\delta^{13}C$–$\delta^{18}O$ Covariance Plot

Results from Spirit Lake indicate three distinct groupings of data (Fig. 2.5). The first and oldest termed the "Ice Melt" group from 12,700–11,900 yr BP includes the glacio-lacustrine silts and clays from the lower five meters of the core. The second group, from 11,900-11,600 years BP, represents a transition from "Ice Melt" into the "Holocene" and is termed "Transition" as it represents the largest $\delta^{18}O_{carb}$ offset. The third group is the "Holocene" from 11,600 years BP to present that makes up the bulk of the temporal record. Evaluating the relationship between $\delta^{13}C$–$\delta^{18}O$ values through time provides information on how limnological changes influenced the isotope budgets within the lake (Li and Ku, 1997). Isotopic analysis of samples from the underlying carbonaceous bedrock (Hancock Member) reveals an oxygen isotope value ($\delta^{18}O$: –8.6‰$_{VPDB}$, located off-scale in Fig. 2.5) that is distinct from lake marl, thus, $\delta^{18}O_{carb}$ values likely reflect environmental conditions with minimal contributions from detrital carbonate. Carbon isotope values are linked to changes in carbon sources, where lower values are associated with increased incorporation of dissolved inorganic carbon from ground and surface water sourced from terrestrial vegetation, or respired soil CO_2 (Leng and Marshall, 2004); higher $\delta^{13}C$ values being related to increased C sourcing from atmospheric CO_2 exchange. The full Spirit Lake $\delta^{13}C_{carb}$ record is discussed in a sister paper Timsic et al. (in prep).

Fig. 2.5 clearly illustrates the bimodal distribution of $\delta^{18}O_{carb}$ values of Spirit Lake as well as a change in the $\delta^{13}C$–$\delta^{18}O_{carb}$ relationship between deglaciation and the Holocene, reflecting a major shift in limnological conditions. During the melting of the Cassiar Lobe of the Cordilleran Ice Sheet the Spirit Lake area was overlain by a large proglacial lake (Watson) that drained through the Cowley Creek outlet channel to the north of Spirit Lake into the Yukon River. As ice retreated south of Carcross and withdrew from Bennett Lake, it opened up a new outlet to the south, leading to the abandonment of the Cowley Creek outlet and the draining of glacial Lake Watson (Bond, 2004). It is hypothesized that the change in the $\delta^{13}C$–$\delta^{18}O_{carb}$ relationship between Ice Melt and Holocene data groupings is a result of the draining of glacial Lake Watson and the subsequent isolation of Spirit Lake. The concurrent change in sedimentology and isotope

geochemistry both support this hypothesis which would date the draining of glacial Lake Watson to ~11,550 years BP.

2.5 Discussion

2.5.1 Controls on $\delta^{18}O_{carb}$ Variability

The two primary controls on $\delta^{18}O_{carb}$ values of lake carbonate are water temperature and the $\delta^{18}O_{H2O}$ value of lake water (Stuiver, 1968). Drummond et al. (1995) found that the timing of maximum calcite production was associated with a narrow and consistent range of temperatures suggesting $\delta^{18}O_{carb}$ variability is often related primarily to the $\delta^{18}O_{lakewater}$ value rather than temperature fluctuations. Carbonate formation in the lake can only occur during ice-free periods with conditions conducive to algal growth further suggesting a limited lake water temperature range. $\delta^{18}O_{lakewater}$ values are a more complex variable, affected by air temperature, changes in the seasonality of precipitation, balance between precipitation and evaporation, moisture sources, and changes in local hydrology.

To evaluate the role of air temperature in forcing lake $\delta^{18}O_{carb}$ values via the influence of air temperature on $\delta^{18}O_{lakewater}$ we first calculate its theoretical effect on $\delta^{18}O_{lakewater}$ values. In high latitude regions mean annual air temperature is strongly correlated with $\delta^{18}O_{precipitation}$ and has an average relationship of 0.6‰/°C (Dansgaard, 1964; Rozanski et al., 1992). The fractionation relationship for calcite at modern summer lake temperatures (15°C) is –0.22‰/°C (Kim and O'Neil, 1997) combining these factors results in a carbonate fractionation of 0.38‰/°C air temperature change. The range in $\delta^{18}O_{carb}$ values observed at Spirit Lake is greater than 6.5‰ equating to a temperature change greater than 17°C—clearly unreasonable and not supported by any other regional climate proxies. For example, a summary of Holocene Thermal Maximum temperatures in the western Arctic suggests an average difference of +1.6±0.8°C compared with modern temperatures (Kaufman et al., 2004). The range of Holocene $\delta^{18}O_{carb}$ values (2.5‰) equates to a temperature change of ~7°C, which means that other factors are equally if not more important when interpreting lake carbonate records in this region.

Changes in the seasonality of precipitation could force $\delta^{18}O_{lakewater}$ values (e.g. Drummond et al., 1995) due to the difference in $\delta^{18}O_{precipitation}$ values of average summer and winter precipitation (GNIP weighted summer mean = –18.2‰; weighted winter mean = –24.3‰). The 6.1‰ offset between summer and winter $\delta^{18}O_{precipitation}$ values of precipitation is large enough to

invoke the observed change in the $\delta^{18}O_{carb}$ record however the magnitude of change required to invoke this change is unrealistic. The weighted annual average $\delta^{18}O$ value of precipitation is –21.6‰$_{VSMOW}$. Modeling the weighted contributions of different seasons and adjusting the mass balance to invoke a 2.5‰ shift (*i.e.* range in Holocene values) in annual average of $\delta^{18}O_{carb}$ values requires a >90% increase in winter precipitation for periods with lower $\delta^{18}O_{precipitation}$ values and a >90% increase in summer precipitation during periods of higher $\delta^{18}O_{precipitation}$ values. This wholesale change in the seasonal distribution of precipitation is unlikely for the Holocene and therefore it is assumed that changes in the seasonal distribution of precipitation represents only a minor effect on overall variability in $\delta^{18}O$ values. Even short-term variability in $\delta^{18}O_{carb}$ values, up to 1.4‰ between adjacent $\delta^{18}O_{carb}$ values in the Holocene, requires a >50% increase in summer precipitation followed by a >50% increase in winter precipitation, which is not observed in the historical record. In addition, a recently updated summary on the controls on North Pacific $\delta^{18}O_{precipitation}$ values indicates that both proxy data and models show little evidence that temperature, precipitation amount, or seasonality play a dominant role on the regional $\delta^{18}O$ values of precipitation (Anderson et al., 2016). Instead, atmospheric circulation patterns and local effective moisture conditions are responsible for variability in $\delta^{18}O_{precipitation}$ values.

The balance between precipitation and evaporation, or effective moisture, plays an important role in $\delta^{18}O_{lakewater}$ variability. Increased evaporation preferentially removes ^{16}O resulting in higher $\delta^{18}O_{lakewater}$ values in the remaining water, leading to higher $\delta^{18}O_{carb}$ values. This is thought to be the dominant environmental control on $\delta^{18}O_{lakewater}$ values at the nearby evaporation sensitive Marcella Lake (Anderson et al., 2005b), and also likely plays an important role at Spirit Lake as shown by the intermediary position of the $\delta^{18}O_{lakewater}$ value of Spirit Lake along the local evaporation line (LEL) in Fig. 2.4.

For the southwest Yukon it has been suggested that decreases in Holocene $\delta^{18}O_{precipitation}$ (Fisher et al., 2004) and hence $\delta^{18}O_{carb}$ (Anderson et al., 2005a) values are related to a deeper/stronger AL that draws moisture from more southerly sources. These air masses undergo increased Rayleigh fractionation as they pass over the Coast Mountains leading to increased distillation (Fisher et al., 2004; Anderson et al., 2005a). Therefore, $\delta^{18}O_{ice}$ values at Mt. Logan are principally a proxy for the relative ratio of meridional versus zonal flow (Fisher et al., 2008). However, comparing isotope-enabled GCM-based circulation patterns with the $\delta^{18}O_{ice}$ record from Mt. Logan, Field et al. (2010) found that during cooler periods, deeper ALs were associated

with elevated $\delta^{18}O_{ice}$ values and lower values with the opposite meteorological conditions. A comparison of Mt. Logan ice accumulation data with large-scale atmospheric circulation patterns finds a positive relationship between ice accumulation and North Pacific storminess (Rupper et al., 2004) agreeing with the GCM-models. Increased snow accumulation at Mt. Logan is associated with an enhanced trough-ridge system over the northeast Pacific; consistent with increased southerly flow that supplies warm moist air to the coastal region (Rupper et al., 2004). Although these studies agree that strong, eastward ALs bring more moisture to the coastal region, they differ in their interpretation of the isotopic record. However, a comparison of 20th century Mt. Logan accumulation values with major Pacific climate modes (e.g. Pacific Decadal Oscillation) indicates a complex relationship that varies temporally (Moore et al., 2002), reinforcing the dynamic relationship between North Pacific climate and the characteristics of Mt. Logan ice. In addition, Mt. Logan is on the windward side of the Coastal Mountain Range, in contrast to both Jellybean Lake and Spirit Lake located in the interior on the leeward side of the rain shadow of these mountains. Preliminary data from an inland site in Alaska (King Salmon; 58°41'21"N, 156°39'37"W) correlates $\delta^{18}O_{precipitation}$ values with specific storm events indicates Pacific-sourced moisture had values around $-7‰_{VSMOW}$ compared with $-18‰_{VSMOW}$ for more continental-sourced moisture (Wang and Wooller, 2008). Therefore, moisture sourced from more continental air masses would have lower $\delta^{18}O$ values indicating the continentality of moisture will also play an important role in the $\delta^{18}O_{lakewater}$ at Spirit Lake. In summary, $\delta^{18}O_{carb}$ values at Spirit Lake will reflect a combination of geographical effects based on the continentality of the study site, and changes in the seasonality of precipitation and evaporation rates (effective moisture), apparent from the assessment of modern climatological conditions.

2.5.2 Modern Seasonality of Precipitation

The modern seasonal distribution of precipitation is skewed towards the summer months (Fig. 2.2), an average of 17% of total annual precipitation falling from January to April at Whitehorse. However, the spring freshet associated with the melting of snow accumulated over the winter months must also be considered as a source of lake water, along with the dominant summer precipitation. Evaporative effects are limited to summer months (due to winter ice cover) therefore, changes in summer precipitation-evaporation patterns should exhibit significant effects on lakewater $\delta^{18}O_{lakewater}$ values and hence $\delta^{18}O_{carb}$ values through the Holocene. Using historical

monthly precipitation totals from Whitehorse (http://climate.weather.gc.ca/) from 1942-1994 (a period without data gaps) we have calculated monthly average values and then subtracted this from the record to create a precipitation anomaly series (Fig. 2.6). The precipitation anomaly series shows that extreme precipitation events at Whitehorse occur predominantly during summer months (June to September) with only one smaller event occurring in March. This suggests that the largest deviations in precipitation amounts falling at Whitehorse are related to variations in summertime atmospheric conditions. It is important to note here that coastal regions (i.e. 200 km west of Spirit Lake) exhibit a strikingly different situation with strong relationships to wintertime conditions. Comparison of modern stream flow with atmospheric circulation patterns reveals a strong influence of topography at coastal versus interior sites (Cayan and Peterson, 1989). Indeed, physiographic boundaries such as mountains and coastlines can have a dramatic effect on local climate conditions leading to inverse responses compared with adjacent areas (Mock et al., 1998). Similarly, in Alaska coastal sites are heavily influenced by winter patterns including the AL pressure system whereas interior sites exhibit a positive relationship between stream flow and remote high-pressure systems in the central North Pacific (Cayan and Peterson, 1989), signifying the importance of the summertime high-pressure atmospheric conditions in the North Pacific on precipitation trends at interior sites.

2.5.3 The Younger Dryas and Transition into the Holocene at Spirit Lake

The $\delta^{18}O_{carb}$ record for Spirit Lake (Fig. 2.7A) exhibits a large decrease in $\delta^{18}O_{carb}$ values from 12,000 years BP to 11,500 years BP. This is contemporaneous with the end of the Younger-Dryas and is marked here by a decrease in the mean $\delta^{18}O_{carb}$ value from $-13.9‰_{VPDB}$ in the Younger Dryas (Y-D) to $-15.7‰_{VPDB}$ in the Holocene. $\delta^{18}O_{carb}$ values from before 12,000 years BP have a larger range and kurtosis (5.4‰; 1.98) compared with the Holocene (2.4‰; 0.39), suggesting more dynamic environmental variability in the lake's pre-Holocene history.

The large shift in $\delta^{18}O_{carb}$ values at Spirit Lake related to the transition from the Y-D into the Early Holocene is broadly synchronous with several other regional and global climate records of End-Y-D climatic effects. Regionally, the –1.8‰ shift in $\delta^{18}O_{carb}$ values at Spirit Lake is associated with: –4.5‰ shift in $\delta^{18}O_{carb}$ of molluscs in a southeastern Alaskan lake (Fig. 2.7E) (Yu et al., 2008); cool and dry conditions in southern Alaska (Edwards et al., 2001; Kokorowski et al., 2008; Kaufman et al., 2010); a positive shift in $\delta^{18}O_{ice}$ values in ice cores from Mt. Logan

in the St. Elias Mountains (Fig 2.7H) (Fisher et al., 2008), and increases in North Pacific SSTs off Vancouver Island (Fig 2.7D) (Kienast and McKay, 2001) and northern California (Fig. 2.7C; Barron et al., 2003) indicating that the influence of the end of the Y-D was widespread along the western margin of North America.

The post-Younger Dryas decrease in Spirit Lake $\delta^{18}O_{carb}$ values is somewhat coincident with a –4.5‰ shift in the $\delta^{18}O_{carb}$ values of molluscs at Hundred Mile Lake (Yu et al., 2008). Hundred Mile Lake and Spirit Lake share similar climatological settings, within the rain shadow of coastal mountains. The –4.5‰ shift in $\delta^{18}O_{carb}$ values of molluscs between 11,000 and 10,300 years BP is slightly younger and larger than that of Spirit Lake, but Hundred Mile Lake is roughly a quarter the size of Spirit Lake, perhaps resulting in greater sensitivity to climatic change. The difference in the timing of the Y-D at these two locales could be related to variability in the reservoir correction used in the derivation of age models. Yu et al. (2008) used biogenic carbonates to derive an age model that included a constant reservoir correction, however based on the large temporal variability in the reservoir correction observed at Spirit Lake (7,730 to 2,130 years BP) it's possible that similar variability exists at Hundred Mile Lake, and that the –4.5‰ shift is in fact concurrent with the end of the Y-D. Yu et al. (2008) suggest that a change in atmospheric circulation patterns is likely responsible for a shift in moisture sources, leading to this large change in lake $\delta^{18}O$ values. Specifically, a change in the seasonality and source of moisture with increases in continental precipitation with lower $\delta^{18}O_{H2O}$ values, however, the mechanism forcing these changes remains unknown. Cooling along with a drop in lake levels coincident with the Younger Dryas has been previously reported from many lakes in southern Alaska (Edwards et al., 2001; Kokorowski et al., 2008). However, spatial (Kokorowski et al., 2008) and temporal (Kaufman et al., 2010) variability in the overall effects exist within the region, reflecting the heterogeneity of regional physiography.

$\delta^{18}O_{ice}$ values from nearby Mt. Logan display a concurrent shift towards higher values at the end of the Y-D (Fisher et al., 2008), though with a more gradual rise to the Holocene Maximum and extremely large variability in comparison to the Greenland ice cores. The $\delta^{18}O_{ice}$ record from Mt. Logan is thought to be source-related rather than a function of air temperature, as observed in Greenland (Fisher et al., 2004). Therefore, the interpretation of the Mt. Logan $\delta^{18}O_{ice}$ record is complicated by a combination of moisture source effects and temperature, possibly explaining the large perturbations in the Mt. Logan record during the Holocene.

The two North Pacific SST records (Kienast and McKay, 2001; Barron et al., 2003) display sharp departures from cooler Y-D temperatures to warmer Holocene SSTs, increasing 6 °C (Fig. 2.7). This shift to warmer Holocene SSTs occurs slightly after the shift at Spirit Lake and other atmospheric sensitive proxy records (e.g. NGRIP, GISP2, Hulu Cave), however this could be related to the lower sample resolution of these records relative to the Spirit Lake record. Paleoceanographic proxy evidence from coastal Gulf of Alaska indicates that sea-ice disappeared (Barron et al., 2009), and productivity increased around 11,700 years BP (Addision et al., 2012), coincident with the end of the Y-D at Spirit Lake. The inverse relationship between SSTs and $\delta^{18}O_{carb}$ values at Spirit Lake suggests that when sea surface temperatures increase, $\delta^{18}O_{carb}$ values decrease. This likely arises as the result of higher SSTs enhancing marine evaporation leading to increased moisture advection to the Spirit Lake region. The resulting precipitation would increase effective moisture, reducing the effects of lake evaporation, and lowering the $\delta^{18}O_{lakewater}$ value. During periods with decreased SSTs, less moisture is transported to Spirit Lake and evaporation becomes more important, resulting in elevated $\delta^{18}O_{lakewater}$ values. Therefore, cooler (warmer) periods are dryer (wetter), and are reflected by higher (lower) $\delta^{18}O_{carb}$ values at Spirit Lake. This relationship implies an intimate link between northeastern Pacific SSTs and terrestrial atmospheric conditions, despite the potential effects of the Coast Mountain rain shadow on Spirit Lake. This effect is predominantly evident during larger changes in SSTs like at the end of the Y-D, and would be less detectible during the Holocene when changes in moisture sources may overshadow SST-related variability.

2.5.4 Climatological Mechanisms for the Transition

The large shift in the $\delta^{18}O_{carb}$ record from Spirit Lake at the transition from the Y-D to the Holocene is broadly synchronous with many other Y-D records across the globe. Greenland ice core $\delta^{18}O_{ice}$ values (Grootes et al., 1993; NGRIP Members, 2004); Hulu Cave speleothem $\delta^{18}O_{carb}$ values (Wang et al., 2001); and Caribbean SSTs (Lea et al., 2003) represent a small selection of the global set of Y-D-related climate records (Fig. 2.8). The synchronicity in the timing of this transition across the Northern Hemisphere illustrates the global extent of this transition, implicating atmospheric teleconnections. More specifically the $\delta^{18}O_{carb}$ record from Spirit Lake indicates that the North Pacific region underwent significant climatic changes in parallel with many other regions.

In order to invoke a mechanism behind the transition in $\delta^{18}O_{carb}$ values at Spirit Lake, climate models must be evaluated and compared with climate proxy evidence. Modelling suggests that during the LGM an anticyclonic high-pressure cell developed over the Laurentide Ice Sheet that: (a) invigorated the Aleutian Low, increasing its size; and (b) decreased the summer pressure gradient between continental North America and the North Pacific that decreased meridional winds (COHMAP, 1988; Bartlein et al., 1998). Reduced onshore summertime winds would have decreased the amount and distance that maritime moisture would have penetrated into continental North America, resulting in drier summers at Spirit Lake. Sabin and Pisias (1996) use radiolarian based temperature reconstructions to suggest that during the Glacial Period, the North Pacific High was displaced further south such that the AL dominated North Pacific wind patterns. The jet stream and ITCZ were also pushed further south during the Y-D (e.g. Feng et al., 2007; Asmerom et al., 2010; Pak et al., 2012), forcing storm tracks southward and increasing precipitation in the American southwest (Asmerom et al., 2010), which may have been partially the result of the anticyclonic high-pressure cell.

As the ice sheet melted, the Glacial anticyclone high-pressure cell collapsed, diminishing the pressure gradient between the AL and the interior, resulting in a reduction in the size of the AL. This generated the opposite effect on the North Pacific High as the loss of this continental high-pressure cell increased the pressure gradient between the NPH and the continent, invigorating the North Pacific High (COHMAP, 1988). Pacific storm tracks, the ITCZ, and subtropical Pacific waters then began to migrate northward, as recorded by aridification of the American southwest (Polyak et al., 2004; Asmerom et al., 2010), increased North Pacific SSTs (Kienast and McKay, 2001; Barron et al., 2003) and increased Caribbean SSTs (Lea et al., 2003). The invigorated North Pacific High increased summer precipitation at Spirit Lake changing the mean climate from cold, dry evaporation-dominated conditions during the Y-D to relatively warmer and moister conditions post-Y-D reflected by decreasing $\delta^{18}O_{carb}$ values at Spirit Lake. Rising SSTs lead to increasing $\delta^{18}O_{ice}$ values at Mt. Logan, whereas decreased evaporation and wetter conditions at Spirit Lake resulted in decreased $\delta^{18}O_{carb}$ values.

Steffensen et al. (2008) postulate that at the end of the Y-D increasing temperatures in the Southern Hemisphere led to a northern migration of the ITCZ, illustrated by increasing SSTs in the Cariaco Basin (Lea et al., 2003), followed by an intensification of the Pacific Monsoon, exemplified by a synchronous decrease in Chinese speleothem $\delta^{18}O_{carb}$ values at Hulu Cave

(Wang et al., 2001) (Fig. 2.8). This increased moisture reduced atmospheric dust concentrations in the high-resolution NGRIP dust and Ca concentration records (Steffensen et al., 2008). This suggests that atmospheric reorganization could have begun in the low latitudes and migrated northward, forcing abrupt atmospheric change that is recorded in northern latitude atmospheric proxies.

Hendy and Kennett (1999) used coupled foraminiferal records from the North Pacific to postulate that climate change during Dansgaard-Oeschger cycles is transferred through atmospheric change. Amplified responses in $\delta^{18}O$ values of surface species compared with thermocline species, suggest that atmospheric reorganization was responsible for transmitting global climate signals in the ocean, and the synchronicity of marine and atmospheric records provides evidence of a strong atmospheric-oceanic coupling (Hendy and Kennett, 1999). This may explain the slight lag in SST rise in the North Pacific compared with atmospheric-sensitive proxies (Fig 2.8: Spirit Lake, NGRIP, GISP2 CH_4). Even under modern conditions changes in atmospheric circulation precede changes in ocean conditions in the North Pacific by about 2-3 months (Trenberth and Hurrell, 1994).

We postulate that the collapse of the Glacial anticyclone and the subsequent removal of a North American continental blocking center greatly affected Northern Hemisphere atmospheric circulation patterns causing a reorganization of North Pacific atmospheric circulation patterns. A major change in the seasonality of precipitation is the result of an increase in summer precipitation to the interior of the Yukon, which locally decreased evaporation and lowered $\delta^{18}O_{carb}$ values at Spirit Lake. These changes in atmospheric circulation patterns lead to changes in ocean wind-drift surface currents that are reflected by increasing SSTs following the atmospheric reorganization to its Holocene state.

2.5.5 The Holocene $\delta^{18}O_{carb}$ Record

The Early Holocene is typified by significantly lower $\delta^{18}O_{carb}$ values than the earlier Younger Dryas, including the lowest $\delta^{18}O_{carb}$ values of the Holocene. Total $\delta^{18}O_{carb}$ variability during the Holocene is ~2.5‰, comparable to that observed at Jellybean Lake (Fig. 2.9; Anderson et al., 2005c). $\delta^{18}O_{carb}$ values through the Holocene reflect effective moisture at Spirit Lake related to precipitation:evaporation with warmer and/or drier conditions conducive to enhanced evaporation resulting in higher $\delta^{18}O_{carb}$ values. The beginning of the Holocene in the southwest

Yukon was warmer than mean conditions during the last Glacial Period as evidenced from local glaciology (Bond, 2004) and pollen (Cwynar, 1988), North Pacific SSTs (Kienast and McKay, 2001; Barron et al., 2003), and manifested as lower Spirit Lake $\delta^{18}O_{carb}$ values immediately following the Deglacial. During the beginning of the Holocene, Spirit Lake $\delta^{18}O_{carb}$ values increase from 11,500 to 9,000 years BP (Fig. 2.9) suggesting drier conditions, consistent with increased aridity at Marcella Lake (Anderson et al., 2005b); and cooler and drier conditions at Upper Fly Lake in the southwest Yukon (Bunbury and Gajewski, 2009).

Following 9,000 years BP, Spirit Lake $\delta^{18}O_{carb}$ decrease until ~8,000 years BP when they level off until reaching their Holocene minimum at ~6,250 years. The timing of the Holocene Thermal Maximum (HTM) varied significantly in the western Arctic occurring from about 10,000 years BP to 7,000 years BP in the Spirit Lake region (Kaufman et al., 2004) coincident with maximum solar insolation values (Fig. 2.7A; Laskar, 2004), and reduced glacial activity (Denton and Stuiver, 1966; 1967). A trend towards higher $\delta^{18}O_{carb}$ values around 9,000 years BP suggests decreased effective moisture in the region the result of warm, dry conditions. Sand dunes at Carcross, just south of Spirit Lake, were active during the beginning of the HTM (~10ka) further suggesting dry conditions, until dune stabilization occurred at ~9,000 years BP, suggesting that effective moisture increased after ~9,000 years BP in concert with the establishment of regional boreal forests in the region (Wolfe et al., 2011), a hypothesis supported by local pollen (Cwynar, 1988) and lake level records from Marcella Lake (Anderson et al., 2005b). After 9,000 years BP $\delta^{18}O_{carb}$ values decrease as effective moisture in the region increases until conditions stabilize at ~8,000 years BP (See 1 in Fig. 2.9).

The Mid-Holocene is characterized by stabilization of regional climate and environmental conditions as it is during this time (~8,000 years BP) that local eustatic sea level stabilized (Mann and Streveler, 2008); and $\delta^{18}O_{carb}$ values from Spirit Lake reach their Holocene average, –15.7‰ (~5,500 years BP, see 2 in Fig. 2.9). $\delta^{18}O_{carb}$ values from Spirit Lake reflect an increase in effective moisture compared to the Early Holocene maximum (Fig. 2.9) indicating relatively moist conditions compared to the Early Holocene. Vegetation records from northern British Columbia also suggest that wetter conditions prevailed from 7,000-4,000 years BP (Hebda, 1995)

Ice patches (alpine ice accumulations with insufficient mass to flow like glaciers) near Spirit Lake renew growth from 5,500-3,840 yr BP (Farnell et al., 2004), perhaps related to the increase

in effective moisture to the region as suggested by decreased in $\delta^{18}O_{carb}$ values from 4,500 to 3,800 years BP (Fig. 2.9). Neoglaciation began in Alaska at 4,400 years BP (Ellis and Calkin, 1984) and radiolarian based SST reconstructions show North Pacific cooling occurred from 5,500-3,000 years BP (Sabin and Pisias, 1996), suggesting a period of regional cooling.

At ~3,750-2,500 years BP there is a steady increase in average $\delta^{18}O_{carb}$ values at Spirit Lake (see 3 to 4 in Fig. 2.9), concurrent with increased $\delta^{18}O_{carb}$ values at Jellybean Lake (Fig. 2.9, Anderson et al., 2005b), suggesting a return to drier conditions on the central Pacific Northwest coast. After ~1,000 years BP, the accuracy of the age model decreases due to sediment loss in the top core section. Unfortunately, accurate evaluation of the expression of the Little Ice Age cannot be determined due to poor temporal resolution near the top of our core. Overall, Late Holocene climate is characterized by minor fluctuations in effective moisture in the Spirit Lake region.

2.6 Conclusions

Spirit Lake $\delta^{18}O_{carb}$ data represents the longest continuous lake carbonate record from the southwest Yukon Territory. Core chronology extends back to the Pleistocene-Holocene transition documenting the climate history of southwestern Yukon Territory. Sedimentology indicates two major periods of deposition: rapidly deposited glacio-lacustrine silts and clays, shifting to post-glacial authigenic carbonate production at ~11,500 years BP. Core stratigraphy and $\delta^{18}O_{carb}$ values indicate that the draining of glacial Lake Watson occurred ~11,550 years BP, helping to better elucidate the poorly understood chronology of Deglacial events in the southwest Yukon.

$\delta^{18}O_{lakewater}$ values are controlled by a combination of evaporation and seasonality of precipitation. Therefore, the $\delta^{18}O_{carb}$ record from Spirit Lake provides a proxy for local effective moisture. Modern precipitation in the region is higher in the summer months, observed in both regional stream flow (Cayan and Peterson, 1989) and meteorological data. This indicates that variability in summer precipitation regimes will have a significant effect on $\delta^{18}O_{lakewater}$ values.

The long-term $\delta^{18}O_{carb}$ record from Spirit Lake exhibits an abrupt transition in climate and limnological conditions during the end of the Y-D that is coincident with other paleoclimate records from the region and globally. This likely represents significant changes in atmospheric circulation patterns following the reduction of ice sheets on North America, and subsequent

alterations to the interactions between continental and marine weather patterns. Spirit Lake $\delta^{18}O_{carb}$ values decrease during the transition into the Holocene, suggesting an increase in effective moisture to the region. It is postulated that this increase in effective moisture is related to increased penetration of maritime moisture, caused by an intensification and northern migration of the North Pacific High following the collapse of the glacial anticyclone associated with the shrinking Laurentian Ice Sheet. Concurrent increases in SSTs and the northern migration of the ITCZ, jet stream, and Pacific storm tracks leads to contemporaneous shifts in climate throughout the Northern Hemisphere, suggesting major atmospheric reorganization.

The Holocene $\delta^{18}O_{carb}$ record is significantly less variable than during the Late Pleistocene. The HTM is exemplified by the highest Spirit Lake $\delta^{18}O_{carb}$ values concurrent with other regional evidence for warm conditions. Modern-like conditions at Spirit Lake are reached ~5,500 years BP similar to other regional evidence. Unfortunately, during the vibra-coring process sediment representing the Late Holocene including the Little Ice Age was disturbed, preventing evaluation of this period in the Spirit Lake record.

The long, continuous lake sediment archive from Spirit Lake provides a unique view into regional paleoclimatology and specifically effective moisture in the southwest Yukon Territory. Interpretation of the Spirit Lake record confirms that the intensity and position of North Pacific pressure centers are important in controlling moisture to the region, however, NE Pacific sea surface temperatures also play an important role in moisture advection to coastal areas.

2.7 Relationship with Overarching Theme of Thesis

The oxygen-isotope record from Spirit Lake illustrates how authigenic lake carbonate records long-term changes in North Pacific atmospheric pressure systems combined with Pacific SST variability through the Holocene. By using a sub-centennial sampling resolution paleoclimatic information pertaining to the strength and position of both the Aleutian low and North Pacific High pressure systems can be resolved from the broader, long-term changes in Pacific SST. This information coupled with modern isotope hydrology provides a quantitative approach to assessing moisture source regions and provides insight into changes in atmospheric circulation patterns through the Holocene.

Although the sub-centennial sampling resolution employed in this study is useful for assessing long term changes in atmospheric circulation patterns it cannot resolve higher

frequency climate oscillations such as the Pacific Decadal Oscillation (PDO) or El Niño Southern Oscillation (ENSO). In the next chapter, authigenic lake carbonates are sampled at sub-decadal resolution allowing for important climate information associated with PDO and ENSO variability through the Holocene to be resolved.

2.8 Acknowledgements

D. Besic and M. Mamchur provided field and lab assistance, A. Bangsund for lab assistance, and the Geology 498 paleoclimate class for their assistance in sample processing. G. Lowey of the Yukon Geological Survey is thanked for providing a hand specimen of the Hancock Fm. for isotopic analysis. NSERC DGS grant to A.W. Kingston, and NSERC Discovery grant to W.P. Patterson helped fund this research.

2.9 References

Addison, J. A., Finney, B. P., Dean, W. E., Davies, M. H., Mix, A. C., Stoner, J. S., & Jaeger, J. M. (2012). Productivity and sedimentary $\delta^{15}N$ variability for the last 17,000 years along the northern Gulf of Alaska continental slope. Paleoceanography, 27(1) PA1206.

Anderson, L. (2005). Holocene climate of the southwest Yukon Territory, Canada, inferred from lake-level and isotope analyses of small carbonate lakes. Ph.D. dissertation, University of Massachusetts Amherst. pp. 171.

Anderson, L., Abbott, M. B., Finney, B. P., & Edwards, M. E. (2005). Palaeohydrology of the Southwest Yukon Territory, Canada, based on multiproxy analyses of lake sediment cores from a depth transect. The Holocene, 15(8), 1172-1183.

Anderson, L., Abbott, M. B., Finney, B. P., & Burns, S. J. (2005). Regional atmospheric circulation change in the North Pacific during the Holocene inferred from lacustrine carbonate oxygen isotopes, Yukon Territory, Canada. Quaternary Research, 64(1), 21-35.

Anderson, L., Abbott, M. B., Finney, B. P., & Burns, S. J. (2007). Late Holocene moisture balance variability in the southwest Yukon Territory, Canada. Quaternary Science Reviews, 26(1), 130-141.

Anderson, L., Berkelhammer, M., Barron, J. A., Steinman, B. A., Finney, B. P., & Abbott, M. B. (2016). Lake oxygen isotopes as recorders of North American Rocky Mountain hydroclimate:

Holocene patterns and variability at multi-decadal to millennial time scales. Global and Planetary Change, 137, 131-148.

Asmerom, Y., Polyak, V. J., & Burns, S. J. (2010). Variable winter moisture in the southwestern United States linked to rapid glacial climate shifts. Nature Geoscience, 3(2), 114-117.

Barron, J. A., Heusser, L., Herbert, T., & Lyle, M. (2003). High-resolution climatic evolution of coastal northern California during the past 16,000 years. Paleoceanography, 18(1). 1020.

Barron, J. A., Bukry, D., Dean, W. E., Addison, J. A., & Finney, B. (2009). Paleoceanography of the Gulf of Alaska during the past 15,000 years: results from diatoms, silicoflagellates, and geochemistry. Marine Micropaleontology, 72(3), 176-195.

Bartlein, P. J., Anderson, K. H., Anderson, P. M., Edwards, M. E., Mock, C. J., Thompson, R. S., Webb, R.S., Webb III, T. & Whitlock, C. (1998). Paleoclimate simulations for North America over the past 21,000 years: features of the simulated climate and comparisons with paleoenvironmental data. Quaternary Science Reviews, 17(6), 549-585.

Bond, J.D., (2004). Late Wisconsinan McConnell glaciation of the Whitehorse map area (105D), Yukon. In: Yukon Exploration and Geology 2003, D.S. Emond and L.L. Lewis (eds), Yukon Geological Survey, 73–88.

Brook, E. J., Harder, S., Severinghaus, J., Steig, E. J., & Sucher, C. M. (2000). On the origin and timing of rapid changes in atmospheric methane during the last glacial period. Global Biogeochemical Cycles, 14(2), 559-572.

Bunbury, J., & Gajewski, K. (2009). Postglacial climates inferred from a lake at treeline, southwest Yukon Territory, Canada. Quaternary Science Reviews, 28(3), 354-369.

Cayan, D. R., & Peterson, D. H. (1989). The influence of North Pacific atmospheric circulation on streamflow in the west. Geophysical Monograph, 55, 375-397.

Clegg, B. F., Clarke, G. H., Chipman, M. L., Chou, M., Walker, I. R., Tinner, W., & Hu, F. S. (2010). Six millennia of summer temperature variation based on midge analysis of lake sediments from Alaska. Quaternary Science Reviews, 29(23), 3308-3316.

Clegg, B. F., & Hu, F. S. (2010). An oxygen-isotope record of Holocene climate change in the south-central Brooks Range, Alaska. Quaternary Science Reviews, 29(7), 928-939.

COHMAP Members, (1988). Climatic changes of the last 18,000 years: Observations and model simulations. Science 241, 1043–1052.

Coplen, T. B., Kendall, C., & Hopple, J. (1983). Comparison of stable isotope reference samples.

Cwynar, L. C. (1988). Late Quaternary vegetation history of Kettlehole Pond, southwestern Yukon. Canadian Journal of Forest Research, 18(10), 1270-1279.

Dansgaard, W. (1964). Stable isotopes in precipitation. Tellus 16, 436–468.

Deevey Jr, E. S., Gross, M. S., Hutchinson, G. E., & Kraybill, H. L. (1954). The natural C14 contents of materials from hard-water lakes. Proceedings of the National Academy of Sciences of the United States of America, 40(5), 285.

Denton, G. H., & Stuiver, M. (1966). Neoglacial chronology, northeastern Saint Elias Mountains, Canada. American Journal of Science, 264(8), 577-599.

Denton, G. H., & Stuiver, M. (1967). Late Pleistocene Glacial Stratigraphy and Chronology, Northeastern St Elias Mountains, Yukon Territory, Canada. Geological Society of America Bulletin, 78(4), 485-510.

Drummond, C. N., Patterson, W. P., & Walker, J. C. (1995). Climatic forcing of carbon-oxygen isotopic covariance in temperate-region marl lakes. Geology, 23(11), 1031-1034.

Edwards, M. E., Mock, C. J., Finney, B. P., Barber, V. A., & Bartlein, P. J. (2001). Potential analogues for paleoclimatic variations in eastern interior Alaska during the past 14,000 yr: atmospheric-circulation controls of regional temperature and moisture responses. Quaternary Science Reviews, 20(1), 189-202.

Ellis, J. M., & Calkin, P. E. (1984). Chronology of Holocene glaciation, central Brooks Range, Alaska. Geological Society of America Bulletin, 95(8), 897-912.

Environment Canada (2013). Climate Data from 1971-2000 Canadian Climate Normals taken from Whitehorse weather station 60°42'34"; 135°04'07"; elevation: 706m. REF: Environment Canada, 2013 http://climate.weatheroffice.gc.ca/climate_normals.

Farnell, R., Hare, P. G., Blake, E., Bowyer, V., Schweger, C., Greer, S., & Gotthardt, R. (2004). Multidisciplinary investigations of alpine ice patches in southwest Yukon, Canada: Paleoenvironmental and paleobiological investigations. Arctic, 247-259.

Feng, X., Reddington, A. L., Faiia, A. M., Posmentier, E. S., Shu, Y., & Xu, X. (2007). The changes in North American atmospheric circulation patterns indicated by wood cellulose. Geology, 35(2), 163-166.

Field, R. D., Moore, G. W. K., Holdsworth, G., & Schmidt, G. A. (2010). A GCM‐based analysis of circulation controls on $\delta^{18}O$ in the southwest Yukon, Canada: Implications for climate reconstructions in the region. Geophysical Research Letters, 37(5). L05706.

Fisher, D.A., Wake, C., Kreutz, K., Yalcin, K., Steig, E., Mayewski, P., Anderson, L., Zheng, J., Rupper, S., Zdanowicz, C., Demuth, M., Waszkiewicz, M., Dahl-Jensen, D., Goto-Azuma, K., Bourgeois, J.B., Koerner, R.M., Sekerka, J., Osterberg, E., Abbott, M.B., Finney, B.P., & Burns, S.J. (2004). Stable isotope records from Mount Logan, Eclipse ice cores and nearby Jellybean Lake. Water cycle of the North Pacific over 2000 years and over five vertical kilometers: Sudden shifts and tropical connections. Géographie Physique et Quaternaire 58, 337–352.

Fisher, D., Osterberg, E., Dyke, A., Dahl-Jensen, D., Demuth, M., Zdanowicz, C., Bourgeois, J., Koerner, R.M., Mayewski, P., Wake, C., Kreutz, K., Steig, E., Zheng, J., Yalcin, K., Goto-Azuma, K., Luckman, B., & Rupper, S. (2008). The Mt. Logan Holocene-late Wisconsinan isotope record: tropical Pacific-Yukon connections. The Holocene 18, 667–677.

Grootes, P. M., Stuiver, M., White, J. W. C., Johnsen, S., & Jouzel, J. (1993). Comparison of oxygen isotope records from the GISP2 and GRIP Greenland ice cores. Nature, 366, 552-554.

Hebda, R. J. (1995). British Columbia vegetation and climate history with focus on 6 ka BP. Géographie Physique et Quaternaire, 49(1), 55-79.

Hendy, I. L., & Kennett, J. P. (1999). Latest Quaternary North Pacific surface-water responses imply atmosphere-driven climate instability. Geology, 27(4), 291-294.

Kaufman, D. S., Ager, T. A., Anderson, N. J., Anderson, P. M., Andrews, J. T., Bartlein, P. J., & Dyke, A. S. (2004). Holocene thermal maximum in the western Arctic (0–180 W). Quaternary Science Reviews, 23(5), 529-560.

Kaufman, D. S., Anderson, R. S., Hu, F. S., Berg, E., & Werner, A. (2010). Evidence for a variable and wet Younger Dryas in southern Alaska. Quaternary Science Reviews, 29(11), 1445-1452.

Kienast, S. S., & McKay, J. L. (2001). Sea surface temperatures in the subarctic northeast Pacific reflect millennial ‐ scale climate oscillations during the last 16 kyrs. Geophysical Research Letters, 28(8), 1563-1566.

Kim, S. T., & O'Neil, J. R. (1997). Equilibrium and nonequilibrium oxygen isotope effects in synthetic carbonates. Geochimica et Cosmochimica Acta, 61(16), 3461-3475.

Kokorowski, H. D., Anderson, P. M., Mock, C. J., & Lozhkin, A. V. (2008). A re-evaluation and spatial analysis of evidence for a Younger Dryas climatic reversal in Beringia. Quaternary Science Reviews, 27(17), 1710-1722.

Lamoureux, S. F., & Gilbert, R. (2004). Physical and chemical properties and proxies of high latitude lake sediments. In Long-term Environmental Change in Arctic and Antarctic Lakes (pp. 53-87). Springer Netherlands.

Laskar, J., Robutel, P., Joutel, F., Gastineau, M., Correia, A. C. M., & Levrard, B. (2004). A long-term numerical solution for the insolation quantities of the Earth. Astronomy & Astrophysics, 428(1), 261-285.

Lea, D. W., Pak, D. K., Peterson, L. C., & Hughen, K. A. (2003). Synchroneity of tropical and high-latitude Atlantic temperatures over the last glacial termination. Science, 301(5638), 1361-1364.

Leng, M. J., & Marshall, J. D. (2004). Palaeoclimate interpretation of stable isotope data from lake sediment archives. Quaternary Science Reviews, 23(7), 811-831.

Li, H.C., & Ku, T.L. (1997). $\delta^{13}C$-$\delta^{18}O$ covariance as a paleohydrological indicator for closed-basin lakes. Palaeogeography, Palaeoclimatology, Palaeoecology 133, 69–80.

MacDonald, G. M., Beukens, R. P., Kieser, W. E., & Vitt, D. H. (1987). Comparative radiocarbon dating of terrestrial plant macrofossils and aquatic moss from the "ice-free corridor" of western Canada. Geology, 15(9), 837-840.

Mantua, N. J., & Hare, S. R. (2002). The Pacific decadal oscillation. Journal of oceanography, 58(1), 35-44.

Menounos, B., Osborn, G., Clague, J. J., & Luckman, B. H. (2009). Latest Pleistocene and Holocene glacier fluctuations in western Canada. Quaternary Science Reviews, 28(21), 2049-2074.

Mock, C. J., Bartlein, P. J., & Anderson, P. M. (1998). Atmospheric circulation patterns and spatial climatic variations in Beringia. International Journal of Climatology, 18(10), 1085-1104.

Moore, G. W. K., Holdsworth, G., & Alverson, K. (2002). Climate change in the North Pacific region over the past three centuries. Nature, 420(6914), 401-403.

Mott, R. J. (1975). Palynological studies of lake sediment profiles from southwestern New Brunswick. Canadian Journal of Earth Sciences, 12(2), 273-288.

NGRIP Members (2004). High-resolution record of Northern Hemisphere climate extending into the last interglacial period. Nature 431, 147–151.

NOAA, NOWData NOAA Online Climate Data, Accessed 2013-10-04 http://www.nws.noaa.gov/climate/xmacis.php?wfo=pajk.

Overland, J. E., Adams, J. M., & Bond, N. A. (1999). Decadal variability of the Aleutian Low and its relation to high-latitude circulation*. Journal of Climate, 12(5), 1542-1548.

Pak, D. K., Lea, D. W., & Kennett, J. P. (2012). Millennial scale changes in sea surface temperature and ocean circulation in the northeast Pacific, 10–60 kyr BP. Paleoceanography, 27(1). PA1212.

Pisias, N. G., Mix, A. C., & Heusser, L. (2001). Millennial scale climate variability of the northeast Pacific Ocean and northwest North America based on radiolaria and pollen. Quaternary Science Reviews, 20(14), 1561-1576.

Polyak, V. J., Rasmussen, J. B., & Asmerom, Y. (2004). Prolonged wet period in the southwestern United States through the Younger Dryas. Geology, 32(1), 5-8.

Reimer, P.J., Baillie, M.G.L., Bard, E., Bayliss, A., Beck, J.W., Blackwell, P.G., Bronk Ramsey, C., Buck, C.E., Burr, G.S., Edwards, R.L., Friedrich, M., Grootes, P.M., Guilderson, T.P., Hajdas, I., Heaton, T.J., Hogg, A.G., Hughen, K.A., Kaiser, K.F., Kromer, B., McCormac, F.G., Manning, S.W., Reimer, R.W., Richards, D.A., Southon, J.R., Talamo, S., Turney, C.S.M., van der Plicht, J., & Weyhenmeyer, C.E. (2009). IntCal09 and Marine09 radiocarbon age calibration curves, 0-50,000 years cal BP. Radiocarbon, 51(4), 1111–1150.

Rodionov, S. N., Bond, N. A., & Overland, J. E. (2007). The Aleutian Low, storm tracks, and winter climate variability in the Bering Sea. Deep Sea Research Part II: Topical Studies in Oceanography, 54(23), 2560-2577.

Roots, E. F. (1989). Climate change: high-latitude regions. Climatic Change, 15(1-2), 223-253.

Rozanski, K., Araguás-Araguás, L., & Gonfiantini, R. (1992). Relation between long-term trends of oxygen-18 isotope composition of precipitation and climate. Science, 258(5084), 981-985.

Rupper, S., Steig, E. J., & Roe, G. (2004). The relationship between snow accumulation at Mt. Logan, Yukon, Canada, and climate variability in the North Pacific. Journal of Climate, 17(24), 4724-4739.

Sabin, A. L., & Pisias, N. G. (1996). Sea surface temperature changes in the northeastern Pacific Ocean during the past 20,000 years and their relationship to climate change in northwestern North America. Quaternary Research, 46(1), 48-61.

Sawada, K., & Handa, N. (1998). Variability of the path of the Kuroshio ocean current over the past 25,000 years. Nature, 392(6676), 592-595.

Spooner, I. S., Barnes, S., Baltzer, K. B., Raeside, R., Osborn, G. D., & Mazzucchi, D. (2003). The impact of air mass circulation dynamics on Late Holocene paleoclimate in northwestern North America. Quaternary International, 108(1), 77-83.

Stabeno, P. J., Bond, N. A., Hermann, A. J., Kachel, N. B., Mordy, C. W., & Overland, J. E. (2004). Meteorology and oceanography of the Northern Gulf of Alaska. Continental Shelf Research, 24(7), 859-897.

Steffensen, J.P., Andersen, K.K., Bigler, M., Clausen, H.B., Dahl-Jensen, D., Fischer, H., Goto-Azuma, K., Hansson, M., Johnsen, S.J., Jouzel, J., Masson-Delmotte, V., Popp, T., Rasmussen, S.O., Röthlisberger, R., Ruth, U., Stauffer, B., Siggaard-Andersen, M.L., Sveinbjörnsdóttir, Á.E., Svensson, A., & White, J.W.C. (2008). High-resolution Greenland ice core data show abrupt climate change happens in few years. Science, 321, p. 680–684.

Stuiver, M. (1968). Oxygen-18 content of atmospheric precipitation during last 11,000 years in the Great Lakes region. Science, 162(3857), 994-997.

Talbot, M. R. (1990). A review of the palaeohydrological interpretation of carbon and oxygen isotopic ratios in primary lacustrine carbonates. Chemical Geology: Isotope Geoscience Section, 80(4), 261-279.

Trenberth, K. E., & Hurrell, J. W. (1994). Decadal atmosphere-ocean variations in the Pacific. Climate Dynamics, 9(6), 303-319.

Walker, M.J.C., Berkelhammer, M., Björck, S., Cwynar, L.C., Fisher, D.A., Long, A.J., Lowe, J.J., Newnham, R.M., Rasmussen, S.O., & Weiss, H. (2012). Formal subdivision of the Holocene Series/Epoch: a Discussion Paper by a Working Group of INTIMATE (Integration of ice-core, marine and terrestrial records) and the Subcommission on Quaternary Stratigraphy (International Commission on Stratigraphy). Journal of Quaternary Science 27, 649–659.

Wang, X. C., & Geurts, M. A. (1991). Late Quaternary pollen records and vegetation history of the southwest Yukon Territory: A review. Géographie Physique et Quaternaire, 45(2), 175-193.

Wang, Y. J., Cheng, H., Edwards, R. L., An, Z. S., Wu, J. Y., Shen, C. C., & Dorale, J. A. (2001). A high-resolution absolute-dated late Pleistocene monsoon record from Hulu Cave, China. Science, 294(5550), 2345-2348.

Wang, Y., & Wooller, M.J. (2008). Report: Increasing coverage of Alaska within the global network of isotopes in precipitation. USGS State Water Resources Research Institute Program: Report as of FY2007 for 2007AK64B.

Wiles, G. C., Lawson, D. E., Lyon, E., Wiesenberg, N., & D'Arrigo, R. D. (2011). Tree-ring dates on two pre-Little Ice Age advances in Glacier Bay National Park and Preserve, Alaska, USA. Quaternary Research, 76(2), 190-195.

Wolfe, S., Bond, J., & Lamothe, M. (2011). Dune stabilization in central and southern Yukon in relation to early Holocene environmental change, northwestern North America. Quaternary Science Reviews, 30(3), 324-334.

Yu, Z., Walker, K. N., Evenson, E. B., & Hajdas, I. (2008). Lateglacial and early Holocene climate oscillations in the Matanuska Valley, south-central Alaska. Quaternary Science Reviews, 27(1), 148-161.

Table 2.1: Radiocarbon Dates

Sample ID	Lab ID	Core Depth (cm)	$\delta^{13}C$ (‰, VPDB)	Conventional Ages	Calibrated Ages	Reservoir Corrected Ages	Material
Sl-1	NZA-33609	14.2	-35.6	2363±25	2361	**919**	Carophyte
SL-20	*NZA-33939*	*22.5*	*-25.4*	*1349±25*	*1286*	***1286***	*Charcoal*
SL-2	NZA-33612	30.3	-34.8	3266±25	3490	**1858**	Carophyte
SLG-2	NZA-33667	30.4	-6.5	3281±45	3511	**1878**	Gastropod shell
SL-3	NZA-33610	49.3	-34.2	4033±25	4482	**2627**	Carophyte
SL-4	NZA-33611	95.4	-36.0	5557±30	6349	**3951**	Carophyte
SL-7	NZA-33607	165.5	-1.4	6855±30	7682	**4459**	Marl sediment
SL-13	NZA-33666	278	-9.7	8916±50	10039	**5493**	Gastropod shell
SL-15	NZA-33670	348	-8.8	10290±55	12078	**6708**	Gastropod shell
SL-16a	*NZA-33644*	*407.6*	*-23.4*	*8156±55*	*9105*	***9105***	*Several insect bodies (midges)*
SL-21	NZA-34001	503.8	-0.5	16020±70	19163	**11865**	Marl
SL-19	*NZA-33613*	*503.8*	*-27.2*	*9984±35*	*11433*	***11433***	*Wood*
SL-16	NZA 33643	275.5	-25.4	8308±60	12078	-	Plant material
SL-22	NZA 33998	22.5	-1.1	3202±35	3490	-	Marl sediment

Terrestrial dates *italicized,* rejected dates greyed

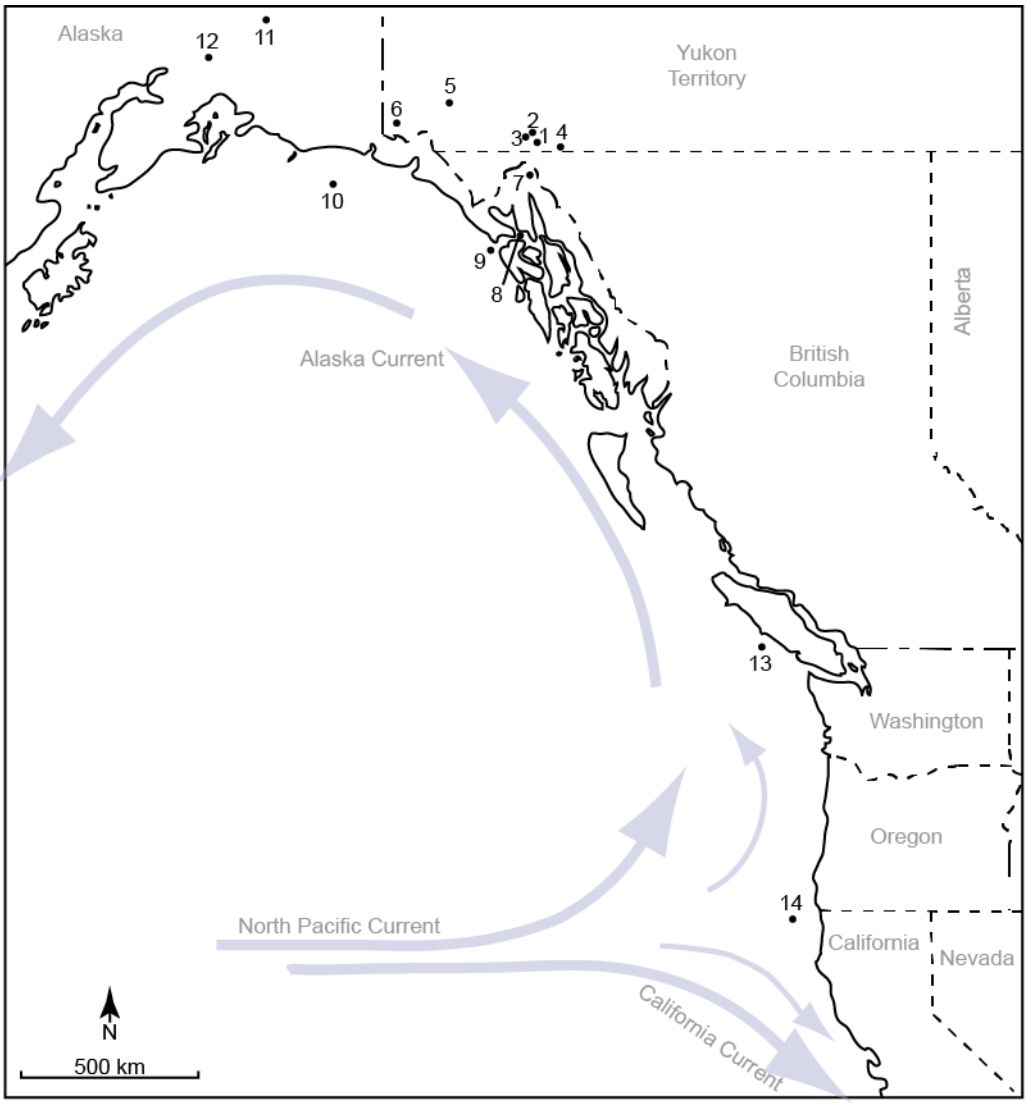

Figure 2.1: Map of study region including some of the locations discussed in the text. 1. Spirit Lake (this study) and Jellybean Lake (Anderson et al., 2005b); 2. Whitehorse; 3. Alpine ice patches (Farnell et al., 2004); 4. Marcella Lake (aka Kettlehole Pond, Cwynar, 1988; Anderson et al., 2005a); 5. Kluane Lake Research Station (Denton and Stuiver 1966, 1967; Gajewski et al., 2014); 6. Mt. Logan ice core (Fisher et al., 2004); 7. White Pass (Lamoureux and Cockburn, 2005); 8. Glacier Bay, Alaska (Mann and Streveler, 2008); 9. Yabobi Sea Valley marine core EW0408-66JC (Barron et al., 2009; Addison et al., 2012); 10. Kayak slope marine core EW0408-85JC (Barron et al., 2009; Addison et al., 2012); 11. Moose Lake (Clegg et al., 2010); 12. Hundred Mile Lake (Yu et al., 2008); 13. Marine core: JT96-09-pc (Kienast and McKay, 2001); 14. ODP Site 1019 (Barron et al., 2003).

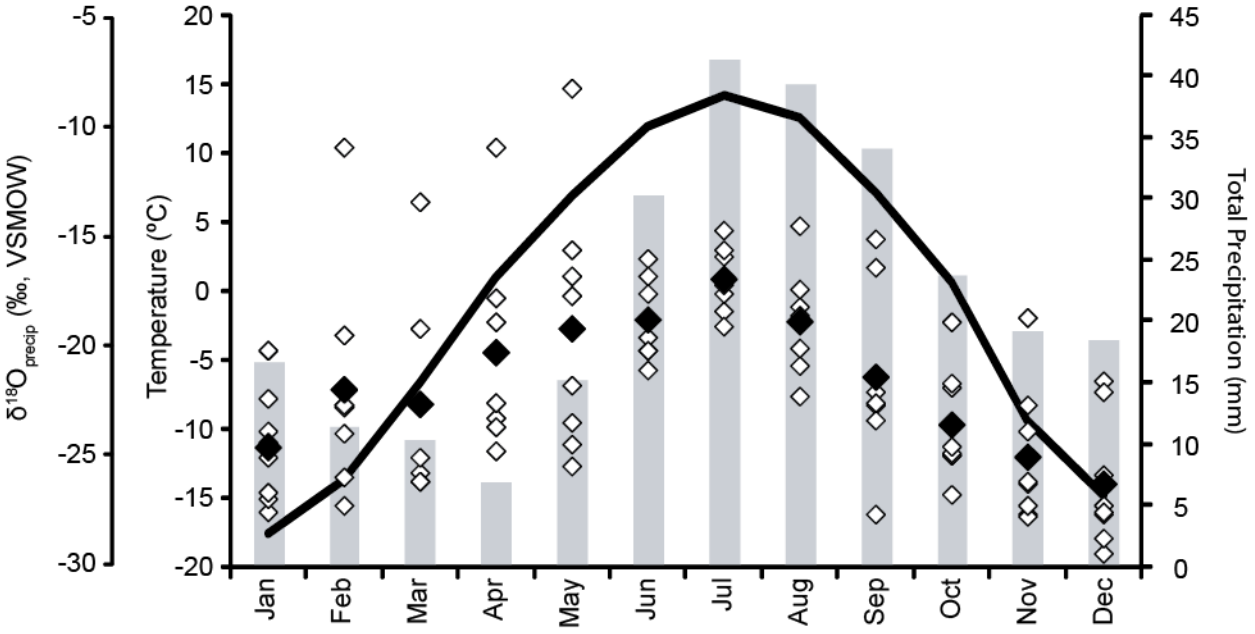

Figure 2.2: Average precipitation (grey bars) and temperature (blank line) at Whitehorse, Canada (Canada Climate Normals) plotted with average monthly $\delta^{18}O$precipitation values from each monitoring year (open diamonds) and average $\delta^{18}O$precipitation values of each month for all years (solid diamonds) from IAEA's Global Network of Isotopes in Precipitation (1965-1989).

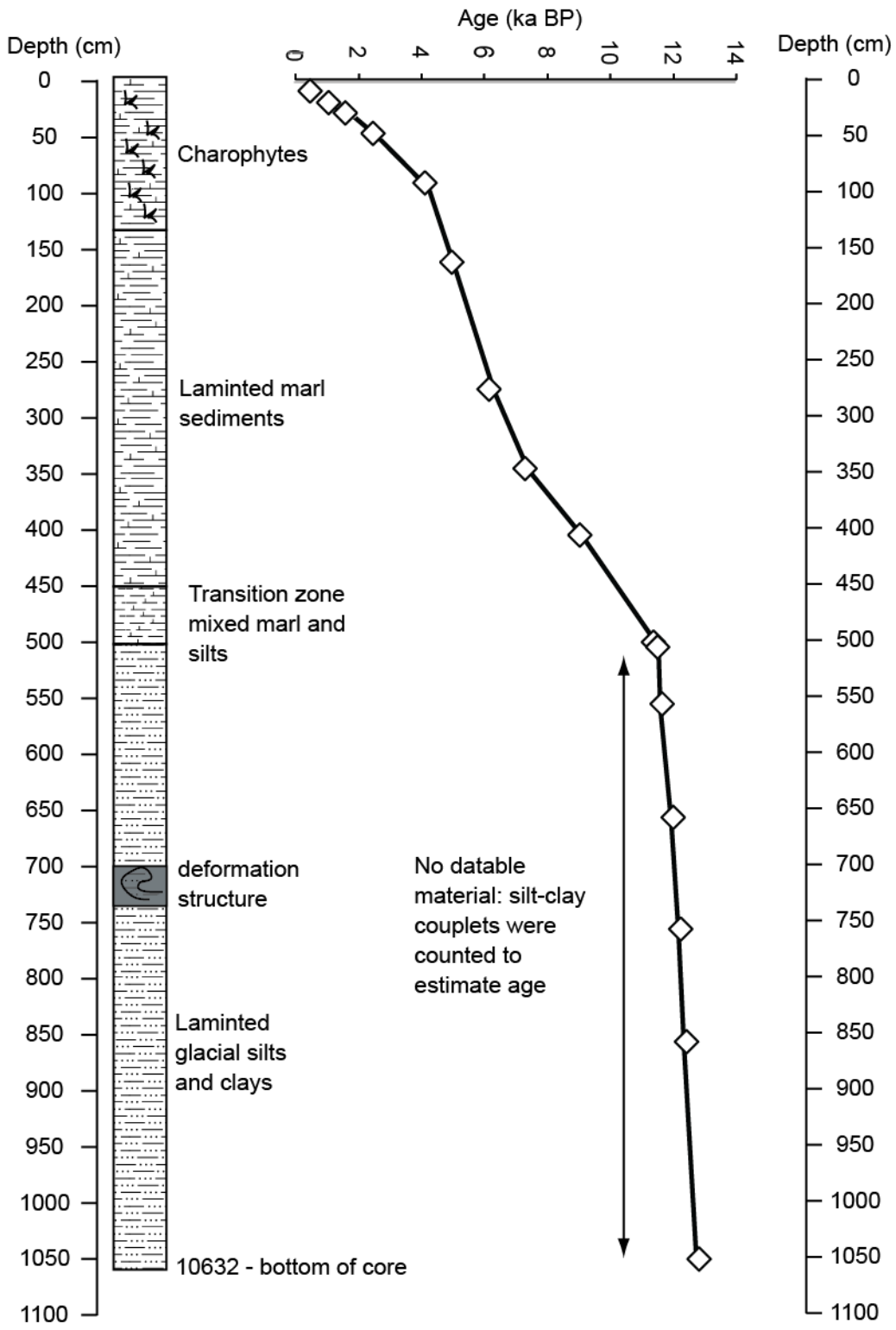

Figure 2.3: Age model and simplified stratigraphy of Spirit Lake core. Radiocarbon ages are calibrated using Calib 6.0 according to Reimer et al. (2009).

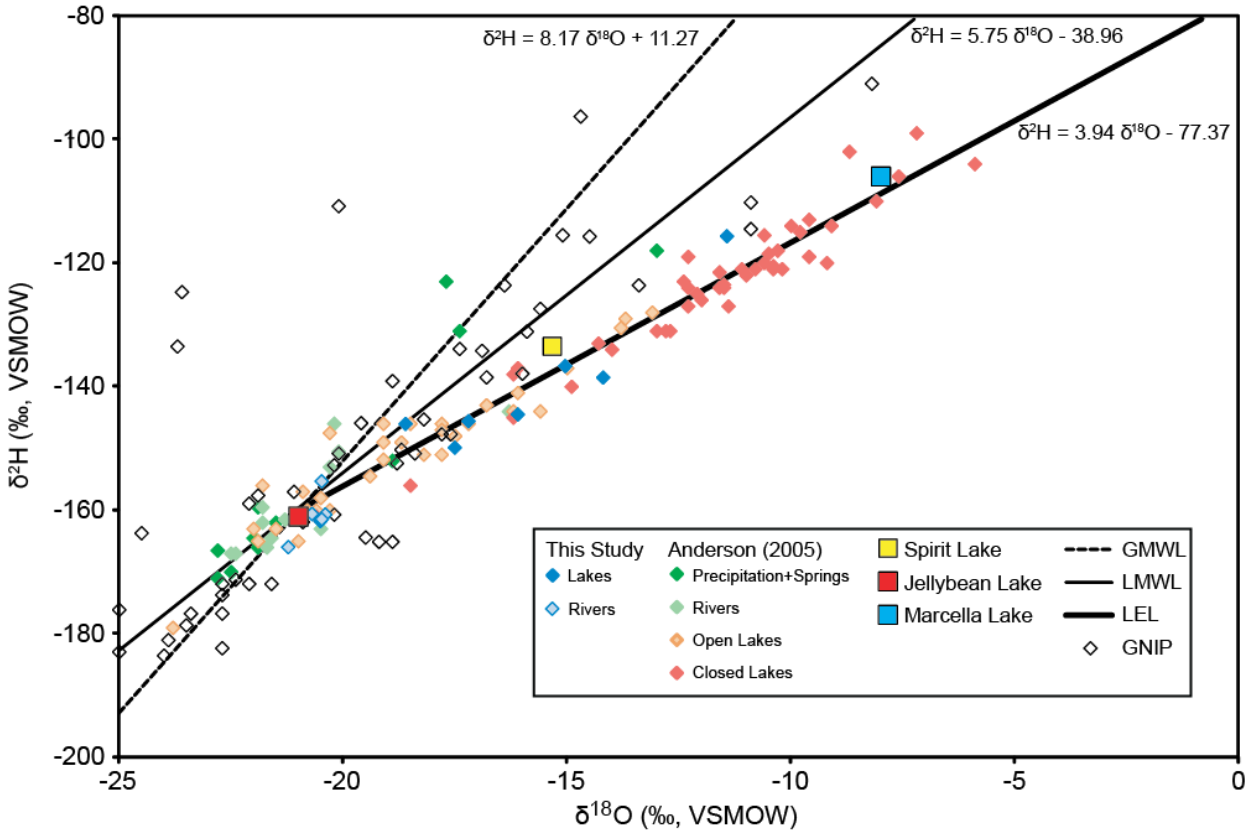

Figure 2.4: Hydrological isotope data from the Yukon. Including data from the Global Network of Isotopes in Precipitation, Anderson (2005), and this study. Global meteoric water line (GMWL), local meteoric water line (LMWL), and the local evaporation line (LEL) are also plotted with their respective equations.

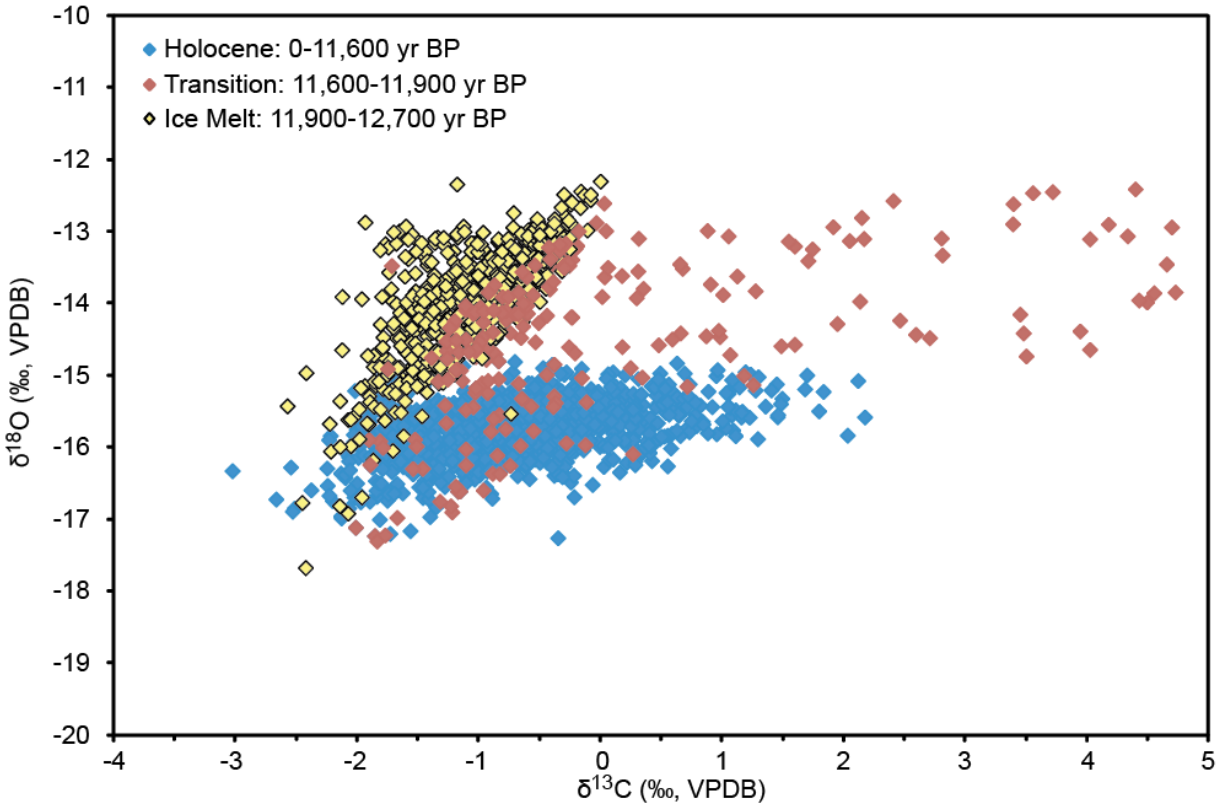

Figure 2.5: Plot of the covariance of $\delta^{13}C$–$\delta^{18}O$ values. Three different sub-groups have been chosen based on age and their $\delta^{13}C$–$\delta^{18}O$ relationship.

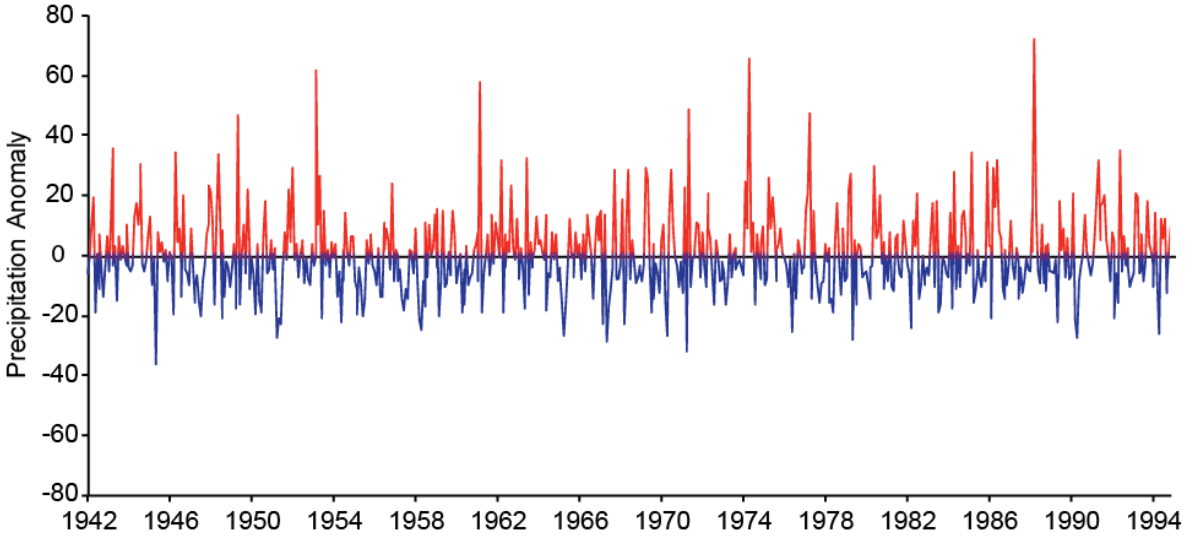

Figure 2.6: Precipitation anomaly plot from Whitehorse monthly precipitation totals 1942-1994. Red: positive anomalies, blue: negative anomalies compared with average monthly precipitation total.

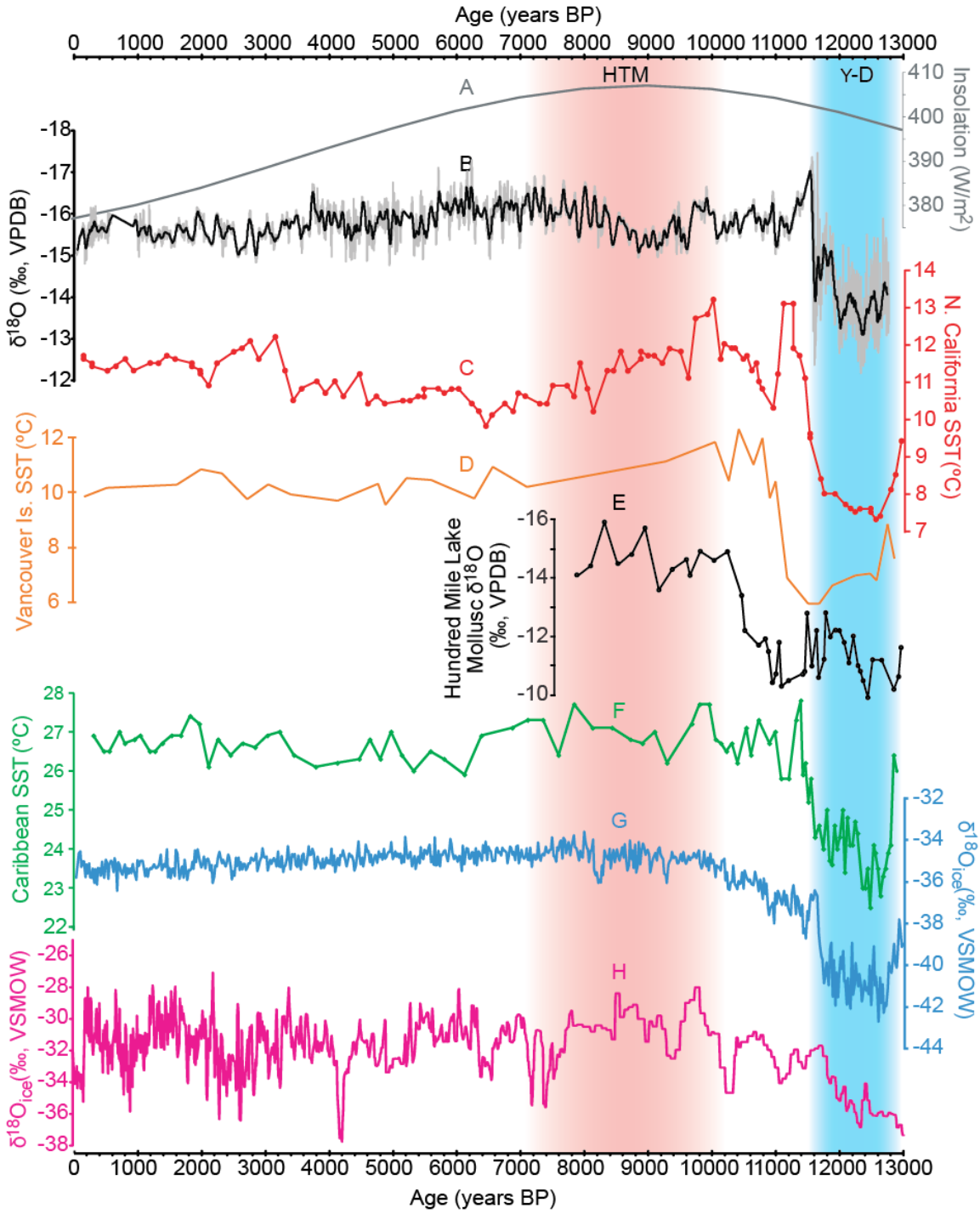

Figure 2.7: Pleistocene-Holocene $\delta^{18}O_{carb}$ record from Spirit Lake including some globally and locally significant climate events. A. Mean insolation 60°N, 90-180°W (Laskar, 2004); B. Spirit Lake $\delta^{18}O_{carb}$ (this study); C. North California alkenone SSTs (Barron et al., 2003); D. West Vancouver Island alkenone SSTs (Kienast and McKay, 2001); E. Molluscan $\delta^{18}O_{carb}$ (Yu et al., 2008); F. Caribbean SSTs based on foraminiferan Mg/Ca ratios (Lea et al., 2003); G. Greenland ice core $\delta^{18}O_{ice}$ (NGRIP Dating Group, 2006); H. Mt Logan ice core $\delta^{18}O_{ice}$ (Fisher et al., 2004). Holocene Thermal Maximum (HTM) based on Kaufman et al. (2004) shown in red shading; Younger Dryas (Y-D) shown in blue shading.

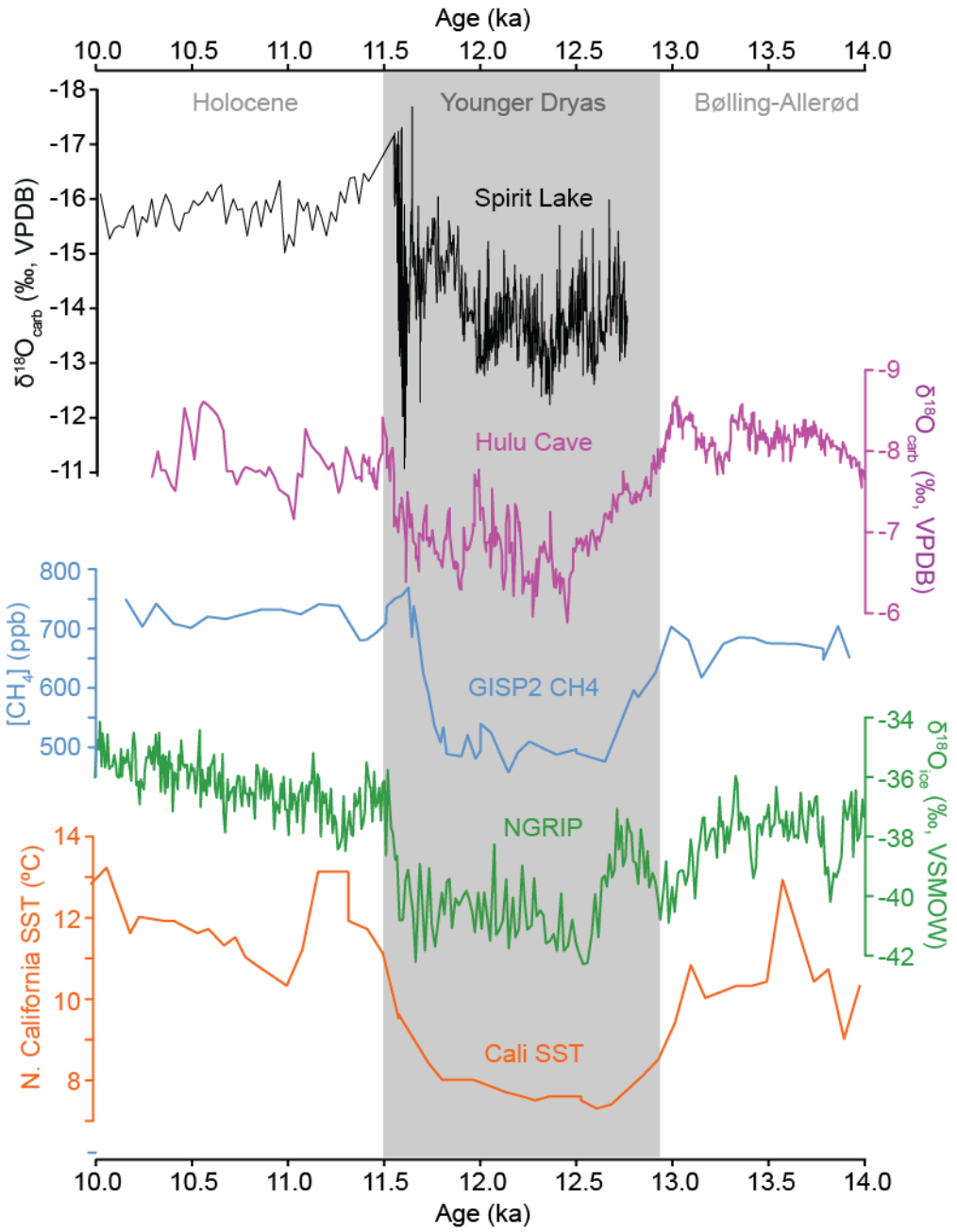

Figure 2.8: Climate records from the Younger Dryas. Spirit Lake (this study); Hulu Cave $\delta^{18}O_{carb}$ (Wang et al., 2001); GISP2 CH_4 concentrations (Brook et al., 2000); NGRIP $\delta^{18}O_{ice}$ (NGRIP Dating Group, 2006); California SSTs (Barron et al., 2003).

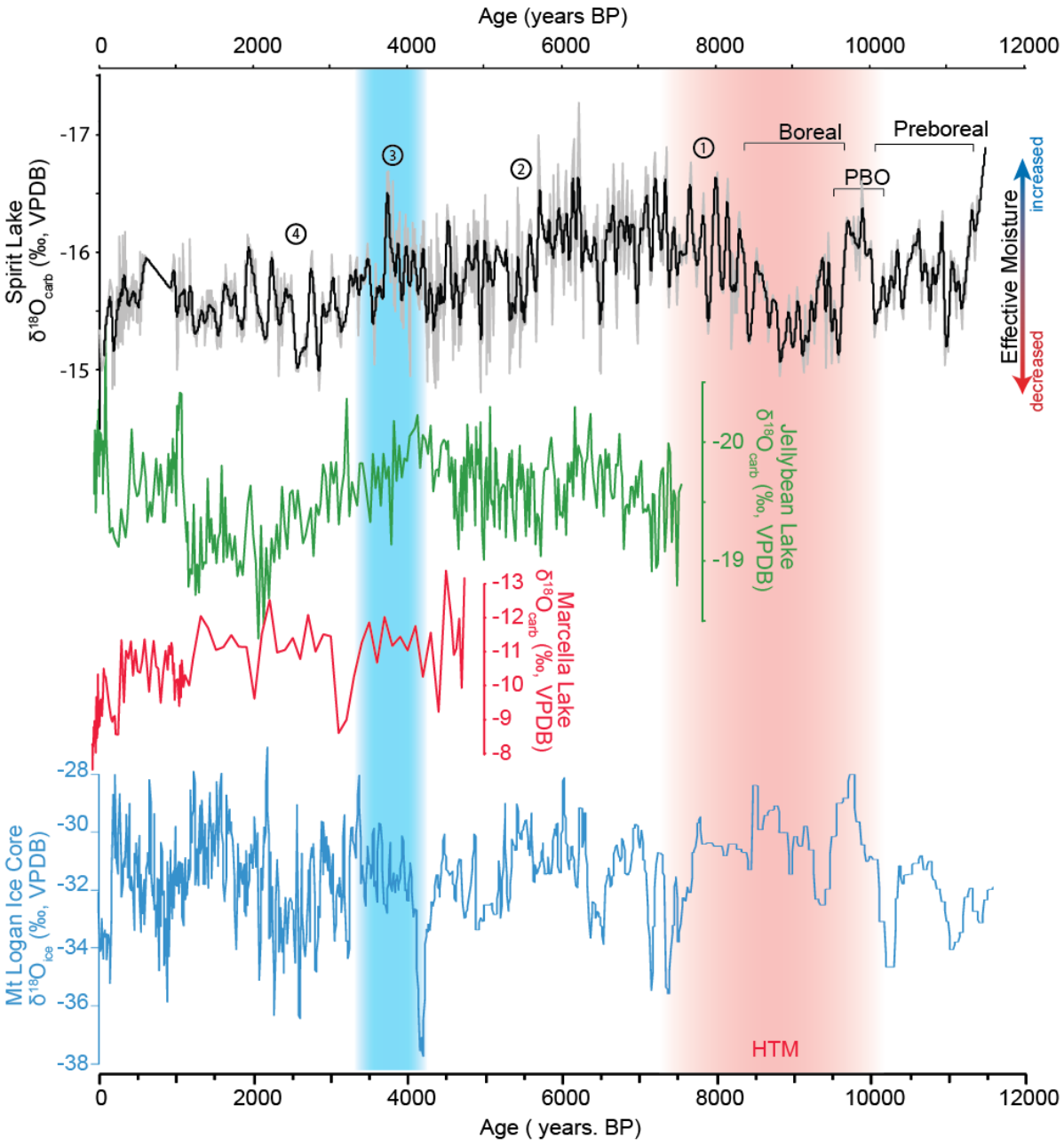

Figure 2.9: Holocene climate synthesis for the southwest Yukon Territory. Circuled numbers described in text. Note y-axis reversed on Spirit Lake, Jellybean Lake, and Marcella $\delta^{18}O_{carb}$ records. A. Spirit Lake $\delta^{18}O_{carb}$ (this study); B. Jellybean $\delta^{18}O_{carb}$ (Anderson et al., 2005c); C. Marcella Lake $\delta^{18}O_{carb}$ (Anderson et al., 2005b); D. Mt. Logan $\delta^{18}O_{ice}$ (Fisher et al., 2004).

CHAPTER 3

HIGH-RESOLUTION RECORD OF PALEOPRECIPITATION OVER CENTRAL NORTH AMERICA: IMPLICATIONS FOR THE PACIFIC/NORTH AMERICAN PATTERN AND MID-HOLOCENE CLIMATE CHANGE

3.1 Abstract

Stable isotope analysis of authigenic lake carbonate from the southern boundary of the boreal forest provides for a more detailed understanding of Holocene climate change in central North America. The southern boundary of the boreal forest is precipitation-limited, making it particularly sensitive to changes in atmospheric circulation patterns. Stable isotope analysis of lake sediment from this region can provide information on precipitation variability in the region through time and insight as to how changes in atmospheric circulation might be responsible for this variability. Isotope values record moisture source information, helping to elucidate changes in atmospheric circulation patterns through time. We present a high-resolution (millimeter scale) 8,000-year record of climate from central Saskatchewan, detailing climate change in the region from the Early to Late Holocene. $\delta^{18}O$ values of precipitation from the region are significantly correlated with the Pacific/North American (PNA) Index (Birks and Edwards, 2009) implying that paleoprecipitation $\delta^{18}O$ records can be used as a proxy for the PNA Index. The Early to Mid-Holocene (8,000 to 4,200 years BP) is characterized by significant variability in $\delta^{13}C$ and $\delta^{18}O$ values, implying more variable moisture sources, suggesting a more prevalent PNA pattern. This stronger PNA pattern induces increased meridional flow, resulting in a greater variety of moisture sources to the study region. The Mid- to Late Holocene (4,200 to 1,750 years BP) exhibits a more muted PNA pattern with a reduction in the variety of moisture sources due to more zonal flow, evident from reduced variability in $\delta^{18}O$ values. After 1,750 years BP the PNA pattern is re-established coincident with the onset of ENSO conditions in the Pacific.

Keywords: Oxygen isotopes, lake carbonate, Pacific North American, ENSO, Pacific Decadal Oscillation, Holocene

3.2 Introduction

In North America, climate teleconnections such as the Pacific/North America (PNA) pattern have been correlated with regional continental precipitation and temperature patterns (e.g. Leathers et al., 1991; Shabbar et al, 2006; Trouet and Taylor, 2010). For example, anomalous circulation related to strong PNA has been implicated in the decrease in sea ice in the western Arctic in 2007 (L'Heureux et al., 2008), and a reduction in springtime snow depth across much of North America (Ge et al., 2009; Trouet and Taylor, 2010). Modern $\delta^{18}O$ anomalies of precipitation from the central North American region have been significantly correlated with the PNA pattern via the PNA index (Birks and Edwards, 2009). This suggests that high-resolution records of $\delta^{18}O$ values of paleoprecipitation can be used as a proxy for the PNA index through time. However, climate patterns such as the PNA pattern, El Niño Southern Oscillation (ENSO), and the Pacific Decadal Oscillation (PDO) typically vary on the order of years in contrast to the majority of paleoclimate records are typically multi-decadal in resolution at best, resulting in the inability of these records to resolve important Pacific climate phenomenon, thereby limiting their utility for evaluation of these processes. Proxy records require a sub-decadal resolution to adequately assess the role climate modes play in North American climate during the Holocene. Saskatchewan lies near a node of the PNA pattern, and is therefore, an ideal location for investigating changes in this climate pattern over time. Analysis of historical precipitation anomaly patterns in Saskatchewan indicates that Saskatchewan circulation patterns have global correlations (Cayan et al., 1998), *i.e.* atmospheric teleconnections. Authigenic lake carbonate is known to archive environmental information during carbonate precipitation (e.g. Stuiver, 1968; Talbot, 1990; Leng and Marshall, 2004). Lacustrine carbonate records information about the $\delta^{18}O$ value of lake water and lake temperature, providing a history of Holocene paleoprecipitation $\delta^{18}O$ values, in laminated lake sediment. We present a high-resolution (millimeter scale, 1–3 years) lake carbonate record from the southern boreal forest region in central Saskatchewan, Canada (Fig. 3.1) detailing climate change including variability in the PNA pattern over the past 8,000 years.

3.2.1 PNA Pattern and Climate

The PNA pattern is the most prevalent mode of atmospheric variability across continental North America. The PNA is a teleconnection pattern first described by Wallace and Gutzler

(1981) with four centers of action close to 1) the Aleutian Islands, 2) Hawaii, 3) Gulf of Mexico coastal region in the United States, and 4), Alberta which is adjacent to the study site (Fig. 3.2). During a positive PNA, deep Aleutian Lows develop with a high-pressure center over western Canada leading to the development of a prevalent ridge-trough pattern (Wallace and Gutzler, 1981). This ridge-trough pattern forces increased meridional flow as cold Arctic air flows southward in troughs and warm air flows northward in ridges (Fig. 3.2). Comparison of isotope values of precipitation across Canada (Birks and Edwards, 2009) and the contiguous United States (Liu et al., 2011) suggests a strong correlation with the PNA teleconnection pattern (Fig. 3.3a). A robust correlation exists between the PNA index and precipitation isotope values in central Canada with positive isotope anomalies associated with positive PNA (PNA^{+}) indices and negative isotope anomalies with negative PNA (PNA^{-}) indices (Birks and Edwards, 2009). This implies that the prevalent ridge-trough pattern and related meridional flow associated with a positive PNA index results in moisture with a more varied distillation history transported to western Canada (Birks and Edwards, 2009). Atmospheric circulation patterns and related moisture source regions associated with the PNA dominate local climate conditions in controlling precipitation isotope values, hinting at the potential value of precipitation isotope proxy studies in the reconstruction atmospheric circulation through the Holocene (Liu et al., 2011).

3.2.2 Pacific Climate Oscillations and western Canadian climate

ENSO is the second largest contributor to interannual variability of the climate in western Canada, following only the seasonal cycle in importance (Shabbar, 2006). Warm phases of ENSO (El Niño) are associated with heating of the eastern tropical Pacific leading to the formation of a poleward-propagating Rossby wave that induces a positive PNA pattern (Shabbar, 2006) resulting in positive temperature anomalies beginning in northwestern Canada then extending eastward (Shabbar and Khandekar, 1996). Precipitation is also affected by ENSO with decreased precipitation patterns associated with the first winter following El Niño conditions in the western portion of Canada (Shabbar et al., 1997). In addition, El Niño periods are associated with a higher likelihood of extreme warm temperature anomalies in western Canada (Shabbar, 2006) that could have a significant effect on evaporation potential at the study site.

Changes to the sea surface temperatures (SST) structure of the North Pacific can impose significant effects on the climate in western Canada. Bonsal et al. (1993) provide evidence of a link between North Pacific SST anomaly patterns and extended drought on the Canadian prairies through a disruption of upper atmosphere (Rossby) winds. PDO is a pattern of SST anomalies that occurs in the North Pacific on a time scale of around 20-30 years (Hare and Francis, 1995). Positive (negative) PDO phases arise when eastern Pacific (along the northwest coast of North America) SSTs warm (cools) and the central Pacific cools (warms) (Mantua and Hare, 2002). When positive phases of PDO and ENSO occur in concert there is a considerable increase in temperature in western Canada, while negative phases have the opposite effect (Bonsal et al., 2001). Periods of positive PNA patterns are related to warm phases of PDO and ENSO that can be exacerbated during periods when PDO and ENSO are in phase (Trouet and Taylor, 2010). The robust evidence for teleconnections between North Pacific SST regimes and precipitation-temperature patterns in western Canada highlights the importance of the state of the Pacific Ocean including associated atmospheric and ocean oscillations on the climate of western Canada.

3.3 Site Locality

Sturgeon Lake is located in central Saskatchewan, Canada in northern-central part of North America (Fig. 3.1). The lake occupies the bottom of a 60 m deep valley formed in the drainage channel into former glacial lake Saskatchewan ~11,500 years BP (Christiansen, 1979). Currently a weir located at the east end of the lake maintains lake levels artificially. This is a hydrologically open lake with an inflow at the western margin and outflow at the eastern margin resulting in lake water with a relatively short residence time. The lake has an area of ~13 km^2 with maximum depth of 8 m and is classified as a cold polymictic lake (Lewis, 1983), as it is too shallow to develop a thermocline. It is moderately saline with total dissolved solids ~486 ppm (Rawson and Moore, 1944; Moore, 1952). Sturgeon Lake overlies predominantly dolomitic glacial sediment that provides the source of ions in the lake for marl precipitation (Kupsch, 1956).

Average precipitation and temperature values for Wynyard (51°45’56”N, 104°10’46”) over a 30-year period stretching from 1971-2000 (Canada Climate Normals) are shown in Fig. 3.4. Wynyard was chosen over Prince Albert (the closest weather station) because the Global

Network for Isotopes in Precipitation (GNIP) operated a station at Wynyard providing detailed information on isotopes in precipitation from this area. The climates of Prince Albert and Wynyard are almost identical therefore, the Wynyard climate data is assumed to be reflective of the climate at Sturgeon Lake as the region is relatively climatologically homogenous. Average monthly temperatures range from -17°C in January to 18°C in July. Precipitation peaks in the summer months with monthly average of 75mm in June and dips to 13mm in February with a fairly low average annual precipitation of 415 mm. $\delta^{18}O$ values of precipitation from the GNIP Wynyard station essentially track air temperature with higher temperatures resulting in higher $\delta^{18}O$ values (Fig. 3.4). The region is dominated by air masses from the Pacific being along the path of strongest Westerlies however incursions from the Arctic occur during winter months (Bryson and Hare, 1974).

3.4 Methods

3.4.1 Lake Carbonate Record

A five-meter long Livingstone push core composed of laminated marl and silt layers with varying amounts of organic matter was collected from the shore of Sturgeon Lake. Laminae throughout the core suggest little sediment mixing via bioturbation. Seven samples of terrestrial organic matter were used to construct the age model and radiocarbon history of the lake in order to avoid the effects of reservoir effects, which can be large in marl lake systems. Descriptions of these samples are included with the ^{14}C ages in Table 3.1.

Aliquots of carbonate were extracted from the core such that only fine grain marl sediment was taken. Shell debris and other non-carbonate material was removed prior to placing these samples into stainless steel sample boats. Sample boats were then heated to 200°C *in vacuo* for one hour in order to eliminate potential contamination from organic matter and volatiles in the sediment that may interfere with the isotope analyses. Carbonate samples were subsequently analyzed using a Kiel IV automated carbonate preparation device directly coupled to a ThermoFinnigan MAT 253 mass spectrometer and calibrated using NBS-19 at the University of Saskatchewan. All results are reported in standard per mil notation (‰) relative to VPDB. Standard deviation of replicate NBS-19 analyses was better than 0.04‰ for $\delta^{13}C$ and 0.07‰ for $\delta^{18}O$.

3.4.2 Local Meteoric Water Sampling

Regional meteoric waters were sampled from several streams, lakes and rivers in August 2009. Water samples were collected in 100 mL Nalgene containers that were rinsed with the water sample before filling and capping with no headspace. Capped samples were taped and transported back to the Saskatchewan Isotope Laboratory where they were analyzed for $\delta^{18}O$ and $\delta^{2}H$ values on a Picarro L1102-*i* Isotopic Liquid Water Analyzer based on wavelength-scanned cavity ring down spectroscopy (WS-CRDS).

3.4.3 Time Series Analyses

One of the unique qualities of this dataset is the large number of samples that allows for high-resolution time series analysis in order to evaluate cyclicity in the data that could be related to cyclical climate phenomenon such as ENSO or PDO. The time series analyses employed in this study include Singular Spectrum Analysis (Ghil et al., 2002); the Multitaper Method (MTM; Thomson, 1982) and wavelet analysis (Torrence and Compo, 1998; Grindsted et al., 2004). Multiple methods are employed in order to prevent spurious results due to method-specific spectral artifacts (e.g. aliasing). If periodicity is observed using multiple methods, there is a greater degree of confidence in its robustness.

Data pre-processing was conducted to make the dataset suitable for time series analysis. This includes reproducing the time series with equal sample spacing. First, a curve was fit to the data using Time Curve software created by Bruce Eglington (available from: http://sil.usask.ca/Eglington/bme_software.htm). This program uses the cubic spline method to produce a curve through the data, allowing for extra data points to be added in between samples in order to standardize the frequency of data. This does not add extra spectral information to the data but instead permits the interpolation of values at even spacing without losing information during scaling caused by the age model. The following parameters were used in order to create the spline for both $\delta^{13}C$ and $\delta^{18}O$: Students t multiplier (1.96); Minimum standard deviation (0.02); Required smoothing precision (0.001); Average every (0.005) age units; Number of spline points (n=20,000). Spline model results were then validated by comparing the model with the original data, any model data points that were mis-representative of the actual data (i.e. anomalously different than the original data series) were removed prior to statistical analysis.

A MATLAB program was then used to interpolate the data such that there is an even spacing between data points resulting in a constant time step. A time step of 1 year was used, as this was the maximum sampling frequency based on the age model. This series was then detrended by fitting a 2nd order polynomial to the data that was subsequently subtracted from the dataset. This series was then input into the MTM routine in the kSpectra program to generate MTM spectra using a resolution of 2 and 3 tapers. This was compared to AR(1) red noise to evaluate the significance (Mann and Lees, 1996). Only frequencies with a confidence level greater than 95% were used. Wavelet analysis was performed using combination of MATLAB programs incorporating the work of Ghil et al. (2002) performing wavelet analysis using the Morlet mother wavelet, with no zero padding (modified by B. Eglington) and a cross wavelet analysis program by Grinsted et al. (2004).

3.5 Results

3.5.1 Core Stratigraphy and Age Model

An age model constructed from the seven radiocarbon dates is shown in Fig. 3.5. Core chronology reveals a continuous lake record extending back from about 0 years BP (present: 1950 AD) to around 8,000 years BP. Currently there is a significant age gap between the youngest dates from the core-top to the mid-core dates. This has resulted in an assumption of a linear age-depth relationship from approximately 5,000 yr BP to present. It is understood that this is a significant assumption that may change with the addition of more dates, however the correlation of the record with other regional climate records throughout the Holocene suggests some validity to this model.

Timescale errors also have significant impacts on spectral estimation for time series analyses. Timing errors cause a smearing of the intensity of spectral energy over a larger number of frequencies resulting in less defined spectral peaks (Rhines and Huybers, 2011) decreasing the distinguishability of spectral peaks and increasing the frequency uncertainty for these spectral peaks (Mudelsee et al., 2009). The major consequence of this is a lower degree of confidence in the frequency of the cyclicity determined via spectral analysis. The lack of dates in this study between 5,000 yr BP and present represents a large hiatus that introduces timescale error that is difficult to quantify without additional dates and therefore cannot be accurately incorporated into the spectral analysis presented. Therefore, in this study an assumption has been made that the age

model is robust and timescale errors have been ignored. This means that the periodicities calculated using spectral analysis are not completely accurate as they do not record the full scale of the errors in the age model. It is acknowledged that to assess the full significance of cyclicity in climate data accurate determination of all timescale error sources must be determined and incorporated in spectral analysis (Mudelsee et al., 2012).

3.5.2 Regional Water Isotope Hydrology

The Global Network for Isotopes in Precipitation (GNIP) program of the IAEA has operated several sampling stations in the Sturgeon Lake region, and although none of the stations are within 200 km of the study site, a composite of all data reveals similar regional $\delta^{18}O$-$\delta^{2}H$ trends from these stations. The location of these stations is shown on Fig. 3.1. $\delta^{18}O$-$\delta^{2}H$ values from these stations create a local meteoric water line (LMWL) as shown in Fig. 3.4. Additionally, a compilation of surface water data from Saskatchewan are plotted creating a local evaporation line (LEL). Surface water samples are grouped based on their location within the Climatic Moisture Index system separating sites into three zones: northern Boreal Forest, transitional Aspen Parkland, and southern Grasslands; related to their balance between precipitation and potential evaporation (Hogg, 1994). The main difference between Boreal Forest sites, Aspen Parkland sites, and Grassland sites is that the southern sites (Aspen and Grassland) are further along the LEL and whereas Boreal Forest sites have a full range of values along the LEL depending on the characteristics of the lake. Open system lakes with shorter water residence times will have isotope values that are more reflective of precipitation compared with closed system lakes with longer water residence times that have evolved to higher isotope values due to evaporation. Sturgeon Lake is a shallow open lake that occupies an old drainage channel with inflow from the northwest and outflow to the southeast suggesting its isotopic values should be minimally influenced by evaporitic effects. As shown in (Fig. 3.4) Sturgeon Lake plots near the intersection of the LEL and the LMWL, implying it is less affected by evaporation and thus lake water should provide an accurate proxy for precipitation values. Therefore, oxygen isotope values of authigenic lake carbonate from Sturgeon Lake should provide a good proxy of paleoprecipitation $\delta^{18}O$ values.

3.5.3 Carbonate Stable Isotope Analyses

Oxygen isotope values of lake carbonate are controlled by lake temperature and lake water $\delta^{18}O_{H2O}$ values. $\delta^{18}O_{H2O}$ values of lake water are in turn affected by $\delta^{18}O$ values of precipitation and lake water evaporation. $\delta^{18}O$ values of precipitation are affected by air temperature, relative humidity, the seasonal distribution of precipitation, and the source of precipitation, which is related to atmospheric circulation patterns. Lake carbonate $\delta^{18}O$ values exhibit a range of 5.8‰ over the entire record, such that if temperature was assumed to be the only control over $\delta^{18}O$ variability it would equate to over 23ºC (4.2ºC/1‰; Kim and O'Neil, 1997) change in lake water temperature. This is unreasonably high and therefore cannot be the only source of $\delta^{18}O$ variability (*e.g.* Diefendorf and Patterson, 2008). Furthermore, the period of maximum calcium precipitation is closely related to maximum lake water temperatures, therefore, it is unlikely that a wide range of temperatures are recorded during calcite precipitation (Drummond et al., 1995). In addition, short-term variations of up to 18ºC (4.5‰) are equally unlikely and point to other causes of lake water carbonate $\delta^{18}O$ variability. Carbonate $\delta^{18}O$ values are interpreted to predominantly reflect the variability in the $\delta^{18}O$ values of precipitation related to changes in atmospheric circulation and air temperature. The average isotope values of dolomite from the region are $\delta^{13}C = 4.0‰_{VPDB}$ and $\delta^{18}O = –2.4‰_{VPDB}$ (Liu and Qing, 2010), over 4‰ greater than the highest $\delta^{18}O$ value and about 7.5‰ greater than the average of all $\delta^{18}O$ values suggesting that the influence of detrital carbonate is negligible.

The Sturgeon Lake isotope record (Fig. 3.6a) displays the highest $\delta^{18}O$ values of the entire record with average values of –8.2‰ from 8,000-7,500 yr BP. Subsequently, $\delta^{18}O$ values decrease until ~6,500 yr BP., at which point $\delta^{18}O$ values average –9.9‰ from 6,500–4,300 yr BP, with high short-term variability. After 4,300 yr BP there is a significant decrease in $\delta^{18}O$ values followed by a recovery with values leveling off to an average of –10.6‰ for the remainder of the record (4,300–0 yr BP).

The Early to Mid-Holocene (8,000 to 4,200 yr BP) is characterized by greater variability in $\delta^{18}O$ values, represented by multiple large, short-lived fluctuations (up to 4.5‰ in $\delta^{18}O$), especially in the time period 8,000-5,500 yr BP (Fig. 3.6b). Spectral analysis (MTM) of the Early to Mid-Holocene portion (8,000 to 4,000 yr BP) of the Sturgeon Lake $\delta^{18}O$ time series indicates three robust periodicities 6.25, 3.2, and 2.6 years (Fig. 3.7). Notably, MTM analysis of the entire 8,000-year record provides only one robust periodicity (6.6 years), prevalent throughout all

windows of the MTM analyses conducted, similar to the 3-5-year periodicity of ENSO (e.g. Graham and White, 1988). Wavelet analysis of the Mid-Holocene exhibits consistent robust periodicities of ~16 years and ~6.6 years (Fig. 3.8). Periodicites greater than ~16 years are present but are not consistent through this portion of the record.

After 4,200 yr BP short term variance decreases appreciably until about 1,800 yr BP when there is a modest increase. This suggests that the Mid-Holocene was subject to increased rapid environmental change compared to the Late Holocene, that underwent more gradual change. It appears that modern-like conditions began approximately 1,800 years ago when average $\delta^{13}C$ and $\delta^{18}O$ values as well as short-term variance approached modern values. Wavelet analysis shows a reduction of decadal to multidecadal period cyclicity after 4,200 yr BP, that last until about 1,800 yr BP, when there is a recovery of the multidecadal band (Fig. 3.8).

3.6 Discussion

3.6.1 $\delta^{18}O$ as a Proxy for the Strength of the PNA

Oxygen isotope analysis of local modern precipitation indicates a strong positive correlation between precipitation $\delta^{18}O$ anomalies and PNA index, highlighting the importance of atmospheric circulation on isotopic labeling in the study region (Birks and Edwards, 2009). PNA^+ phases have increased meridional flow across central North America (Fig. 3.2) resulting in moisture derived from more southerly sources, transferring heat to the study region along with higher precipitation $\delta^{18}O$ values, producing positive $\delta^{18}O$ anomalies and warmer temperatures in the study region (Birks and Edwards, 2009). Meridional flow leads to moisture migrating northward before penetrating the Canadian Cordillera, undergoing less isotope distillation, resulting in moisture sources with higher $\delta^{18}O$ values, changing the typical $\delta^{18}O$-temperature relationship (Fig. 3.3b) in the study area (Birks and Edwards, 2009). Periods of PNA^- are related to increased zonal flow across central North America as moisture is transported across the southern Canadian Cordillera, where it undergoes intensive Rayleigh distillation. This results in moisture with lower $\delta^{18}O$ values as the slope of the $\delta^{18}O$-temperature relationship increases (Fig. 3.3b) and less heat is transported to the study region (Birks and Edwards, 2009).

Isotope hydrology from Sturgeon Lake (Fig. 3.4) suggests that lake water $\delta^{18}O$ values are reflective of precipitation values, and hence the strength and sign of the PNA pattern should also affect $\delta^{18}O$ values of lake water. If variability in the $\delta^{18}O$ value of lake water dominates the $\delta^{18}O$

values of authigenic lake carbonate (see discussion above), variations in the PNA pattern through the Mid- to Late Holocene should be recorded in the Sturgeon Lake carbonate $\delta^{18}O$ archive.

Climatologically, periods of PNA^+ are associated with higher regional temperatures, less precipitation and a higher $\delta^{18}O$-temperature relationship resulting in higher precipitation $\delta^{18}O$ values on average (Birks and Edwards, 2009). Higher temperatures coupled with decreased rainfall can increase evaporation potential, resulting in higher lake water $\delta^{18}O$ values. Therefore, lake water $\delta^{18}O$ values should be higher during PNA^+ phases. Conversely, during PNA^- phases there are typically lower temperatures and an increased gradient in the $\delta^{18}O$-temperature relationship (Fig. 3.3; Birks and Edwards, 2009). Cooler temperatures reduce evaporation potential and when combined with lower $\delta^{18}O$ values of precipitation, result in lower lake water $\delta^{18}O$ values during PNA^- phases. Therefore, lower lake carbonate $\delta^{18}O$ values are associated with PNA^- phases and higher values with PNA^+ phases. The strength of the PNA index should also be recorded in the lake carbonate $\delta^{18}O$ values. However, lacking a robust historical record of lake carbonate $\delta^{18}O$ values to compare with instrumental records of PNA (only extends back to 1950 AD) it is difficult to calibrate quantitatively, therefore the record is treated as a qualitative record of PNA through time.

Qualitatively assessing the strength of the PNA should be relatively straightforward as a strong PNA pattern with large PNA^- and PNA^+ shifts will be associated with greater differences in the precipitation $\delta^{18}O$ values in the study region, reflected as increased $\delta^{18}O$ variability in the Sturgeon Lake carbonate $\delta^{18}O$ record. Figure 3.6b displays the 30-year variance in $\delta^{18}O$ values from Sturgeon Lake versus time to illustrate how the strength of the PNA pattern may have varied through time.

3.6.2 $\delta^{18}O$ and the Strength of the PNA Through the Holocene

The Early to Mid-Holocene (8,000 to 4,000 yr BP) is characterized by high variability and an average $\delta^{18}O$ value of $-9.4‰_{VSMOW}$, that is 1.2‰ higher than the average of the rest of the Sturgeon Lake record. This hints at a dominance of PNA^+-like conditions across the Early to Mid-Holocene. Increased meridional flow into the region brings warmer and drier conditions and promotes evaporation coupled with higher $\delta^{18}O$ values of precipitation that drives lake water $\delta^{18}O$ values higher. Faunal and sedimentological evidence from regional lakes suggest increased

aridity during this period (Dean et al., 1996; Dean, 1997; Valero-Garces et al., 1997; Schwalb and Dean, 2002), and sand dunes from the Sturgeon Lake region show activity from 7,500 to 4,800 years BP, also indicating arid conditions during this period (Wolfe et al., 2006). In addition, palynological and geochemical records from Moore Lake located ~300 km to the northeast and Chappice Lake located ~450 km southwest of Sturgeon Lake both show periods of short-lived fluctuations between moist and arid conditions during the Mid-Holocene (Hickman and Schweger, 1996; Vance et al., 1992). Similarly, large shifts in $\delta^{18}O$ values at Sturgeon Lake suggest significant changes in effective moisture that supports the interpretation of records these local lakes. A combination of PNA^{+}-like conditions coupled with large fluctuations in regional aridity may have amplified short-term changes in lake water $\delta^{18}O$ values, resulting in increased variance in the $\delta^{18}O$ record at Sturgeon Lake.

At ~4,000 years BP (beginning of the Late Holocene) $\delta^{18}O$ variability decreases and remains low until ~1,800 yr BP. This period displays the lowest variability from the entire Holocene record and is fairly consistent with the exception of one spike in variability centered around 2,790 yr BP (Fig. 3.6b). Low variability in $\delta^{18}O$ values at Sturgeon Lake indicates a transition to consistent moisture sources. In addition, $\delta^{18}O$ values are on average lower than in the previous period (8,000-4,000 yr BP), perhaps indicating moisture underwent increased Rayleigh fractionation associated with more zonal flow bringing with it cooler and possibly moister conditions decreasing evaporative effects and leading to a decrease in $\delta^{18}O$ values in Sturgeon Lake. Other regional lakes also suggest wetter and cooler conditions in the Late Holocene Period after 4,000 yr BP (Vance et al., 1992; Hickman and Schweger, 1996; Valero-Garces et al., 1997; Schwalb and Dean, 2002). This period of decreased variability and lower $\delta^{18}O$ values at Sturgeon Lake may be related to a weakening of the PNA pattern and a dominance of PNA^{-}-like conditions resulting in enhanced zonal flow.

After ~1,800 yr BP $\delta^{18}O$ variability increases again and remains elevated for the remainder of the record. Average $\delta^{18}O$ values over this period increase 0.5‰ compared to the previous period, suggesting the development of PNA^{+}-like conditions with increased meridional flow bringing more heat and precipitation with higher $\delta^{18}O$ values to the region. This also seems to represent the development of the modern PNA pattern in the Sturgeon Lake region. Interestingly, this is

also coincident with the onset of modern-like ENSO conditions based on Holocene ENSO proxies.

3.6.3 Relationship of PNA with other Pacific Climate Phenomenon

One of the unique aspects of the PNA is its four "centers of action" that influence a large geographic area via atmospheric teleconnections to different regions of North America. This means that knowledge of strength of the PNA may help predict climate on a broader geographical scale. Therefore, the presence of the PNA pattern may also hint at the prevalence of other Pacific climate phenomenon such as ENSO and PDO. Periods of PNA^+ pattern are related to warm phases of PDO and ENSO which can be exacerbated during periods when PDO and ENSO are in phase (Trouet and Taylor, 2010). ENSO and PDO records both comparably correlate with wintertime pressure anomalies (Fig. 3.9) similar to the PNA (compare with Fig. 3.2). Therefore, it is likely that during periods when these climate oscillations were active they could influence the state and strength of the PNA, recorded in the lake carbonate $\delta^{18}O$ values.

Figure 3.10 shows a compilation of Holocene ENSO records alongside Sturgeon Lake $\delta^{18}O$ variability. Sturgeon Lake $\delta^{18}O$ values exhibit three distinct periods over the past 5,000 years. Mid-Holocene variance is high, reflecting a strong PNA signal followed by low variability and a weakening of the PNA, and subsequently around 1,800 yr BP variability increases. The Holocene ENSO records (Fig.3.10b-d) generally show a similar timing for the development of ENSO in the latter part of the Late Holocene, and weak ENSO activity during the early part of the Late Holocene. Reconstructions of ENSO during the Holocene suggest distinct changes in the prevalence of El Niño and La Niña like conditions (Rein et al., 2005; Makou et al., 2010). ENSO state-specific marine biomarkers from the Peru margin provide evidence of decreased El Niño conditions during the Mid-Holocene (Fig. 3.10d) with an increase in El Niño and La Niña like conditions beginning around 2,000 yr BP (Makou et al., 2010). The Sturgeon Lake record indicates a prevalence of PNA^- conditions with enhanced zonal flow over North America similar to climate patterns during modern La Niña conditions supporting this theory. Although proxy evidence generally agrees that ENSO conditions varied during the Holocene, the timing of these variations is more poorly constrained. Most studies agree that ENSO-like conditions increased after 2,000 years BP (Moy et al., 2002; Rein et al., 2005; Conroy et al., 2008; Makou et al., 2010), however, some suggest a Mid-Holocene enhancement of ENSO conditions occurring

around 4,000 years BP (Conroy et al., 2008) or 7,000 years BP (Moy et al., 2002). Recent work in the Galapagos suggests that the Early-Mid Holocene (9,200-5,500 years BP) was punctuated by periods of intense ENSO activity of a century in duration (Zhang et al., 2014). Heightened $\delta^{18}O$ variability at Sturgeon Lake also hints at Pacific climate variability and suggests large fluctuations in the state of the PNA pattern supporting highly variable ENSO during early Mid-Holocene.

Warm phases of the PDO have been shown to be associated with drought conditions in the Pacific Northwest region of North America (Mantua, et al., 1997). This was used to develop a high-resolution Holocene reconstruction of PDO from lake sediment (Nelson et al., 2011), that indicates multidecadal variability in drought-like conditions. Notably, this record exhibits strong periodicities in the multidecadal frequency band (16-64) during the Mid-Holocene that gradually weaken after 4,000 years BP (Nelson et al., 2011), attributed to changes in the thermal structure of Pacific SSTs. This decrease in strength of the multidecadal band around 4,000 years BP is reproduced in the wavelet analysis of Sturgeon Lake $\delta^{18}O$ values (Fig. 3.8), however, Sturgeon Lake displays a recovery after about 2,000 years BP coincident with the onset of Late Holocene ENSO activity. A reconstruction of PDO over the past millennium from tree-ring data (Macdonald and Case, 2005) correlates well with the Sturgeon Lake record, especially the portion after 345 years BP ($r=0.5$, $p<0.05$), indicating a substantial relationship between Pacific SST variability and $\delta^{18}O$ values at Sturgeon Lake (Fig. 3.11). The strong correlation between the PDO proxy and the Sturgeon Lake record implies that Pacific SST structure is important in forcing atmospheric circulation patterns at Sturgeon Lake. In addition, this suggests that with improved age control the $\delta^{18}O$ values at Sturgeon Lake can be used to as a proxy for the PDO extending the Holocene PDO record back further in time then previous studies (e.g. Biondi et al., 2001; D'Arrigo et al., 2001; Macdonald and Case, 2005). The interaction of Pacific Ocean and atmospheric patterns forces long-term variability in the $\delta^{18}O$ values at Sturgeon Lake illustrating the importance of the Pacific influence on North American climate.

3.6.4 The 4,200-year Event and the Mid to Late Holocene Transition

The end of relatively high $\delta^{18}O$ values and variability during the Early to Mid-Holocene (~8,000 to ~4,000 yr BP) is coincident with the 4,200 yr Event (Bond Event 3), characterized by drought conditions in the central United States (Booth et al., 2005), Africa (Gasse, 2000), the

Middle East (Cullen et al., 2000), and parts of Asia (Dixit et al., 2014). The 4,200-year event is a globally correlated period of climate change with widespread impacts (Walker et al., 2012). Locally, there is evidence from peat records of increased precipitation and rapid peat accumulation suggesting a wet period in adjacent Alberta (Yu et al., 2003). This is in contrast to widespread evidence of severe drought further to the south in mid-continental United States (Dean et al., 1996). As noted by Booth et al. (2005) many higher latitude regions show evidence of wetter and/or cooler conditions around 4,200 years BP, in contrast to low and mid-latitude sites. Dettinger et al. (1998) used modern conditions to show an interannual-decadal seesaw in precipitation patterns along the west coast about 40ºN latitude related to tropical and subtropical conditions affecting Pacific storm paths causing a redistribution of moisture over North America. Furthermore, the higher latitude sites are generally situated above the southern limit of the jet stream, which may also shed light on the cause of this dichotomy. As shown at Sturgeon Lake, $\delta^{18}O$ values decrease to Holocene minima around the 4,200-year event suggesting cooler, wetter conditions. Variability in $\delta^{18}O$ values also decreases to the lowest Holocene values, suggesting a reduction in the development of the PNA^{+} pattern over the study site. The lack of a PNA^{+} pattern is a result of a trend toward more zonal upper tropospheric flow over North America, and indicates a reduction of the PDO/ENSO effects on continental North American climate. Zonal flow directs Pacific storms onto the northwestern USA (Trouet and Taylor, 2010) and is associated with elevated snowfall in PNA^{-}. Western Canadian glaciers underwent an advance around 4,200 years BP (Menounos et al, 2008), which may be a reflection of transition to PNA^{-} dominant conditions with increased zonal flow over North America resulting in increased precipitation and lower temperatures in the regional mountains. Using a combination of lake and speleothem records from two nodes of the PNA pattern Liu et al. (2014) present evidence to suggest that the boundary from the Mid-Holocene to the Late-Holocene marks a transition from a period of frequent PNA^{+} state to PNA^{-} supporting the Sturgeon Lake record highlighting the importance of the PNA on North American climate.

3.7 Conclusions

High-resolution paleoclimate records are required to resolve higher frequency climate oscillations such as ENSO and PDO and more accurately assess their variability through the Holocene. $\delta^{18}O$ records from lake carbonate provide a history of $\delta^{18}O$ precipitation variability in

central Saskatchewan allowing us to assess past changes in moisture sources. High-resolution sampling and analysis of a marl lake core at Sturgeon Lake over the last 8,000 years reveals significant changes in atmospheric circulation over Saskatchewan related to regional and global climate change. $\Delta\delta^{18}O$ values of precipitation in this region are significantly related to the PNA Index (Birks and Edwards, 2009), suggesting the lake carbonate record can be used as a proxy for the PNA index through the Holocene. Sturgeon Lake is located near the northern continental "center of action" of the PNA pattern and therefore changes in the PNA index are reflected in $\delta^{18}O_{H2O}$ values of precipitation at Sturgeon Lake. As PNA is sensitive to Pacific SST and sea level pressure patterns including the presence and strength of climate oscillations such as ENSO and PDO the $\delta^{18}O$ record from Sturgeon Lake provides a high-resolution record of these climate oscillations over the past 8,000 years.

The transition from the Mid to Late Holocene is associated with a marked decrease in aridity and a decrease in temperature in the study region, likely the result of a move to more prevalent PNA^- conditions after 4,200 years BP. ENSO and the PDO are known to excite the PNA pattern and this record indicates the development of PNA^+ like conditions around 1,800 years BP contemporaneous with the development ENSO in the Southern Hemisphere. This combined ENSO+PDO-excited PNA pattern at Sturgeon Lake indicates that the effects of ENSO on North American climate occurred contemporaneously, after its onset in the Late Holocene around 1,800 years BP. High $\delta^{18}O$ variability in the Mid-Holocene record indicates the possibility of enhanced ENSO-like behavior in the Pacific in the Mid-Holocene. The manifestation of which is amplified at Sturgeon Lake due to warm arid conditions associated with the Holocene Thermal Maximum. The 4,200-year event represents the transition from a warm PNA^+ prevalent period to a cooler PNA^- period and is represented by the lowest $\delta^{18}O$ values from the entire record.

Sturgeon Lake $\delta^{18}O$ values record long-term changes in atmospheric circulation patterns that have been attributed to changes in the strength and state of the PNA. Variations in $\delta^{18}O$ values of lake carbonate reflect changes in moisture source regions, with high values attributed to enhanced meridional flow and lower values with enhanced zonal flow. The cause of atmospheric circulation variability is linked with changes in the SST structure in the Pacific Ocean.

3.8 Relationship with Overarching Theme of Thesis

The oxygen isotope record from Sturgeon Lake provides insight into the variability of decadal climate variability in central North America. Sub-decadal sampling resolution permits evaluation of how Pacific climate oscillations such as PDO and ENSO varied through the Holocene. Oxygen isotope analysis of lake carbonates provided a proxy for the $\delta^{18}O$ values of precipitation that are intrinsically related to their source regions, which varied depending on the state of these Pacific climate oscillations.

Records with sub-decadal resolution provide valuable insight in climate variability occurring over multiple years, however, increasing to sub-seasonal resolution provides in-depth information about paleoenvironmental conditions. In the next chapter, bivalve shells are sampled at sub-seasonal resolution in order to illustrate how paleoenvironmental information about their life histories and depositional characteristics is stored in the $\delta^{18}O$ and $\delta^{13}C$ values of shell carbonate.

3.9 Acknowledgements

Mitch Mamchur is acknowledged for his laboratory assistance. NSERC DGS grant to A.W. Kingston, and NSERC Discovery grant to W.P. Patterson helped fund this research.

3.10 References

Barnston, A. G., & Livezey, R. E. (1987). Classification, seasonality and persistence of low-frequency atmospheric circulation patterns. Monthly weather review, 115(6), 1083-1126.

Biondi, F., Gershunov, A., & Cayan, D. R. (2001). North Pacific decadal climate variability since 1661. Journal of Climate, 14(1), 5-10.

Birks, S. J., & Edwards, T. W. D. (2009). Atmospheric circulation controls on precipitation isotope–climate relations in western Canada. Tellus B, 61(3), 566-576.

Bonsal, B. R., Chakravarti, A. K., & Lawford, R. G. (1993). Teleconnections between north Pacific SST anomalies and growing season extended dry spells on the Canadian Prairies. International Journal of Climatology, 13(8), 865-878.

Bonsal, B. R., Shabbar, A., & Higuchi, K. (2001). Impacts of low frequency variability modes on Canadian winter temperature. International Journal of Climatology, 21(1), 95-108.

Booth, R. K., Jackson, S. T., Forman, S. L., Kutzbach, J. E., Bettis, E. A., Kreigs, J., & Wright, D. K. (2005). A severe centennial-scale drought in midcontinental North America 4200 years ago and apparent global linkages. The Holocene, 15(3), 321-328.

Bryson, R. A., & Hare, F. K. (Eds.). (1974). Climates of North America (Vol. 11, pp. 1-47). Amsterdam, The Netherlands: Elsevier. Cayan, D.R., Dettinger, M.D., Diaz, H.F., & Graham, N.E., 1998. Decadal variability of precipitation over western North America. Journal of Climate 11, p. 3148–3166.

Christiansen, E. A. (1979). The Wisconsinan deglaciation, of southern Saskatchewan and adjacent areas. Canadian Journal of Earth Sciences, 16(4), 913-938.

Conroy, J. L., Overpeck, J. T., Cole, J. E., Shanahan, T. M., & Steinitz-Kannan, M. (2008). Holocene changes in eastern tropical Pacific climate inferred from a Galápagos lake sediment record. Quaternary Science Reviews, 27(11), 1166-1180.

Cullen, H. M., Hemming, S., Hemming, G., Brown, F. H., Guilderson, T., & Sirocko, F. (2000). Climate change and the collapse of the Akkadian empire: evidence from the deep sea. Geology, 28(4), 379-382.

d'Arrigo, R., Villalba, R., & Wiles, G. (2001). Tree-ring estimates of Pacific decadal climate variability. Climate Dynamics, 18(3-4), 219-224.

Dean, W. E. (1997). Rates, timing, and cyclicity of Holocene eolian activity in north-central United States: evidence from varved lake sediments. Geology, 25(4), 331-334.

Dean, W. E., Ahlbrandt, T. S., Anderson, R. Y., & Bradbury, J. P. (1996). Regional aridity in North America during the middle Holocene. The Holocene, 6(2), 145-155.

Diefendorf, A. F., Patterson, W. P., Mullins, H. T., Tibert, N., & Martini, A. (2006). Evidence for high-frequency late Glacial to mid-Holocene (16,800 to 5500 cal yr BP) climate variability from oxygen isotope values of Lough Inchiquin, Ireland. Quaternary research, 65(1), 78-86.

Dettinger, M. D., Cayan, D. R., Diaz, H. F., & Meko, D. M. (1998). North-south precipitation patterns in western North America on interannual-to-decadal timescales. Journal of Climate, 11(12), 3095-3111.

Dixit, Y., Hodell, D. A., & Petrie, C. A. (2014). Abrupt weakening of the summer monsoon in northwest India~ 4100 yr ago. Geology, 42(4), 339-342.

Drummond, C. N., Patterson, W. P., & Walker, J. C. (1995). Climatic forcing of carbon-oxygen isotopic covariance in temperate-region marl lakes. Geology, 23(11), 1031-1034.

Gasse, F. (2000). Hydrological changes in the African tropics since the Last Glacial Maximum. Quaternary Science Reviews, 19(1), 189-211.

Ge, Y., Gong, G., & Frei, A. (2009). Physical mechanisms linking the winter Pacific-North American teleconnection pattern to spring North American snow depth. Journal of Climate, 22(19), 5135-5148.

Ghil, M., Allen, M.R., Dettinger, M.D., Ide, K., Kondrashov, D., Mann, M.E., Robertson, A.W., Saunders, A., Tian, Y., Varadi, F., & Yiou, P. (2002). Advanced spectral methods for climatic time series. Reviews of Geophysics 40, p. 1-1–1-41.

Graham, N. E., & White, W. B. (1988). The El Niño cycle: a natural oscillator of the Pacific Ocean—atmosphere system. Science, 240(4857), 1293-1302.

Grinsted, A., Moore, J. C., & Jevrejeva, S. (2004). Application of the cross wavelet transform and wavelet coherence to geophysical time series. Nonlinear processes in geophysics, 11(5/6), 561-566.

Hare, S. R., & Francis, R. C. (1995). Climate change and salmon production in the Northeast Pacific Ocean. Canadian Special Publication of Fisheries and Aquatic Sciences, 357-372.

Hickman, M., & Schweger, C. E. (1996). The Late Quaternary palaeoenvironmental history of a presently deep freshwater lake in east-central Alberta, Canada and palaeoclimate implications. Palaeogeography, Palaeoclimatology, Palaeoecology, 123(1), 161-178.

Hogg, E. H. (1994). Climate and the southern limit of the western Canadian boreal forest. Canadian Journal of Forest Research, 24(9), 1835-1845.

Kim, S. T., & O'Neil, J. R. (1997). Equilibrium and nonequilibrium oxygen isotope effects in synthetic carbonates. Geochimica et Cosmochimica Acta, 61(16), 3461-3475.

Kupsch, W.O. (1956). The Geology of the Sturgeon Lake Marl Deposit. *In* Sturgeon Lake Marl Deposit. Report of Investigations no. 8. Province of Saskatchewan, Department of Mineral Resources.

L'Heureux, M. L., Kumar, A., Bell, G. D., Halpert, M. S., & Higgins, R. W. (2008). Role of the Pacific‐North American (PNA) pattern in the 2007 Arctic sea ice decline. Geophysical Research Letters, 35(20). L20701.

Leathers, D. J., Yarnal, B., & Palecki, M. A. (1991). The Pacific/North American teleconnection pattern and United States climate. Part I: Regional temperature and precipitation associations. Journal of Climate, 4(5), 517-528.

Leng, M. J., & Marshall, J. D. (2004). Palaeoclimate interpretation of stable isotope data from lake sediment archives. Quaternary Science Reviews, 23(7), 811-831.

Lewis Jr, W. M. (1983). A revised classification of lakes based on mixing. Canadian Journal of Fisheries and Aquatic Sciences, 40(10), 1779-1787.

Liu, J. & Qing, H. (2010): Oxygen and carbon isotopic geochemistry of dolomite in the Mississippian Midale strata, Steelman area, southeastern Saskatchewan; in Summary of Investigations 2010, Volume 1, Saskatchewan Geological Survey, Sask. Ministry of Energy and Resources, Misc. Rep. 2010-4.1, Paper A-3, 11p.

Liu, Z., Kennedy, C. D., & Bowen, G. J. (2011). Pacific/North American teleconnection controls on precipitation isotope ratios across the contiguous United States. Earth and Planetary Science Letters, 310(3), 319-326.

Liu, Z., Yoshimura, K., Bowen, G. J., Buenning, N. H., Risi, C., Welker, J. M., & Yuan, F. (2014). Paired oxygen isotope records reveal modern North American atmospheric dynamics during the Holocene. Nature Communications, 5. p. 3701.

MacDonald, G. M., & Case, R. A. (2005). Variations in the Pacific Decadal Oscillation over the past millennium. Geophysical Research Letters, 32(8). L08703.

Makou, M. C., Eglinton, T. I., Oppo, D. W., & Hughen, K. A. (2010). Postglacial changes in El Niño and La Niña behavior. Geology, 38(1), 43-46.

Mann, M. E., & Lees, J. M. (1996). Robust estimation of background noise and signal detection in climatic time series. Climatic Change, 33(3), 409-445.

Mantua, N. J., Hare, S. R., Zhang, Y., Wallace, J. M., & Francis, R. C. (1997). A Pacific interdecadal climate oscillation with impacts on salmon production. Bulletin of the American Meteorological Society, 78(6), 1069-1079.

Mantua, N. J., & Hare, S. R. (2002). The Pacific decadal oscillation. Journal of oceanography, 58(1), 35-44.

Menounos, B., Clague, J. J., Osborn, G., Luckman, B. H., Lakeman, T. R., & Minkus, R. (2008). Western Canadian glaciers advance in concert with climate change circa 4.2 ka. Geophysical Research Letters, 35(7). L07501.

Moore, J. E. (1952). The entomostraca of southern Saskatchewan. Canadian Journal of Zoology, 30(6), 410-450.

Moy, C. M., Seltzer, G. O., Rodbell, D. T., & Anderson, D. M. (2002). Variability of El Niño/Southern Oscillation activity at millennial timescales during the Holocene epoch. Nature, 420(6912), 162-165.

Mudelsee, M., Scholz, D., Röthlisberger, R., Fleitmann, D., Mangini, A., & Wolff, E. W. (2009). Climate spectrum estimation in the presence of timescale errors. Nonlinear Processes in Geophysics, 16(1), 43-56.

Mudelsee, M., Fohlmeister, J., & Scholz, D. (2012). Effects of dating errors on nonparametric trend analyses of speleothem time series. Climate of the Past, 8(5), 1637-1648.

Nelson, D.B., Abbott, M.B., Steinman, B., Polissar, P.J., Stansell, N.D., Ortiz, J.D., Rosenmeier, M.F., Finney, B.P., & Riedel, J. (2011). Drought variability in the Pacific Northwest from a 6,000-yr lake sediment record. Proceedings of the National Academy of Sciences 108, p. 3870–3875.

Rawson, D.S., & Moore, J.E. (1944). The saline lakes of Saskatchewan. Canadian Journal of Research, D, 22, 141–201.

Rein, B., Lückge, A., Reinhardt, L., Sirocko, F., Wolf, A., & Dullo, W. C. (2005). El Niño variability off Peru during the last 20,000 years. Paleoceanography, 20(4). PA4003.

Rhines, A., & Huybers, P. (2011). Estimation of spectral power laws in time uncertain series of data with application to the Greenland Ice Sheet Project 2 $\delta^{18}O$ record. Journal of Geophysical Research: Atmospheres, 116(D1).

Schwalb, A., & Dean, W. E. (2002). Reconstruction of hydrological changes and response to effective moisture variations from North-Central USA lake sediments. Quaternary Science Reviews, 21(12), 1541-1554.

Shabbar, A. (2006). The impact of El Niño-Southern oscillation on the Canadian climate. Advances in Geosciences, 6, 149-153.

Shabbar, A., Bonsal, B., & Khandekar, M. (1997). Canadian precipitation patterns associated with the Southern Oscillation. Journal of Climate, 10(12), 3016-3027.

Shabbar, A., & Khandekar, M. (1996). The impact of El Niño‐Southern Oscillation on the temperature field over Canada: Research note. Atmosphere-Ocean, 34(2), 401-416.

Stuiver, M. (1968). Oxygen-18 content of atmospheric precipitation during last 11,000 years in the Great Lakes region. Science, 162(3857), 994-997.

Talbot, M. R. (1990). A review of the palaeohydrological interpretation of carbon and oxygen isotopic ratios in primary lacustrine carbonates. Chemical Geology: Isotope Geoscience Section, 80(4), 261-279.

Thomson, D.J. (1982). Spectrum estimation and harmonic analysis. Proceedings of the IEEE 70, 1055-1096.

Torrence, C., & Compo, G. P. (1998). A practical guide to wavelet analysis. Bulletin of the American Meteorological Society, 79(1), 61-78.

Trouet, V., & Taylor, A. H. (2010). Multi-century variability in the Pacific North American circulation pattern reconstructed from tree rings. Climate Dynamics, 35(6), 953-963.

Valero-Garcés, B. L., Laird, K. R., Fritz, S. C., Kelts, K., Ito, E., & Grimm, E. C. (1997). Holocene climate in the Northern Great Plains inferred from sediment stratigraphy, stable isotopes, carbonate geochemistry, diatoms, and pollen at Moon Lake, North Dakota. Quaternary Research, 48(3), 359-369.

Vance, R. E., Mathewes, R. W., & Clague, J. J. (1992). 7000-year record of lake-level change on the northern Great Plains: A high-resolution proxy of past climate. Geology, 20(10), 879-882.

Walker, M.J.C., Berkelhammer, M., Bjorck, S., Cwynar, L.C., Fisher, D.A., Long, A.J., Lowe, J.J., Newnham, R.M., Rasmussen, S.O., & Weiss, H. (2012). Formal subdivision of the Holocene Series/Epoch: A discussion paper by a working group of INTIMATE (Integration of ice-core, marine and terrestrial records) and the Subcommission on Quaternary Stratigraphy (International Commission on Stratigraphy). Journal of Quaternary Science 27, 649–659.

Wallace, J. M., & Gutzler, D. S. (1981). Teleconnections in the geopotential height field during the Northern Hemisphere winter. Monthly Weather Review, 109(4), 784-812.

Wolfe, S. A., Ollerhead, J., Huntley, D. J., & Lian, O. B. (2006). Holocene dune activity and environmental change in the prairie parkland and boreal forest, central Saskatchewan, Canada. The Holocene, 16(1), 17-29.

Yu, Z., Campbell, I. D., Campbell, C., Vitt, D. H., Bond, G. C., & Apps, M. J. (2003). Carbon sequestration in western Canadian peat highly sensitive to Holocene wet-dry climate cycles at millennial timescales. The Holocene, 13(6), 801-808.

Zhang, Z., Leduc, G., & Sachs, J. P. (2014). El Niño evolution during the Holocene revealed by a biomarker rain gauge in the Galápagos Islands. Earth and Planetary Science Letters, 404, 420-434.

Table 3.1: Radiocarbon Dates

Core Depth (cm)	Conventional Radiocarbon Age (14C yr BP)	Material Dated	Laboratory Code	Calibrated Age yr BP (2σ confidence interval)
0	1.1844*	Plant Material	GdA-1496	1958.61-1959.2 & 1960.03-1960.04 & 1985.81-1988.82 & 1989.03-1989.05
12.5	1.0051*	Plant Material	GdA-1495	1951.95-1956.18
17.5	1.0148*	Plant Material	GdA-1494	1953.33-1956.27
236.5	4700±50	Plant Material	GdA-1493	5318-5486 & 5508-5581
245	4395±40	Plant Material	GdA-1492	4855-5057 & 5114-5116 & 5187-5214 & 5223-5236 & 5243-5262
264.5	4790±40	Plant Material	GdA-1491	5333-5348 & 5353-5362 & 5366-5371 & 5464-5601
347.7	5645±40	Plant Material	GdA-1490	6314-6498
392.5	5980±40	Plant Material	GdA-1489	6699-6700 & 6722-6937

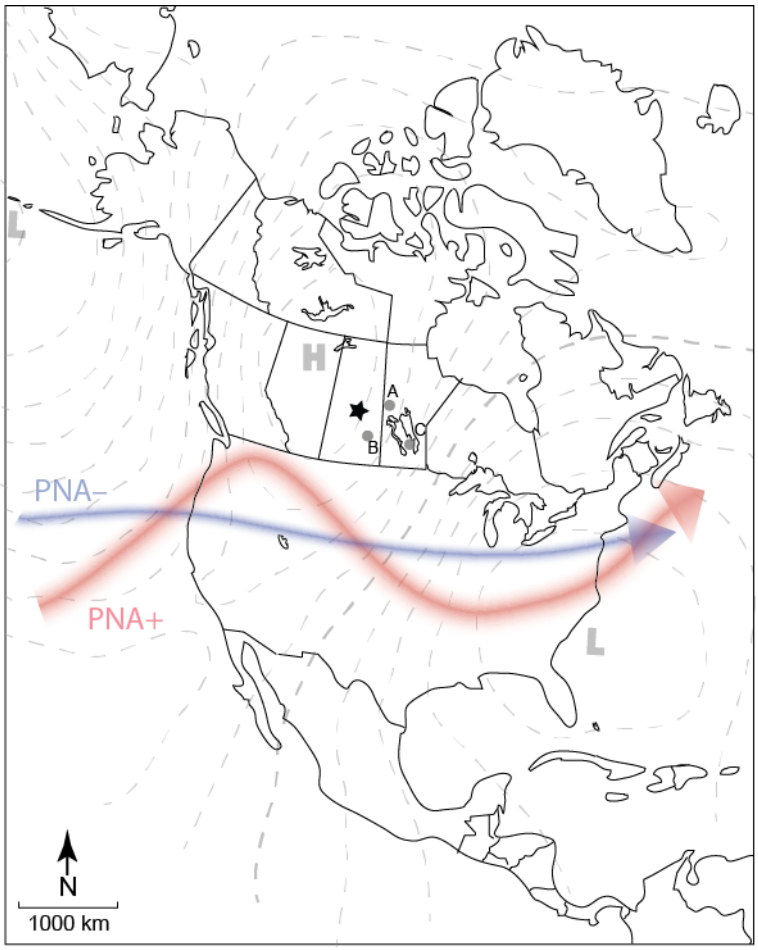

Figure 3.1: Location of study site (star) in relation to three of the four "centers of action" of the PNA pattern (light grey dashed lines) based on Barnston and Livezey, (1987) and the state of 700mb flow under PNA+ and PNA– conditions based (Leather et al., 1991). The three GNIP locations are shown (grey circles): A. The Pas, B. Wynyard, C. Gimli.

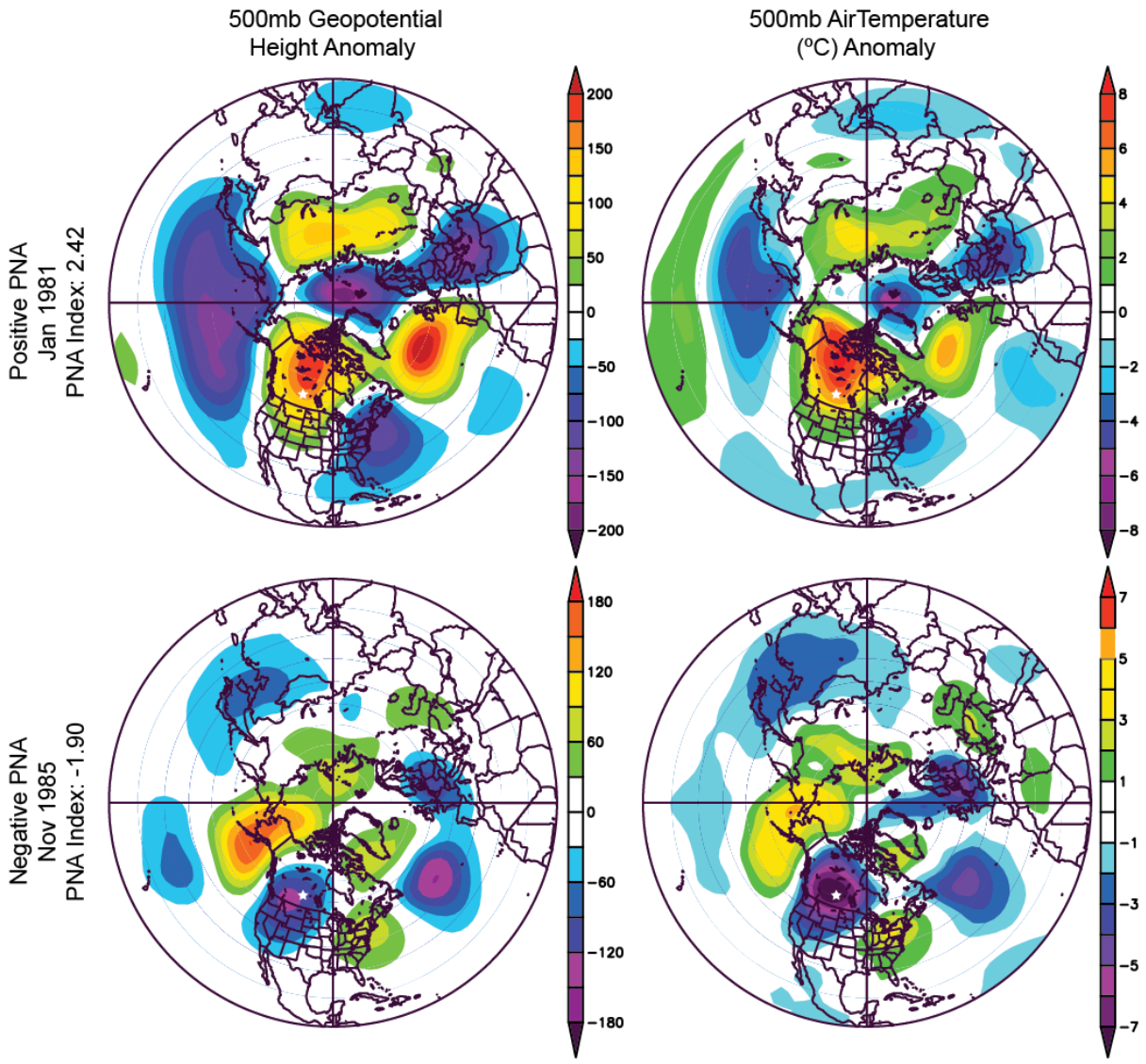

Figure 3.2: NCEP/NCAR reanalysis composite anomaly maps for PNA+ and PNA– states including 500mb geopotential heights and 500mb air temperatures. Study site denoted by white star. Note proximity of study site to the center of the PNA dipole.

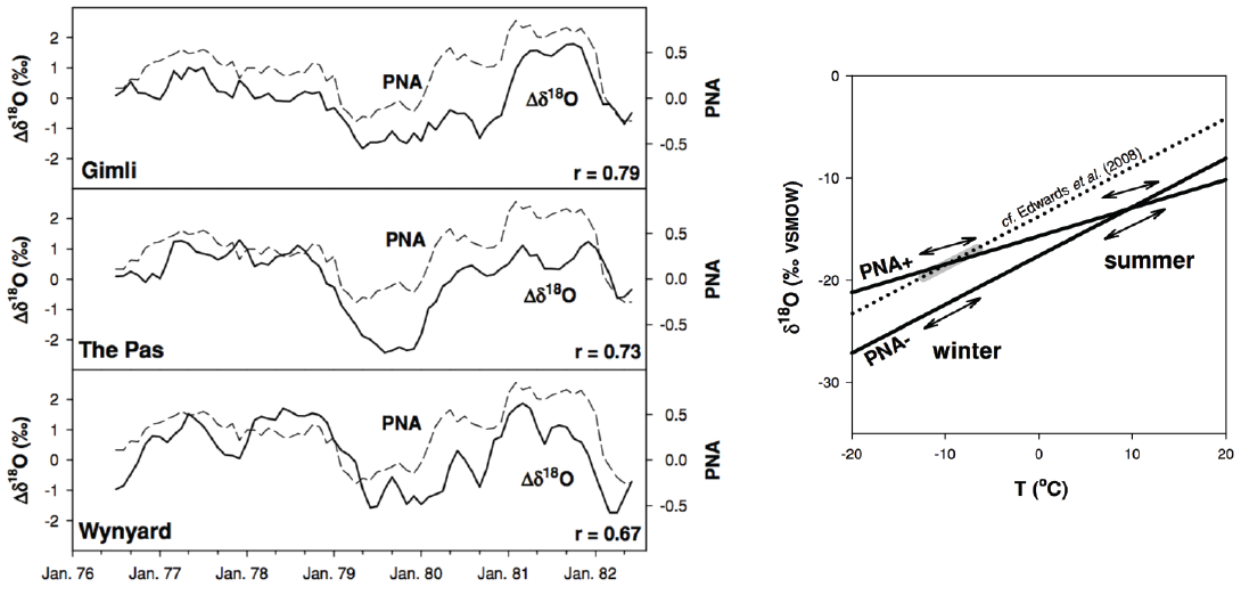

Figure 3.3: $\Delta\delta^{18}O$ plotted with the state of PNA for three GNIP stations (shown in Fig. 1) showing the strong correlation between isotope anomalies and the PNA Index (reproduced from Birks and Edwards, 2009); Changes in the Dansgaard $\delta^{18}O$-temp relationships based on the state of the PNA index (reproduced from Birks and Edwards, 2009).

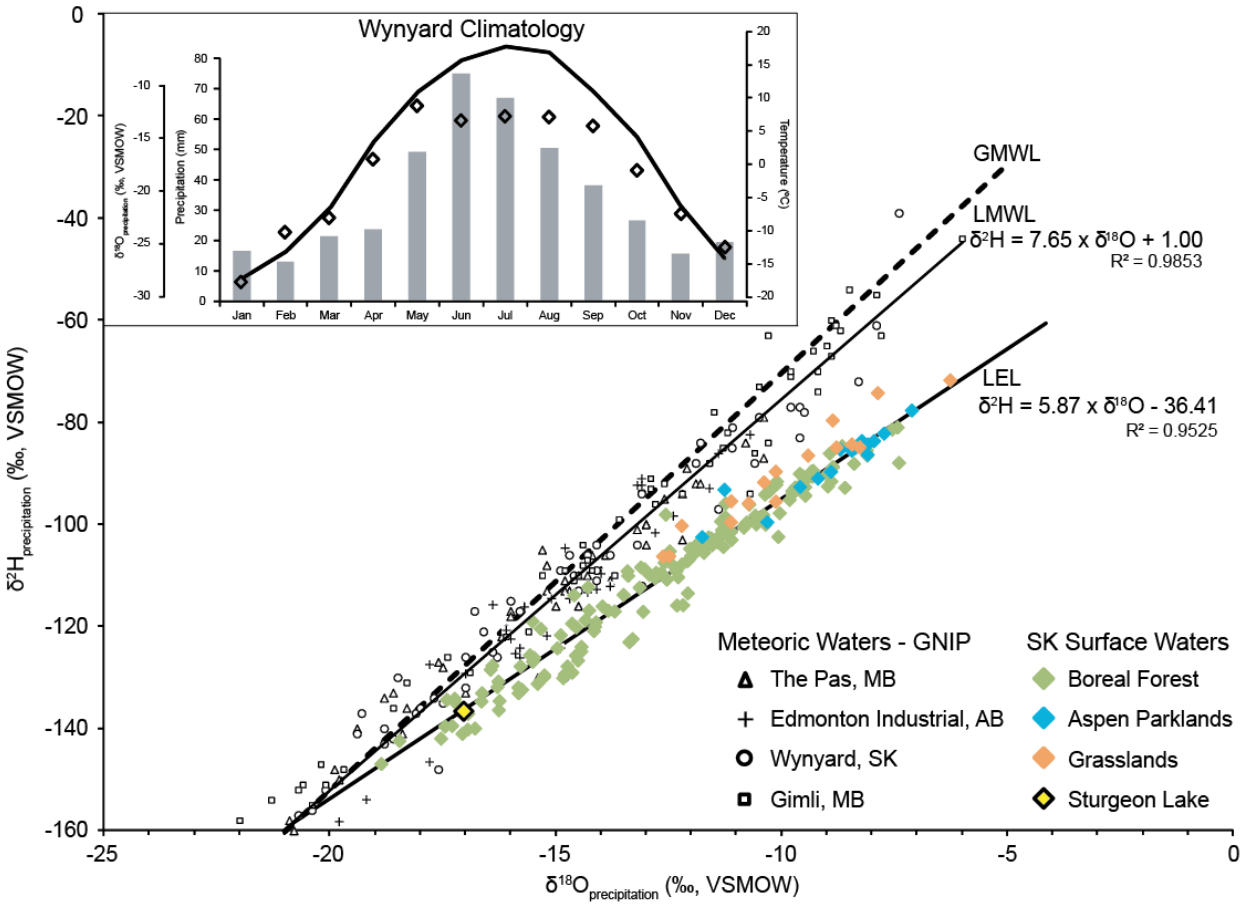

Figure 3.4: Hydrogen and oxygen isotope values of surficial waters from Saskatchewan. Inset: Climatology of Wynyard plotted alongside average GNIP isotope values of precipitation. GMWL: global meteoric water line; LMWL: local meteoric water line; LEL: local evaporation line.

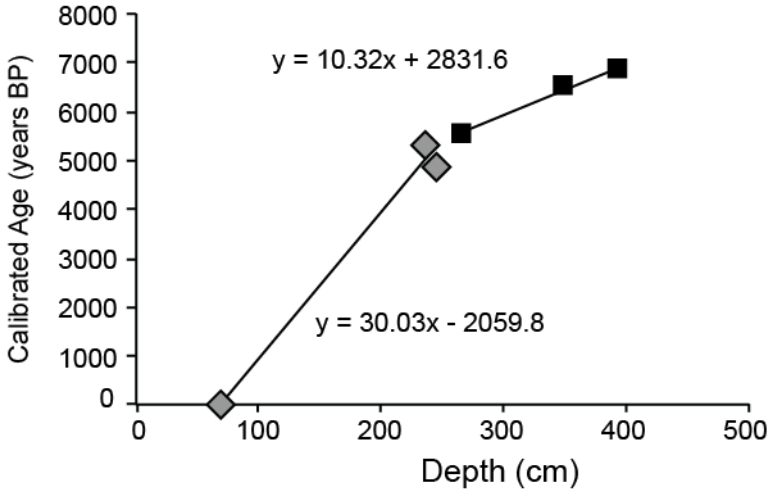

Figure 3.5: Age model of Sturgeon Lake core based on seven radio-carbon dates.

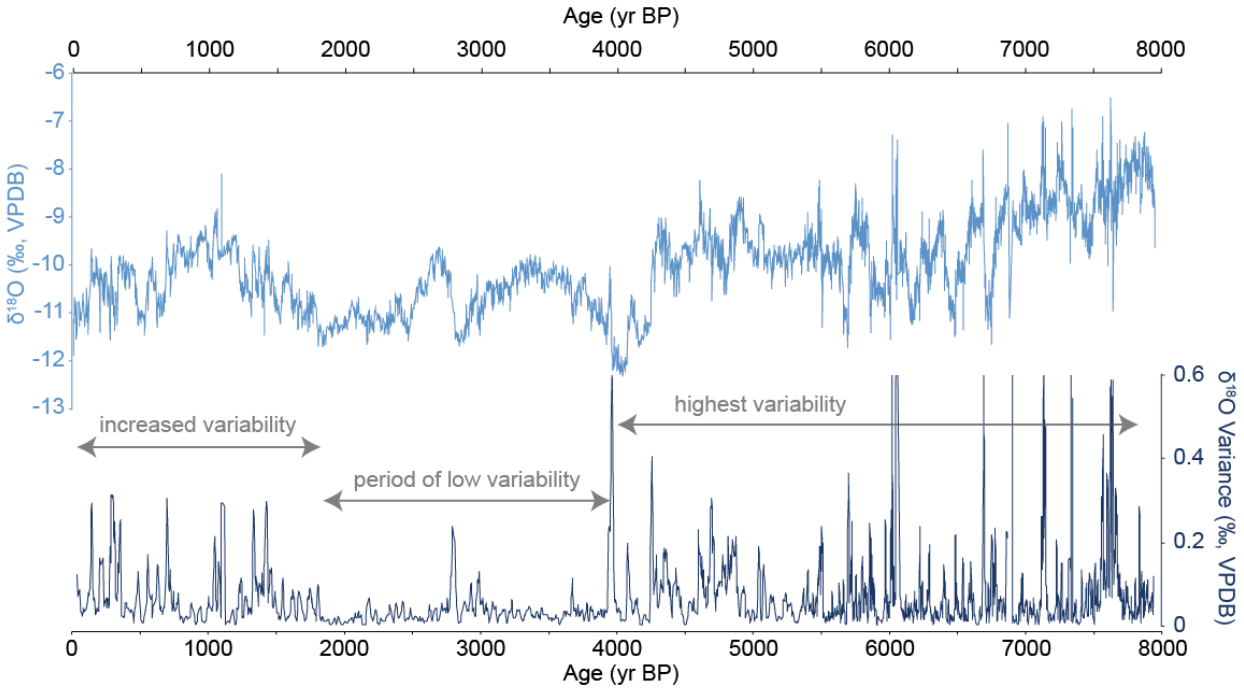

Figure 3.6: Sturgeon Lake carbonate $\delta^{18}O$ values plotted against time along with 30-year variance in $\delta^{18}O$ values.

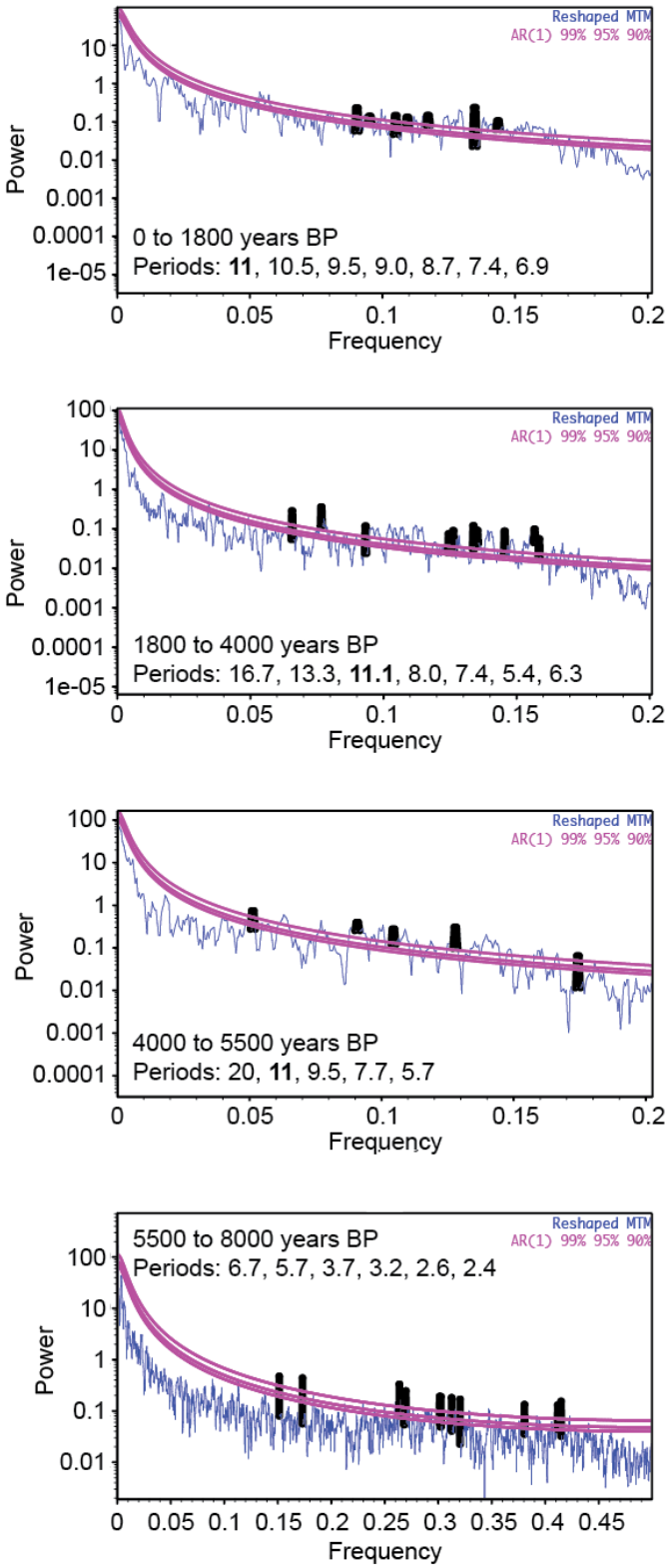

Figure 3.7: Multi Taper Method spectral analysis of four time slices of the Sturgeon Lake $\delta^{18}O$ values. See text for details.

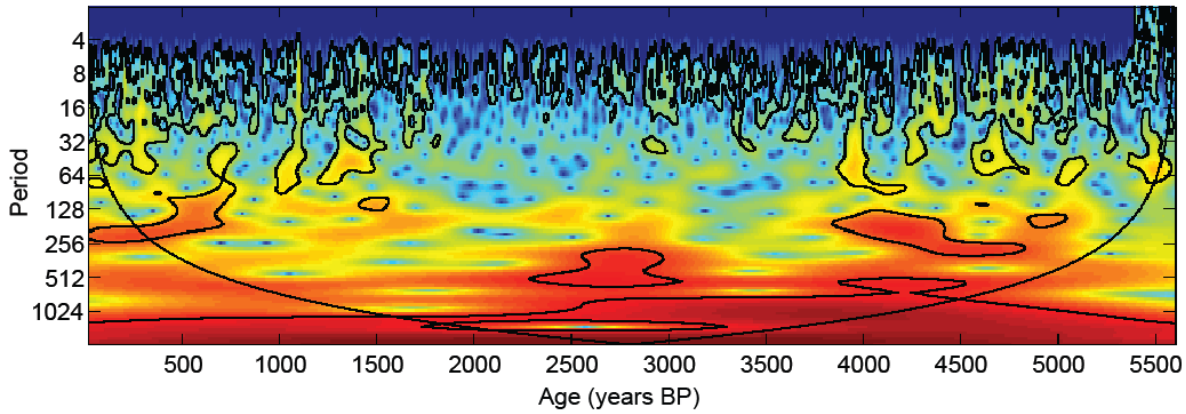

Figure 3.8: Wavelet analysis of the final 5,600 years of the Sturgeon Lake $\delta^{18}O$ record. Strong spectral power is represented by warm colors and cool colors of weak strength. The solid cone denotes the areas where edge effects due to time series anaysis method become problematic. Areas enclosed by solid black lines represent regions where spectral strength is greater than the red noise signal. Note the decrease in the multidecadal band during the period from ~4,000-1,800 years BP. See text for more details.

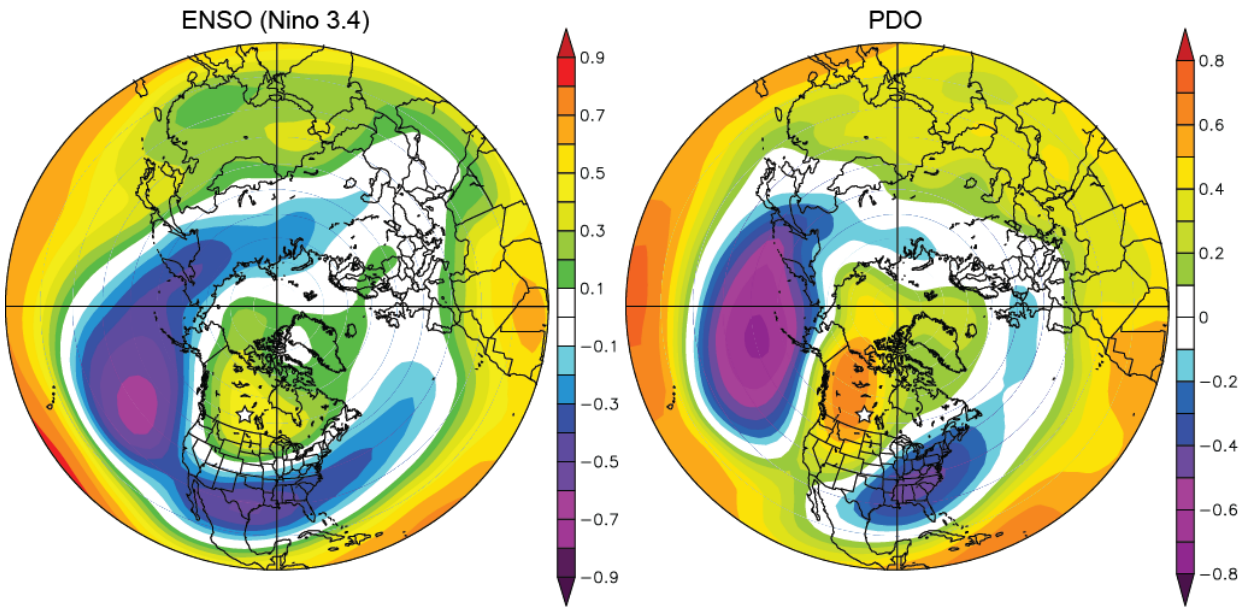

Figure 3.9: NCEP/NCAR reanalysis of the seasonal correlation of (a) ENSO (based on the Nino 3.4 index) and (b) PDO with December to February 500mb geopotential heights. Note similarities between the expression of the PNA and the 500mb geopotential height pattern, compare with Fig. 2.

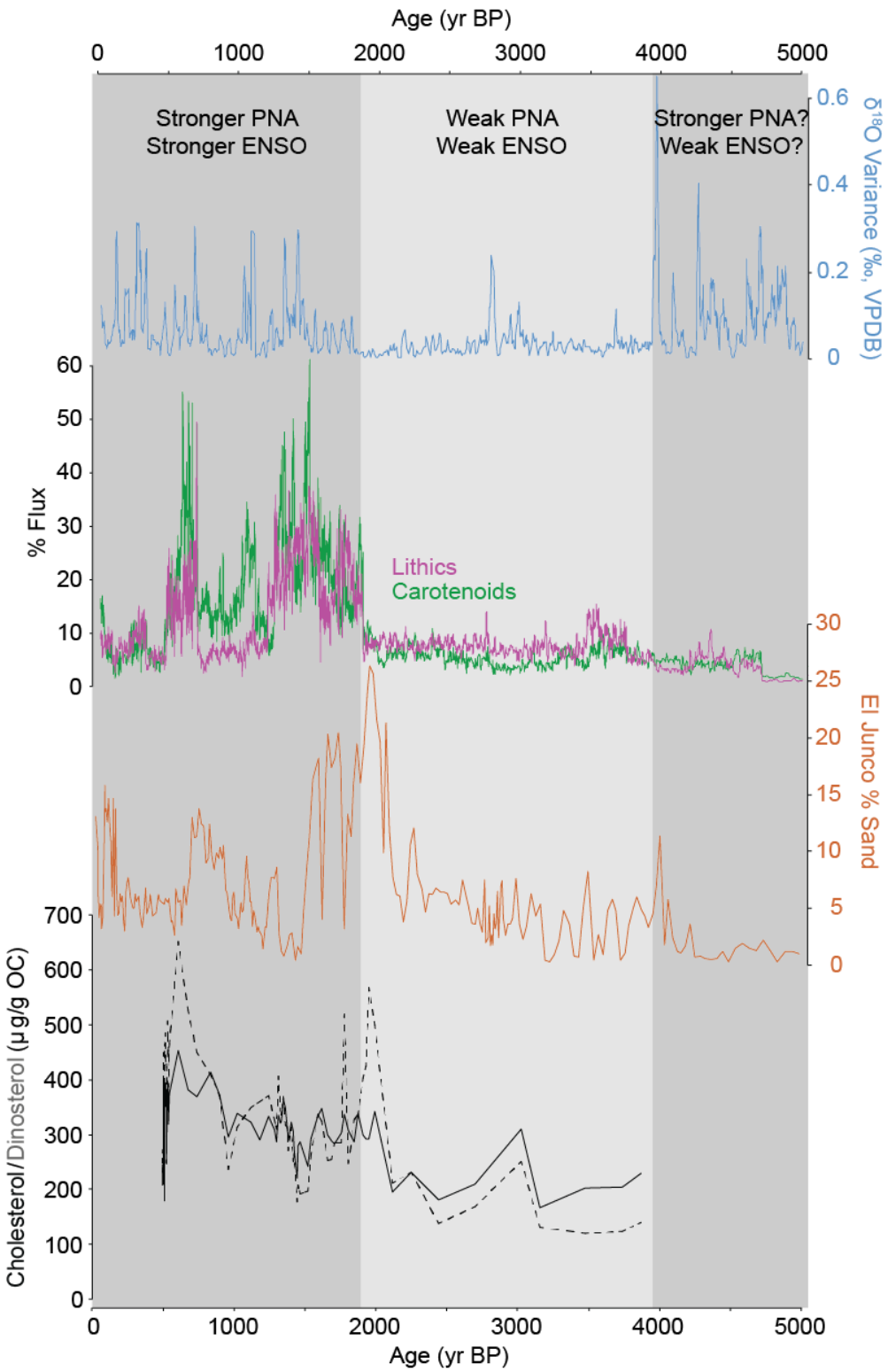

Figure 3.10: Sturgeon Lake $\delta^{18}O$ variability and Holocene records of ENSO variability. A. Sturgeon Lake $\delta^{18}O$ variability. B. Peru marine sediment record (Rein et al., 2005). C. Galápagos lake sediment record (Conroy et al., 2008). D. Ocean productivity biomarkers from Peru margin region (Makou et al., 2010).

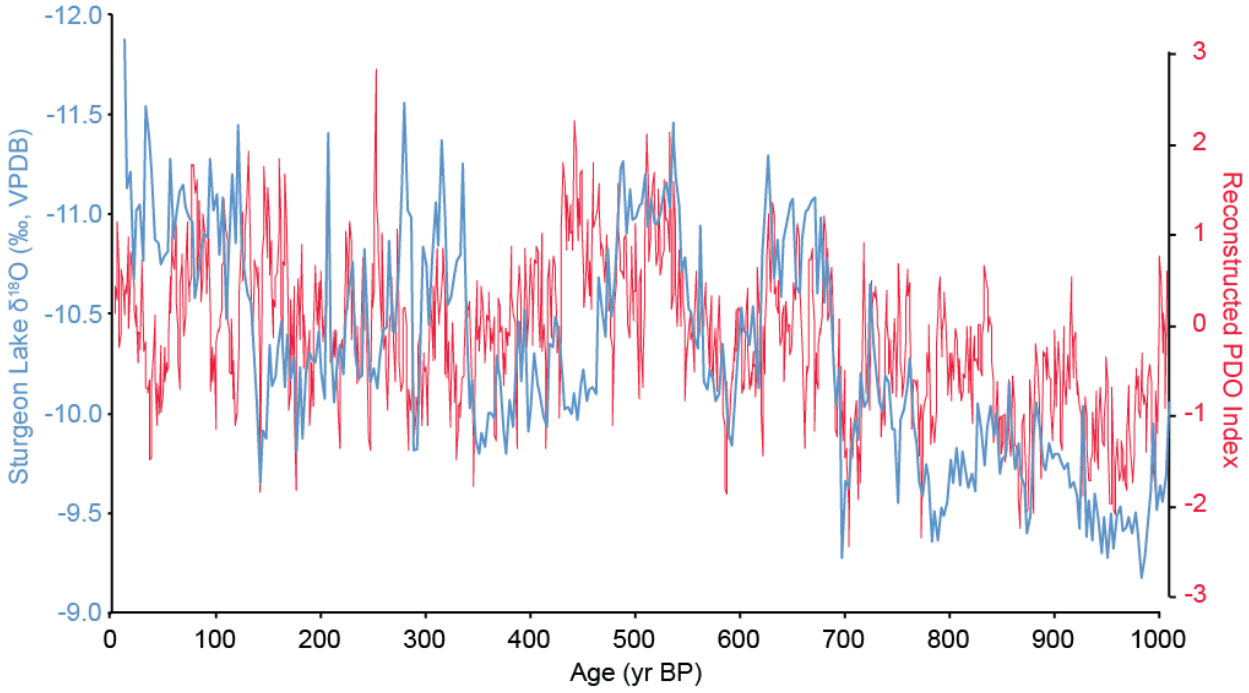

Figure 3.11: Reconstruction of PDO over the past 1000 years based on coupled tree-ring data (Macdonald and Case, 2005) plotted alongside Sturgeon Lake $\delta^{18}O$ values. Note inverted scale on the Sturgeon Lake $\delta^{18}O$ data series.

CHAPTER 4
ORIGIN OF SHELL-RICH DEPOSITS: EVIDENCE FROM SEASONAL VARIATIONS IN STABLE ISOTOPE VALUES OF BIVALVE SHELLS

4.1 Abstract

In this study, seasonality of shells within a shell-rich sedimentary unit are used to determine the likely origin of a sedimentary unit suspected to be a tsunami deposit. Tsunami events deposit sedimentary units that can be difficult to distinguish from storm deposits using standard sedimentological techniques alone. The seasonality of "single-event" sedimentary units can provide insight into their origin by comparing the season of deposition with historical records of storms and tsunamis because oxygen and carbon isotope profiles from bivalves record environmental conditions during growth to the time of death. By analyzing the environmental conditions at the time of death we can determine the season of the depositional event. Comparison of the season of the event with historical records of large storms and tsunamis determines the likelihood as to whether a particular deposit is tsunamigenic or a storm event. Using three different species of bivalves from the suspected tsunamite at Sur, Sultanate of Oman we observe a late spring to early summer timing of deposition. Comparison of this timing with historic tsunami and large storm events suggests that the large tropical cyclone of 1890CE is the likely source of this deposit.

Keywords: Tsunami deposit; tempestite; oxygen isotope; carbon isotope; bivalvia

4.2 Introduction

Determination of the depositional nature of shell-rich units in the geologic record can be problematic. Distinguishing between storm deposits, tsunamites, and lag deposits can be difficult based on sedimentary characteristics alone and therefore additional techniques that may provide further insight into the depositional characteristics of shell-rich units would be of great value. Seasonality records of a population of bivalves within a shell-rich unit can potentially provide information on both the season of deposition and potentially the length of time a deposit took to form. Studies of seasonal variation in $\delta^{18}O$ values of shells have been used extensively to assess long and short-term variations of water temperature in climatic and oceanographic applications,

but studies applying the use of seasonal variation in $\delta^{18}O$ values of bivalves to infer depositional characteristics of shell-rich units are lacking. In this study, a technique is presented for utilizing seasonal records from bivalves for sedimentological analysis of shell-rich deposits to develop an understanding of the processes responsible for unit formation. Differences in the development of shell-rich overwash deposits by single-event processes such as storms, tsunamis, mass mortality, etc., will impart seasonality profiles that are distinct from slow processes such as winnowing and lag deposit formation.

Tsunamis and large coastal storm events can have disastrous effects on coastal populations. The catastrophic Indian Ocean tsunami on December 26th, 2004; Hurricane Katrina in 2005; and the March 11th, 2011 tsunami in Japan represent three recent examples of coastal events that caused extensive damage to coastal economies, infrastructure, and high death-tolls among populations. The ability to link storm and tsunami deposits with specific storms, or tsunami events could aid in determining periodicity of such events and improve risk assessment. In addition, characterization of large storm and tsunami events in the past is essential for our understanding of how future events may affect coastal areas (*e.g.* Dunbar and Weaver, 2008). Critical to this is the ability to correlate events with specific deposits in the geologic record. This could help determine how storm tracks, earthquake magnitude, and landslide size, as well as geographic location are related to sediment deposition at specific sites, better quantifying risk assessments of coastal environments. This is particularly relevant in areas that lack long-term historic records (*e.g.* the Americas) where it would be possible to link local tempestites (storm deposits) and tsunamites (tsunami deposits) with events in areas with longer historical records (*e.g.* Asia and Europe).

Traditional radiometric dating techniques can provide useful ranges in age but typically have errors on the order of 50-100 years that in regions prone to storms and seismic activity may bracket multiple events. However, using a combination of radiometric dating and a sub-seasonal microanalytical technique we can determine both the absolute age and season of the event, thereby providing much tighter constraints, linking deposits with specific events. Dendrochronology has been used as a sub-seasonal dating technique in the past (*e.g.* Jacoby *et al.*, 1997; Atwater *et al.*, 2005) but its use is limited to sites containing multiple trees that survived the event and are still well preserved. Bivalves, however, are abundant in coastal regions and are often incorporated in tsunamites (Hindson and Andrade, 1999; Hindson *et al.*,

1999; Kortekaas and Dawson, 2007; Donato *et al.*, 2008) and tempestites (Jelgersma *et al.*, 1995; Kortekaas and Dawson, 2007; Morton *et al.*, 2007). Because environmental conditions are recorded in the stable-isotope geochemistry of bivalve shells (*e.g.* Krantz *et al.*, 1987), shell chemistry profiles can be developed that characterize the season of death. Additionally, shell carbonate often has a greater preservation potential than wood and can therefore be utilized not only to evaluate the historic record, and over geologic timescales as bivalve isotope seasonality is known to preserve in deep geologic time (*e.g.* Ivany and Runnegar, 2010).

As bivalves grow they are sequentially secreting shell carbonate along the margins of their shells, thereby archiving environmental conditions through time. Shell oxygen isotope values ($\delta^{18}O_{shell}$) are controlled by water temperature and the oxygen isotope value of ambient water (*e.g.* Epstein *et al.*, 1953; Grossman and Ku, 1986). Bivalves secrete shell carbonate in isotopic equilibrium except for a limited number of species (*e.g.* Fastovsky *et al.*, 1993). Carbon isotope values of bivalve shells ($\delta^{13}C_{shell}$) are predominantly controlled by the carbon isotope value of dissolved inorganic carbonate ($\delta^{13}C_{DIC}$) with offsets related to diet and metabolism, as well as bivalve physiology (Tanaka *et al.*, 1986; McConnaughey *et al.*, 1997; Wurster and Patterson, 2001; Lorrain *et al.*, 2004; Gillikin *et al.*, 2006, 2007, 2009; McConnaughey and Gillikin, 2008; Poulain *et al.*, 2010). Therefore, $\delta^{18}O_{shell}$ values from shallow water species should provide a record of sea surface temperatures (SSTs) and $\delta^{18}O$ values of seawater while $\delta^{13}C_{shell}$ serves as a proxy for $\delta^{13}C_{DIC}$ values and metabolism.

To assess the potential of this technique we address two hypotheses: (1) stable isotope profiles derived from bivalves can be used to determine the season of deposition of this shell-rich unit; and (2) using the season of deposition information in collaboration with historic archives of large storms and tsunamis, we can infer information about the mechanism responsible for deposition of this shell-unit by corroborating the geologic and historical records. In order to accomplish this, it must first be demonstrated that (a) seasonal changes in environmental conditions are faithfully recorded in bivalve shell isotope records; and (b) that these specimens lived contemporaneously. To assess whether bivalves are accurately recording environmental conditions a comparison of measured SSTs and $\delta^{18}O_{shell}$ –calculated temperatures is first preformed. If environmental conditions are accurately recorded, the range in measured SST and SST calculated from carbonate should be similar. Determination of whether the bivalves lived concurrently is evaluated by comparing the temporal variability in $\delta^{18}O_{shell}$ profiles and timing of death. This

includes a comparison of the coherence of seasonal $\delta^{18}O_{shell}$ minima and maxima as well as other minor trends in the profiles that should be similar in contemporaneous individuals.

4.2.1 Theoretical Framework

Tsunamis and large storms are high-energy events that can transport and deposit a large amount of sediment. Bivalve species inhabiting the littoral zone can be incorporated into, and entombed by, the resulting deposits. The transportation process can have two outcomes, either: (a) the bivalves are buried within the deposit and expire, thereby preserving the season of the event as the timing of death (*i.e.* at the shell margin); or (b) they survive the event and are transported to another distinct environment where their isotopic geochemistry can incur a significant (measurable) change (*c.f.* McConnaughey and Gillikin, 2008). Accurate assessment of changes in isotope values due to relocation requires an understanding of the environmental isotope geochemistry at both the source and depositional areas. This can be accomplished by analyzing bivalves from both the autochthonous (at the site of the tsunamite) and allochthonous environments. Therefore, it is desirable to have species from several habitats (*i.e*. offshore marine and lagoonal). We have included offshore bivalves as well as lagoonal species known to live at the site of deposition.

Articulated bivalves are targeted, as they are assumed to have undergone transportation *alive* and therefore record environmental conditions up until the transportation event. Disarticulated specimens could have expired previous to the storm or tsunami event and therefore would not be indicative of the conditions at the timing of the event. It is assumed that the high-energy of the storm or tsunami wave(s) will dislodge any previously expired articulated valves transported by the event.

4.3 Study Site

4.3.1 Sur Lagoon, Sultanate of Oman

Sur (22°35’03N, 59°31’55E) is located on the Northeastern coast of the Sultanate of Oman in the Arabian Sea, in the northern Indian Ocean (Fig. 4.1). The Sur lagoon is a roughly horseshoe shaped lagoon located adjacent to the town of Sur (Fig. 4.2). The lagoon is microtidal (~1.2 m) with surface elevations varying by about ±2 m above mean sea level (Donato *et al.*, 2008b).

Sediment is dominated by very-fine sand on the lagoon surface and mud in the mangroves and elevated lagoonal margins.

The Arabian Sea experiences biannual monsoons, with the stronger summer/southwest monsoon (June-September) occurring when southeasterly surface winds from the southern hemisphere expand into the northern hemisphere becoming southwesterlies (Hamilton, 1979). During the southwest monsoon, the Somali current increases and parallels the Omani coast, causing strong upwelling of nutrient-rich waters along the coast that lead to the formation of phytoplankton blooms in the summer months (Brock and McClain, 1992) and some cooling of surface waters (Colburn, 1975). Most severe cyclone activity experienced by the Sultanate of Oman is related to the southwest monsoon. The winter/northeast monsoon (November-March) comes upon the reversal of these winds, but is typically less intense than the summer/southwest monsoon (Cadet and Diehl, 1984).

4.3.2 The Tsunamite

The lagoonal sediment at Sur includes a deposit previously interpreted by Donato *et al*. (2008a, 2008b) as a tsunamite based on shell taphonomy and particle size distribution. This interpreted tsunamite contains abundant whole and fragmented bivalve shell material, including several species from different ecological settings (*e.g*. offshore, lagoonal, deep burrowing, etc.). Test pits and cores excavated in the Sur lagoon recovered a laterally extensive shell-rich unit. This unit contained high proportions of allochthonous species with articulated valves, in addition to lagoonal species (Donato *et al*., 2008a). Shell taphonomy was dominated by angular fragmentation, damage associated with shell on shell impacts and turbulent flow. Shells had minimal evidence of edge rounding or encrustation suggesting rapid burial with minimal exposure. Sedimentological analysis (particle-size distributions) (Donato *et al.*, 2008b) subsequently showed the tsunamite to be poorly sorted, and more heterogeneous than normal lagoonal sediment. Moreover, particle size analysis indicated textual trends in the tsunami unit suggesting multiple phases of sedimentation consistent with other tsunamigenic deposits. Detailed images of the deposit are shown in Donato *et al*. (2008b).

4.3.3 Tsunamis Events in Oman

At least seven tsunami events are known to have occurred in the Arabian Sea during the last ~200 years. A compilation of these events including date, source location, wave height and a short description detailing the likely effects on the coast of Oman is provided in Table 4.1. Most of these events likely had minimal effects on the Omani coasts. The tsunami event most likely to have had serious effects on the Omani coast was one on November 28th, 1945. This event was caused by an 8.1 Mw thrust earthquake on the Makran subduction zone off the coast of Pakistan that triggered a tsunami, causing extensive damage and more than 4,000 deaths in Pakistan, Iran, western India, and Oman (Pararas-Carayannis, 2006). The epicenter was on the coast of Pakistan, approximately 550 km northeast of Sur. Although historical records of tsunami occurrence on the Omani coast are limited; damage caused by the 1945 tsunami were reported at Sur (Ambraseys and Melville, 1982, p. 89). Numerical modeling of this event has been conducted by several authors including Dominey-Howes *et al*. (2007) who suggest that minimal effects would have been observed on the Omani coast; and Heidarzadeh *et al*. (2008) who found runups of about 0.5 m were possible. Evidence of larger wave heights (~3 m) have come from one eyewitness account (Okal, personal communication, 2008; in Heidarzadeh *et al.*, 2008).

4.3.4 Bivalve Species

Three bivalve species were examined in this study *Paphia* (*Protapes) sinuosa* (Lamarck, 1818), *Tellina (Quidnipagus) palatum* (Iredale, 1929), and *Anodontia edentula* (Linnaeus, 1758), (Fig. 4.2). *P. sinuosa* is an infaunal offshore species (Bosch *et al.*, 1995) with an aragonitic shell inhabiting the offshore subtidal marine zone (Bosch *et al.*, 1995). *T. palatum* is also an infaunal offshore species (Bosch *et al.*, 1995) with an aragonitic shell, known to burrow deeply (Gibbs, 1978). Stable isotope records from *P. sinuosa* and *T. palatum* should reflect offshore marine environmental conditions and therefore $\delta^{18}O_{shell}$–calculated temperatures can be compared with measured local sea surface temperatures to evaluate the ability of bivalve oxygen isotope profiles to record the full seasonal range of temperatures measured. *A. edentula* is an infaunal lagoonal/mangrove species living in fine grain sediment ~1m below the sediment surface within the exaerobic zone (Primavera *et al.*, 2002). Isotopic profiles from *A. edentula* provide a record of environmental conditions at or near the site of sampling trench therefore representing the autochthonous species in this study. Individuals that survive the transportation event and

continue to secrete shell carbonate after burial should re-equilibrate shell chemistry to an isotopic composition similar to that of *A. edentula*.

4.4 Methods

4.4.1 *Sample Collection and Micromilling*

Articulated bivalves were directly sampled from the shell-rich unit exposed in test pits dug into Sur Lagoon (Fig. 4.2). Multiple specimens of three different species were collected for isotopic analysis. A total of eight bivalve specimens were analyzed in this study. Left and right valves were separated and cleaned with deionized water in an ultrasonic bath. Right valves were affixed to glass microscope slides and the surface of the shell to be sampled was removed in order to eliminate potential adhering organic contaminates or surface features that may interfere with micromilling or sampling procedures. A custom computer-controlled robotic micromilling apparatus (Wurster et al., 1999) was used to mill samples at a high spatial resolution concordant with growth banding (Fig. 4.3). Bivalve slides are placed on the three-dimensional micropositioning stage below a fixed high-precision dental drill. Growth banding is digitized and characterized by cubic splines that are used to calculate the desired number of intermediate 3D sampling paths.

4.4.2 $\delta^{18}O$ and $\delta^{13}C$ Analyses of Carbonates

Carbonate samples are collected in stainless steel cups and roasted *in vacuo* at 200°C for one hour to remove water and volatile organic contaminants that may interfere with the isotopic values of carbonates. All stable isotope analyses were obtained using a Finnigan Kiel-IV carbonate preparation device directly coupled to the dual-inlet sample introduction system of a Finnigan MAT 253 isotope ratio mass spectrometer in the Saskatchewan Isotope Laboratory, University of Saskatchewan. Twenty to fifty micrograms of carbonate were reacted at 75°C with three drops of anhydrous (100%) phosphoric acid for 420 seconds. The evolved CO_2 is then cryogenically purified before being passed to the mass spectrometer for analysis. Isotope ratios are corrected for acid fractionation and ^{17}O contribution using the Craig correction (Craig, 1957), and reported in standard delta notation relative to the VPDB scale. Data is directly calibrated against the international standard NBS-19. Precision and accuracy of data is monitored through

the routine analysis of NBS-19, and in-house standards that have been calibrated against NBS-19. Precision/accuracy of $\delta^{13}C$ and $\delta^{18}O$ values is 0.05‰ and 0.11‰ respectively.

4.4.3 Adjustments to $\delta^{18}O_{shell}$ Profile Abscissa

The abscissa of each $\delta^{18}O_{shell}$ value has been initially assigned a value equal to its order in the sampling sequence, or sample number. This was subsequently adjusted to account for variable growth rates between bivalves by matching the positions of seasonal minima and maxima in $\delta^{18}O_{shell}$ values on the abscissa axis. Growth rates can vary significantly, even among a population of sessile bivalves in close proximity due to their age, food availability, resource competition, and predation (Schöne *et al.*, 2003; Peterson, 1982). We use the software program Analyseries (Paillard *et al.*, 1995), that utilizes a combination of user selected "tie points" and an algorithm to adjust the time axis of multiple specimens to a common time scale. By this method, the abscissa of one profile series can be matched to a reference series. The reference series is denoted as the solid line in all bivalve isotope profile plots. $\delta^{13}C$ and $\delta^{18}O$ profiles are plotted against adjusted sample number such that values closest to the graph's origin represent the final period of growth, and hence the conditions at the time of death.

4.5 Results and Discussion

4.5.1 Bivalve Isotope Profiles and Seasonal Timing of Death

Before a bivalve species can be used for seasonality analysis we must determine if the organism is secreting shell carbonate in isotope equilibrium with seawater. Bivalves must secrete shell carbonate in isotopic equilibrium with seawater, or the disequilibrium fractionation must be known in order to accurately calculate SSTs at the timing of death and hence predict the seasonality of death. In order to assess the ability of these species to accurately record annual SST variation, we compare measured local SSTs with $\delta^{18}O_{shell}$-calculated temperatures. Measured SSTs are obtained from NOAA's Coral Reef Watch programs via the National Environmental Satellite Data and Information Service (NESDIS). Average monthly temperatures (from January 2001 to June 2009) are plotted along with monthly maxima and minima in figure 4.4 (NESDIS, 2009). Maximum temperatures (33 °C) occur in July and minimum temperatures in February (22 °C). Summer months can have periods of reduced SSTs during strong upwelling

events caused by the southwest monsoon as seen by the drop in minimum temperatures in August.

$\delta^{18}O$-calculated temperatures (T, in K) are determined using the carbonate-temperature relationship of Grossman and Ku (1986) modified by Dettman et al (1999). Modifications were made to correct for differences in the scales used and to directly relate the fractionation factor (α) to the temperature relationship that provides an accurate equation for any $\delta^{18}O_{water}$ value:

$$10^3 \ln\alpha_{(aragonite\text{-}water)} = 2.559 \times (10^6 \times T^{-2}) + 0.715 \qquad (4.1)$$

where

$$\alpha_{(aragonite\text{-}water)} = (1000 + \delta^{18}O_{shell}) / (1000 + \delta^{18}O_{water}) \qquad (4.2)$$

The oxygen isotope value of seawater ($\delta^{18}O_{water}$) in the region is 0.5‰ (±0.1‰) VSMOW based on an average of 40 oxygen isotope measurements from the area (Ganssen and Kroon, 1991). $\delta^{18}O_{shell}$ values in Eqn. 4.2 are converted from the VPDB to VSMOW scale using the equation from NIST (1992) and Coplen *et al.* (1983):

$$\delta^{18}O_{VSMOW} = 1.03092 \times (\delta^{18}O_{VPDB}) + 30.92 \qquad (4.3)$$

$\delta^{18}O$ calculated temperatures are presented alongside all $\delta^{18}O_{shell}$ profiles for comparison with measured SSTs from figure 4.4.

P. sinuosa $\delta^{18}O_{shell}$ values range from –1.9 to 0.1‰$_{VPDB}$ corresponding to temperatures ranging from 22°C to 33°C (Fig. 4.5). The similarity in the range of $\delta^{18}O$-calculated temperatures and measured temperature range (22 °C to 33 °C) confirms that this species is secreting shell carbonate in isotopic equilibrium with seawater and are therefore accurately recording seasonal variations in SSTs. Because seasonal changes in SSTs can account for all of the $\delta^{18}O_{shell}$ variability, intra-annual changes in $\delta^{18}O_{water}$ must be minimal, thus providing negligible contributions to $\delta^{18}O_{shell}$ variability. $\delta^{18}O_{shell}$ profiles of all three *P. sinuosa* specimens exhibit excellent reproducibility of seasonal $\delta^{18}O_{shell}$ maxima and minima (see winter and summer values in Fig. 4.5) suggesting that all three specimens lived during the same time period. $\delta^{18}O_{shell}$ values at the timing of death are also similar providing compelling evidence for the concurrency of these three specimens. Even a small fluctuation around adjusted sample number

16 is reproduced in all three specimens. $\delta^{13}C_{shell}$ profiles (not shown) of these three specimens are also very similar further implying these three specimens lived and died at the same time.

T. palatum $\delta^{18}O_{shell}$ values range from –1.7 to –0.1‰ VPDB corresponding to a temperature range of 23 °C to 32 °C (Fig. 4.6), this is slightly less than the measured SST range, possibly due to the deeper burrowing depth of *T. palatum* (Gibbs, 1978) that would moderate seasonal temperature variability. Similar to *P. sinuosa* the seasonal SST fluctuations can account for all of the *T. palatum* $\delta^{18}O_{shell}$ variability, indicating that seasonal changes in $\delta^{18}O_{water}$ are negligible. Similarities in measured and $\delta^{18}O_{shell}$–calculated SSTs suggests that *T. palatum* is also secreting shell carbonate in isotopic equilibrium with seawater as does *P. sinuosa*—indicating that both offshore species are accurately recording seasonal variations in SSTs. Although *T. palatum* $\delta^{18}O_{shell}$ profiles accurately record seasonal variations in SSTs, *T. palatum* is somewhat problematic species for seasonality analysis, especially as individuals age. In some longer living bivalve species there is a tendency later in life, of punctuated growth such that shell secretion is not continuous (*c.f.* Harrington, 1989). During this period of discontinuous growth there are many growth cessations or times when shell secretion does not occur. This truncation of the $\delta^{18}O_{shell}$ profile leads to temporal gaps in the $\delta^{18}O_{shell}$ record resulting in discontinuous SST histories. Bivalves exhibiting punctuated growth represent incomplete environmental records making their use for reconstructing seasonality more difficult, and highlight the benefit of obtaining detailed analysis of multiple species.

A. edentula inhabit the lagoonal tidal flats and represent a species living at the sampling site, thus providing a proxy for environmental conditions at the site of deposition. The lagoonal habitat of *A. edentula* is subjected to tidal flooding and intense evaporation associated with high air temperatures. These effects will significantly alter the oxygen isotope value of local water used by the bivalve in shell secretion. Therefore, the sinusoidal shape of the $\delta^{18}O_{shell}$ profiles associated with seasonal shifts in SSTs typically observed in the offshore species is not apparent in *A. edentula* $\delta^{18}O_{shell}$ records. Thus, the lagoonal habitat of *A. edentula* makes it difficult to use $\delta^{18}O_{shell}$ profiles in seasonality studies, although it does provide a reference frame for the oxygen isotope values of shell secreted at the site of deposition (location of tsunamite). *A. edentula* $\delta^{18}O_{shell}$ values range from –1.1 to 0.6‰$_{VPDB}$, exhibiting slightly higher values than offshore species due to higher $\delta^{18}O_{water}$ values caused by higher evaporation in the warm lagoonal environment relative to offshore marine waters.

Despite difficulties in the use of *A. edentula* $\delta^{18}O_{shell}$ and $\delta^{13}C_{shell}$ profiles (Fig. 4.7) show excellent inter specimen reproducibility—convincing evidence of concomitant life histories for these specimens. $\delta^{13}C_{shell}$ is not directly proportional to SST and therefore $\delta^{13}C_{shell}$ cannot be used to determine the season of the event. Nonetheless, variations in $\delta^{13}C_{shell}$ values are still valuable for interspecies seasonality analysis. The time period recorded in the $\delta^{13}C_{shell}$ records of *A. edentula* can be assessed by comparison with *P. sinuosa* $\delta^{13}C_{shell}$ records to determine if both of these species perished at the same time during the same event. Before $\delta^{13}C_{shell}$ records of two species can be directly compared, species-specific ontogenic effects must be accounted for. This is essential because large ontogenic decreases in $\delta^{13}C_{shell}$ values are evident in *A. edentula* profiles, but weak in *P. sinuosa* profiles. This gradual decrease in $\delta^{13}C_{shell}$ with age is prevalent in many species of bivalves (*e.g.* Krantz *et al.*, 1987, Elliot *et al.*, 2003, Lorrain *et al.*, 2004, Gillikin *et al.*, 2007), generally regarded as an increase in the incorporation of metabolic ^{12}C into shell carbonate. Therefore, in order to compare $\delta^{13}C_{shell}$ records between these two species this ontogenic overprint is removed first. A linear trendline of *A. edentula* data (Fig. 4.7) provides a rough approximation of ontogenic decreases in $\delta^{13}C_{shell}$ values while preserving any potential seasonal variations in $\delta^{13}C_{shell}$ values. Detrending $\delta^{13}C_{shell}$ values eliminates the unidirectional ontogenic trend. Figure 4.8 illustrates the detrended *A. edentula* $\delta^{13}C_{shell}$ data alongside *P. sinuosa* $\delta^{13}C_{shell}$ data after abscissae adjustments using the Analyseries program. $\delta^{13}C_{shell}$ profiles of *A. edentula* and *P. sinuosa* exhibit excellent correspondence in $\delta^{13}C$ variability values indicating that the same environmental conditions were responsible for $\delta^{13}C_{shell}$ variability of both species confirming that they were contemporaries.

4.5.2 Seasonality of Death and Implications for the Seasonality of the Deposit

$\delta^{18}O_{shell}$ records from the three *P. sinuosa* specimens just prior to death are trending toward lower $\delta^{18}O_{shell}$ values, suggesting a seasonal increase in temperature, that indicates they died in late spring to early summer. Terminal $\delta^{18}O_{shell}$ values (recorded days before death) from the three *P. sinuosa* specimens are 29.4 °C, 29.2 °C, and 28.6 °C SSTs for specimens 1a, 2a, and 3a respectively. SSTs at Sur (Fig. 4.4) trend towards this temperature from May-June, further suggesting a late spring to early summer time of deposition.

The deposit has been assigned a late-spring/early-summer seasonality based on bivalve $\delta^{18}O_{shell}$ profiles. To evaluate potential depositional events, the seasonality of the deposit with the storm and tsunami events summarized in Table 4.1 and 4.2 to determine the probability of each

event in terms of its timing and the seasonality of the deposit. Most of the tsunami events in Table 1 occurred in the late fall to early winter time period. Those that occur in during summer months have only centimeter-scale amplitudes. Events of this magnitude are unlikely to generate deposits with the observed amount of shell material, suggesting that these events are unlikely candidates.

Severe cyclones are exceedingly rare in the Arabian Sea (Fritz *et al.*, 2010) and historically only three large tropical cyclones are known to have impacted the northern Omani coast (Table 4.2). British historical records (Bailey, 1988) document evidence of large storms on May 2, 865 A.D. and June 4th and 5th, 1890 A.D. (the Super Cyclone); both of which had large storm surges and severely impacted coastal populations. High-resolution storm surge modeling estimated that peak storm surge heights for the 1890 A.D. event were 5.4 m (Blount *et al.*, 2010). The most recent event, Cyclone Gonu, occurred after sampling for this study (August 3-7, 2007), however large storm surge heights including high water marks greater than 5m were observed. Effects of the storm surge were found to extend several kilometers inland (Fritz *et al.*, 2010) illustrating the magnitude of potential effects possible from severe storms in the region. The 1890 "Super" cyclone occurred in early June and had a storm surge significantly higher than any of the tsunami wave heights. The seasonality of the deposit based on $\delta^{18}O_{shell}$ records agrees with this timing, suggesting that this is a likely candidate. The 865 A.D. cyclone event occurred in early May, implicating it as a potential candidate for the source event as well. One issue with the 865 A.D. event is that the estimated cyclone track (see Fig. 4.1), seems to have made landfall significantly north of Sur at Muscat (Blount *et al.*, 2010). This would mean smaller storm surge heights at Sur and suggests that the 1890 A.D. event is a better candidate for the source of the deposit at Sur.

The distinction between storm and tsunami deposits is complicated by similar hydrodynamic processes and depositional characteristics. Several studies have addressed the distinguishing characteristics for the identification of tsunamigenic versus storm deposits (Nanayama *et al.*, 2000; Goff *et al.*, 2004; Tuttle *et al.*, 2004; Dawson and Stewart, 2007; Kortekaas and Dawson, 2007; Morton *et al.*, 2007). Unfortunately, differences in the number of sedimentary sub-units within both tsunami and storm deposits (Nanayama *et al.*, 2000; Morton *et al.*, 2007); the poorly sorted nature of both types of deposits (however, tsunamites are generally more poorly sorted) (Morton *et al.*, 2007), and the similarity in micropaleotological and geochemical signatures of both deposits (Kortekaas and Dawson, 2007) make it difficult to develop a general method to

distinguish tsunami and storm deposits. This means that there is no universal approach that can be applied to the identification of all tsunami or storm deposits and methods must be tailored to the specific deposit.

The similarities in the sedimentology of tsunamites and tempestites means that we need to use all available proxies to assess the type of depositional event. Here we present an alternative to the tsunamigenic origin that was originally proposed by Donato *et al.*, (2008a) based on bivalve isotope profiles. The ultimate cause of this shell-rich unit at Sur lagoon will likely only be determined after the application of more analytical techniques.

4.6 Conclusions

- The two offshore species (*P. sinuosa* and *T. palatum*) analyzed are secreting shell carbonate in isotopic equilibrium and therefore are accurately recording seasonal fluctuations in SSTs at Sur. This means they have the potential to be used as a seasonality index for their host deposits.
- Stable isotope profiles from *T. palatum* exhibit punctuated growth during the final period of growth. As this is the period most pertinent to this study, the specimens of this species cannot be used in a seasonality study. Younger specimens of this species that have not transitioned into punctuated growth have the potential to be used as a seasonality proxy provided a detailed growth history study is performed prior.
- Inter-specimen similarities in the $\delta^{18}O_{shell}$ profiles of *P. sinuosa*; and the $\delta^{13}C_{shell}$ profiles of *A. edentula* indicate coeval life histories. Interspecies similarities in $\delta^{13}C_{shell}$ profiles of *P. sinuosa* and *A. edentula* provides a temporal link between these two species and suggests that all six specimens lived and died contemporaneously.
- The timing of death based on a combination of $\delta^{18}O_{shell}$ and $\delta^{13}C_{shell}$ records indicates a similar season of death for all specimens and therefore suggests a single-event cause for this deposit.
- The bivalves judged to be useful for seasonality studies (*P. sinuosa* and *A. edentula*) suggest that this unit was deposited in the late spring to early summer months. As no significant tsunami events are known to have impacted the Omani coast in the late spring to early summer months an alternate source has been suggested.

- The Super Cyclone of 1890 A.D. that occurred on June 4-5th is proposed as the source of this shell-rich unit. The large storm surge associated with this event and its summer timing make it a better candidate as the source of this unit.

The use of seasonality proxies applied to geological deposits can be of great utility in the future as the use of chemical signatures in faunal material is extended. This includes the use of different chemical proxies (*e.g.* stable isotopes, trace elements, etc.) as well as different species (*e.g.* marine vs. terrestrial organisms, gastropods, etc.). It has been suggested that the use of geochemical signatures in the identification of paleotsunami deposits has been under-utilized (Chagué-Goff, 2010). We agree with Chagué-Goff (2010) that, alone, it will not provide unequivocal evidence of the tsunamigenic nature of a deposit but it will provide additional quantitative evidence to be used along with other proxies. Our primary goal was to link the geologic and historical record and it is hoped that this could be extended to link well-dated tsunami deposits located in areas of the world lacking historic archives with known events. Locations with multiple tsunami units could use this technique to delineate the boundaries of specific event deposits. This could help in risk assessment scenarios by linking specific magnitude events with their associated deposits. Great storm and tsunami events of human through human history can be ascribed to specific seasons, thereby further defining their impact on societies. Additionally, this technique can be used to assess whether a sedimentological unit is a single-event or a lag deposit.

The use of seasonality must be approached with some caution, as there are limitations to its applicability. For example, short-lived species may share a common season of death due to environmental (*e.g.* large temperature or salinity changes) or biological stress (*e.g.* reproduction) an inaccurate interpretation could result. Lastly, the mixing of multiple specimens of a single species from different environments could be an issue for certain euryhaline species.

4.7 Relationship with Overarching Theme of Thesis

In this study, bivalves were sampled at sub-seasonal resolution in order to evaluate their life histories and provide insight into their deposition. This represents the highest resolution sampling strategy employed in this dissertation. Sub-seasonally resolved records archive seasonal shifts in weather and environmental conditions and hint at, but do not show climate

information, that must be acquired through longer-term sampling. This final study illustrates how increasing the sampling resolution results in different types of paleoenvironmental information being obtained. Therefore, by employing a wide variety of sampling resolutions a diversity of paleoenvironmental information is attained showing the power high-resolution studies, but also demonstrates the need to evaluate the research question prior to selecting a sampling resolution.

4.8 Acknowledgements

A. Bangsund is acknowledged for lab assistance. Bivalve specimens collected by J. Pilarczyk and made available by E. Reinhardt (McMaster University). NSERC DGS grant to A.W. Kingston, and NSERC Discovery grant to W.P. Patterson helped fund this research.

4.9 References

Ambraseys, N.N., & Melville, C.P. (1982). *A History of Persian Earthquakes*, Cambridge University Press. 219 p.

Atwater, B.F., Satoko, M., Kenji, S., Yoshinobu, T., Kazue, U., & Yamaguchi, D.K., 2005. The Orphan Tsunami of 1700 – Japanese Clues to a Parent Earthquake in North America. University of Washington Press / U.S. Geological Survey. Professional Paper 1707. 141 p.

Bailey, R.W. (Ed.) (1988). Records of Oman: 1867–19460, 12 vols. Archive Editions, Buckinghamshire, England. 7500 p.

Blount, C., Fritz, H. M., & Al-Harthy, A. H. M. (2010). Coastal vulnerability assessment based on historic tropical cyclones in the Arabian Sea. In Indian Ocean Tropical Cyclones and Climate Change (pp. 207-214). Springer Netherlands.

Bosch, D.T., Dance, S.P., Moolenbeek, R.G., & Oliver, P.G. (1995). Seashells of eastern Arabia: Dubai, Motivate Publishing, 296 p.

Brock, J., & McClain, C. (1992). Interannual variability in phytoplankton blooms observed in the northwestern Arabian Sea during the southwest monsoon. Journal of Geophysical Research, 97(1), 733-750.

Cadet, D. L., & Diehl, B. C. (1984). Interannual variability of surface fields over the Indian Ocean during recent decades. Monthly Weather Review, 112(10), 1921-1935.

Chagué-Goff, C. (2010). Chemical signatures of palaeotsunamis: A forgotten proxy? Marine Geology, 271(1), 67-71.

Colburn, J.G. (1975). *The thermal structure of the Indian Ocean*. East-West Centre Press. University of Hawaii. 173 p.

Coplen, T. B., Kendall, C., & Hopple, J. (1983). Comparison of stable isotope reference samples. Nature 302, 236-238.

Craig, H. (1957). Isotopic standards for carbon and oxygen and correction factors for mass-spectrometric analysis of carbon dioxide. Geochimica et Cosmochimica Acta, 12(1), 133-149.

Dawson, A. G., & Stewart, I. (2007). Tsunami deposits in the geological record. Sedimentary Geology, 200(3), 166-183.

Dominey-Howes, D., Cummins, P., & Burbidge, D. (2007). Historic records of teletsunami in the Indian Ocean and insights from numerical modelling. Natural Hazards, 42(1), 1-17.

Donato, S. V., Reinhardt, E. G., Boyce, J. I., Rothaus, R., & Vosmer, T. (2008). Identifying tsunami deposits using bivalve shell taphonomy. Geology, 36(3), 199-202.

Donato, S. V., Reinhardt, E. G., Boyce, J. I., Pilarczyk, J. E., & Jupp, B. P. (2009). Particle-size distribution of inferred tsunami deposits in Sur Lagoon, Sultanate of Oman. Marine Geology, 257(1), 54-64.

Dunbar, P. K., & Weaver, C. S. (2008). US States and Territories National Tsunami Hazard Assessment: Historical Record and Sources for Waves. Washington, DC: US Department of Commerce, National Oceanic and Atmospheric Administration. 59 p.

Elliot, M., DeMenocal, P. B., Linsley, B. K., & Howe, S. S. (2003). Environmental controls on the stable isotopic composition of *Mercenaria mercenaria*: potential application to paleoenvironmental studies. Geochemistry, Geophysics, Geosystems, 4(7). 1056.

Epstein, S., Buchsbaum, R., Lowenstam, H. A., & Urey, H. C. (1953). Revised carbonate-water isotopic temperature scale. Geological Society of America Bulletin, 64(11), 1315-1326.

Fritz, H. M., Blount, C. D., Albusaidi, F. B., & Al-Harthy, A. H. M. (2010). Cyclone Gonu storm surge in Oman. Estuarine, Coastal and Shelf Science, 86(1), 102-106.

Ganssen, G., & Kroon, D. (1991). Evidence for Red Sea surface circulation from oxygen isotopes of modern surface waters and planktonic foraminiferal tests. Paleoceanography, 6(1), 73-82.

Gibbs, P. E. (1978). Macrofauna of the intertidal sand flats on low wooded islands, northern Great Barrier Reef. Philosophical Transactions of the Royal Society B: Biological Sciences, 284(999), 81-97.

Gillikin, D. P., De Ridder, F., Ulens, H., Elskens, M., Keppens, E., Baeyens, W., & Dehairs, F. (2005). Assessing the reproducibility and reliability of estuarine bivalve shells (*Saxidomus giganteus*) for sea surface temperature reconstruction: implications for paleoclimate studies. Palaeogeography, Palaeoclimatology, Palaeoecology, 228(1), 70-85.

Gillikin, D. P., A. Lorrain, S. Bouillon, P. Willenz, & F. Dehairs (2006), Stable carbon isotopic composition of *Mytilus edulis* shells: Relation to metabolism, salinity, $\delta^{13}C_{DIC}$ and phytoplankton, Organic Geochemistry 37, 1371-1382.

Gillikin, D. P., A. Lorrain, & F. Dehairs, (2007), A large metabolic carbon contribution to the $\delta^{13}C$ record in marine aragonitic bivalve shells. Geochimica et Cosmochimica Acta 71, 2936-2946.

Gillikin, D. P., Hutchinson, K. A., & Kumai, Y. (2009). Ontogenic increase of metabolic carbon in freshwater mussel shells (*Pyganodon cataracta*). Journal of Geophysical Research: Biogeosciences (2005–2012), 114(G1). G01007.

Goff, J., McFadgen, B. G., & Chagué-Goff, C. (2004). Sedimentary differences between the 2002 Easter storm and the 15th-century Okoropunga tsunami, southeastern North Island, New Zealand. Marine geology, 204(1), 235-250.

Grossman, E. L., & Ku, T. L. (1986). Oxygen and carbon isotope fractionation in biogenic aragonite: temperature effects. Chemical Geology: Isotope Geoscience section, 59, 59-74.

Hamilton, M.G. (1979). *The South Asian Summer Monsoon*, Edward Arnold, Melbourne, Australia. 72 p.

Harrington, R. J. (1989). Aspects of growth deceleration in bivalves: Clues to understanding the seasonal $\delta^{18}O$ and $\delta^{13}C$ record —A comment on Krantz et al. (1987). Palaeogeography, Palaeoclimatology, Palaeoecology, 70(4), 399-403.

Heidarzadeh, M., Pirooz, M. D., Zaker, N. H., & Synolakis, C. E. (2008). Evaluating tsunami hazard in the northwestern Indian Ocean. Pure and applied geophysics, 165(11-12), 2045-2058.

Hindson, R. A., & Andrade, C. (1999). Sedimentation and hydrodynamic processes associated with the tsunami generated by the 1755 Lisbon earthquake. Quaternary International, 56(1), 27-38.

Hindson, R., Andrade, C., & Parish, R. (1998). A microfaunal and sedimentary record of environmental change within the late Holocene sediments of Boca do Rio (Algarve, Portugal). Geologie en Mijnbouw, 77(3-4), 311-321.

Ivany, L. C., & Runnegar, B. (2010). Early Permian seasonality from bivalve $\delta^{18}O$ and implications for the oxygen isotopic composition of seawater. Geology, 38(11), 1027-1030.

Jacoby, G. C., Bunker, D. E., & Benson, B. E. (1997). Tree-ring evidence for an AD 1700 Cascadia earthquake in Washington and northern Oregon. Geology, 25(11), 999-1002.

Jelgersma, S., Stive, M. J. F., & Van der Valk, L. (1995). Holocene storm surge signatures in the coastal dunes of the western Netherlands. Marine Geology, 125(1), 95-110.

Jordan, B. R. (2008). Tsunamis of the Arabian Peninsula a guide of historic events. Science of Tsunami Hazards, 27(1), 31.

Kortekaas, S., & Dawson, A. G. (2007). Distinguishing tsunami and storm deposits: an example from Martinhal, SW Portugal. Sedimentary Geology, 200(3), 208-221.

Krantz, D. E., Williams, D. F., & Jones, D. S. (1987). Ecological and paleoenvironmental information using stable isotope profiles from living and fossil molluscs. Palaeogeography, Palaeoclimatology, Palaeoecology, 58(3), 249-266.

Lorrain, A., Paulet, Y. M., Chauvaud, L., Dunbar, R., Mucciarone, D., & Fontugne, M. (2004). $\delta^{13}C$ variation in scallop shells: increasing metabolic carbon contribution with body size? Geochimica et Cosmochimica Acta, 68(17), 3509-3519.

McConnaughey, T. A., Burdett, J., Whelan, J. F., & Paull, C. K. (1997). Carbon isotopes in biological carbonates: respiration and photosynthesis. Geochimica et Cosmochimica Acta, 61(3), 611-622.

McConnaughey, T. A., & Gillikin, D. P. (2008). Carbon isotopes in mollusk shell carbonates. Geo-Marine Letters, 28(5-6), 287-299.

Morton, R. A., Gelfenbaum, G., & Jaffe, B. E. (2007). Physical criteria for distinguishing sandy tsunami and storm deposits using modern examples. Sedimentary Geology, 200(3), 184-207.

Nanayama, F., Shigeno, K., Satake, K., Shimokawa, K., Koitabashi, S., Miyasaka, S., & Ishii, M. (2000). Sedimentary differences between the 1993 Hokkaido-nansei-oki tsunami and the 1959 Miyakojima typhoon at Taisei, southwestern Hokkaido, northern Japan. Sedimentary Geology, 135(1), 255-264.

NESDIS (2009). National Environmental Satellite, Data and Information Service, virtual station: Oman-Muscat. Website: http://coralreefwatch.noaa.gov/satellite/index.html. [Accessed June 2009]

Paillard, D., Labeyrie, L., & Yiou, P. (1996). Macintosh program performs time‐series analysis. Eos, Transactions American Geophysical Union, 77(39), 379-379. (Available at http://www.agu.org/eos_elec/96097e.html)

Pararas-Carayannis, G. (2006). The potential of tsunami generation along the Makran Subduction Zone in the northern Arabian Sea: Case study: The earthquake and tsunami of November 28, 1945. Science of Tsunami Hazards, 24(5), 358-384.

Peterson, C. H. (1982). The importance of predation and intra-and interspecific competition in the population biology of two infaunal suspension-feeding bivalves, *Protothaca staminea* and *Chione undatella*. Ecological Monographs, 437-475.

Poulain, C., Lorrain, A., Mas, R., Gillikin, D. P., Dehairs, F., Robert, R., & Paulet, Y. M. (2010). Experimental shift of diet and DIC stable carbon isotopes: Influence on shell $\delta^{13}C$ values in the Manila clam *Ruditapes philippinarum*. Chemical Geology, 272(1), 75-82.

Primavera, J. H., Lebata, M. J. H. L., Gustilo, L. F., & Altamirano, J. P. (2002). Collection of the clam *Anodontia edentula* in mangrove habitats in Panay and Guimaras, central Philippines. Wetlands Ecology and Management, 10(5), 363-370.

Schöne, B., Tanabe, K., Dettman, D. L., & Sato, S. (2003). Environmental controls on shell growth rates and $\delta^{18}O$ of the shallow-marine bivalve mollusk *Phacosoma japonicum* in Japan. Marine Biology, 142(3), 473-485.

Tanaka, N., Monaghan, M. C., & Rye, D. M. (1986). Contribution of metabolic carbon to mollusc and barnacle shell carbonate. Nature 320, 520-523.

Tuttle, M. P., Ruffman, A., Anderson, T., & Jeter, H. (2004). Distinguishing tsunami from storm deposits in eastern North America: the 1929 Grand Banks tsunami versus the 1991 Halloween storm. Seismological Research Letters, 75(1), 117-131.

Wurster, C. M., Patterson, W. P., & Cheatham, M. M. (1999). Advances in micromilling techniques: a new apparatus for acquiring high-resolution oxygen and carbon stable isotope values and major/minor elemental ratios from accretionary carbonate. Computers & Geosciences, 25(10), 1159-1166.

Table 4.1

Historical tsunami events with impacts in the Arabian Sea (adapted from Jordan, 2008). N.R – no record, Neg. – negligible.

Date	Source Location	Max Wave Height	Description
A.D. 1819, 16 June	Gujrat, India	N.R.	Large earthquake in western India generated a large tsunami – the wave would have arrived in Arabia in about four hours, but there is no record of effects in the Arabian Peninsula
A.D. 1845	Kutch, India	N.R.	An earthquake was followed by a small tsunami – this event was probably too small to have affected the Arabian Peninsula.
A.D. 1851	Makran, Pakistan	N.R.	An earthquake occurred off of the Makran coast with an epicenter west of the better known 1945 earthquake epicenter and tsunami.
A.D. 1883, 8 August	Krakatau, Indonesia	<13 cm	The eruption of the Krakatau volcano generated a large tsunami, that was measured worldwide. A station located in the Gulf of Aden measured a small tsunami 13 cm in height. No other records are apparent for Arabia.
A.D. 1945, 28 November	Makran, Pakistan	0.1-3 m	A large earthquake off of the southern coast of Pakistan generated a large tsunami that devastated the region, killing more than 4,000 people. This wave may have also swept into the Persian Gulf and washed out a large sandbar at Ras al-Khaimah, UAE.
A.D. 1983, 30 November	Chagos Archipelago	Neg.	An earthquake at the Island of Diego Garcia produced a small tsunami (1.5 m high) - its small size did not produce any recordable impacts on the Arabian Peninsula, but future events from the same location could.

A.D. 2004, 26 December	Aceh, Indonesia	2.5 m	An extremely large (?) earthquake generated a 10-15 m high tsunami that killed over 225,000 people. It had minor impacts along the southern Arabian coast.

Table 4.2

Large historical storm events (based on Bailey, 1988; Blount et al., 2010; Fritz et al., 2010).

Date	Storm Surge Height	Description
A.D. 865, 2 May	4.75 m (est.)	Mostly affected the areas northwest of Muscat, with minimal effects in the Sur area.
A.D. 1890, 4-5 June	5.4 m (est.)	Super Cyclone is thought to have paralleled the shore from around Sur to north of Muscat. Causes significant damage along the coast to date plantations and other agriculture that required 15 years for recovery.
A.D. 2007, 3-7 June	5.1 m	Super Cyclone Gonu, the most intense tropical cyclone on record in the Arabian Sea, reached Tropical Cyclone strength on June 3rd. Intensified to Category 5 status on June 4th, after which it diminished slightly before making landfall near Sur on June 5th. On June 6th it turned north towards the Makran Coast of Iran.

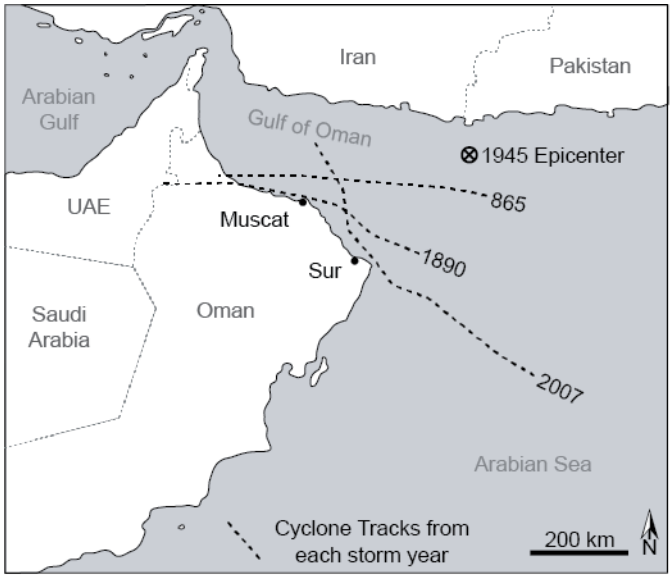

Figure 4.1: Map of study site including storm tracks of severe tropical cyclones recorded on the Arabian Peninsula. 865 and 1890 storm tracks are based on models of Blount et al. (2010); 2007 storm track from Fritz et al. (2009).

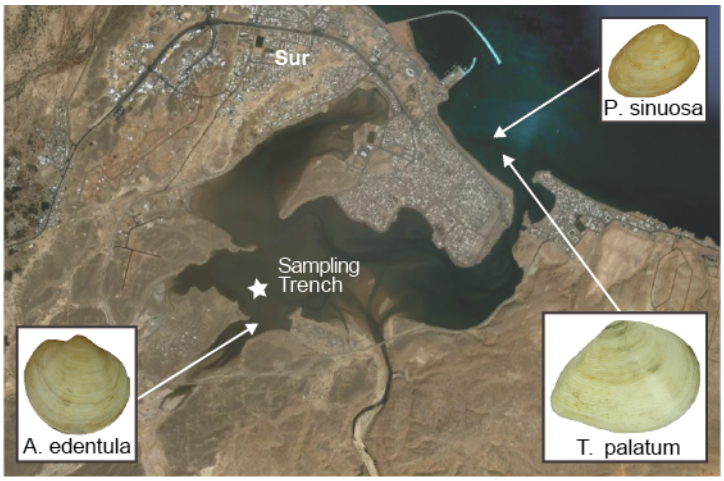

Figure 4.2: Aerial image of Sur lagoon including the habitats of the bivalve species used in this study (arrowed) as well as the sampling trench (star).

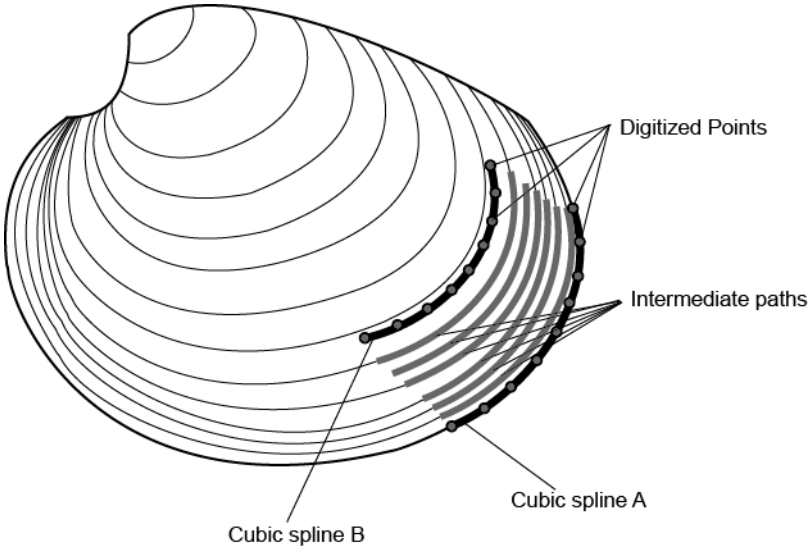

Figure 4.3: Schematic of micromilling sampling procedure.
See text for details

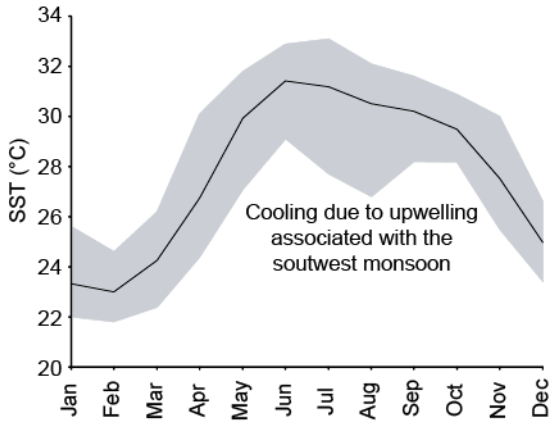

Figure 4.4: Average monthly sea surface temperatures from area (solid line) including range of maximum and minimum monthly values (interval). Based on NOAA's National Environmental Satellite Data and Information Service.

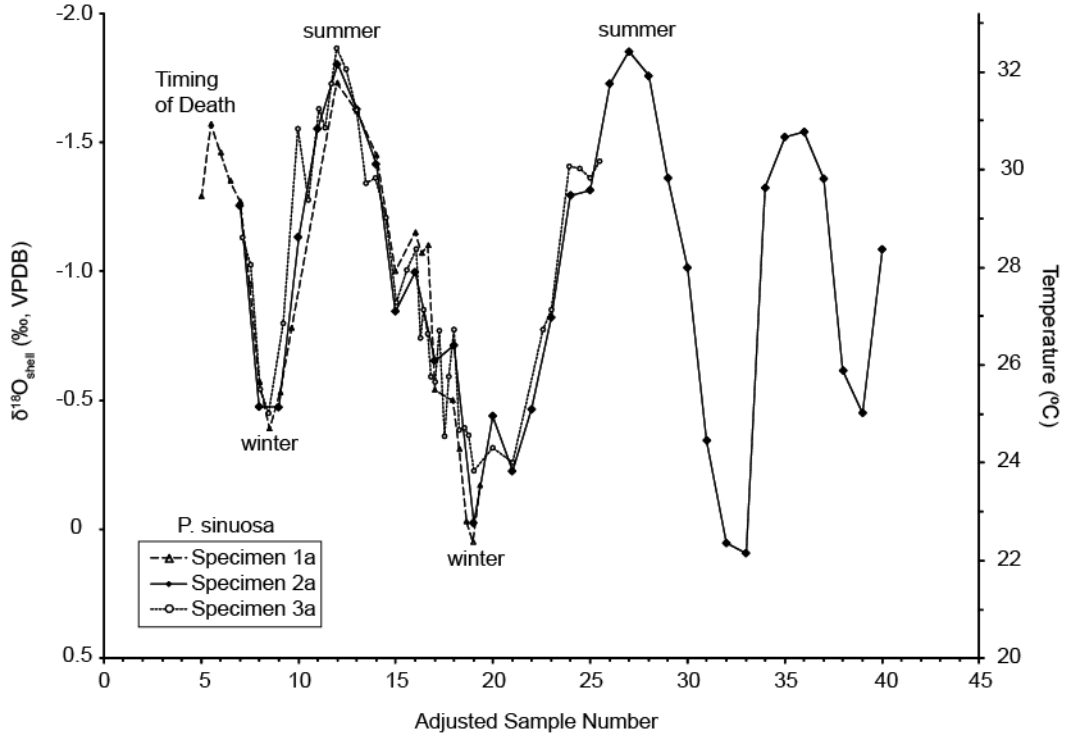

Figure 4.5: $\delta^{18}O_{shell}$ profiles of three *P. sinuosa* specimens.

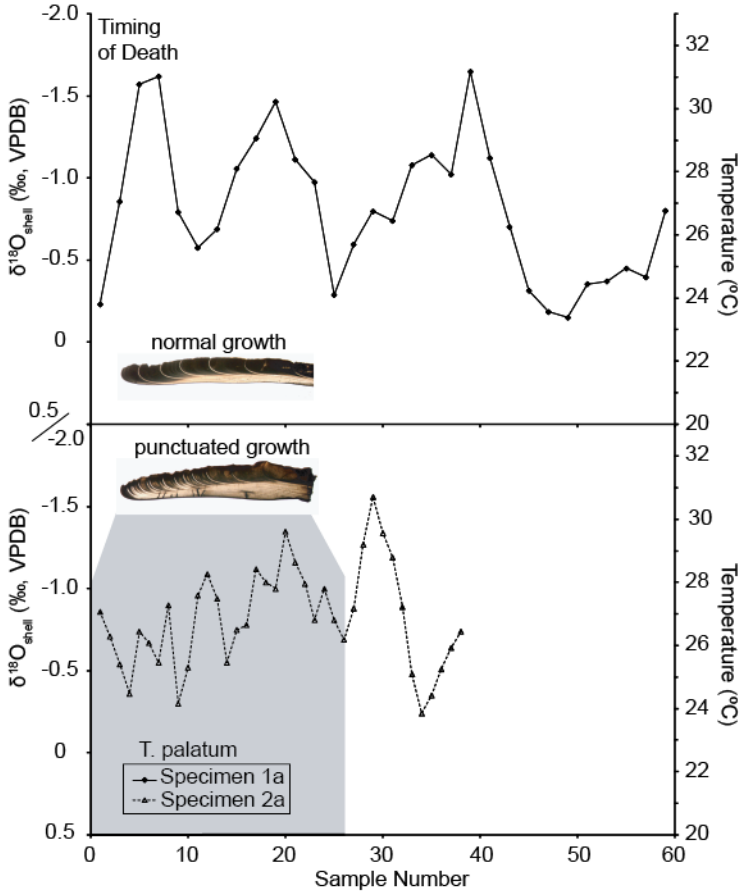

Figure 4.6: $\delta^{18}O_{shell}$ profiles of two *T. palatum* specimens. Grey areas represent the period of punctuated growth (see text). Bivalve images are two specimens of *S. giganteus* which have more defined growth banding thus providing a better visual example of punctuated growth. Images courtesy of M. Burchell.

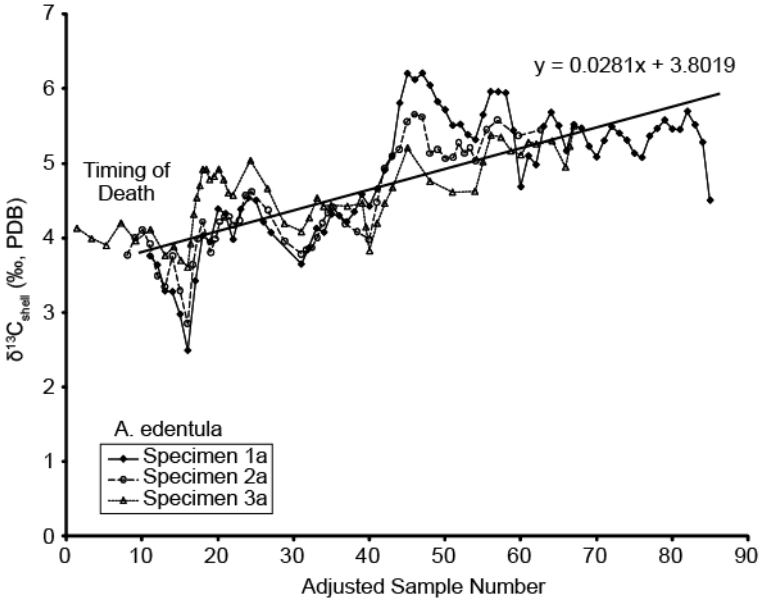

Figure 4.7: $\delta^{13}C_{shell}$ profiles of three *A. edentula* specimens. A linear regression of specimen 1a is included which is used to detrend *A. edentula* $\delta^{13}C_{shell}$ data for figure 9, see text for details.

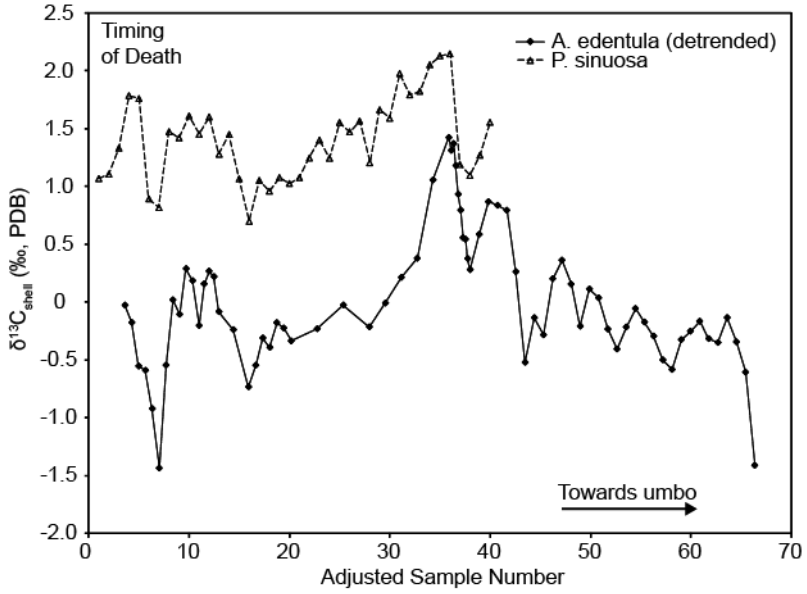

Figure 4.8: Comparison of $\delta^{13}C_{shell}$ profiles of *A. edentula* and *P. sinuosa*.

CHAPTER 5
CONCLUDING SUMMARY

This dissertation focused on improving our understanding of how paleoenvironmental information is archived in biogenic carbonates by focusing on the use of high-resolution sampling to evaluate paleoenvironmental change. Biogenic carbonates are useful archives of paleoenvironmental information because they record information about ambient environmental conditions during their formation. Therefore, long-term records of biogenic carbonates provide long-term records of environmental conditions.

Traditionally, these studies have been conducted with low temporal resolution owing to analytical or economical restrictions. Although these records provide valuable information surrounding long-term climatic change, they lack the resolution to resolve the short-term climatic oscillations that drive environmental change. Climate oscillations such as the PDO or ENSO have dramatic effects on North American climate, but have periods of six and 60 years, respectively. Therefore, a sub-decadal sampling strategy must be employed in order to resolve these drivers of climate. Furthermore, varying the sampling resolution diversifies the nature of information generated. For example, when investigating seasonal changes in sea surface temperatures using a sub-seasonal sampling strategy we can evaluate the paleoenvironmental histories archived in bivalves' shells elucidating the depositional histories stored in these biogenic carbonates.

The objective of this thesis was to increase knowledge of past environmental variability using high-resolution sampling strategies and illustrate the advantages of various sampling resolution strategies. The objectives were achieved using three separate studies employing sampling resolutions ranging from sub-centennial to sub-seasonal and assessing how these different resolutions affect the quality and types of paleoenvironmental information generated from the stable isotope analysis of biogenic carbonates.

The first study employed a sub-centennial resolution, the lowest of the three studies, to assess centennial scale climate variability in the Yukon Territory. This enabled the resolution of long-term shifts in climate such as the Pleistocene-Holocene transition and several large climate shifts in the Holocene (e.g. Holocene Thermal Maximum,

Preboreal, Preboreal Oscillation, and the Tiedemann Neoglaciation). While this technique was appropriate for resolving long-term climate patterns, it lacked the ability to evaluate decadal-scale climate oscillations, which are the driving factors behind these climate shifts and require a higher resolution sampling strategy.

The second study used a sub-decadal sampling strategy that greatly increased the resolution of data resulting in the ability to resolve decadal-scale climate oscillations. This permitted dominant climate oscillations such as the PDO and ENSO to be resolved illustrating how their prevalence changed through the Holocene and the associated effects on central North American climate. An additional advantage of higher resolution studies is the potential to utilize time series analysis techniques (e.g. wavelet analysis, Multi Taper Method, etc.) to assess how these climate oscillations varied through time, including both their presence and strength. This enhances our ability to develop accurate models of how these climate oscillations varied through time and their effects on climate.

The final study employed sub-seasonal stable isotope analysis of bivalve shells in order to assess past environmental conditions with the ultimate goal of evaluating the timing of deposition for a shell-rich overwash deposit. Increasing the resolution to this degree significantly changed the type information gained from the analysis. In this case records of weather and oceanographic conditions over several years are generated. Long-term climatic trends are not resolved with this technique, however, paleoenvironmental information still provides unique insight into the history of this deposit thereby improving our understanding of tempestite and tsunamite depositional processes.

High temporal resolution stable isotope analysis provides insight into environmental conditions at unprecedented resolution in each of the respective studies. Despite the merits of each of the techniques used in these studies, they all have specific limitations stemming from cost of analyses, analytical uncertainty, age controls, and assumptions made. In this final concluding synopsis, a summary of the major findings is reported along with the limitations of the methods utilized in each study. Finally, suggestions for future research directions are addressed with respect to each study.

5.1 Chapter 2: "Late Quaternary climate change in the southwest Yukon Territory: evidence from oxygen isotope analysis of authigenic lake carbonate"

5.1.1 Summary

This study provided the longest lake sediment isotope record from the Yukon Territory detailing climate change across the Pleistocene-Holocene transition through most of the Holocene. It employed a sub-centennial sampling resolution to provide paleoclimatic information pertaining to long-term changes in atmospheric circulation patterns. Results from this study contributed to our understanding of (a) the chronology of deglacial events in the region; (b) the importance of summer precipitation patterns in controlling effective moisture in the Yukon; and (c) elucidating how the interaction between continental glacial anticyclonic atmospheric circulation and North Pacific marine atmospheric circulation resulted in decreased precipitation in the southern Yukon Territory during the Pleistocene. Previously our knowledge of the timing of deglacial events was poor (e.g. Bond, 2004); using isotopic and sedimentological evidence, this study helped resolve the timing of the draining of Glacial Lake Watson, a major deglaciation event in southwestern Yukon. The majority of studies on the climate of the Pacific Northwest implicate the strength and position of the Aleutian Low pressure center in controlling precipitation patterns in the region. Although winter precipitation is important along the Pacific Northwest coast especially with regard to the freshet, summer precipitation patterns were largely ignored. This study illustrates how the Spirit Lake region is dominated by summer precipitation in the rain shadow of the Coast Mountains and implicated variations in the strength of the North Pacific High pressure center in controlling the amount of summer precipitation at Spirit Lake and thus the effective moisture in the region. Finally, high $\delta^{18}O$ values from the Pleistocene are interpreted to be a consequence of interactions between the Glacial anticyclone and North Pacific High pressure center that resulted in decreased summer precipitation to the region during the Late Glacial. Blocking of the North Pacific High concluded following the breakup of the Laurentian Ice Sheet, resulting in an increase in summer precipitation during the warmer Holocene period.

5.1.2 Limitations and Assumptions

The major limitation of this study was age control. The dissolved carbonate pool in Late Glacial water at Spirit Lake was dominated by bicarbonate dissolved from local

Triassic limestones and dolostones underlying Spirit Lake. This means that the ^{14}C pool in the lake was extremely low, or "dead", resulting in extremely large reservoir effects on radiocarbon dates derived from materials sourcing carbon from this "dead" pool. If the reservoir effect was constant through time, then a simple correction could be made. However, it was found to vary through the Holocene and therefore the use of aquatic material for dating was compromised. This greatly reduced the number of acceptable radiocarbon dates and consequently the resolution of the age model. Furthermore, the latter half of the record was devoid of dateable material resulting in an age model based on varve counting. This relies on the assumption that one couplet is equal to one year. Despite these age-related limitations the Spirit Lake oxygen isotope record seems to match well with other regional paleoclimate records justifying the accuracy of the age model developed.

In addition to age model uncertainties, several assumptions were made about the relationship between the $\delta^{18}O_{carb}$ values of carbonate and environmental conditions. It was assumed that the majority of variation in the $\delta^{18}O_{carb}$ values was related to changes in $\delta^{18}O_{lakewater}$ values and that water temperature and changes in the seasonality of precipitation played only a minor role. While these assumptions seem valid, there is always the potential that one or both of these assumptions may be invalid during some portions of the isotope record.

5.1.3 Suggested Future Research

The results of this study suggest several areas for future research related to the Pleistocene-Holocene transition and changes in North Pacific air circulation patterns. In this study it was hypothesized that air circulation patterns of the southern Yukon Territory during the Pleistocene were affected by Glacial anticyclonic air circulation patterns resulting in a suppression of North Pacific High pressure system. It would be interesting to see if there is other proxy evidence suggesting similar changes or even records capable of modeling the magnitude of these effects. It's possible that dendrochronology records may be able to test this hypothesis. The top portion of the core was disturbed due to the coring process, however, because marl formation is still active in Spirit Lake, a high-resolution study of the uppermost layers of marl could be used to

calibrate the Spirit Lake oxygen isotope record with historical climate records. This would not only be of great use in assessing climate change during the Anthropocene, but would also greatly increase the value of the whole Spirit Lake record.

5.2 Chapter 3 "Holocene variability in the Pacific/North American pattern from an 8,000-year lake carbonate oxygen isotope record"

5.2.1 Summary

This study reported the highest resolution lake carbonate record from central North America detailing Holocene climate change. Sub-decadal sampling resolution provided an opportunity to resolve important Pacific climate phenomena such as the PDO and ENSO. Saskatchewan is situated near one of the nodes of the Pacific/North American pattern and because of this, $\delta^{18}O_{H2O}$ values in precipitation can be used as a proxy for the strength and sign of the PNA (e.g. Birks and Edwards, 2009). The Sturgeon Lake oxygen isotope record utilized this relationship in order to illustrate how the PNA has varied through the Holocene. The record indicated that the Early to Mid-Holocene was characterized by large fluctuations between PNA^+ and PNA^- patterns as illustrated by large variations in $\delta^{18}O_{carb}$ values. After a negative excursion in $\delta^{18}O_{carb}$ values associated with the globally correlated 4,200-year event, a decrease in $\delta^{18}O_{carb}$ values and variability signaled a dominance of PNA^--like conditions with increased zonal flow to the region. Finally, after ~1,800 years BP there was increased influence of PNA^+ and associated meridional flow as exhibited by higher $\delta^{18}O_{carb}$ variability. Modern PNA conditions were also intrinsically linked to Pacific climate phenomenon such as ENSO and PDO through ocean-atmosphere interactions. For example, modern La Niña phases of ENSO are typically associated with PNA^- patterns. Holocene records of ENSO suggest a Mid-Holocene dominance of La Niña-like conditions (Makou et al., 2010) that correlates well with a contemporaneous dominance of PNA^- conditions shown by the Sturgeon Lake $\delta^{18}O_{carb}$ record. This highlights the potential value of high-resolution records from the nodes of major climate patterns in assessing past climatic change on large geographical scales.

5.2.2 Limitations and Assumptions

In this study the primary limitation was, again, age control. Radiocarbon dates from this core are unevenly distributed, resulting in a well-constrained bottom half and a poorly constrained upper half. This could be mitigated by the addition of several dates from the upper portion of the core. However, despite these temporal uncertainties, correlations between the Sturgeon Lake record and a tree-ring record from Alberta (Macdonald and Case, 2005) suggest that the age model is sufficiently accurate for comparison with other regional climate proxies. Lack of calibration of $\delta^{18}O_{carb}$ values with the PNA Index is a limitation resulting in the inability to quantify changes in the PNA Index through time. As such, the Sturgeon Lake $\delta^{18}O_{carb}$ record is restricted to evaluating changes in the PNA qualitatively. Lastly, similar to the previous study, an assumption was made that water temperature had minimal influences on $\delta^{18}O_{carb}$ values. Again this may have not been the case throughout the record, but is difficult to quantify and therefore effects of water temperature were likely of minimal importance.

5.2.3 Suggested Future Research

Future research in this area should focus on the calibration of the $\delta^{18}O_{carb}$ signal with the strength and sign of the PNA Index. Carbonate precipitation is ongoing in the lake and therefore a high-resolution record from the uppermost sediment could be extracted and then compared with modern climate conditions in order to better constrain the relationship between the PNA Index and $\delta^{18}O_{carb}$ values. If this were combined with additional dates from the top section of the core it would better constrain the chronology of the core allowing for more accurate correlation with other regional climate proxy records. Comparison of this record with other climate proxy records sensitive to the PNA, PDO, and ENSO would serve to quantify whether this lake carbonate $\delta^{18}O$ archive is accurately recording Holocene changes in the PNA, PDO, and ENSO. These climate oscillations significantly affect global climate (e.g. strength of the Atlantic hurricane season or drought in Africa) and our ability to generate accurate models of how these climate phenomena varied in the past would greatly assist in creating better predictions about their future variability.

5.3 Chapter 4, "Using seasonal variations in the stable isotope values of bivalve shells to determine the origin of shell-rich overwash deposits"

5.3.1 Summary

This study illustrated how high-resolution isotope analysis of bivalves from a suspected tsunami deposit can be seasonally dated to help connect the geological and historical record. The sub-seasonal sampling strategy provided in-depth information about environmental conditions throughout the bivalves' life histories permitting an evaluation of the depositional characteristics of the sedimentary host unit. Results of this study illustrated that in order to accurately conduct seasonality analysis, marine bivalves inhabiting offshore environments secreting shell carbonate consistently throughout the year are required. In this study, one species was found to have punctuated growth and did not precipitate shell carbonate throughout the year, resulting in temporal gaps in the isotope profile, thus making it unsuitable for seasonality analysis. Oxygen isotope profiles from a lagoonal species illustrated the challenge of using species which experience rapid changes to ambient water oxygen isotope compositions, in this case due to evaporation and tidal flooding cycles. Ultimately, a combination of carbon and oxygen isotope profiles were used to determine the coeval life histories of bivalves from the sampled overwash deposit. Comparison of bivalve $\delta^{18}O$-derived temperatures with measured seasonal SST changes lead to a conclusion that this shell-rich overwash unit was deposited in late spring/early summer. An analysis of historical records of tsunami and storm events in the region suggests that "the Super Cyclone" of June 1890 is a more likely candidate than the previously suggested tsunami of late November 1945 (Donato et al., 2008).

5.3.2 Limitations and Assumptions

The limitations of this technique are generally related to the ability of different bivalve species to accurately record specific environmental conditions. Species that live in lagoonal environments are more susceptible to varying ambient water $\delta^{18}O$ values, which make it difficult to model SST from these bivalves' $\delta^{18}O_{carb}$ values. Therefore, offshore marine species that secrete carbonate throughout the year are typically required for seasonality analysis, although they may be difficult to obtain in some study areas. The

lack of any absolute age dating of this unit is also a limitation that could be easily solved with the addition of radiocarbon dates of shells from within the unit. Lastly, it was assumed that the $\delta^{18}O$ value of seawater was constant throughout the year. This was presumed to be a reasonably appropriate assumption based on the minimal changes in values derived from the Global Seawater $\delta^{18}O$ database, but this was not directly characterized.

5.3.3 Suggested Future Research

This study was essentially a proof-of-concept for using this technique for seasonally dating single-event geological deposits and therefore has considerable potential for future research. The use of bivalves in archiving environmental conditions has received much attention, however their use in seasonality analysis has only recently been gaining popularity outside of archaeological studies. Future research using this method could extend to other tsunamigenic deposits including both those that are modern and/or well-characterized and ancient deposits. Seasonally dating deposits could also be used to correlate tsunamigenic units over large geographical areas, thereby assisting in correlation of the magnitude of an event with the resulting expression in the geological record. This would be beneficial for risk assessment applications, enabling one to model the potential risk of certain areas to the impacts of tsunamis or storm surge of different magnitudes.

5.4 References

Birks, S. J., & Edwards, T. W. D. (2009). Atmospheric circulation controls on precipitation isotope–climate relations in western Canada. Tellus B, 61(3), 566-576.

Bond, J. D. (2004). Late Wisconsinan McConnell glaciation of the Whitehorse map area (105D), Yukon. Yukon Exploration and Geology. Yukon Geological Survey, 73-88.

Donato, S. V., Reinhardt, E. G., Boyce, J. I., Rothaus, R., & Vosmer, T. (2008). Identifying tsunami deposits using bivalve shell taphonomy. Geology, 36(3), 199-202.

MacDonald, G. M., & Case, R. A. (2005). Variations in the Pacific Decadal Oscillation over the past millennium. Geophysical Research Letters, 32(8), L08703.

Makou, M. C., Eglinton, T. I., Oppo, D. W., & Hughen, K. A. (2010). Postglacial changes in El Niño and La Niña behavior. Geology, 38(1), 43-46.

APPENDIX A: SPIRIT LAKE OXYGEN ISOTOPE DATA and XRD Data

Depth	Age	$\delta^{13}C$	$\delta^{18}O$
cm	yr BP	VPDB	VPDB
0	291	-1.34	-15.34
0.5	313	-1.79	-14.99
1	335	-1.52	-15.10
1.5	357	-1.63	-15.42
2	380	-1.81	-15.50
2.5	402	-1.97	-15.77
3	424	-1.91	-15.66
3.1	428	-1.41	-14.85
3.2	433	-1.50	-14.99
3.3	437	-1.60	-15.26
3.4	441	-1.59	-15.08
3.5	446	-1.55	-14.87
3.6	450	-1.45	-15.14
3.7	455	-1.61	-15.28
3.8	459	-1.57	-15.22
3.9	464	-1.91	-15.58
4	468	-1.96	-15.53
4.1	472	-2.02	-15.21
4.2	477	-1.94	-15.62
4.3	481	-1.97	-15.71
4.4	486	-1.96	-15.18
4.5	490	-1.94	-15.67
4.6	495	-1.89	-15.63
4.7	499	-1.88	-15.35
4.8	503	-1.90	-15.65
4.9	508	-2.07	-16.13
5	512	-1.98	-15.69
5.1	517	-0.02	-15.24
5.2	521	-1.83	-15.27
5.3	525	-1.90	-15.75
5.4	530	-1.99	-15.85
5.5	534	-1.89	-15.22
5.6	539	-1.99	-16.14
5.7	543	-2.01	-15.75
5.8	548	-2.11	-16.04
5.9	552	-1.80	-15.35
6	556	-1.87	-15.97
6.1	561	-1.88	-15.53
6.2	565	-1.72	-16.17
6.3	570	-0.58	-15.59
6.4	574	-0.39	-15.92
6.5	579	-1.40	-15.42
6.6	583	-0.67	-15.72
6.7	587	-1.67	-15.59
6.8	592	-1.66	-15.49
6.9	596	-1.69	-15.60
7	601	-1.64	-15.69

Depth	Age	$\delta^{13}C$	$\delta^{18}O$
cm	yr BP	VPDB	VPDB
7.1	605	-1.34	-15.35
7.2	609	-1.60	-15.53
7.3	614	-1.63	-15.62
7.4	618	-1.75	-15.44
7.5	623	-1.77	-15.71
7.6	627	-1.62	-15.46
7.7	632	-1.61	-15.60
7.8	636	-1.64	-15.78
7.9	640	-1.75	-15.79
8	645	-1.71	-15.58
8.1	649	-1.12	-15.42
8.2	654	-1.75	-15.81
8.3	658	-1.76	-15.72
8.4	663	-1.73	-15.67
8.5	667	-1.69	-15.54
8.6	671	-1.63	-15.76
8.7	676	-1.66	-15.59
8.8	680	-1.66	-15.59
8.9	685	-1.43	-15.58
9	689	-1.60	-15.75
9.1	693	-0.58	-15.40
9.2	698	-1.35	-15.52
9.3	702	-1.25	-15.40
9.4	707	-1.61	-15.52
9.5	711	-1.58	-15.69
9.6	716	-1.62	-15.61
9.7	720	-1.70	-15.57
9.8	724	-0.72	-15.63
9.9	729	-0.48	-15.30
10	733	-1.61	-16.00
10.1	738	-1.04	-15.42
10.2	742	-1.55	-15.93
10.3	747	-1.53	-15.61
10.4	751	-1.57	-15.98
10.5	755	-1.56	-15.85
10.6	760	-1.64	-15.85
10.7	764	-1.68	-15.73
10.8	769	-1.68	-15.80
10.9	773	-1.70	-15.89
11	778	-1.86	-15.97
17.1	1047	-1.40	-15.67
17.2	1052	-1.96	-15.83
17.3	1056	-2.03	-15.92
17.4	1060	-2.22	-15.84
17.5	1065	-1.98	-15.98
17.6	1069	-1.87	-15.92
17.7	1074	-1.88	-15.87

Depth	Age	$\delta^{13}C$	$\delta^{18}O$
cm	yr BP	VPDB	VPDB
17.8	1078	-1.96	-15.53
17.9	1083	-2.03	-15.82
18	1087	-1.79	-15.13
18.1	1091	-1.09	-15.69
18.2	1096	-1.71	-15.00
18.3	1100	-1.67	-15.22
18.4	1105	-1.72	-15.47
18.5	1109	-1.84	-15.84
18.6	1114	-1.70	-15.95
18.7	1118	-1.72	-15.47
18.8	1122	-1.69	-15.82
18.9	1127	-1.77	-15.42
19	1131	-1.72	-15.64
19.1	1136	-1.33	-15.45
19.2	1140	-1.72	-15.43
19.3	1145	-1.81	-16.07
19.4	1149	-1.80	-15.78
19.6	1158	-1.73	-15.65
19.7	1162	-1.69	-15.69
19.8	1167	-1.56	-15.69
19.9	1171	-1.43	-15.43
20	1175	-1.23	-15.47
20.1	1180	-0.20	-15.32
20.2	1184	-1.00	-15.47
20.3	1189	-1.10	-15.40
20.4	1193	-0.83	-15.49
20.5	1198	-0.68	-15.65
20.6	1202	-0.79	-15.50
20.7	1206	-1.85	-16.11
20.9	1215	-1.07	-15.62
21	1220	-1.16	-15.56
21.1	1224	-1.41	-15.68
21.2	1229	-0.34	-15.34
21.3	1233	-0.88	-15.45
21.4	1237	-0.71	-15.40
21.5	1242	-1.00	-15.29
21.6	1246	-1.05	-15.40
21.7	1251	-1.08	-15.33
21.8	1255	-1.07	-15.28
21.9	1259	-1.05	-15.32
22	1264	-1.12	-15.20
22.1	1268	-1.12	-15.23
22.2	1273	-1.41	-15.52
22.3	1277	-1.10	-15.31
22.4	1282	-1.10	-15.38
22.5	1286	-1.21	-15.38
22.6	1293	-1.31	-15.40

Depth	Age	$\delta^{13}C$	$\delta^{18}O$
cm	yr BP	VPDB	VPDB
22.7	1301	-1.00	-15.36
22.8	1308	-1.18	-15.50
22.9	1315	-1.37	-15.54
23	1323	-1.25	-15.49
23.1	1330	-0.94	-15.62
23.2	1337	-0.33	-15.41
23.3	1345	-0.42	-15.49
23.4	1352	-0.74	-15.58
23.5	1359	-0.71	-15.39
23.6	1367	-0.89	-15.49
23.7	1374	-0.22	-15.21
23.8	1381	-0.65	-15.38
24	1396	-0.97	-15.32
24.1	1403	0.44	-15.68
24.2	1411	-0.67	-15.42
24.3	1418	-0.18	-15.68
24.4	1425	-1.35	-15.37
24.5	1433	-1.44	-15.68
24.6	1440	-1.57	-15.49
24.7	1447	-1.52	-15.48
24.8	1455	-1.49	-15.68
24.9	1462	-1.19	-15.47
25	1469	-1.02	-15.68
25.1	1477	-0.93	-15.35
25.2	1484	-1.16	-15.61
25.3	1491	-0.82	-15.44
25.4	1499	-1.09	-15.48
25.5	1506	-1.08	-15.50
25.6	1513	-1.13	-15.56
25.7	1521	-1.10	-15.45
25.8	1528	-1.23	-15.58
25.9	1535	-1.17	-15.53
26	1543	-0.84	-15.25
26.1	1550	-0.71	-15.18
26.2	1557	-0.84	-15.26
26.3	1565	-0.62	-15.29
26.4	1572	-0.89	-15.35
26.5	1579	-0.79	-15.39
26.6	1587	-0.66	-15.38
26.7	1594	-0.71	-15.20
26.8	1601	-0.65	-15.46
26.9	1609	-0.84	-15.20
27	1616	-0.88	-15.47
27.1	1623	-0.71	-15.50
27.2	1631	-0.95	-15.68
27.3	1638	-1.00	-15.74
27.4	1645	-1.13	-15.69

Depth	Age	$\delta^{13}C$	$\delta^{18}O$
cm	yr BP	VPDB	VPDB
27.5	1653	-1.26	-15.75
27.6	1660	-1.12	-15.56
27.7	1667	-0.84	-15.79
27.8	1675	-1.00	-15.63
27.9	1682	-1.13	-15.90
28	1689	-0.96	-15.73
28.1	1697	-1.04	-15.60
28.2	1704	-1.17	-15.68
28.3	1711	-1.06	-15.67
28.4	1719	-1.07	-15.69
28.6	1733	-0.21	-15.49
28.7	1741	-0.59	-15.75
28.8	1748	-0.45	-15.44
28.9	1755	-0.75	-15.56
29	1763	-0.88	-15.76
29.1	1770	-0.32	-15.44
29.3	1785	-0.83	-15.52
29.4	1792	-0.76	-15.65
29.5	1799	-0.96	-15.64
29.7	1814	-1.16	-15.82
29.8	1821	-1.06	-15.66
29.9	1829	-1.16	-15.68
30	1836	-0.99	-15.47
30.1	1843	-0.52	-15.35
30.2	1851	-0.85	-15.29
30.3	1858	-0.90	-15.44
30.4	1878	-0.95	-15.41
30.5	1882	-0.82	-15.39
30.6	1886	-0.86	-15.39
30.7	1890	-0.63	-15.30
30.8	1894	-0.63	-15.40
30.9	1898	-0.89	-15.38
31	1902	-1.02	-15.44
31.1	1906	-0.23	-15.24
31.2	1910	-0.73	-15.33
31.3	1914	-0.70	-15.38
31.4	1918	-0.77	-15.28
31.5	1922	-0.63	-15.35
30.1	1843	-0.52	-15.35
30.2	1851	-0.85	-15.29
30.3	1858	-0.90	-15.44
30.4	1878	-0.95	-15.41
30.5	1882	-0.82	-15.39
30.6	1886	-0.86	-15.39
30.7	1890	-0.63	-15.30
30.8	1894	-0.63	-15.40
30.9	1898	-0.89	-15.38

Depth	Age	$\delta^{13}C$	$\delta^{18}O$
cm	yr BP	VPDB	VPDB
31	1902	-1.02	-15.44
31.1	1906	-0.23	-15.24
31.2	1910	-0.73	-15.33
31.3	1914	-0.70	-15.38
31.4	1918	-0.77	-15.28
31.5	1922	-0.63	-15.35
31.6	1926	-0.48	-15.33
31.7	1930	-0.50	-15.29
31.9	1937	-0.66	-15.93
32	1941	-0.67	-15.68
30.6	1886	-0.86	-15.39
30.7	1890	-0.63	-15.30
30.8	1894	-0.63	-15.40
30.9	1898	-0.89	-15.38
31	1902	-1.02	-15.44
31.1	1906	-0.23	-15.24
31.2	1910	-0.73	-15.33
31.3	1914	-0.70	-15.38
31.4	1918	-0.77	-15.28
31.5	1922	-0.63	-15.35
31.6	1926	-0.48	-15.33
31.7	1930	-0.50	-15.29
31.9	1937	-0.66	-15.93
32	1941	-0.67	-15.68
32.1	1945	-0.26	-15.42
32.2	1949	-0.49	-15.86
32.3	1953	-0.90	-15.78
32.5	1961	-0.65	-15.92
32.7	1969	-1.61	-16.15
32.8	1973	-1.39	-16.08
32.9	1977	-1.39	-16.12
33	1981	-1.29	-16.06
33.1	1985	-1.44	-16.06
33.2	1989	-1.31	-16.06
33.3	1993	-0.88	-15.95
33.4	1997	-1.63	-16.07
33.5	2001	-1.46	-15.97
33.6	2005	-0.40	-15.66
33.7	2009	-0.87	-15.71
33.8	2013	-1.54	-15.94
33.9	2017	-1.48	-15.84
34	2021	-1.46	-16.02
34.1	2025	-1.79	-15.89
34.2	2029	-1.45	-15.82
34.3	2033	-1.45	-15.76
34.4	2037	-1.39	-15.74
34.5	2040	-1.47	-15.75

Depth	Age	$\delta^{13}C$	$\delta^{18}O$
cm	yr BP	VPDB	VPDB
34.6	2044	-1.41	-15.93
34.7	2048	-1.45	-15.72
34.8	2052	-1.34	-15.58
34.9	2056	-1.58	-15.84
35	2060	-1.33	-15.94
35.1	2064	-1.06	-15.32
35.2	2068	-1.50	-15.55
35.3	2072	-1.53	-15.60
35.4	2076	-1.40	-15.54
35.5	2080	-1.35	-15.48
35.6	2084	-1.27	-15.42
35.7	2088	-1.15	-15.45
35.8	2092	-1.29	-15.38
35.9	2096	-1.37	-15.53
36	2100	-1.31	-15.49
36.1	2104	-1.71	-15.51
36.2	2108	-1.19	-15.47
36.3	2112	-1.21	-15.44
36.4	2116	-1.18	-15.49
36.5	2120	-1.19	-15.45
36.6	2124	-1.11	-15.35
36.7	2128	-1.14	-15.42
36.8	2132	-1.08	-15.30
36.9	2136	-1.16	-15.40
37	2140	-1.11	-15.40
37.5	2159	-0.95	-15.23
38	2179	-0.43	-15.26
38.5	2199	-0.82	-15.46
39	2219	-1.48	-15.86
39.5	2239	-0.49	-16.00
40	2258	-1.70	-15.86
40.5	2278	-0.91	-15.43
41	2298	-1.40	-15.86
41.5	2318	0.10	-14.95
42	2338	-0.82	-15.78
42.5	2358	-0.25	-15.21
43	2377	-0.58	-15.82
43.5	2397	-0.16	-15.57
44	2417	-0.80	-15.73
44.5	2437	-0.40	-15.49
45	2457	-1.16	-15.81
45.5	2476	-0.55	-15.41
46	2496	-0.60	-15.31
46.5	2516	0.20	-14.99
47	2536	-0.30	-14.99
47.5	2556	0.13	-15.15
48	2575	-0.08	-15.18

Depth	Age	$\delta^{13}C$	$\delta^{18}O$
cm	yr BP	VPDB	VPDB
48.5	2595	0.73	-15.12
49	2615	-0.30	-15.31
49.5	2633	-0.18	-15.03
50	2647	-0.64	-15.57
50.5	2661	-0.81	-15.64
51	2676	-0.87	-15.94
51.5	2690	-1.19	-16.01
52	2705	-0.50	-15.46
52.5	2719	-1.25	-15.72
53	2733	-0.31	-15.29
53.5	2748	-0.36	-15.15
54	2762	0.63	-14.83
54.5	2776	0.95	-15.01
55	2791	0.02	-15.41
55.5	2805	-0.06	-15.66
56	2819	0.64	-15.56
56.5	2834	0.05	-15.40
57	2848	0.11	-15.41
57.5	2863	-0.19	-15.58
58	2877	-0.14	-15.53
58.5	2891	-0.28	-15.42
59	2906	-1.19	-15.98
59.5	2920	-0.27	-15.74
60.5	2949	-0.67	-15.56
61	2963	-0.35	-15.28
61.5	2977	-1.07	-15.80
62	2992	0.54	-15.27
62.5	3006	-0.25	-15.20
63	3020	-0.36	-15.50
63.5	3035	-0.41	-15.36
64	3049	-0.36	-15.38
64.5	3064	-0.36	-15.51
65	3078	0.15	-15.59
65.5	3092	-0.59	-15.62
66	3107	-0.95	-15.98
66.5	3121	-0.98	-15.79
67	3135	-0.56	-15.62
67.5	3150	-0.75	-15.72
68	3164	-0.94	-15.91
68.5	3178	-1.13	-15.96
69	3193	0.10	-15.29
69.5	3207	-1.04	-15.79
70	3222	-0.45	-15.81
70.5	3236	-0.39	-15.80
71	3250	-0.29	-15.73
71.5	3265	-0.20	-15.75
72	3279	-0.25	-15.91

Depth	Age	$\delta^{13}C$	$\delta^{18}O$
cm	yr BP	VPDB	VPDB
72.5	3293	-0.90	-16.07
73	3308	-0.13	-15.82
73.5	3322	-0.94	-15.93
74	3336	-0.28	-15.45
74.5	3351	-0.88	-15.58
75	3365	-0.20	-15.05
75.5	3379	-1.72	-15.91
76	3394	0.35	-15.54
76.5	3408	-0.60	-15.70
77	3423	-0.22	-15.68
77.5	3437	-0.69	-15.78
78	3451	-0.15	-15.60
79	3480	-0.85	-15.89
79.1	3483	-0.96	-16.10
79.2	3486	-1.17	-16.27
79.3	3489	-1.39	-16.21
79.4	3491	-1.39	-16.38
79.5	3494	-1.39	-16.38
79.6	3497	-1.36	-16.26
79.7	3500	-1.45	-16.47
79.8	3503	-1.63	-16.64
79.9	3506	-1.45	-16.68
80	3509	-1.85	-16.47
80.1	3512	-1.75	-16.62
80.2	3514	-1.68	-16.52
80.3	3517	-1.84	-16.68
80.4	3520	-1.79	-16.56
80.5	3523	-1.73	-16.61
80.6	3526	-1.49	-16.55
80.7	3529	-1.34	-16.37
80.8	3532	-1.36	-16.07
80.9	3535	-1.47	-16.03
81.3	3546	-1.58	-15.75
81.4	3549	-1.71	-15.83
81.6	3555	-1.82	-15.95
81.7	3558	-1.84	-15.88
81.8	3560	-1.95	-16.11
81.9	3563	-2.07	-16.19
82	3566	-2.38	-16.59
82.1	3569	-2.55	-16.28
82.2	3572	-3.03	-16.33
82.5	3581	0.01	-15.55
82.6	3583	-0.33	-15.67
82.7	3586	-0.26	-15.60
82.8	3589	-0.40	-15.57
82.9	3592	-0.44	-15.50
83	3595	-0.53	-15.55

Depth	Age	$\delta^{13}C$	$\delta^{18}O$
cm	yr BP	VPDB	VPDB
83.1	3598	-0.51	-15.82
83.2	3601	-0.69	-16.04
83.3	3603	-0.52	-15.75
83.4	3606	-0.45	-15.95
83.5	3609	-0.59	-16.00
83.6	3612	-0.64	-16.18
83.7	3615	-0.60	-16.03
83.8	3618	-0.79	-16.09
83.9	3621	-0.80	-16.08
84	3624	-0.82	-15.95
84.1	3626	-0.99	-16.25
84.2	3629	-0.79	-16.16
84.3	3632	-1.09	-16.06
84.4	3635	-1.45	-16.08
84.5	3638	-1.06	-16.34
84.6	3641	-1.11	-16.11
84.7	3644	-1.00	-15.83
84.8	3647	-1.00	-15.68
84.9	3649	-1.02	-15.71
85	3652	-1.03	-15.72
85.1	3655	-0.93	-15.54
85.2	3658	-0.96	-15.46
85.3	3661	-1.02	-15.44
85.4	3664	-0.99	-15.41
85.5	3667	-1.01	-15.52
85.6	3670	-1.06	-15.41
85.7	3672	-1.06	-15.58
85.8	3675	-1.00	-15.36
85.9	3678	-0.89	-15.77
86	3681	-0.92	-15.85
86.1	3684	-0.93	-15.68
86.2	3687	-0.97	-15.68
86.3	3690	-1.09	-15.67
86.4	3693	-1.19	-16.13
86.5	3695	-1.36	-16.01
86.6	3698	-1.14	-16.18
86.7	3701	-1.18	-16.25
86.8	3704	-2.23	-15.89
86.9	3707	-1.18	-16.03
87	3710	-1.11	-16.32
87.1	3713	-1.02	-15.99
87.2	3715	-1.01	-16.02
87.3	3718	-0.91	-15.86
87.4	3721	-0.86	-15.81
87.5	3724	-0.94	-16.00
87.6	3727	-0.87	-16.13
87.7	3730	-0.95	-16.01

Depth	Age	$\delta^{13}C$	$\delta^{18}O$
cm	yr BP	VPDB	VPDB
87.8	3733	-0.89	-16.05
87.9	3736	-0.83	-16.20
88	3738	-0.64	-15.88
88.1	3741	-0.31	-15.92
88.2	3744	-0.68	-15.81
88.3	3747	-0.34	-15.23
88.4	3750	-0.22	-15.39
88.5	3753	-0.28	-14.95
88.6	3756	-0.28	-15.43
88.7	3759	-0.31	-15.50
88.8	3761	-0.42	-15.79
88.9	3764	-0.33	-15.87
89	3767	-0.22	-15.86
89.1	3770	-0.01	-15.99
89.2	3773	-0.14	-16.04
89.3	3776	-0.48	-16.04
89.4	3779	-0.48	-16.10
89.5	3782	-0.73	-16.20
89.6	3784	-0.84	-16.25
89.7	3787	-0.50	-16.04
89.8	3790	-0.51	-15.88
89.9	3793	-0.53	-15.82
90	3796	-0.43	-15.82
90.1	3799	-0.42	-15.92
90.2	3802	-0.46	-15.84
90.3	3805	-1.15	-16.06
90.4	3807	-1.14	-16.19
90.5	3810	-0.83	-15.99
90.7	3816	-0.87	-15.93
90.8	3819	-0.72	-16.06
90.9	3822	-0.57	-15.80
91	3825	-0.46	-15.68
91.1	3828	-0.40	-15.65
91.2	3830	-0.38	-15.76
91.3	3833	-0.67	-15.64
91.4	3836	-0.39	-15.64
91.5	3839	-0.19	-15.61
91.6	3842	-0.36	-15.58
91.7	3845	-0.54	-15.78
91.8	3848	-0.46	-15.77
91.9	3850	-0.58	-15.57
92	3853	-0.40	-15.53
92.1	3856	-0.29	-15.52
92.2	3859	-0.33	-15.51
92.3	3862	-0.59	-15.70
92.4	3865	-0.78	-16.06
92.5	3868	-0.71	-15.80

Depth	Age	$\delta^{13}C$	$\delta^{18}O$
cm	yr BP	VPDB	VPDB
92.6	3871	-0.67	-15.84
92.7	3873	-0.66	-15.67
92.8	3876	-0.65	-15.60
92.9	3879	-0.69	-15.65
93	3882	-0.72	-15.80
93.1	3885	-0.67	-16.13
93.2	3888	-0.69	-16.10
93.3	3891	-0.90	-15.99
93.4	3894	-0.99	-16.21
93.5	3896	-0.99	-16.26
93.6	3899	-0.82	-16.06
93.7	3902	-0.86	-16.21
93.8	3905	-0.61	-16.07
93.9	3908	-0.83	-16.25
94	3911	-0.78	-16.21
94.1	3914	-0.38	-15.89
94.2	3917	-0.36	-15.76
94.3	3919	-0.39	-15.64
94.4	3922	-0.18	-15.56
94.5	3925	-0.23	-15.53
94.6	3928	-0.18	-15.65
94.7	3931	-0.27	-15.50
94.8	3934	0.02	-15.32
94.9	3937	-0.19	-15.42
95	3940	0.06	-14.98
95.1	3942	-0.16	-14.90
95.2	3945	-0.20	-15.23
95.3	3948	-0.22	-15.15
95.4	3951	-0.22	-15.32
95.5	3952	-0.21	-15.19
95.6	3952	-0.27	-15.46
95.7	3953	-0.34	-15.53
95.8	3954	-0.38	-15.59
96.1	3956	-1.14	-15.98
96.2	3957	-1.30	-16.04
96.3	3958	-1.38	-15.87
96.4	3958	-1.36	-16.02
96.5	3959	-1.26	-15.64
96.9	3962	-1.45	-15.96
97	3963	-1.40	-15.95
97.1	3963	-1.36	-15.88
97.2	3964	-1.48	-15.76
97.3	3965	-1.34	-15.90
97.4	3965	-1.20	-15.92
97.5	3966	-1.00	-15.70
97.6	3967	-1.20	-15.65
97.7	3968	-0.97	-15.70

Depth	Age	$\delta^{13}C$	$\delta^{18}O$
cm	yr BP	VPDB	VPDB
97.8	3968	-0.88	-15.83
97.9	3969	-0.84	-15.67
98	3970	-0.92	-15.78
98.1	3971	-0.89	-15.90
98.2	3971	-0.94	-15.82
98.3	3972	-0.84	-15.80
98.4	3973	-0.79	-15.88
98.5	3973	-0.80	-15.81
98.6	3974	-0.94	-15.83
98.7	3975	-0.87	-16.01
98.8	3976	-0.87	-16.10
98.9	3976	-1.05	-15.91
99	3977	-0.84	-15.78
99.1	3978	-0.87	-15.65
99.2	3979	-1.05	-15.92
99.3	3979	-0.75	-15.74
99.4	3980	-0.62	-15.34
99.5	3981	-0.43	-15.51
99.6	3981	-0.63	-15.32
100.6	3989	-0.83	-15.81
101.6	3996	-0.67	-15.34
101.9	3998	-0.60	-15.10
102	3999	-0.72	-14.95
102.1	4000	-0.47	-14.90
102.2	4000	-0.57	-15.31
102.3	4001	-0.39	-15.16
102.4	4002	-0.67	-15.34
102.5	4002	-0.69	-15.30
102.6	4003	-0.68	-15.57
102.7	4004	-0.59	-15.33
102.8	4005	-0.52	-15.49
102.9	4005	-0.59	-15.37
103	4006	-0.52	-15.14
103.1	4007	-0.53	-15.14
103.2	4008	-0.47	-15.03
103.3	4008	-0.48	-15.04
103.4	4009	-0.40	-14.85
103.5	4010	-0.47	-15.26
103.6	4010	-0.50	-15.18
103.7	4011	-0.57	-15.11
103.8	4012	-0.78	-15.35
103.9	4013	-0.95	-15.68
104	4013	-0.88	-15.58
104.1	4014	-0.81	-15.66
104.2	4015	-0.83	-15.75
104.4	4016	-0.53	-15.41
104.5	4017	-0.77	-15.03

Depth	Age	$\delta^{13}C$	$\delta^{18}O$
cm	yr BP	VPDB	VPDB
104.6	4018	-0.72	-15.44
104.7	4018	-0.71	-15.26
104.8	4019	-1.25	-15.86
104.9	4020	-0.65	-16.22
105.1	4021	-0.98	-16.33
105.2	4022	-1.00	-16.32
105.3	4023	-1.15	-16.11
105.4	4023	-0.47	-15.85
105.5	4024	-0.63	-15.77
105.6	4025	-0.70	-15.82
105.7	4026	-0.75	-15.84
105.8	4026	-0.58	-15.70
105.9	4027	-0.90	-15.91
106	4028	-1.04	-16.12
106.1	4029	-0.97	-15.98
106.2	4029	-0.85	-15.68
106.6	4032	0.96	-14.92
107.6	4039	-0.94	-15.98
108.6	4047	-0.92	-15.62
109.6	4054	0.23	-15.44
110.6	4061	-0.62	-15.90
111.6	4068	-0.84	-15.67
112.6	4076	-0.39	-15.26
113.6	4083	-0.68	-15.76
114.6	4090	0.02	-15.47
115.6	4097	0.35	-16.07
116.6	4105	-0.68	-16.40
117.6	4112	-1.62	-16.27
118.6	4119	-0.62	-16.19
119.6	4126	-1.43	-16.25
120.8	4135	-1.49	-16.03
121.8	4142	-0.83	-15.68
122.8	4150	-0.54	-15.22
123.8	4157	-0.41	-15.09
123.9	4158	-0.47	-15.46
124	4158	-0.82	-15.71
124.1	4159	-0.98	-15.95
124.2	4160	-1.04	-15.83
124.3	4160	-1.03	-15.88
124.4	4161	-1.36	-16.30
124.5	4162	-1.22	-16.02
124.6	4163	-1.27	-16.02
124.7	4163	-1.21	-16.10
124.8	4164	-1.14	-16.11
124.9	4165	-1.03	-16.09
125	4166	-1.25	-16.08
125.1	4166	-0.86	-15.70

Depth	Age	$\delta^{13}C$	$\delta^{18}O$
cm	yr BP	VPDB	VPDB
125.2	4167	-0.89	-15.61
125.3	4168	-0.71	-15.48
125.4	4168	-0.63	-15.45
125.5	4169	-0.67	-15.56
125.6	4170	-0.64	-15.50
125.7	4171	-0.44	-15.22
125.8	4171	-0.55	-15.56
125.9	4172	-1.31	-15.68
126	4173	-0.53	-15.55
126.1	4173	-0.62	-15.62
126.2	4174	-0.67	-15.78
126.3	4175	-0.62	-15.60
126.4	4176	-0.41	-15.58
126.5	4176	-0.57	-15.61
126.6	4177	-0.69	-15.74
126.7	4178	-0.57	-15.70
126.8	4179	-0.68	-15.85
126.9	4179	-0.70	-15.81
127	4180	-0.65	-15.80
127.1	4181	-0.63	-15.81
127.2	4181	-0.69	-15.84
127.3	4182	-0.53	-15.84
127.4	4183	-0.68	-15.84
127.5	4184	-0.63	-16.03
127.6	4184	-0.84	-16.06
127.7	4185	-0.98	-16.13
127.8	4186	-0.93	-16.07
128.8	4193	-0.36	-15.87
129.8	4200	-0.54	-15.16
130.8	4208	-0.98	-15.72
131.8	4215	-0.67	-15.26
132.8	4222	-0.32	-15.22
133.8	4229	-0.60	-15.87
134.8	4237	-0.40	-15.84
135.8	4244	-0.52	-15.63
136.8	4251	-0.91	-15.81
137.8	4258	-0.30	-15.65
140	4274	-1.09	-16.24
141	4281	-0.85	-15.71
142	4289	-1.33	-16.17
143	4296	-1.42	-16.01
144	4303	-0.84	-15.66
145	4310	-1.07	-15.87
146	4318	-0.99	-15.66
147	4325	-1.40	-16.35
148	4332	-1.10	-15.53
149	4339	-1.61	-16.17

Depth	Age	$\delta^{13}C$	$\delta^{18}O$
cm	yr BP	VPDB	VPDB
150	4347	-0.78	-16.26
151	4354	-0.48	-15.94
152	4361	-1.48	-16.25
153	4368	-0.19	-15.24
154	4376	-0.71	-14.81
155	4383	-1.29	-15.48
155.2	4384	0.27	-15.43
155.3	4385	0.48	-15.38
155.4	4386	0.67	-15.40
155.6	4387	0.54	-15.52
155.7	4388	0.28	-15.57
155.8	4389	-0.07	-15.61
155.9	4389	0.09	-15.71
156	4390	0.35	-15.40
156.1	4391	0.28	-15.48
156.2	4392	0.05	-15.31
156.4	4393	0.59	-15.23
156.6	4395	0.19	-15.30
156.7	4395	0.01	-15.59
156.8	4396	-0.36	-15.60
156.9	4397	-0.30	-15.54
157	4397	-0.35	-15.76
157.1	4398	-0.17	-15.62
157.2	4399	-0.32	-15.66
157.3	4400	-0.23	-15.46
157.4	4400	-0.35	-15.67
157.7	4402	-0.35	-15.77
157.8	4403	-0.90	-15.70
157.9	4404	-0.81	-15.72
158	4405	-1.18	-16.10
159	4412	-1.04	-16.01
160	4419	-0.25	-16.48
160.1	4420	-0.30	-16.38
160.2	4421	-0.63	-16.19
160.3	4421	-0.59	-16.44
160.4	4422	0.03	-16.27
160.5	4423	-0.28	-16.20
160.6	4423	-0.21	-16.05
160.7	4424	-0.38	-16.06
160.8	4425	0.10	-15.76
160.9	4426	0.33	-15.64
161	4426	0.27	-16.03
161.1	4427	0.80	-15.64
161.2	4428	0.39	-15.75
161.3	4429	0.11	-15.45
161.4	4429	0.16	-15.17
161.5	4430	0.46	-15.44

Depth	Age	$\delta^{13}C$	$\delta^{18}O$
cm	yr BP	VPDB	VPDB
161.6	4431	0.49	-14.97
161.7	4431	0.21	-15.26
161.8	4432	0.42	-15.15
162	4434	0.19	-15.58
162.4	4437	0.27	-15.85
162.8	4439	0.55	-16.26
162.9	4440	0.42	-16.19
163	4441	0.07	-16.17
163.1	4442	0.59	-15.81
163.2	4442	-0.10	-15.90
163.3	4443	0.69	-15.76
163.4	4444	0.95	-15.81
163.6	4445	0.45	-15.93
163.7	4446	0.34	-16.05
163.8	4447	0.40	-16.08
164	4448	0.21	-15.97
164.1	4449	0.36	-16.00
164.2	4450	1.08	-15.55
164.3	4450	1.49	-15.32
164.4	4451	2.12	-15.07
164.6	4452	0.79	-15.70
164.7	4453	0.49	-15.88
164.8	4454	0.26	-15.97
164.9	4455	0.73	-15.79
165	4455	0.43	-15.94
166	4464	-0.02	-15.92
167	4473	-0.22	-15.76
168	4482	-0.12	-15.73
169	4491	0.10	-15.29
170	4500	-1.14	-16.00
171	4510	-0.80	-15.86
172	4519	-0.88	-16.10
184	4629	-1.14	-15.84
185	4638	-1.58	-16.26
186	4647	-1.36	-16.22
187	4657	-0.48	-15.43
188	4666	-0.89	-15.64
189	4675	-0.33	-14.97
189.1	4676	0.29	-15.44
189.2	4677	0.27	-15.34
189.3	4678	0.17	-15.56
189.4	4679	0.16	-15.45
189.5	4680	0.63	-15.30
189.6	4681	-0.50	-15.37
189.7	4681	-0.56	-15.39
189.8	4682	0.15	-15.45
189.9	4683	-0.09	-15.45

Depth	Age	$\delta^{13}C$	$\delta^{18}O$
cm	yr BP	VPDB	VPDB
190	4684	0.48	-15.14
190.1	4685	0.04	-15.37
190.2	4686	0.27	-15.25
190.3	4687	0.14	-15.45
190.4	4688	-0.63	-15.30
190.5	4689	-0.37	-15.46
190.6	4690	-0.49	-15.49
190.7	4691	0.12	-15.38
190.8	4692	0.11	-15.51
190.9	4692	0.14	-15.76
191	4693	-0.06	-15.74
191.1	4694	-0.63	-15.98
191.2	4695	-0.64	-15.92
191.3	4696	-0.42	-15.83
191.4	4697	0.04	-15.57
191.5	4698	0.09	-15.61
191.6	4699	0.66	-15.84
191.7	4700	0.92	-15.44
191.8	4701	0.59	-15.48
191.9	4702	0.51	-15.40
192	4703	-0.45	-15.71
192.1	4703	-0.06	-15.59
192.2	4704	0.28	-15.44
192.3	4705	0.27	-15.69
192.4	4706	0.24	-15.86
192.5	4707	0.10	-15.80
192.6	4708	-0.01	-15.75
192.7	4709	-0.44	-15.20
192.8	4710	-0.42	-15.72
192.9	4711	-0.23	-15.55
193	4712	0.30	-15.61
194	4721	0.68	-15.32
195	4730	-0.16	-15.40
196	4739	-0.59	-15.57
197	4749	-0.73	-15.45
198	4758	-1.28	-16.55
199	4767	-1.16	-15.77
200	4776	-0.30	-16.40
201	4785	-0.46	-15.02
202	4794	-0.92	-15.40
203	4804	-0.54	-16.17
204	4813	-1.12	-15.34
205	4822	-0.87	-15.47
206	4831	-1.14	-15.39
207	4840	-0.41	-15.39
208	4850	-0.38	-15.48
209.1	4860	-0.24	-16.01

Depth	Age	$\delta^{13}C$	$\delta^{18}O$
cm	yr BP	VPDB	VPDB
210	4868	-0.17	-15.66
211	4877	-0.70	-16.14
212	4886	-0.30	-16.20
213	4896	-0.62	-16.27
214	4905	-0.68	-16.22
215	4914	-0.63	-15.85
216	4923	-0.67	-16.02
217	4932	-0.77	-15.70
218	4942	-1.00	-15.87
219	4951	-0.70	-15.94
220	4960	-0.26	-15.24
221	4969	-0.40	-15.67
222	4978	-0.81	-15.68
223	4987	-2.13	-16.99
224	4997	-2.02	-16.69
225	5006	-1.43	-16.29
226	5015	-2.10	-16.42
227	5024	-1.52	-16.19
228	5033	-1.21	-16.25
229	5043	-1.42	-16.11
230	5052	-1.77	-16.19
231	5061	-1.57	-16.23
232	5070	-0.34	-15.90
233	5079	-0.44	-16.06
234	5089	-0.30	-16.27
235	5098	-0.66	-15.97
236	5107	-0.99	-16.39
237	5116	-1.32	-16.49
238	5125	-0.59	-16.11
239	5135	-0.28	-15.39
240	5144	-0.75	-15.81
241	5153	-1.98	-16.65
242	5162	-0.56	-15.98
243	5171	-0.96	-15.88
244	5181	-1.24	-16.12
245	5190	-1.27	-16.05
246	5199	-1.75	-16.74
247	5208	-0.90	-16.21
248	5217	-1.04	-16.44
249	5226	-1.30	-16.18
250	5236	-0.62	-16.24
251	5245	-0.87	-15.89
252	5254	-0.99	-16.32
253	5263	-0.12	-15.64
254	5272	-1.05	-15.97
255	5282	-2.00	-16.50
256	5291	-0.22	-16.69

Depth	Age	$\delta^{13}C$	$\delta^{18}O$
cm	yr BP	VPDB	VPDB
257	5300	-0.49	-16.16
258	5309	-0.76	-16.17
259	5318	-0.55	-15.75
260	5328	-0.29	-15.96
261	5337	0.00	-15.72
262	5346	-0.90	-16.24
263	5355	-0.90	-16.65
264	5364	-2.07	-16.85
265	5374	-2.13	-16.96
266	5383	-0.58	-16.20
267	5392	0.41	-15.59
268	5401	-1.47	-16.27
269	5410	-1.48	-16.05
270	5419	-1.46	-16.70
271	5429	-0.35	-17.26
272	5438	-0.89	-16.71
274	5456	-0.89	-15.83
275	5465	-1.21	-16.14
276	5475	-0.11	-15.27
277	5484	-0.70	-16.09
278	5493	-0.38	-16.39
279	5510	-1.29	-16.08
280	5528	-1.43	-16.10
281	5545	-1.21	-15.94
282	5562	-0.88	-15.93
283.4	5587	-0.74	-15.92
284.4	5604	-0.73	-15.87
285.4	5621	-0.63	-16.24
286.4	5639	-1.06	-16.12
287.4	5656	-0.95	-16.16
287.5	5658	-0.88	-16.26
287.6	5660	-1.06	-16.30
287.7	5661	0.03	-15.97
287.8	5663	0.08	-15.90
287.9	5665	0.55	-15.83
288	5667	0.84	-15.64
288.1	5668	1.16	-15.58
288.2	5670	0.23	-15.88
288.3	5672	0.38	-15.91
288.4	5674	-0.22	-15.81
288.5	5675	0.27	-15.90
288.6	5677	-1.12	-16.40
288.7	5679	-1.54	-16.37
288.8	5680	-1.00	-16.34
288.9	5682	0.52	-15.85
289	5684	0.63	-15.77
289.1	5686	1.17	-15.50

Depth	Age	$\delta^{13}C$	$\delta^{18}O$
cm	yr BP	VPDB	VPDB
289.2	5687	1.48	-15.40
289.3	5689	1.06	-15.45
289.4	5691	0.67	-15.50
289.5	5693	0.64	-15.54
289.6	5694	2.17	-15.58
289.7	5696	1.46	-15.58
289.8	5698	1.80	-15.49
289.9	5700	1.22	-15.58
290	5701	0.01	-15.64
290.1	5703	-0.11	-15.62
290.2	5705	0.18	-15.58
290.3	5706	1.70	-15.00
290.4	5708	1.08	-15.17
290.5	5710	1.45	-15.12
290.6	5712	0.82	-15.42
290.7	5713	1.05	-15.25
290.8	5715	0.32	-15.74
290.9	5717	-0.09	-15.90
291	5719	-0.13	-15.78
291.1	5720	0.46	-15.28
291.2	5722	0.44	-15.16
291.3	5724	0.56	-15.12
291.4	5726	0.69	-14.97
292.4	5743	-1.34	-16.10
293.4	5760	-0.91	-15.36
294.4	5778	-1.72	-16.22
295.4	5795	-1.89	-16.11
296.4	5812	-1.02	-15.92
297.4	5830	-2.24	-16.53
298.5	5849	-1.53	-16.02
299.4	5864	-1.60	-16.24
300.4	5882	-1.25	-16.08
301.4	5899	-2.20	-16.74
302.4	5917	-1.25	-16.40
303.4	5934	-1.00	-15.64
304.4	5951	-0.84	-15.35
305.4	5969	-1.67	-16.51
306.4	5986	-1.44	-16.51
307.3	6002	-1.47	-15.85
308.3	6019	-1.69	-16.24
309.3	6036	-1.90	-16.75
310.3	6054	-1.05	-15.81
311.3	6071	-1.37	-15.94
312.3	6088	-1.43	-16.37
313.3	6106	-1.84	-16.60
314.6	6128	-0.24	-15.78
315.5	6144	-0.24	-16.08

Depth	Age	$\delta^{13}C$	$\delta^{18}O$
cm	yr BP	VPDB	VPDB
316.5	6161	0.21	-16.21
317.5	6179	-0.07	-16.52
318.5	6196	-0.24	-15.85
319.5	6213	0.16	-16.35
320.5	6231	1.36	-15.43
321.5	6248	-0.02	-15.22
322.5	6265	-1.39	-15.87
323.5	6283	-1.88	-16.28
324.5	6300	-2.14	-16.36
325.5	6317	-1.23	-15.99
326.5	6335	0.29	-16.19
327.5	6352	-0.35	-16.37
328.5	6370	-1.41	-16.72
329.5	6387	-1.15	-16.13
330.5	6404	-1.74	-16.65
331.5	6422	-1.08	-16.03
332.5	6439	-0.14	-15.72
333.5	6456	-0.79	-15.78
334.5	6474	-1.44	-16.08
335.5	6491	-2.67	-16.72
336.5	6508	-2.51	-16.84
337.5	6526	-2.10	-16.38
338.5	6543	-2.06	-16.32
339.5	6560	0.28	-16.24
340.5	6578	-0.19	-15.92
341.5	6595	-1.27	-16.15
342.5	6613	-1.17	-15.89
343.5	6630	-1.70	-16.64
344.5	6647	-1.82	-16.49
345.5	6665	-2.53	-16.89
346.5	6682	-1.81	-15.77
347.5	6699	-1.00	-15.53
348.5	6728	-1.49	-15.85
349.5	6768	-1.60	-16.13
350.5	6809	-2.25	-16.29
351.5	6849	-1.48	-15.55
352.5	6889	-1.30	-16.14
353.5	6929	-1.17	-15.88
354.5	6969	-1.77	-16.06
355.5	7010	-1.42	-15.90
356.5	7050	-1.72	-16.34
357.5	7090	-1.97	-16.76
358.5	7130	-2.02	-15.95
359.5	7171	-1.50	-16.16
360.5	7211	-1.97	-15.71
361.5	7251	-1.78	-16.11
362.5	7291	-1.58	-16.08

Depth	Age	$\delta^{13}C$	$\delta^{18}O$
cm	yr BP	VPDB	VPDB
363.5	7331	-1.80	-16.50
364.5	7372	-1.35	-15.75
365.5	7412	-0.33	-15.31
366.5	7452	0.19	-15.62
367.5	7492	-0.50	-16.09
369.5	7573	-2.23	-16.67
370.5	7613	-1.69	-16.01
371.5	7653	-1.62	-15.70
372.5	7693	-1.42	-15.65
373.5	7734	-1.64	-16.20
374.5	7774	-1.42	-16.62
375.5	7814	-0.85	-15.75
375.6	7818	-0.61	-15.73
375.7	7822	-0.51	-15.70
375.8	7826	-0.25	-15.77
375.9	7830	-0.43	-15.75
376	7834	0.29	-15.58
376.1	7838	0.55	-15.37
376.2	7842	0.53	-15.18
376.3	7846	0.71	-15.43
376.4	7850	0.24	-15.54
376.5	7854	0.20	-15.57
376.6	7858	-0.03	-15.68
376.7	7862	-0.46	-15.99
376.8	7866	-0.49	-15.91
376.9	7870	0.18	-15.85
377.1	7878	0.50	-15.85
377.2	7882	0.88	-15.80
377.3	7886	1.09	-15.76
377.4	7890	1.11	-15.84
377.5	7894	1.03	-15.73
377.6	7898	0.17	-15.48
377.7	7902	0.25	-15.48
377.8	7907	0.47	-15.66
377.9	7911	0.16	-15.69
378	7915	-0.48	-15.70
378.1	7919	0.02	-15.55
378.2	7923	-0.11	-15.63
378.3	7927	-0.12	-15.60
378.4	7931	0.10	-15.48
378.5	7935	-0.15	-15.52
378.6	7939	-0.21	-15.64
378.7	7943	-0.27	-15.96
378.8	7947	0.06	-16.00
378.9	7951	0.03	-15.62
379	7955	-0.26	-16.05
379.1	7959	-0.44	-16.21

Depth	Age	$\delta^{13}C$	$\delta^{18}O$
cm	yr BP	VPDB	VPDB
379.2	7963	-0.50	-16.21
379.3	7967	-0.37	-16.22
379.4	7971	-0.40	-16.27
379.5	7975	-1.34	-16.34
380.5	8015	0.41	-15.99
381.5	8055	-0.86	-16.07
382.5	8096	-0.17	-15.77
383.5	8136	0.33	-15.28
384.5	8176	0.11	-15.22
385.5	8216	1.11	-15.48
386.5	8256	-0.02	-15.71
387.5	8297	-1.48	-16.03
388.5	8337	-1.77	-15.74
390	8397	-0.70	-15.89
391	8437	-0.18	-15.59
392	8478	-0.62	-15.75
393	8518	-0.16	-15.24
394	8558	0.14	-15.51
395	8598	0.09	-15.63
396	8638	0.56	-15.54
397	8679	0.78	-15.55
398	8719	1.19	-14.95
399	8759	1.68	-15.19
400	8799	1.03	-15.24
401	8840	0.72	-15.29
402	8880	0.75	-15.63
403	8920	0.89	-15.22
404	8960	1.27	-15.21
405	9000	0.33	-15.26
406	9041	0.25	-15.70
407	9081	1.05	-15.43
408	9115	1.40	-15.20
409	9139	1.23	-14.98
410	9164	-0.39	-15.56
411	9188	0.31	-15.05
412	9212	0.78	-15.37
413	9237	1.00	-15.63
414	9261	1.46	-15.55
415	9286	1.83	-15.23
416	9310	0.40	-15.81
417	9334	0.85	-15.68
418	9359	1.29	-15.88
419	9383	0.20	-15.91
420	9408	-0.12	-15.98
421	9432	1.30	-15.02
422	9457	0.10	-16.16
423	9481	2.03	-15.83

Depth	Age	$\delta^{13}C$	$\delta^{18}O$
cm	yr BP	VPDB	VPDB
424	9505	0.47	-15.05
425	9530	0.29	-15.59
426	9554	1.16	-15.51
427	9579	1.14	-15.16
428	9603	1.08	-15.06
430	9652	-0.61	-15.82
431	9676	-1.07	-15.93
432	9701	-1.33	-16.29
433	9725	-1.79	-16.25
434	9750	-1.21	-16.19
435	9774	-1.84	-16.06
436	9798	-1.79	-16.30
437	9823	-1.37	-15.84
438	9847	-1.59	-16.30
439	9872	-1.27	-15.76
440	9896	-2.06	-16.60
441	9920	-0.61	-16.24
442	9945	-0.73	-15.95
443	9969	-0.93	-15.98
444	9994	-0.51	-15.99
445	10018	-1.24	-16.10
446	10043	-0.88	-15.72
447	10067	-0.03	-15.28
448	10091	0.27	-15.48
449	10116	-0.20	-15.54
450	10140	-0.64	-15.49
451	10165	-0.56	-15.75
452	10189	-1.24	-15.90
453	10213	-0.57	-15.34
454	10238	-0.32	-15.70
455	10262	-0.13	-15.60
456	10287	0.58	-16.01
457	10311	-0.14	-15.51
458	10335	-0.17	-15.83
459	10360	-0.33	-16.10
460	10384	-0.37	-15.92
461	10409	0.01	-15.56
462	10433	-0.36	-15.43
463	10458	-0.16	-15.75
464	10482	-0.77	-15.77
465	10506	-0.26	-15.99
466	10531	0.12	-15.90
467	10555	-0.59	-15.99
468	10580	-1.05	-16.14
469	10604	-0.42	-15.97
470	10628	-0.67	-16.18
471	10653	-0.82	-16.27

Depth	Age	$\delta^{13}C$	$\delta^{18}O$
cm	yr BP	VPDB	VPDB
472	10677	-0.50	-15.57
473	10702	-0.82	-15.88
473.5	10714	-0.49	-16.02
474.5	10738	-0.85	-15.81
475.5	10763	-0.46	-15.84
476.5	10787	-0.51	-15.34
477.5	10812	-0.64	-15.84
478.5	10836	0.40	-15.97
479.5	10860	-0.33	-15.50
480.5	10885	-1.04	-16.00
481.5	10909	-0.37	-15.77
483.5	10958	-1.13	-16.35
484.5	10982	0.05	-15.04
485.5	11007	-0.93	-15.37
486.5	11031	0.08	-15.16
487.5	11056	-0.44	-16.01
488.5	11080	-0.78	-15.80
489.5	11105	-0.53	-15.95
490.5	11129	-0.02	-15.44
491.5	11153	-0.20	-15.89
492.5	11178	-0.05	-15.68
493.5	11202	-0.44	-15.35
494.5	11227	-0.75	-15.78
495.5	11251	-0.42	-15.60
496.5	11275	-0.47	-16.14
497.5	11300	-0.62	-15.93
498.5	11324	-0.22	-16.39
499.5	11349	-0.31	-16.41
500.5	11373	-0.59	-15.92
501.5	11398	-1.11	-16.48
502.5	11422	-0.93	-16.33
511.5	11642	-1.56	-17.16
513.5	11691	-0.57	-15.88
514.5	11715	-1.73	-17.20
515.5	11739	-1.40	-16.97
516.5	11748	-0.73	-16.12
517.5	11749	-1.46	-16.56
518.5	11750	-1.22	-16.18
519.5	11752	-1.11	-16.49
520.5	11753	-0.94	-16.56
521.5	11754	-0.94	-15.91
522.5	11756	-1.82	-17.00
523	11756	-1.13	-14.87
523.5	11757	-1.07	-15.74
524	11758	-0.91	-16.31
524.5	11758	-1.35	-16.83
525	11759	-0.58	-16.19

Depth	Age	$\delta^{13}C$	$\delta^{18}O$
cm	yr BP	VPDB	VPDB
525.5	11760	-0.69	-15.76
526	11761	-0.78	-15.74
526.5	11761	-1.11	-16.25
527	11762	-1.17	-16.61
527.1	11762	-0.84	-14.80
527.2	11762	-0.81	-13.91
527.3	11762	-0.97	-14.47
527.4	11762	-1.53	-15.89
527.5	11763	-1.15	-16.61
527.6	11763	-0.74	-16.25
527.7	11763	-0.28	-15.94
527.8	11763	-1.11	-15.48
527.9	11763	-1.86	-17.23
528	11763	-2.01	-17.12
528.1	11763	-1.51	-15.98
528.2	11763	-1.03	-15.17
528.3	11764	-0.78	-14.22
528.4	11764	-0.91	-13.83
528.5	11764	-1.11	-14.50
528.6	11764	-1.11	-14.09
528.7	11764	-1.22	-14.30
528.8	11764	-1.39	-14.75
528.9	11764	-1.75	-14.91
529	11765	-1.27	-14.65
529.1	11765	-1.05	-14.14
529.2	11765	-1.17	-14.67
529.3	11765	-0.96	-14.26
529.4	11765	-1.18	-14.91
529.5	11765	-0.57	-15.43
529.6	11765	-0.85	-16.11
529.7	11766	-0.13	-15.97
529.8	11766	-1.67	-16.98
529.9	11766	-1.03	-14.66
530	11766	-0.61	-13.63
530.1	11766	-0.78	-14.10
530.2	11766	-0.87	-13.74
530.3	11766	-0.99	-14.05
530.4	11766	-1.03	-14.12
530.5	11767	-1.11	-14.03
530.6	11767	-1.20	-14.24
530.7	11767	-1.34	-15.08
530.8	11767	-1.26	-14.77
530.9	11767	-1.46	-16.29
531	11767	-1.54	-16.30
531.1	11767	-0.55	-15.77
531.2	11768	-0.93	-15.07
531.4	11768	-1.90	-16.24

Depth	Age	$\delta^{13}C$	$\delta^{18}O$
cm	yr BP	VPDB	VPDB
531.5	11768	-1.79	-16.00
531.6	11768	-1.19	-14.92
531.7	11768	-0.56	-13.88
531.8	11768	-0.61	-14.12
531.9	11768	-0.60	-14.14
532	11769	-0.70	-14.14
532.1	11769	-1.72	-13.47
532.2	11769	-0.41	-13.38
532.3	11769	-0.30	-13.46
532.4	11769	-0.34	-13.26
532.5	11769	-0.29	-13.16
532.6	11769	-0.26	-13.43
532.7	11770	-0.60	-14.03
532.8	11770	-0.67	-13.84
532.9	11770	-0.30	-13.50
533	11770	-0.34	-13.18
533.1	11770	-0.43	-13.22
533.2	11770	-0.54	-13.46
533.3	11770	-0.76	-13.91
533.4	11771	-0.64	-13.56
533.5	11771	-0.64	-14.00
533.6	11771	-0.81	-14.13
533.7	11771	-0.89	-14.40
533.8	11771	-0.99	-14.54
533.9	11771	-1.26	-15.05
534	11771	-1.02	-14.63
534.1	11771	-1.08	-14.67
534.2	11772	-1.27	-14.53
534.3	11772	-1.27	-14.53
534.4	11772	-1.19	-14.51
534.5	11772	-1.24	-14.34
534.6	11772	-0.96	-14.11
534.7	11772	-0.92	-13.84
534.8	11772	-0.88	-14.09
534.9	11773	-0.64	-14.32
535.9	11774	-0.43	-13.76
536.9	11775	-1.11	-16.03
537.9	11777	-0.18	-12.99
538.7	11778	-0.21	-14.69
538.8	11778	0.27	-16.09
538.9	11778	-0.89	-16.36
539	11778	-0.83	-16.37
539.1	11778	-0.96	-16.60
539.2	11778	-0.66	-15.97
539.3	11779	0.34	-15.03
539.4	11779	0.48	-14.58
539.5	11779	0.18	-13.61

Depth	Age	$\delta^{13}C$	$\delta^{18}O$
cm	yr BP	VPDB	VPDB
539.6	11779	-0.65	-15.32
539.7	11779	-1.19	-16.54
539.8	11779	-1.32	-16.75
539.9	11779	-1.22	-16.90
540	11779	-1.23	-16.82
540.1	11780	-1.77	-17.22
540.2	11780	-1.84	-17.31
540.3	11780	-1.27	-15.66
540.4	11780	-0.68	-14.15
540.5	11780	-0.51	-14.27
540.6	11780	-0.39	-13.70
540.7	11780	0.90	-13.73
540.8	11781	-0.44	-14.17
540.9	11781	0.01	-13.90
541	11781	0.03	-13.63
541.1	11781	-0.23	-13.04
541.2	11781	-0.41	-13.11
541.3	11781	-0.35	-13.30
541.4	11781	0.04	-12.99
541.5	11781	0.03	-12.61
541.6	11782	-0.04	-12.88
541.7	11782	0.31	-13.09
541.8	11782	-0.27	-13.02
541.9	11782	-0.19	-13.20
542	11782	-0.26	-13.47
542.1	11782	-0.27	-13.27
542.2	11782	-0.23	-13.39
542.3	11783	-0.42	-13.80
542.4	11783	-0.21	-13.24
542.5	11783	-0.35	-13.44
542.6	11783	-0.41	-13.49
542.7	11783	0.35	-13.79
542.8	11783	0.88	-12.99
542.9	11783	1.05	-13.06
543	11784	2.41	-12.57
543.1	11784	3.55	-12.46
543.2	11784	4.40	-12.41
543.3	11784	2.17	-13.10
543.4	11784	1.60	-13.20
543.5	11784	3.39	-12.62
543.6	11784	7.79	-12.62
543.7	11784	10.11	-12.52
543.8	11785	0.31	-13.55
543.9	11785	2.05	-13.13
544	11785	1.74	-13.24
544.1	11785	1.91	-12.93
544.2	11785	3.72	-12.45

Depth	Age	$\delta^{13}C$	$\delta^{18}O$
cm	yr BP	VPDB	VPDB
544.3	11785	7.52	-12.08
544.4	11785	6.47	-12.42
544.5	11786	6.46	-12.64
544.6	11786	4.18	-12.90
544.7	11786	7.11	-12.46
544.9	11786	2.15	-12.81
545	11786	6.39	-12.36
545.1	11786	6.90	-12.82
545.2	11786	7.76	-12.08
545.3	11787	4.98	-12.96
545.4	11787	6.17	-12.91
545.5	11787	1.71	-13.41
545.6	11787	0.06	-13.50
545.7	11787	1.12	-13.62
545.8	11787	0.67	-13.51
545.9	11787	0.30	-13.92
546	11788	1.55	-13.14
546.1	11788	3.39	-12.89
546.2	11788	2.81	-13.33
546.3	11788	0.65	-13.45
546.4	11788	1.27	-13.82
546.5	11788	4.02	-13.10
546.6	11788	2.80	-13.09
546.7	11789	-0.93	-14.60
546.8	11789	-0.23	-14.19
546.9	11789	2.13	-13.97
547	11789	-0.66	-14.48
547.1	11789	-0.24	-14.19
547.2	11789	13.67	-13.18
547.3	11789	1.07	-14.71
547.4	11789	8.88	-13.81
547.5	11790	7.46	-14.17
547.6	11790	1.49	-14.59
547.7	11790	0.98	-14.46
547.8	11790	-0.54	-14.53
548	11790	0.25	-14.89
548.1	11790	9.73	-14.33
548.2	11791	9.69	-13.63
548.3	11791	11.48	-12.86
548.4	11791	7.82	-14.19
548.5	11791	3.48	-14.41
548.6	11791	8.45	-13.18
548.7	11791	10.53	-12.73
548.8	11791	3.50	-14.73
548.9	11791	6.60	-14.42
549	11792	0.97	-14.38
549.1	11792	-0.97	-15.11

Depth	Age	$\delta^{13}C$	$\delta^{18}O$
cm	yr BP	VPDB	VPDB
549.2	11792	-0.86	-14.70
549.3	11792	-1.03	-14.74
549.4	11792	-1.28	-15.42
549.5	11792	-0.26	-14.60
549.6	11792	-1.15	-14.93
549.8	11793	4.70	-12.94
550	11793	4.02	-14.64
550.1	11793	-1.27	-14.94
550.2	11793	-1.81	-15.91
550.3	11793	-1.90	-15.89
550.4	11794	-0.38	-15.29
550.5	11794	4.65	-13.45
550.6	11794	9.64	-11.14
550.7	11794	9.16	-11.47
550.8	11794	5.28	-12.19
550.9	11794	1.60	-14.57
551	11794	1.18	-15.00
551.6	11795	10.67	-12.76
551.7	11795	12.36	-12.12
551.8	11795	9.74	-13.48
552.2	11796	4.49	-13.98
552.3	11796	9.15	-13.07
552.4	11796	14.33	-12.04
552.5	11796	14.95	-11.96
552.6	11797	17.24	-11.39
552.7	11797	25.98	-11.48
552.8	11797	14.59	-14.23
552.9	11797	26.64	-11.34
553	11797	14.07	-12.14
553.1	11797	7.81	-13.29
553.2	11797	2.46	-14.23
553.3	11797	10.65	-12.43
553.4	11798	21.04	-11.80
553.5	11798	17.03	-12.50
553.6	11798	23.65	-12.47
553.7	11798	12.38	-12.89
553.8	11798	6.87	-13.66
553.9	11798	18.51	-12.27
554	11798	9.78	-13.45
554.1	11799	18.95	-11.70
554.2	11799	15.38	-12.77
554.3	11799	18.96	-12.39
554.4	11799	16.90	-12.80
554.5	11799	11.63	-13.30
554.6	11799	9.71	-13.97
554.7	11799	8.51	-13.50
554.8	11799	0.71	-15.15

Depth	Age	$\delta^{13}C$	$\delta^{18}O$
cm	yr BP	VPDB	VPDB
554.9	11800	1.26	-15.13
555	11800	2.59	-14.43
555.1	11800	0.87	-14.45
555.2	11800	4.73	-13.84
555.3	11800	17.02	-12.90
555.4	11800	11.29	-13.47
555.5	11800	7.94	-14.10
555.6	11801	-0.38	-14.85
555.7	11801	-0.67	-15.11
555.8	11801	-0.15	-15.03
556.8	11802	4.43	-13.95
557.8	11804	3.94	-14.38
558.7	11805	6.06	-13.41
558.8	11805	9.23	-13.39
558.9	11805	6.89	-12.82
559	11805	4.33	-13.06
559.1	11805	14.12	-12.64
559.2	11805	16.16	-12.90
559.3	11806	4.55	-13.85
559.4	11806	5.95	-13.54
559.5	11806	5.30	-13.72
559.6	11806	0.66	-14.41
559.7	11806	-0.74	-14.41
559.8	11806	-0.94	-14.78
559.9	11806	1.95	-14.28
561.1	11808	3.45	-14.15
562.1	11809	2.71	-14.48
563.1	11811	1.01	-13.88
564.1	11812	5.22	-13.59
565.1	11813	0.59	-14.50
565.9	11815	-0.44	-14.99
566	11815	-1.14	-15.07
566.1	11815	0.18	-14.60
566.2	11815	-0.84	-15.05
566.3	11815	-0.37	-15.38
566.4	11815	-0.83	-15.55
566.5	11815	-0.93	-15.24
566.6	11815	-0.39	-15.43
566.7	11816	-0.88	-15.60
566.8	11816	-1.03	-15.23
566.9	11816	-0.90	-15.78
567	11816	-1.05	-15.44
568	11817	-0.12	-15.37
568.1	11817	-1.62	-15.84
568.2	11818	-1.47	-15.56
568.3	11818	-1.71	-16.05
568.4	11818	-2.45	-16.77

Depth	Age	$\delta^{13}C$	$\delta^{18}O$
cm	yr BP	VPDB	VPDB
568.5	11818	-2.42	-17.68
568.6	11818	-2.08	-16.92
568.7	11818	-2.15	-16.81
568.8	11818	-1.96	-16.69
568.9	11819	-2.05	-15.98
569	11819	-1.87	-16.18
569.5	11820	-1.21	-14.78
570.5	11824	-1.49	-15.06
571.5	11827	-1.43	-15.23
572.5	11831	-1.28	-14.64
573.5	11834	-1.60	-14.98
574.5	11838	-1.01	-14.31
575.5	11841	-1.04	-13.84
576.4	11844	-1.12	-14.48
577.5	11848	-2.08	-15.61
577.6	11849	-1.91	-15.68
577.7	11849	-2.03	-15.57
577.8	11849	-1.98	-15.88
577.9	11850	-1.94	-15.14
578	11850	-1.58	-14.92
578.1	11850	-0.97	-14.21
578.2	11851	-1.08	-14.46
578.3	11851	-1.30	-14.51
578.4	11851	-1.18	-14.58
578.5	11852	-1.37	-14.85
578.6	11852	-1.85	-15.14
578.7	11852	-1.78	-14.72
578.8	11853	-1.61	-14.65
578.9	11853	-1.51	-15.06
579	11853	-1.54	-14.67
579.1	11854	-1.43	-14.45
579.2	11854	-1.16	-14.23
579.3	11854	-1.02	-14.10
579.4	11855	-1.20	-14.99
579.5	11855	-0.78	-13.96
579.6	11855	-0.83	-13.97
579.7	11856	-0.78	-14.05
579.8	11856	-0.78	-13.90
579.9	11857	-0.77	-13.89
580	11857	-0.74	-13.89
580.1	11857	-0.96	-14.15
580.2	11858	-1.01	-14.07
580.3	11858	-1.10	-14.00
580.4	11858	-1.02	-13.87
580.5	11859	-1.18	-12.34
580.6	11859	-0.90	-13.86
580.8	11860	-0.73	-13.95

Depth	Age	$\delta^{13}C$	$\delta^{18}O$
cm	yr BP	VPDB	VPDB
580.9	11860	-0.89	-13.69
581	11860	-0.97	-13.54
581.1	11861	-0.86	-13.56
581.2	11861	-0.74	-13.45
581.3	11861	-0.96	-13.67
581.4	11862	-0.91	-14.07
581.5	11862	-0.96	-14.10
582.5	11866	-1.31	-14.93
583.5	11869	-0.87	-14.15
584.5	11872	-0.83	-14.39
585.5	11876	-1.48	-15.12
586.5	11879	-0.74	-13.85
587.5	11883	-1.05	-14.34
588.5	11886	-1.10	-14.29
589.4	11889	-1.30	-14.68
590.5	11893	-1.38	-14.84
591.5	11897	-1.70	-15.24
592.5	11900	-1.69	-15.51
593.5	11904	-1.53	-14.89
594.5	11907	-1.33	-15.11
595.5	11911	-1.65	-15.11
596.5	11914	-1.31	-14.84
597.5	11918	-1.90	-15.29
598.6	11921	-1.72	-15.20
599.5	11925	-1.92	-15.66
600.5	11928	-1.79	-15.19
601.5	11931	-1.98	-15.47
602.5	11935	-2.23	-15.67
603.5	11938	-2.06	-15.61
604.5	11942	-1.18	-14.76
605.5	11945	-1.01	-14.14
606.5	11949	-0.87	-14.48
607.5	11952	-2.22	-16.05
608.6	11956	-1.55	-15.00
609.5	11959	-1.74	-14.78
610.5	11963	-1.23	-14.52
611.5	11966	-0.97	-14.34
612.5	11970	-1.54	-14.94
613.5	11973	-1.45	-14.98
614.5	11977	-1.87	-14.88
615.5	11980	-1.14	-14.45
616.5	11984	-1.80	-14.71
617.5	11987	-1.49	-14.30
618.6	11991	-1.75	-14.89
619.5	11994	-1.52	-14.85
620.5	11997	-1.86	-15.08
621.5	12001	-1.55	-14.93

Depth	Age	$\delta^{13}C$	$\delta^{18}O$
cm	yr BP	VPDB	VPDB
622.5	12004	-1.44	-14.90
623.6	12008	-1.26	-14.70
624.5	12011	-1.77	-15.63
625.5	12015	-1.61	-15.35
626.5	12018	-1.41	-15.04
627.5	12022	-1.74	-15.24
628.5	12025	-1.75	-15.00
629.5	12029	-1.97	-15.17
630.5	12032	-2.14	-15.35
631.5	12036	-1.90	-15.37
632.5	12039	-1.68	-14.47
633.5	12043	-1.09	-14.37
634.5	12046	-1.21	-14.96
635.5	12049	-1.58	-15.08
636.5	12053	-1.60	-15.17
637.5	12056	-1.64	-15.51
638.5	12060	-1.18	-14.77
639.5	12063	-1.23	-14.56
640.5	12067	-0.84	-14.08
641.5	12070	-0.74	-13.87
642.5	12074	-1.04	-14.26
643.5	12077	-1.42	-14.81
644.5	12081	-0.71	-13.56
645.5	12084	-0.89	-13.97
646.5	12088	-0.56	-13.45
647.5	12091	-0.65	-13.63
648.5	12095	-1.60	-14.67
649.5	12098	-1.03	-14.25
650.5	12102	-1.54	-14.41
651.5	12105	-0.90	-13.80
652.5	12108	-1.38	-14.06
653.5	12112	-1.26	-13.81
654.5	12115	-1.36	-13.97
655.5	12119	-1.71	-13.97
656.5	12122	-1.34	-13.93
657.5	12126	-1.68	-14.01
658.5	12129	-1.37	-13.80
659.5	12133	-1.21	-13.98
660.5	12136	-1.43	-13.77
661.5	12140	-1.80	-13.90
662.5	12143	-1.27	-13.98
663.5	12147	-1.66	-14.41
664.5	12150	-1.58	-14.07
665.5	12154	-1.18	-13.59
666.5	12157	-0.86	-13.50
667.5	12160	-1.08	-13.64
668.5	12164	-0.52	-12.88

Depth	Age	$\delta^{13}C$	$\delta^{18}O$
cm	yr BP	VPDB	VPDB
670.2	12168	-0.51	-12.86
671.2	12170	-0.76	-13.15
672.2	12173	-0.79	-13.15
673.3	12175	-0.62	-13.15
673.5	12175	-1.21	-13.93
673.6	12176	-1.56	-14.27
673.7	12176	-1.60	-14.36
673.8	12176	-1.86	-14.72
673.9	12176	-1.52	-14.07
674	12177	-1.32	-13.84
674.1	12177	-1.65	-14.13
674.2	12177	-1.47	-13.95
674.3	12177	-1.28	-13.93
674.4	12177	-1.30	-14.07
674.5	12178	-1.20	-13.69
674.6	12178	-1.12	-13.79
674.7	12178	-1.12	-13.73
674.8	12178	-1.24	-13.98
674.9	12179	-1.33	-14.12
675	12179	-1.40	-14.12
675.1	12179	-1.31	-14.04
675.2	12179	-1.45	-14.06
675.3	12179	-1.59	-14.03
675.4	12180	-1.80	-14.63
675.5	12180	-1.79	-14.47
675.6	12180	-1.91	-14.72
675.7	12180	-1.55	-14.08
675.8	12180	-1.23	-13.60
675.9	12181	-1.08	-13.55
676	12181	-0.57	-13.10
676.1	12181	-0.54	-12.97
676.2	12181	-0.60	-12.98
676.3	12182	-0.58	-13.03
676.4	12182	-1.08	-13.50
676.5	12182	-1.36	-13.61
676.6	12182	-0.84	-13.14
676.7	12182	-1.05	-13.16
676.8	12183	-0.97	-13.31
676.9	12183	-0.82	-13.19
677	12183	-0.84	-13.14
677.1	12183	-0.84	-13.10
677.2	12183	-0.74	-13.08
677.3	12184	-1.02	-13.14
677.4	12184	-1.02	-13.28
677.5	12184	-1.04	-13.22
678.5	12186	-1.74	-13.57
679.5	12188	-1.13	-12.93

Depth	Age	$\delta^{13}C$	$\delta^{18}O$
cm	yr BP	VPDB	VPDB
680.5	12191	-1.34	-13.08
681.5	12193	-1.77	-13.17
682.5	12195	-1.51	-13.12
683.5	12197	-1.55	-13.04
684.5	12199	-1.36	-13.16
685.5	12202	-1.58	-13.38
685.6	12202	-1.21	-13.27
685.7	12202	-1.75	-13.22
685.8	12202	-1.66	-13.00
685.9	12202	-1.42	-13.46
686	12203	-1.93	-12.87
686.1	12203	-1.46	-13.32
686.2	12203	-1.29	-13.18
686.3	12203	-1.58	-13.11
686.5	12204	-1.44	-13.28
686.6	12204	-1.61	-13.34
686.7	12204	-1.68	-13.16
686.8	12204	-1.81	-13.25
686.9	12205	-1.52	-13.27
687	12205	-1.06	-13.15
687.1	12205	-1.18	-13.08
687.2	12205	-1.24	-13.32
687.3	12205	-1.07	-13.28
687.4	12206	-1.21	-13.42
687.5	12206	-0.52	-12.82
687.6	12206	-1.47	-13.15
687.7	12206	-0.72	-12.94
687.8	12206	-1.12	-13.61
687.9	12207	-0.79	-13.27
688.5	12208	-1.17	-13.48
689.5	12210	-0.97	-13.83
689.6	12210	-0.96	-14.14
689.7	12211	-1.18	-13.03
689.8	12211	-0.81	-14.19
689.9	12211	-1.08	-14.18
690	12211	-1.05	-13.91
690.1	12211	-0.96	-13.93
690.2	12212	-1.09	-13.88
690.3	12212	-1.05	-14.20
690.4	12212	-0.88	-13.93
690.5	12212	-0.90	-13.79
690.6	12213	-0.76	-13.92
690.7	12213	-0.69	-13.48
690.8	12213	-0.64	-13.48
690.9	12213	-0.64	-13.08
691	12213	-0.58	-13.33
691.1	12214	-0.60	-13.25

Depth	Age	$\delta^{13}C$	$\delta^{18}O$
cm	yr BP	VPDB	VPDB
691.2	12214	-0.63	-13.41
691.3	12214	-0.66	-13.52
691.5	12215	-0.56	-13.33
691.6	12215	-0.72	-13.38
691.7	12215	-0.45	-13.14
691.8	12215	-0.70	-13.27
691.9	12215	-0.46	-13.19
692	12216	-0.47	-13.38
692.1	12216	-0.59	-13.54
692.2	12216	-0.83	-13.60
692.3	12216	-0.75	-13.57
692.4	12216	-0.69	-13.32
692.5	12217	-0.61	-13.37
692.6	12217	-0.65	-13.71
692.7	12217	-0.62	-13.73
692.8	12217	-0.87	-13.82
692.9	12218	-0.76	-13.48
693	12218	-0.98	-13.80
693.1	12218	-1.02	-14.40
693.2	12218	-0.93	-13.89
693.3	12218	-0.69	-13.60
693.4	12219	-0.71	-13.35
693.5	12219	-0.62	-13.38
693.6	12219	-0.76	-13.40
693.7	12219	-0.62	-13.59
693.8	12220	-0.64	-13.66
693.9	12220	-0.57	-13.44
694	12220	-0.71	-13.56
694.1	12220	-1.13	-13.68
694.2	12220	-0.89	-13.83
694.3	12221	-0.97	-14.15
694.4	12221	-1.60	-12.92
694.5	12221	-1.11	-14.08
694.6	12221	-1.16	-13.85
694.7	12221	-1.06	-14.29
694.8	12222	-1.12	-14.31
694.9	12222	-1.02	-14.53
695	12222	-1.25	-13.82
695.1	12222	-1.04	-14.43
695.2	12223	-1.70	-13.01
695.3	12223	-1.32	-14.94
695.4	12223	-1.30	-15.10
695.7	12224	-1.23	-14.73
696.2	12225	-1.69	-15.25
696.7	12226	-1.07	-14.41
697.2	12227	-1.32	-14.92
697.7	12228	-1.02	-13.79

Depth	Age	$\delta^{13}C$	$\delta^{18}O$
cm	yr BP	VPDB	VPDB
698.2	12229	-0.46	-13.29
698.7	12230	-0.59	-13.09
699.2	12231	-0.54	-13.48
699.7	12232	-0.69	-13.39
700.2	12233	-0.87	-13.67
700.7	12234	-0.62	-13.55
701.2	12236	-0.71	-13.57
701.7	12237	-0.70	-13.29
702.2	12238	-0.90	-13.61
702.7	12239	-0.95	-13.59
703.2	12240	-0.80	-13.31
703.7	12241	-0.81	-13.52
704.2	12242	-1.13	-13.91
704.7	12243	-0.99	-13.57
705.2	12244	-0.96	-13.24
705.7	12245	-0.70	-13.54
706.2	12246	-0.87	-13.39
706.7	12248	-0.77	-13.34
707.2	12249	-0.68	-13.47
707.7	12250	-0.86	-13.34
708.2	12251	-0.70	-13.53
708.7	12252	-1.00	-13.81
709.2	12253	-1.04	-13.78
709.7	12254	-0.92	-13.39
710.2	12255	-0.87	-13.59
710.7	12256	-1.09	-13.48
711.2	12257	-1.07	-14.05
711.7	12258	-1.27	-13.67
712.2	12259	-0.97	-13.80
712.7	12261	-0.88	-13.50
713.2	12262	-1.12	-13.00
713.7	12263	-1.03	-13.80
714.2	12264	-1.16	-13.76
714.7	12265	-1.08	-13.81
715.2	12266	-1.32	-13.70
715.7	12267	-1.33	-14.25
716.2	12268	-1.55	-14.31
716.7	12269	-1.45	-14.10
717.2	12270	-0.92	-13.56
717.7	12271	-0.51	-13.20
718.2	12272	-0.55	-13.30
718.7	12274	-0.44	-13.02
719.2	12275	-1.10	-13.64
719.7	12276	-0.55	-13.31
720.2	12277	-0.64	-13.49
720.7	12278	-1.14	-13.98
721.2	12279	-0.77	-13.33

Depth	Age	$\delta^{13}C$	$\delta^{18}O$
cm	yr BP	VPDB	VPDB
721.7	12280	-0.57	-13.35
722.2	12281	-0.84	-14.05
722.7	12282	-0.80	-13.53
723.2	12283	-1.01	-13.90
723.7	12284	-1.48	-14.08
724.2	12285	-1.70	-14.34
724.7	12287	-1.61	-14.29
725.2	12288	-1.60	-14.24
725.7	12289	-1.43	-13.82
726.2	12290	-1.13	-13.85
726.7	12291	-1.54	-13.95
727.2	12292	-0.82	-13.45
727.7	12293	-1.35	-13.84
728.2	12294	-1.49	-14.23
728.7	12295	-2.12	-13.90
729.2	12296	-1.72	-13.80
729.7	12297	-1.61	-13.62
730.2	12299	-1.52	-13.58
730.7	12300	-1.96	-13.94
731.2	12301	-1.43	-13.41
731.7	12302	-1.43	-13.88
732.2	12303	-0.84	-13.51
732.7	12304	-1.60	-13.98
733.2	12305	-1.52	-13.83
733.7	12306	-1.65	-14.48
734.2	12307	-0.92	-13.48
734.7	12308	-1.82	-15.08
735.2	12309	-1.79	-14.61
735.7	12310	-1.60	-14.22
736.7	12313	-1.29	-14.26
737.7	12315	-0.92	-14.13
738.7	12317	-0.87	-13.61
739.7	12319	-1.30	-14.31
740.7	12321	-1.42	-14.20
741.7	12323	-1.39	-13.42
742.7	12326	-1.64	-14.59
743.7	12328	-1.56	-14.54
745.7	12332	-0.96	-14.25
746.7	12334	-0.66	-13.81
747.7	12336	-0.77	-13.67
748.7	12339	-1.13	-14.23
749.7	12341	-1.27	-13.79
750.7	12343	-0.56	-13.33
751.7	12345	-0.88	-13.71
752.7	12347	-0.93	-13.80
753.7	12349	-1.04	-14.17
754.7	12352	-1.37	-14.10

Depth	Age	$\delta^{13}C$	$\delta^{18}O$
cm	yr BP	VPDB	VPDB
755.7	12354	-1.55	-13.89
756.7	12356	-0.73	-13.78
757.7	12358	-1.28	-14.42
758.7	12360	-1.50	-14.21
759.7	12363	-1.27	-14.82
760.7	12365	-1.38	-14.41
761.7	12367	-1.52	-14.55
762.7	12369	-1.81	-14.29
763.7	12371	-1.28	-14.30
764.7	12373	-1.37	-13.61
765.7	12376	-1.48	-13.93
766.7	12378	-1.36	-13.09
767.7	12380	-1.26	-13.29
768.7	12382	-1.01	-13.28
769.7	12384	-0.80	-13.52
770.2	12385	-0.76	-13.10
771.2	12387	-0.93	-13.44
772.2	12389	-1.11	-13.56
773.2	12390	-1.19	-13.54
774.2	12392	-1.46	-13.86
775.2	12394	-1.62	-14.20
776.2	12396	-1.26	-13.86
777.2	12398	-2.13	-14.65
778.2	12400	-1.70	-14.28
779.2	12402	-1.55	-14.34
780.2	12403	-1.44	-14.28
781.2	12405	-1.08	-14.37
782.2	12407	-0.92	-14.03
783.2	12409	-1.09	-13.90
784.2	12411	-1.01	-13.60
785.2	12413	-1.37	-13.67
786.2	12414	-1.27	-13.76
787.2	12416	-0.90	-13.36
788.2	12418	-0.86	-13.86
789.2	12420	-0.99	-14.03
790.2	12422	-0.85	-13.43
791.2	12424	-0.91	-13.55
792.2	12426	-0.89	-13.67
793.2	12427	-1.10	-13.77
794.2	12429	-1.43	-14.58
795.2	12431	-1.18	-14.17
796.2	12433	-1.40	-13.91
797.2	12435	-0.88	-13.42
798.2	12437	-0.49	-12.97
799.2	12438	-0.75	-13.64
800.2	12440	-1.02	-14.19
801.2	12442	-1.23	-14.62

Depth	Age	$\delta^{13}C$	$\delta^{18}O$
cm	yr BP	VPDB	VPDB
802.2	12444	-0.40	-12.99
803.2	12446	-0.84	-14.13
804.2	12448	-0.44	-13.33
805.2	12450	-0.63	-13.59
806.2	12451	-0.25	-13.03
807.2	12453	-0.59	-13.43
808.2	12455	-0.65	-13.58
809.2	12457	-0.77	-13.67
810.2	12459	-1.21	-14.26
811.2	12461	-0.25	-12.62
812.2	12462	-0.42	-12.96
813.2	12464	-1.15	-13.71
814.2	12466	-0.86	-13.58
815.2	12468	-1.28	-14.30
816.2	12470	-1.37	-14.39
817.2	12472	-0.37	-13.10
818.2	12474	-0.52	-13.13
819.2	12475	-0.65	-13.51
820.2	12477	-0.51	-13.62
821.2	12479	-0.76	-13.68
822.2	12481	-1.14	-14.47
823.2	12483	-0.50	-13.19
824.2	12485	-0.59	-13.45
825.2	12486	-0.72	-13.66
826.2	12488	-0.97	-13.78
827.2	12490	-0.82	-13.61
828.2	12492	-0.67	-13.70
829.2	12494	-0.40	-13.04
830.2	12496	-0.59	-13.14
831.2	12498	-0.58	-13.34
832.2	12499	-0.55	-12.96
833.2	12501	-0.59	-13.29
834.2	12503	-0.17	-12.67
835.2	12505	-0.16	-12.44
836.2	12507	-1.35	-14.65
837.2	12509	-0.29	-12.80
838.2	12510	-0.77	-13.60
839.2	12512	-0.60	-13.43
840.2	12514	-0.62	-13.45
841.2	12516	-0.54	-13.18
842.2	12518	-0.36	-13.16
843.2	12520	-0.45	-13.79
844.2	12522	-0.46	-13.37
845.2	12523	-0.57	-13.45
846.2	12525	-0.41	-13.40
847.2	12527	-0.13	-12.49
848.2	12529	-0.71	-13.39

Depth	Age	$\delta^{13}C$	$\delta^{18}O$
cm	yr BP	VPDB	VPDB
849.2	12531	-0.45	-13.29
850.2	12533	-0.08	-12.56
851.2	12534	-0.08	-12.48
852.2	12536	-0.38	-13.16
853.2	12538	-0.37	-12.88
854.2	12540	-0.61	-13.32
855.2	12542	-0.48	-12.95
856.2	12544	-0.24	-12.59
857.2	12546	-0.31	-13.08
858.2	12547	0.00	-12.30
859.2	12549	-0.54	-13.09
860.2	12551	-0.48	-13.18
861.2	12553	-0.51	-13.66
862.2	12555	-0.52	-13.66
863.2	12557	-0.93	-13.93
864.2	12558	-0.91	-13.76
865.2	12560	-0.30	-12.48
866.2	12562	-0.65	-13.03
867.2	12564	-1.06	-13.47
868.2	12566	-0.57	-13.01
869.2	12568	-0.32	-12.91
870.2	12570	-0.52	-13.33
871.2	12572	-0.67	-13.34
872.2	12574	-0.67	-13.30
873.2	12576	-0.11	-12.98
874.2	12578	-0.49	-13.16
875.2	12580	-0.77	-13.58
876.2	12582	-0.68	-13.84
877.2	12584	-0.54	-13.49
878.2	12586	-1.05	-14.74
879.2	12587	-0.55	-13.49
880.2	12589	-0.57	-13.51
881.2	12591	-0.63	-13.30
882.2	12593	-0.65	-14.20
883.2	12595	-0.27	-12.89
884.2	12597	-0.68	-13.78
885.2	12599	-0.74	-15.53
886.2	12601	-0.60	-13.06
887.2	12603	-0.42	-13.24
888.2	12605	-0.81	-13.87
889.2	12607	-0.66	-13.96
891.2	12611	-0.79	-13.74
892.2	12613	-0.83	-13.92
893.2	12615	-0.91	-13.97
894.2	12617	-0.94	-14.03
895.2	12619	-0.58	-13.86
896.2	12621	-0.50	-13.20

Depth	Age	$\delta^{13}C$	$\delta^{18}O$
cm	yr BP	VPDB	VPDB
897.2	12623	-0.74	-13.56
898.2	12625	-0.96	-13.77
899.2	12627	-0.41	-12.97
900.2	12629	-0.79	-13.52
901.2	12631	-0.55	-13.35
902.2	12633	-0.74	-13.63
903.2	12635	-0.87	-13.71
904.2	12637	-0.74	-13.19
905.2	12639	-0.70	-13.24
906.2	12641	-0.70	-13.60
907.2	12643	-0.55	-13.65
908.2	12645	-0.99	-13.50
909.2	12647	-0.83	-14.07
910.2	12649	-0.93	-14.03
911.2	12651	-1.20	-14.24
912.2	12653	-1.07	-14.43
913.2	12655	-0.46	-13.49
914.2	12657	-0.65	-13.68
915.2	12659	-0.62	-13.89
916.2	12661	-1.19	-14.54
917.2	12663	-0.78	-13.70
918.2	12665	-0.91	-14.48
919.2	12667	-0.98	-14.76
920.2	12669	-1.20	-14.76
921.2	12671	-0.31	-13.43
922.2	12673	-0.56	-13.65
923.2	12675	-0.76	-13.70
924.2	12677	-0.68	-13.85
925.2	12679	-0.63	-14.18
926.2	12681	-1.07	-14.34
927.2	12683	-1.01	-13.97
928.2	12684	-0.85	-13.81
929.2	12686	-0.65	-13.61
930.2	12688	-0.61	-13.53
931.2	12690	-0.64	-13.37
932.2	12692	-1.30	-14.49
933.2	12694	-1.21	-14.64
934.2	12696	-0.98	-13.17
935.2	12698	-0.44	-13.60
936.2	12700	-1.23	-14.91
937.2	12702	-0.73	-13.61
938.2	12704	-1.02	-13.89
939.2	12706	-0.72	-13.61
940.2	12708	-1.11	-14.21
941.2	12710	-1.02	-13.82
942.2	12712	-1.29	-14.32
943.2	12714	-1.86	-15.43

Depth	Age	$\delta^{13}C$	$\delta^{18}O$
cm	yr BP	VPDB	VPDB
944.2	12716	-1.36	-14.30
945.2	12718	-1.56	-14.76
946.2	12720	-0.42	-13.26
947.2	12722	-0.38	-12.82
948.2	12724	-1.24	-14.19
949.2	12726	-1.45	-14.69
950.2	12728	-0.73	-13.99
951.2	12730	-1.34	-14.68
952.2	12732	-1.03	-13.98
953.2	12734	-1.19	-14.27
954.2	12736	-1.65	-14.89
955.2	12738	-1.74	-14.95
956.2	12740	-1.00	-13.95
957.2	12742	-0.77	-13.40
958.2	12744	-0.24	-12.88
959.2	12746	-0.36	-12.97
960.2	12748	-0.61	-13.51
961.2	12750	-0.41	-13.00
962.2	12752	-1.02	-13.83
963.2	12754	-0.50	-13.41
964.2	12756	-0.61	-13.56
965.2	12758	-1.45	-13.97
966.2	12760	-1.09	-13.49
967.2	12762	-0.50	-13.07
968.2	12764	-0.84	-13.40
969.2	12766	-0.38	-12.88
970.2	12768	-0.26	-12.84
971.2	12770	-1.18	-14.18
972.2	12772	-1.81	-15.47
973.2	12774	-0.82	-13.91
974.2	12776	-1.12	-14.05
975.2	12778	-0.32	-12.66
976.2	12780	-0.56	-13.81
977.2	12781	-0.72	-12.74
978.2	12783	-1.29	-13.08
979.2	12785	-0.97	-13.01
980.2	12787	-0.50	-13.05
981.2	12789	-1.01	-13.17
982.2	12791	-0.47	-13.17
983.2	12793	-0.50	-13.19
984.2	12795	-0.50	-13.04
985.2	12797	-0.51	-13.36
986.2	12799	-0.70	-13.54
987.2	12801	-1.04	-13.91
988.2	12803	-1.05	-13.81
989.2	12805	-1.67	-14.89
990.2	12807	-1.26	-14.22

Depth	Age	$\delta^{13}C$	$\delta^{18}O$
cm	yr BP	VPDB	VPDB
991.2	12809	-0.95	-13.72
992.2	12811	-0.53	-13.43
993.2	12813	-1.01	-13.99
994.2	12815	-0.83	-13.82
995.2	12817	-0.45	-13.44
996.2	12819	-0.57	-13.49
997.2	12821	-0.44	-13.41
998.2	12823	-0.55	-13.62
999.2	12825	-0.47	-13.41
1000.2	12827	-0.51	-13.37
1001.2	12829	-0.82	-13.60
1002.2	12831	-1.01	-13.61
1003.2	12833	-0.81	-13.28
1004.2	12835	-1.11	-13.42
1005.2	12837	-1.16	-13.88
1006.2	12839	-1.14	-13.69
1007.2	12841	-1.02	-14.08
1008.2	12843	-0.85	-13.62
1009.2	12845	-0.54	-13.61
1010.2	12847	-0.64	-14.25
1011.2	12849	-0.93	-14.28
1012.2	12851	-0.69	-14.21
1013.2	12853	-1.07	-14.25
1014.2	12855	-1.45	-15.00
1015.2	12857	-2.14	-15.99
1016.2	12859	-1.36	-14.86
1017.2	12861	-1.22	-14.62
1018.2	12863	-0.74	-13.98
1019.2	12865	-0.32	-13.55
1020.2	12867	-0.66	-13.92
1021.2	12869	-0.78	-13.89
1022.2	12871	-0.94	-14.17
1023.2	12873	-0.79	-14.26
1024.2	12875	-0.78	-14.10
1025.2	12877	-0.50	-13.97
1026.2	12878	-0.58	-13.79
1027.2	12880	-1.23	-14.87
1028.2	12882	-0.79	-14.09
1029.2	12884	-0.85	-14.42
1030.2	12886	-1.21	-14.98
1031.2	12888	-1.51	-15.15
1032.2	12890	-0.70	-13.86
1033.2	12892	-0.78	-13.87
1034.2	12894	-0.64	-13.58
1035.2	12896	-0.72	-13.89
1036.2	12898	-0.98	-14.26
1037.2	12900	-0.88	-14.22

Depth	Age	$\delta^{13}C$	$\delta^{18}O$
cm	yr BP	VPDB	VPDB
1038.2	12902	-1.82	-14.88
1039.2	12904	-2.57	-15.43
1040.2	12906	-2.42	-14.96
1041.2	12908	-1.50	-14.64
1042.2	12910	-0.83	-13.64
1043.2	12912	-0.25	-13.09
1044.2	12914	-0.53	-13.63
1045.2	12916	-1.17	-14.16
1046.2	12918	-1.28	-14.28
1047.2	12920	-0.90	-13.87
1048.2	12922	-0.25	-13.24
1049.2	12924	-0.71	-13.86
1050.2	12926	-0.67	-14.24
1051.2	12928	-1.17	-14.39
1052.2	12930	-1.10	-14.54
1053.2	12932	-1.03	-14.32
1054.2	12934	-1.32	-14.88
1055.2	12936	-0.72	-13.61
1056.2	12938	-0.32	-13.16
1057.2	12940	-0.40	-13.36
1058.2	12942	-0.94	-14.18
1059.2	12944	-0.75	-13.98
1060.2	12946	-0.42	-13.39
1061.2	12948	-0.71	-13.56
1062.2	12950	-0.71	-13.90
1063.2	12952	-0.80	-13.78

Whole Pattern Fitting and Rietveld Refinement

FILE: [Erin-2_AK 801.xrdml] AK 801 @Phi=333.1
SCAN: 10.0049/79.9917/0.01671/90.17(sec)/phi=333, Cu(45kV,40mA), I(p)=18970, 12/03/12 10:57a
PROC: [C:\Documents and Settings\Bruker AXS\MDI Jade 9\Bruker AXS\Creighton Standards.wpf] [Individual FWHM Curve]

☑ K-alpha2 Peak Present
☑ Allow Negative Isotropic B
☑ Allow Negative Occupancy
☑ Apply Anomalous Scattering

[Diffractometer LP] Two-Theta Range of Fit = 10.0 - 70.0(deg)
☑ Specimen Displacement - Cos(Theta) = 0.001101(0.00155)
☐ Monochromator Correction for LP Factor = 1.0
☐ K-alpha2/K-alpha1 Intensity Ratio = 0.5

Profile Shape Function (PSF) for All Phases: pseudo-Voigt, Fixed-BG, Lambda=1.54059Å (Cu/K-alpha1)

Phase ID (6)	Source	I/Ic	Wt%	#L	PC
Calcite - $Ca(CO_3)$	PDF#01-083-0578	2.00(5%)	2.7 (0.2)	19	<None>
Kaolinite; Kaolinite - $Al_2Si_2O_5(OH)_4$	PDF#04-013-3074	0.45(5%)	7.5 (0.7)	198	(001)=0.558
Anorthite - $CaAl_2Si_2O_8$	PDF#04-011-1371	0.34(5%)	13.7 (0.9)	195	<None>
Albite - $NaAlSi_3O_8$	PDF#04-007-5466	0.59(5%)	15.4 (1.0)	198	<None>
Quartz - SiO_2	PDF#04-005-4718	3.50(5%)	20.2 (1.2)	18	(011)=1.000
Orthoclase - $KAlSi_3O_8$	PDF#04-009-3700	0.14(5%)	40.5 (2.7)	139	<None>

XRF(Wt%): Ca=3.1%, K=5.7%, Si=31.0%, Al=9.7%, Na=1.3%, O=48.7%, C=0.3%, H=0.1%

NOTE: Fitting Halted at Iteration 14(4): R=8.96% (E=3.0%, R/E=2.99, P=49, EPS=0.5)

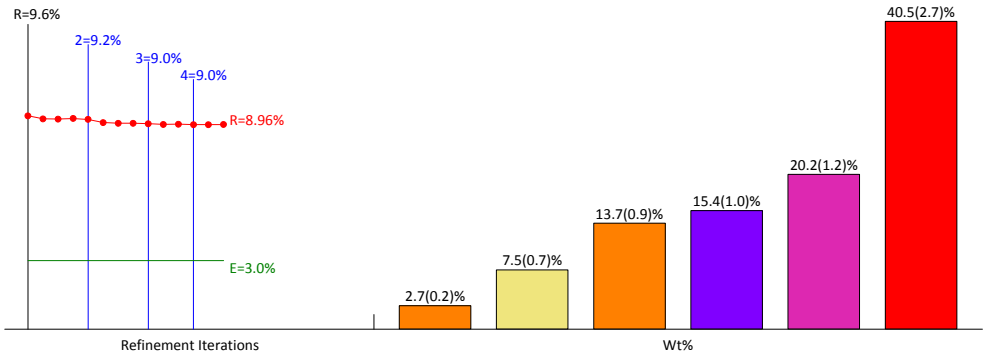

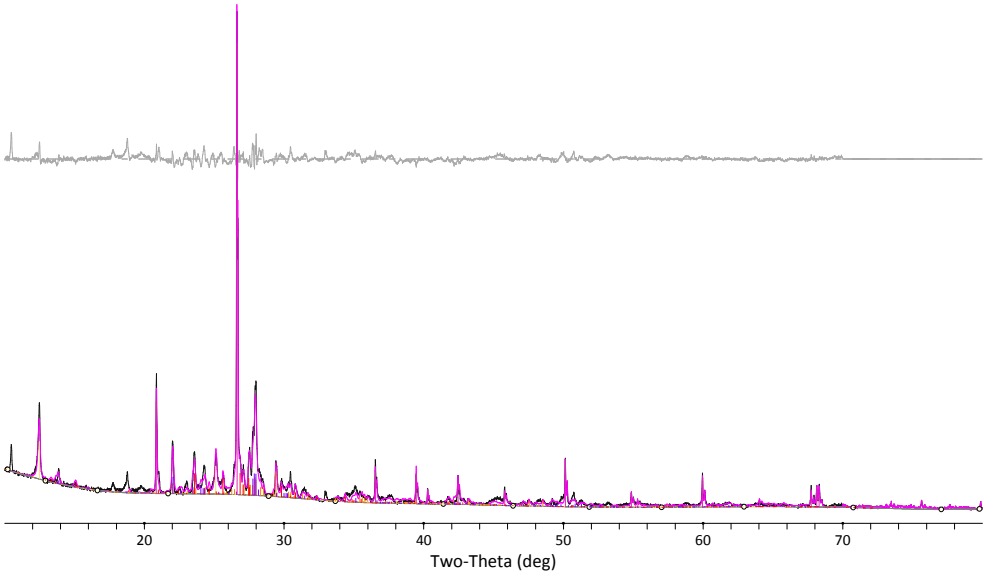

APPENDIX B: STURGEON LAKE ISOTOPE DATA

Depth	Age	$\delta^{13}C$	$\delta^{18}O$
cm	yr BP	VPDB	VPDB
0.65	11.8	-2.10	-11.88
0.651	14.8	-1.33	-11.13
0.652	17.7	-1.83	-11.21
0.653	20.7	-1.30	-10.67
0.654	23.6	-1.18	-11.02
0.655	26.5	-1.51	-11.05
0.656	29.5	-1.41	-10.77
0.657	32.4	-1.43	-11.54
0.658	35.3	-1.47	-11.38
0.659	38.3	-1.93	-11.22
0.66	41.2	-2.07	-10.87
0.661	44.1	-2.02	-10.85
0.662	47.1	-1.54	-10.75
0.663	50.0	-1.54	-10.79
0.664	52.9	-1.90	-10.82
0.665	55.9	-1.86	-11.28
0.666	58.8	-2.00	-10.88
0.667	61.7	-1.55	-10.99
0.668	64.7	-2.53	-11.11
0.669	67.6	-2.15	-11.15
0.67	70.6	-1.92	-11.03
0.671	73.5	-1.64	-10.98
0.672	76.4	-1.54	-10.96
0.673	79.4	-1.56	-10.58
0.674	82.3	-1.58	-10.70
0.675	85.2	-1.68	-10.84
0.676	88.2	-0.92	-10.90
0.677	91.1	-1.49	-10.88
0.678	94.0	-1.73	-11.28
0.679	97.0	-2.05	-11.02
0.68	99.9	-1.89	-11.10
0.681	102.8	-1.40	-10.80
0.682	105.8	-1.56	-11.09
0.683	108.7	-1.63	-10.48
0.684	111.6	-1.54	-10.80
0.685	114.6	-1.91	-11.20
0.686	117.5	-1.62	-10.85
0.687	120.5	-2.50	-11.44
0.688	123.4	-1.84	-10.85

Depth	Age	$\delta^{13}C$	$\delta^{18}O$
cm	yr BP	VPDB	VPDB
0.689	126.3	-1.00	-10.73
0.69	129.3	-1.50	-10.60
0.691	132.2	-1.40	-10.55
0.692	135.1	-1.58	-10.36
0.693	138.1	-1.22	-10.05
0.694	141.0	-0.56	-9.65
0.695	143.9	-1.04	-9.92
0.696	146.9	-1.47	-9.88
0.697	149.8	-1.39	-10.34
0.698	152.7	-1.34	-10.14
0.699	155.7	-1.39	-10.18
0.7	158.6	-1.38	-10.33
0.701	161.5	-1.07	-10.46
0.702	164.5	-1.36	-10.13
0.703	167.4	-1.63	-10.40
0.704	170.4	-1.41	-10.18
0.705	173.3	-1.50	-10.29
0.706	176.2	-1.43	-9.81
0.707	179.2	-1.50	-10.24
0.708	182.1	-1.46	-9.88
0.709	185.0	-1.33	-10.20
0.71	188.0	-1.24	-10.31
0.711	190.9	-1.49	-10.27
0.712	193.8	-1.71	-10.26
0.713	196.8	-1.72	-10.42
0.714	199.7	-1.56	-10.21
0.715	202.6	-1.79	-10.07
0.716	205.6	-1.93	-11.41
0.717	208.5	-1.35	-10.40
0.718	211.4	-1.52	-10.06
0.719	214.4	-1.51	-10.21
0.72	217.3	-1.59	-10.34
0.721	220.3	-1.00	-10.20
0.722	223.2	-1.10	-10.49
0.723	226.1	-1.12	-10.63
0.724	229.1	-2.12	-10.76
0.725	232.0	-1.71	-10.30
0.726	234.9	-1.61	-10.18
0.727	237.9	-1.85	-10.19

Depth	Age	$\delta^{13}C$	$\delta^{18}O$
cm	yr BP	VPDB	VPDB
0.728	240.8	-2.01	-10.83
0.729	243.7	-1.74	-10.40
0.73	246.7	-1.30	-10.15
0.731	249.6	-1.80	-10.23
0.732	252.5	-1.78	-10.13
0.733	255.5	-1.39	-10.28
0.734	258.4	-1.59	-10.42
0.735	261.3	-1.63	-10.43
0.736	264.3	-1.57	-10.86
0.737	267.2	-1.32	-10.42
0.738	270.2	-1.57	-10.41
0.739	273.1	-1.89	-10.69
0.74	276.0	-2.51	-11.14
0.741	279.0	-2.74	-11.56
0.742	281.9	-2.55	-11.02
0.743	284.8	-2.23	-10.98
0.744	287.8	-1.06	-9.82
0.745	290.7	-1.38	-9.82
0.746	293.6	-1.47	-10.41
0.747	296.6	-2.09	-10.83
0.748	299.5	-1.47	-10.74
0.749	302.4	-1.38	-10.45
0.75	305.4	-1.34	-10.79
0.751	308.3	-1.54	-11.06
0.752	311.2	-1.82	-10.84
0.753	314.2	-2.15	-11.37
0.754	317.1	-1.54	-10.97
0.755	320.1	-2.04	-10.54
0.756	323.0	-2.03	-10.58
0.757	325.9	-2.05	-10.70
0.758	328.9	-2.04	-10.77
0.759	331.8	-1.38	-10.79
0.76	334.7	-1.93	-11.25
0.761	337.7	-1.36	-10.50
0.762	340.6	-1.65	-10.03
0.763	343.5	-1.34	-10.17
0.764	346.5	-1.34	-9.87
0.765	349.4	-1.30	-9.80
0.766	352.3	-1.38	-9.91

Depth	Age	$\delta^{13}C$	$\delta^{18}O$
cm	yr BP	VPDB	VPDB
0.767	355.3	-1.40	-9.84
0.768	358.2	-1.24	-10.01
0.769	361.1	-1.45	-10.00
0.77	364.1	-1.30	-9.97
0.771	367.0	-1.08	-10.29
0.772	370.0	-1.37	-10.17
0.773	372.9	-1.47	-9.91
0.774	375.8	-1.32	-9.80
0.775	378.8	-1.34	-10.07
0.776	381.7	-0.55	-9.93
0.777	384.6	-1.11	-10.19
0.778	387.6	-1.36	-10.46
0.779	390.5	-1.45	-10.16
0.78	393.4	-1.20	-10.52
0.781	396.4	-0.85	-9.91
0.782	399.3	-1.69	-10.02
0.783	402.2	-1.58	-10.30
0.784	405.2	-1.53	-10.15
0.785	408.1	-1.66	-10.09
0.786	411.0	-1.47	-9.99
0.787	414.0	-1.03	-9.93
0.788	416.9	-2.02	-10.35
0.789	419.9	-2.58	-10.33
0.79	422.8	-2.54	-10.49
0.791	425.7	-2.15	-10.42
0.792	428.7	-2.18	-10.20
0.793	431.6	-1.80	-10.02
0.794	434.5	-1.83	-10.04
0.795	437.5	-1.67	-10.00
0.796	440.4	-1.68	-10.11
0.797	443.3	-1.36	-9.97
0.798	446.3	-1.42	-10.15
0.799	449.2	-1.31	-10.22
0.8	452.1	-1.58	-10.06
0.801	455.1	-1.66	-10.12
0.802	458.0	-1.81	-10.14
0.803	460.9	-1.72	-10.10
0.804	463.9	-1.82	-10.68
0.805	466.8	-1.19	-10.52

Depth	Age	$\delta^{13}C$	$\delta^{18}O$
cm	yr BP	VPDB	VPDB
0.806	469.8	-2.11	-10.38
0.807	472.7	-1.93	-10.82
0.808	475.6	-2.19	-10.48
0.809	478.6	-2.08	-10.68
0.81	481.5	-2.01	-10.90
0.811	484.4	-2.25	-11.23
0.812	487.4	-1.82	-11.27
0.813	490.3	-1.96	-10.90
0.814	493.2	-2.57	-11.12
0.815	496.2	-2.30	-10.97
0.816	499.1	-2.28	-10.98
0.817	502.0	-2.10	-11.04
0.818	505.0	-2.01	-11.05
0.819	507.9	-2.50	-11.20
0.82	510.8	-2.21	-10.94
0.821	513.8	-2.29	-11.07
0.822	516.7	-2.33	-10.96
0.823	519.7	-2.15	-10.95
0.824	522.6	-2.27	-11.00
0.825	525.5	-2.06	-11.12
0.826	528.5	-2.39	-11.16
0.827	531.4	-2.26	-11.03
0.828	534.3	-2.33	-11.46
0.828	534.3	-2.26	-11.39
0.829	537.3	-2.62	-11.18
0.83	540.2	-2.44	-11.03
0.831	543.1	-1.88	-10.71
0.832	546.1	-2.12	-10.78
0.833	549.0	-1.97	-10.53
0.834	551.9	-2.03	-10.51
0.835	554.9	-1.93	-10.38
0.836	557.8	-1.81	-10.33
0.837	560.7	-2.20	-10.94
0.838	563.7	-1.81	-10.17
0.839	566.6	-1.81	-10.12
0.84	569.6	-1.53	-10.22
0.841	572.5	-1.69	-10.17
0.842	575.4	-1.56	-10.07
0.843	578.4	-1.28	-10.10

Depth	Age	$\delta^{13}C$	$\delta^{18}O$
cm	yr BP	VPDB	VPDB
0.844	581.3	-1.55	-10.35
0.845	584.2	-1.42	-10.19
0.846	587.2	-1.69	-9.90
0.847	590.1	-1.00	-9.84
0.849	596.0	-1.73	-10.29
0.85	598.9	-1.72	-10.53
0.851	601.8	-1.42	-10.41
0.852	604.8	-1.72	-10.40
0.853	607.7	-1.86	-10.34
0.854	610.6	-1.76	-10.54
0.855	613.6	-2.26	-10.25
0.856	616.5	-1.80	-10.13
0.857	619.5	-1.87	-10.81
0.858	622.4	-1.97	-11.09
0.859	625.3	-1.45	-11.29
0.86	628.3	-1.45	-10.90
0.861	631.2	-1.35	-10.68
0.862	634.1	-1.41	-10.87
0.863	637.1	-1.91	-10.58
0.864	640.0	-2.16	-10.87
0.865	642.9	-1.86	-10.96
0.866	645.9	-1.22	-11.05
0.867	648.8	-1.73	-11.08
0.868	651.7	-2.37	-10.64
0.869	654.7	-2.20	-10.60
0.87	657.6	-2.53	-10.88
0.871	660.5	-2.64	-11.01
0.872	663.5	-2.07	-11.03
0.873	666.4	-2.14	-11.07
0.874	669.4	-1.70	-11.08
0.875	672.3	-2.17	-10.60
0.876	675.2	-2.04	-10.98
0.877	678.2	-1.63	-10.56
0.878	681.1	-2.26	-10.78
0.879	684.0	-2.25	-10.64
0.88	687.0	-2.19	-10.24
0.881	689.9	-1.02	-10.04
0.882	692.8	0.69	-10.23
0.883	695.8	-0.57	-9.28

Depth	Age	$\delta^{13}C$	$\delta^{18}O$
cm	yr BP	VPDB	VPDB
0.884	698.7	-0.48	-9.66
0.885	701.6	-0.82	-9.63
0.886	704.6	-1.12	-9.82
0.887	707.5	-0.48	-9.97
0.888	710.4	-0.44	-9.87
0.889	713.4	-0.72	-10.21
0.89	716.3	-1.49	-10.03
0.891	719.3	-0.99	-10.07
0.892	722.2	-0.93	-10.65
0.893	725.1	-1.22	-10.35
0.894	728.1	-1.45	-10.23
0.895	731.0	-1.27	-10.06
0.896	733.9	-0.94	-10.01
0.897	736.9	-0.81	-10.19
0.898	739.8	-0.19	-10.16
0.899	742.7	-1.09	-9.92
0.9	745.7	-1.32	-9.92
0.901	748.6	-1.02	-9.55
0.902	751.5	-1.01	-9.97
0.903	754.5	-0.89	-10.02
0.904	757.4	-1.19	-10.14
0.905	760.3	-1.34	-10.28
0.906	763.3	-1.06	-9.96
0.907	766.2	-1.13	-9.84
0.908	769.2	-1.31	-9.66
0.909	772.1	-1.21	-9.59
0.91	775.0	-1.27	-9.75
0.911	778.0	-0.78	-9.68
0.912	780.9	-0.49	-9.36
0.913	783.8	-0.37	-9.51
0.914	786.8	-0.68	-9.37
0.915	789.7	-1.05	-9.53
0.916	792.6	-0.60	-9.49
0.917	795.6	-1.04	-9.56
0.918	798.5	-1.32	-9.77
0.919	801.4	-0.82	-9.65
0.92	804.4	-0.92	-9.83
0.921	807.3	-1.24	-9.64
0.922	810.2	-0.64	-9.81

Depth	Age	$\delta^{13}C$	$\delta^{18}O$
cm	yr BP	VPDB	VPDB
0.923	813.2	-0.87	-9.70
0.924	816.1	-0.88	-9.63
0.925	819.1	-0.59	-9.70
0.926	822.0	-0.90	-9.61
0.927	824.9	-1.15	-10.05
0.928	827.9	-0.97	-9.92
0.929	830.8	-1.34	-9.74
0.93	833.7	-1.33	-9.92
0.931	836.7	-1.34	-10.04
0.932	839.6	-1.29	-9.89
0.933	842.5	-0.54	-10.01
0.934	845.5	-1.28	-9.70
0.935	848.4	-1.35	-9.78
0.936	851.3	-1.30	-9.79
0.937	854.3	-1.43	-10.16
0.938	857.2	-1.29	-9.92
0.939	860.1	-1.15	-9.73
0.94	863.1	-1.37	-9.85
0.941	866.0	-1.21	-9.69
0.942	869.0	-1.39	-9.64
0.943	871.9	-0.88	-9.40
0.944	874.8	-1.19	-9.49
0.945	877.8	-1.17	-9.91
0.946	880.7	-0.65	-10.06
0.947	883.6	-0.62	-9.94
0.948	886.6	-1.02	-9.75
0.949	889.5	-1.06	-9.72
0.95	892.4	-1.13	-9.85
0.951	895.4	-1.61	-9.78
0.952	898.3	-1.50	-9.80
0.953	901.2	-1.30	-9.80
0.954	904.2	-1.48	-9.76
0.955	907.1	-1.38	-9.72
0.956	910.0	-1.64	-9.75
0.957	913.0	-1.69	-9.63
0.958	915.9	-1.30	-9.66
0.959	918.9	-1.67	-9.59
0.96	921.8	-1.44	-9.42
0.961	924.7	-0.70	-10.04

Depth	Age	$\delta^{13}C$	$\delta^{18}O$
cm	yr BP	VPDB	VPDB
0.962	927.7	-0.94	-9.38
0.963	930.6	-1.15	-9.56
0.964	933.5	-0.94	-9.36
0.965	936.5	-1.00	-9.60
0.966	939.4	-1.13	-9.48
0.967	942.3	-0.70	-9.30
0.968	945.3	-0.87	-9.48
0.969	948.2	-0.85	-9.28
0.97	951.1	-0.87	-9.50
0.971	954.1	-0.70	-9.33
0.972	957.0	-1.06	-9.49
0.973	959.9	-0.51	-9.54
0.974	962.9	-0.77	-9.41
0.975	965.8	-0.37	-9.43
0.976	968.8	-0.60	-9.49
0.977	971.7	-0.87	-9.40
0.978	974.6	-0.61	-9.50
0.979	977.6	-0.76	-9.39
0.98	980.5	-0.61	-9.18
0.981	983.4	-0.69	-9.29
0.982	986.4	-0.83	-9.42
0.983	989.3	-0.94	-9.62
0.984	992.2	-0.09	-9.95
0.985	995.2	-0.89	-9.52
0.986	998.1	-0.61	-9.64
0.987	1001.0	-0.39	-9.56
0.988	1004.0	-1.13	-9.69
0.989	1006.9	-0.87	-10.06
0.99	1009.8	-0.94	-9.83
0.991	1012.8	-1.09	-10.12
0.992	1015.7	-0.76	-9.99
0.993	1018.7	-0.92	-9.88
0.994	1021.6	-0.99	-9.91
0.995	1024.5	-0.55	-10.24
0.996	1027.5	-0.57	-9.93
0.997	1030.4	-1.08	-10.30
0.998	1033.3	-0.80	-9.57
0.999	1036.3	-0.45	-9.71
1	1039.2	-0.77	-9.21

Depth	Age	$\delta^{13}C$	$\delta^{18}O$
cm	yr BP	VPDB	VPDB
1.001	1042.1	-0.62	-9.18
1.002	1045.1	-0.45	-9.33
1.003	1048.0	-0.54	-9.20
1.004	1050.9	-0.74	-9.00
1.005	1053.9	-0.84	-8.89
1.006	1056.8	-1.02	-9.22
1.007	1059.7	-0.77	-9.03
1.008	1062.7	-0.83	-9.41
1.009	1065.6	-0.67	-8.82
1.01	1068.6	-1.52	-9.39
1.011	1071.5	-0.73	-9.76
1.012	1074.4	-0.88	-9.80
1.013	1077.4	-0.83	-9.89
1.014	1080.3	-1.11	-9.70
1.015	1083.2	-0.96	-9.89
1.016	1086.2	-0.66	-9.82
1.017	1089.1	-0.75	-9.80
1.018	1092.0	-0.80	-9.72
1.019	1095.0	-0.94	-9.86
1.02	1097.9	-0.89	-8.10
1.021	1100.8	-0.92	-9.83
1.022	1103.8	-1.09	-9.81
1.023	1106.7	-0.87	-9.78
1.024	1109.6	-1.03	-9.82
1.025	1112.6	-0.83	-9.79
1.026	1115.5	-0.91	-9.78
1.027	1118.5	-1.21	-9.60
1.028	1121.4	-1.18	-9.76
1.029	1124.3	-0.85	-9.80
1.03	1127.3	-1.02	-9.81
1.031	1130.2	-0.95	-9.73
1.032	1133.1	-0.71	-9.64
1.033	1136.1	-0.92	-9.56
1.034	1139.0	-1.02	-9.62
1.035	1141.9	-0.73	-9.49
1.036	1144.9	-0.67	-9.76
1.037	1147.8	-0.62	-9.65
1.038	1150.7	-0.77	-9.66
1.039	1153.7	-0.60	-9.48

Depth	Age	$\delta^{13}C$	$\delta^{18}O$
cm	yr BP	VPDB	VPDB
1.04	1156.6	-0.73	-9.71
1.041	1159.5	-0.47	-9.63
1.042	1162.5	-0.47	-9.73
1.043	1165.4	-0.30	-10.00
1.044	1168.4	-0.41	-9.85
1.045	1171.3	-0.41	-9.49
1.046	1174.2	-0.22	-9.43
1.047	1177.2	-0.58	-9.59
1.048	1180.1	-0.67	-9.59
1.049	1183.0	-0.71	-9.38
1.05	1186.0	-0.59	-9.51
1.051	1188.9	-0.70	-9.40
1.052	1191.8	-0.92	-9.43
1.053	1194.8	-0.94	-9.48
1.054	1197.7	-0.80	-9.50
1.055	1200.6	-0.39	-9.39
1.056	1203.6	-0.87	-9.54
1.057	1206.5	-0.38	-9.38
1.058	1209.4	-0.97	-9.84
1.059	1212.4	-1.26	-9.96
1.06	1215.3	-1.10	-9.79
1.061	1218.3	-0.25	-9.68
1.062	1221.2	-1.15	-9.58
1.063	1224.1	-1.31	-9.92
1.064	1227.1	-1.79	-10.21
1.065	1230.0	-2.06	-10.37
1.066	1232.9	-1.90	-10.27
1.067	1235.9	-1.92	-10.33
1.068	1238.8	-2.06	-10.53
1.069	1241.7	-2.07	-10.36
1.07	1244.7	-2.19	-10.55
1.071	1247.6	-1.94	-10.67
1.072	1250.5	-1.97	-10.43
1.073	1253.5	-1.80	-10.36
1.074	1256.4	-2.07	-10.77
1.075	1259.3	-1.82	-10.46
1.076	1262.3	-1.53	-10.65
1.077	1265.2	-2.11	-10.61
1.078	1268.2	-1.14	-9.85

Depth	Age	$\delta^{13}C$	$\delta^{18}O$
cm	yr BP	VPDB	VPDB
1.079	1271.1	-1.21	-10.49
1.08	1274.0	-1.59	-10.17
1.081	1277.0	-1.40	-10.30
1.082	1279.9	-1.39	-10.19
1.083	1282.8	-1.91	-10.19
1.084	1285.8	-1.29	-10.25
1.085	1288.7	-1.44	-10.58
1.086	1291.6	-1.17	-10.29
1.087	1294.6	-1.25	-10.53
1.088	1297.5	-1.55	-10.56
1.089	1300.4	-1.38	-10.76
1.09	1303.4	-1.23	-10.55
1.091	1306.3	-1.22	-10.53
1.092	1309.2	-1.64	-10.64
1.093	1312.2	-1.71	-10.80
1.094	1315.1	-1.67	-11.08
1.095	1318.1	-1.16	-10.58
1.096	1321.0	-1.19	-10.68
1.097	1323.9	-1.90	-10.46
1.098	1326.9	-0.97	-9.95
1.099	1329.8	-0.23	-9.58
1.1	1332.7	-0.84	-9.70
1.101	1335.7	-0.67	-9.75
1.102	1338.6	-1.09	-9.94
1.103	1341.5	-1.10	-9.79
1.104	1344.5	-1.33	-10.00
1.105	1347.4	-1.44	-10.16
1.106	1350.3	-0.93	-10.53
1.107	1353.3	-1.84	-10.29
1.108	1356.2	-1.88	-10.56
1.109	1359.1	-1.63	-10.34
1.11	1362.1	-1.85	-10.67
1.111	1365.0	-1.31	-10.46
1.112	1368.0	-1.76	-10.65
1.113	1370.9	-1.22	-10.32
1.114	1373.8	-1.19	-9.63
1.115	1376.8	-0.85	-10.06
1.116	1379.7	-1.11	-10.04
1.117	1382.6	-1.14	-10.11

Depth	Age	$\delta^{13}C$	$\delta^{18}O$
cm	yr BP	VPDB	VPDB
1.118	1385.6	-1.59	-10.24
1.119	1388.5	-1.44	-10.39
1.12	1391.4	-0.98	-10.21
1.121	1394.4	-1.51	-10.70
1.122	1397.3	-1.61	-10.46
1.123	1400.2	-1.15	-10.89
1.124	1403.2	-0.89	-10.35
1.125	1406.1	-1.53	-10.76
1.126	1409.0	-1.28	-10.68
1.127	1412.0	-2.28	-11.45
1.128	1414.9	-1.19	-10.10
1.129	1417.9	-1.13	-10.32
1.13	1420.8	-0.63	-10.02
1.131	1423.7	-1.01	-9.69
1.132	1426.7	-0.98	-10.19
1.133	1429.6	-0.95	-9.60
1.134	1432.5	-1.08	-10.16
1.135	1435.5	-1.28	-10.00
1.136	1438.4	-1.48	-10.32
1.137	1441.3	-0.74	-10.09
1.138	1444.3	-1.28	-9.48
1.139	1447.2	-1.68	-10.14
1.14	1450.1	-1.91	-10.19
1.141	1453.1	-1.71	-10.61
1.142	1456.0	-1.89	-10.61
1.143	1458.9	-1.89	-10.63
1.144	1461.9	-1.11	-10.57
1.145	1464.8	-1.50	-10.62
1.146	1467.8	-1.64	-10.13
1.147	1470.7	-1.44	-10.12
1.148	1473.6	-2.05	-10.35
1.149	1476.6	-1.68	-10.23
1.151	1482.4	-2.21	-10.45
1.151	1482.4	-2.30	-10.59
1.152	1485.4	-2.03	-10.59
1.153	1488.3	-2.88	-10.87
1.154	1491.2	-2.31	-10.46
1.155	1494.2	-0.82	-10.98
1.156	1497.1	-2.29	-10.62

Depth	Age	$\delta^{13}C$	$\delta^{18}O$
cm	yr BP	VPDB	VPDB
1.157	1500.0	-2.54	-10.82
1.158	1503.0	-1.75	-10.94
1.159	1505.9	-2.37	-10.70
1.16	1508.8	-2.40	-10.88
1.161	1511.8	-2.11	-11.01
1.162	1514.7	-2.19	-10.97
1.163	1517.7	-2.04	-10.84
1.164	1520.6	-2.44	-11.03
1.165	1523.5	-2.63	-11.08
1.166	1526.5	-2.90	-11.14
1.167	1529.4	-2.98	-11.23
1.168	1532.3	-3.11	-11.03
1.169	1535.3	-2.53	-10.89
1.17	1538.2	-2.46	-10.63
1.171	1541.1	-2.56	-10.77
1.172	1544.1	-2.06	-10.36
1.173	1547.0	-1.90	-10.39
1.174	1549.9	-1.49	-10.33
1.175	1552.9	-2.23	-10.38
1.176	1555.8	-2.07	-10.22
1.177	1558.7	-1.71	-10.58
1.178	1561.7	-1.90	-10.42
1.179	1564.6	-2.06	-10.41
1.18	1567.6	-1.72	-10.19
1.181	1570.5	-1.67	-10.21
1.182	1573.4	-1.92	-10.34
1.183	1576.4	-1.40	-10.15
1.184	1579.3	-1.14	-10.37
1.185	1582.2	-1.76	-10.23
1.186	1585.2	-1.46	-10.37
1.187	1588.1	-1.18	-9.92
1.188	1591.0	-0.98	-10.27
1.189	1594.0	-1.66	-10.35
1.19	1596.9	-2.16	-10.37
1.191	1599.8	-1.72	-10.48
1.192	1602.8	-1.99	-10.50
1.193	1605.7	-1.81	-10.55
1.194	1608.6	-1.98	-10.54
1.195	1611.6	-1.40	-10.94

Depth	Age	$\delta^{13}C$	$\delta^{18}O$
cm	yr BP	VPDB	VPDB
1.196	1614.5	-1.80	-10.19
1.197	1617.5	-1.79	-11.01
1.198	1620.4	-2.26	-10.63
1.199	1623.3	-1.89	-11.11
1.2	1626.3	-2.11	-10.78
1.201	1629.2	-2.47	-10.88
1.202	1632.1	-2.11	-10.71
1.203	1635.1	-1.97	-11.00
1.204	1638.0	-2.13	-10.72
1.205	1640.9	-1.70	-10.88
1.206	1643.9	-2.33	-10.71
1.207	1646.8	-2.04	-10.78
1.208	1649.7	-2.49	-10.58
1.209	1652.7	-1.88	-10.82
1.21	1655.6	-0.97	-10.85
1.211	1658.5	-1.78	-11.35
1.212	1661.5	-0.63	-11.29
1.213	1664.4	-1.27	-11.14
1.214	1667.4	-0.86	-10.49
1.215	1670.3	-1.27	-10.88
1.216	1673.2	-1.50	-10.75
1.217	1676.2	-1.20	-10.88
1.218	1679.1	-1.41	-10.85
1.219	1682.0	-1.20	-10.86
1.22	1685.0	-2.29	-10.74
1.221	1687.9	-1.83	-11.16
1.222	1690.8	-1.13	-11.30
1.223	1693.8	-1.87	-11.18
1.224	1696.7	-1.13	-11.09
1.225	1699.6	-1.83	-11.14
1.226	1702.6	-1.52	-11.06
1.227	1705.5	-2.00	-10.92
1.228	1708.4	-0.69	-10.98
1.229	1711.4	-1.17	-11.25
1.23	1714.3	-1.28	-11.22
1.231	1717.3	-1.48	-10.95
1.232	1720.2	-0.78	-11.01
1.233	1723.1	-0.70	-10.81
1.234	1726.1	-1.01	-10.77

Depth	Age	$\delta^{13}C$	$\delta^{18}O$
cm	yr BP	VPDB	VPDB
1.235	1729.0	-0.82	-10.53
1.236	1731.9	-1.29	-11.39
1.237	1734.9	-1.03	-11.18
1.238	1737.8	-1.04	-10.80
1.239	1740.7	-0.96	-10.89
1.24	1743.7	-1.32	-11.30
1.241	1746.6	-1.51	-10.56
1.242	1749.5	-1.42	-10.67
1.243	1752.5	-1.42	-10.94
1.244	1755.4	-0.78	-11.02
1.245	1758.3	-1.52	-10.63
1.246	1761.3	-1.25	-10.89
1.247	1764.2	-1.67	-10.57
1.248	1767.2	-1.13	-11.21
1.249	1770.1	-1.48	-10.79
1.25	1773.0	-1.23	-10.82
1.251	1776.0	-1.50	-10.62
1.252	1778.9	-1.39	-10.70
1.253	1781.8	-1.24	-10.88
1.254	1784.8	-1.47	-10.79
1.255	1787.7	-1.38	-10.79
1.256	1790.6	-1.39	-10.79
1.257	1793.6	-1.76	-10.91
1.258	1796.5	-1.63	-11.01
1.259	1799.4	-1.63	-11.32
1.26	1802.4	-1.54	-11.33
1.261	1805.3	-1.54	-11.38
1.262	1808.2	-1.42	-11.69
1.263	1811.2	-1.59	-11.39
1.264	1814.1	-2.35	-11.36
1.265	1817.1	-1.89	-11.23
1.266	1820.0	-2.04	-11.21
1.267	1822.9	-1.80	-11.39
1.268	1825.9	-1.92	-11.27
1.269	1828.8	-1.43	-11.38
1.27	1831.7	-1.36	-11.44
1.271	1834.7	-1.65	-11.48
1.272	1837.6	-2.15	-11.52
1.273	1840.5	-2.37	-11.72

Depth	Age	$\delta^{13}C$	$\delta^{18}O$
cm	yr BP	VPDB	VPDB
1.274	1843.5	-2.48	-11.51
1.275	1846.4	-2.63	-11.35
1.276	1849.3	-2.53	-11.67
1.277	1852.3	-2.30	-11.47
1.278	1855.2	-2.56	-11.54
1.279	1858.1	-2.15	-11.46
1.28	1861.1	-2.10	-11.54
1.281	1864.0	-2.32	-11.65
1.282	1867.0	-2.26	-11.51
1.283	1869.9	-2.07	-11.51
1.284	1872.8	-1.93	-11.30
1.285	1875.8	-1.75	-11.27
1.286	1878.7	-1.64	-11.28
1.287	1881.6	-2.17	-11.31
1.288	1884.6	-1.51	-11.33
1.289	1887.5	-1.67	-11.35
1.29	1890.4	-1.90	-11.35
1.291	1893.4	-1.88	-11.20
1.292	1896.3	-2.16	-11.33
1.293	1899.2	-1.64	-11.43
1.294	1902.2	-1.75	-11.27
1.295	1905.1	-1.93	-11.30
1.296	1908.0	-1.91	-11.36
1.297	1911.0	-1.51	-11.51
1.298	1913.9	-2.02	-11.31
1.299	1916.9	-1.47	-11.48
1.3	1919.8	-2.17	-11.18
1.301	1922.7	-2.27	-11.23
1.302	1925.7	-2.09	-11.33
1.303	1928.6	-2.20	-11.13
1.304	1931.5	-2.26	-11.05
1.305	1934.5	-2.33	-11.14
1.306	1937.4	-2.24	-11.21
1.307	1940.3	-1.95	-11.14
1.308	1943.3	-1.77	-11.11
1.309	1946.2	-1.56	-11.08
1.31	1949.1	-1.89	-11.44
1.311	1952.1	-1.74	-11.30
1.312	1955.0	-1.77	-11.43

Depth	Age	$\delta^{13}C$	$\delta^{18}O$
cm	yr BP	VPDB	VPDB
1.313	1957.9	-1.96	-11.44
1.314	1960.9	-1.64	-11.23
1.315	1963.8	-2.04	-11.40
1.316	1966.8	-1.66	-11.37
1.317	1969.7	-2.19	-11.38
1.318	1972.6	-2.23	-11.28
1.319	1975.6	-2.23	-11.24
1.32	1978.5	-2.34	-11.24
1.321	1981.4	-2.12	-11.30
1.322	1984.4	-1.78	-11.36
1.323	1987.3	-1.62	-11.32
1.324	1990.2	-1.27	-11.24
1.325	1993.2	-1.61	-11.31
1.326	1996.1	-1.75	-11.16
1.327	1999.0	-1.52	-11.15
1.328	2002.0	-1.45	-11.07
1.329	2004.9	-1.86	-11.32
1.33	2007.8	-1.64	-11.26
1.331	2010.8	-1.50	-11.09
1.332	2013.7	-1.88	-11.25
1.333	2016.7	-1.84	-11.20
1.334	2019.6	-1.59	-11.34
1.335	2022.5	-1.89	-11.14
1.336	2025.5	-1.96	-11.15
1.337	2028.4	-1.90	-11.17
1.338	2031.3	-1.93	-11.15
1.339	2034.3	-1.96	-10.92
1.34	2037.2	-2.15	-11.11
1.341	2040.1	-2.02	-10.96
1.342	2043.1	-1.99	-11.06
1.343	2046.0	-2.18	-10.96
1.344	2048.9	-2.20	-10.88
1.345	2051.9	-1.77	-10.81
1.346	2054.8	-1.83	-10.73
1.347	2057.7	-1.66	-10.72
1.348	2060.7	-2.29	-10.74
1.349	2063.6	-2.09	-10.88
1.35	2066.6	-1.13	-10.92
1.351	2069.5	-1.82	-10.86

Depth	Age	$\delta^{13}C$	$\delta^{18}O$
cm	yr BP	VPDB	VPDB
1.352	2072.4	-1.88	-10.95
1.353	2075.4	-1.85	-11.09
1.354	2078.3	-1.88	-10.91
1.355	2081.2	-1.84	-11.01
1.356	2084.2	-1.91	-11.34
1.357	2087.1	-1.71	-10.99
1.358	2090.0	-1.81	-10.99
1.359	2093.0	-1.65	-10.78
1.36	2095.9	-1.21	-10.94
1.361	2098.8	-2.01	-11.02
1.362	2101.8	-2.12	-10.81
1.363	2104.7	-2.07	-10.68
1.364	2107.6	-1.82	-11.14
1.365	2110.6	-1.94	-11.05
1.366	2113.5	-1.91	-11.10
1.367	2116.5	-2.05	-11.11
1.368	2119.4	-2.32	-11.01
1.369	2122.3	-2.10	-11.12
1.37	2125.3	-1.96	-11.09
1.371	2128.2	-1.96	-11.23
1.372	2131.1	-1.87	-11.12
1.373	2134.1	-2.34	-11.16
1.374	2137.0	-2.35	-11.20
1.375	2139.9	-2.44	-11.20
1.376	2142.9	-2.52	-11.05
1.377	2145.8	-2.36	-11.08
1.378	2148.7	-2.25	-11.28
1.379	2151.7	-2.08	-11.23
1.38	2154.6	-2.44	-11.15
1.381	2157.5	-2.41	-11.27
1.382	2160.5	-2.36	-11.17
1.383	2163.4	-2.04	-11.66
1.384	2166.4	-1.86	-11.05
1.385	2169.3	-1.78	-11.60
1.386	2172.2	-1.69	-11.04
1.387	2175.2	-2.16	-11.06
1.388	2178.1	-3.44	-10.97
1.389	2181.0	-1.69	-11.15
1.39	2184.0	-2.34	-10.93

Depth	Age	$\delta^{13}C$	$\delta^{18}O$
cm	yr BP	VPDB	VPDB
1.391	2186.9	-2.25	-11.43
1.392	2189.8	-2.12	-11.16
1.393	2192.8	-2.78	-11.25
1.394	2195.7	-2.55	-11.04
1.395	2198.6	-2.50	-11.28
1.396	2201.6	-2.35	-11.20
1.397	2204.5	-2.36	-11.36
1.398	2207.4	-2.49	-11.18
1.399	2210.4	-1.81	-11.26
1.4	2213.3	-1.65	-11.41
1.401	2216.3	-0.92	-11.40
1.402	2219.2	-1.80	-10.95
1.403	2222.1	-2.56	-11.06
1.404	2225.1	-2.26	-11.04
1.405	2228.0	-2.84	-11.00
1.406	2230.9	-2.06	-10.85
1.408	2236.8	-1.80	-11.15
1.409	2239.7	-2.39	-11.11
1.41	2242.7	-2.32	-11.00
1.411	2245.6	-2.20	-11.00
1.412	2248.5	-2.27	-11.02
1.413	2251.5	-2.35	-11.15
1.414	2254.4	-2.44	-11.04
1.415	2257.3	-2.31	-11.06
1.416	2260.3	-2.29	-11.05
1.417	2263.2	-2.34	-11.33
1.418	2266.2	-2.06	-11.11
1.419	2269.1	-1.87	-11.38
1.42	2272.0	-2.22	-11.28
1.421	2275.0	-2.07	-11.26
1.422	2277.9	-1.85	-11.34
1.423	2280.8	-1.37	-11.23
1.424	2283.8	-2.03	-11.10
1.425	2286.7	-2.09	-11.14
1.426	2289.6	-1.75	-11.19
1.427	2292.6	-0.73	-11.43
1.428	2295.5	-1.50	-11.32
1.429	2298.4	-1.93	-11.40
1.43	2301.4	-1.64	-11.20

Depth	Age	$\delta^{13}C$	$\delta^{18}O$
cm	yr BP	VPDB	VPDB
1.431	2304.3	-1.19	-11.32
1.432	2307.2	-1.59	-11.16
1.433	2310.2	-1.44	-10.99
1.434	2313.1	-1.68	-11.44
1.435	2316.1	-1.17	-11.07
1.436	2319.0	-1.08	-11.33
1.437	2321.9	-1.33	-11.30
1.438	2324.9	-1.55	-10.98
1.439	2327.8	-1.44	-11.44
1.44	2330.7	-1.54	-11.11
1.441	2333.7	-1.55	-11.22
1.442	2336.6	-1.25	-10.72
1.443	2339.5	-1.56	-11.28
1.444	2342.5	-1.62	-11.06
1.445	2345.4	-1.39	-11.20
1.446	2348.3	-1.18	-11.04
1.447	2351.3	-1.96	-11.18
1.448	2354.2	-1.47	-11.01
1.449	2357.1	-1.77	-11.11
1.45	2360.1	-1.45	-11.17
1.451	2363.0	-1.17	-11.19
1.452	2366.0	-1.32	-11.15
1.453	2368.9	-0.32	-11.20
1.454	2371.8	-1.22	-10.93
1.455	2374.8	-0.92	-10.59
1.456	2377.7	-1.44	-10.78
1.457	2380.6	-0.93	-10.76
1.458	2383.6	-0.98	-10.79
1.459	2386.5	-0.88	-10.65
1.46	2389.4	-0.77	-11.07
1.461	2392.4	-1.13	-10.75
1.462	2395.3	-0.69	-10.68
1.463	2398.2	-1.19	-10.86
1.464	2401.2	-0.91	-10.69
1.465	2404.1	-1.69	-11.01
1.466	2407.0	-1.03	-10.70
1.467	2410.0	-1.45	-10.78
1.468	2412.9	-0.78	-10.60
1.469	2415.9	-1.08	-10.66

Depth	Age	$\delta^{13}C$	$\delta^{18}O$
cm	yr BP	VPDB	VPDB
1.47	2418.8	-0.98	-11.18
1.471	2421.7	-1.59	-10.89
1.472	2424.7	-1.44	-11.08
1.473	2427.6	-1.81	-11.09
1.474	2430.5	-1.71	-11.27
1.475	2433.5	-1.91	-11.18
1.476	2436.4	-1.33	-11.25
1.477	2439.3	-1.24	-10.95
1.478	2442.3	-1.75	-11.21
1.479	2445.2	-2.15	-11.32
1.48	2448.1	-1.78	-11.18
1.481	2451.1	-2.13	-11.31
1.482	2454.0	-1.93	-11.26
1.483	2456.9	-2.06	-11.42
1.484	2459.9	-2.07	-11.09
1.485	2462.8	-2.28	-11.41
1.486	2465.8	-2.12	-11.29
1.487	2468.7	-2.16	-11.59
1.488	2471.6	-1.70	-11.28
1.489	2474.6	-1.89	-11.43
1.49	2477.5	-1.17	-11.26
1.491	2480.4	-1.77	-11.24
1.492	2483.4	-1.82	-11.22
1.493	2486.3	-2.22	-11.06
1.494	2489.2	-2.01	-10.81
1.495	2492.2	-2.09	-11.01
1.496	2495.1	-2.19	-11.10
1.497	2498.0	-2.02	-11.13
1.498	2501.0	-1.80	-11.01
1.499	2503.9	-1.86	-10.89
1.5	2506.9	-1.93	-10.90
1.501	2509.8	-1.29	-10.91
1.502	2512.7	-1.89	-10.81
1.503	2515.7	-0.97	-10.72
1.504	2518.6	-1.59	-10.82
1.505	2521.5	-2.06	-10.65
1.506	2524.5	-1.36	-10.64
1.507	2527.4	-2.22	-10.46
1.508	2530.3	-2.28	-10.53

Depth	Age	$\delta^{13}C$	$\delta^{18}O$
cm	yr BP	VPDB	VPDB
1.509	2533.3	-1.61	-10.55
1.51	2536.2	-2.25	-10.48
1.511	2539.1	-1.64	-10.79
1.512	2542.1	-1.67	-10.41
1.513	2545.0	-1.46	-10.52
1.514	2547.9	-1.64	-10.51
1.515	2550.9	-1.96	-10.27
1.516	2553.8	-2.01	-10.38
1.517	2556.8	-1.75	-10.39
1.518	2559.7	-1.45	-10.58
1.519	2562.6	-1.70	-10.25
1.52	2565.6	-1.20	-10.42
1.521	2568.5	-1.37	-10.61
1.522	2571.4	-1.98	-10.51
1.523	2574.4	-1.40	-10.63
1.524	2577.3	-2.00	-10.55
1.525	2580.2	-1.92	-10.63
1.526	2583.2	-1.70	-10.62
1.527	2586.1	-1.80	-10.56
1.528	2589.0	-1.95	-10.65
1.529	2592.0	-2.00	-10.43
1.53	2594.9	-1.73	-10.31
1.531	2597.8	-1.25	-10.47
1.532	2600.8	-1.54	-10.45
1.533	2603.7	-2.32	-10.64
1.534	2606.7	-1.01	-10.40
1.535	2609.6	-0.31	-10.41
1.536	2612.5	-1.18	-10.39
1.537	2615.5	-1.38	-10.39
1.538	2618.4	-1.24	-10.14
1.539	2621.3	-1.53	-10.20
1.54	2624.3	-1.29	-10.13
1.541	2627.2	-1.11	-9.98
1.542	2630.1	-1.18	-9.87
1.543	2633.1	-1.33	-9.96
1.544	2636.0	-1.77	-9.86
1.545	2638.9	-0.54	-9.85
1.546	2641.9	-0.78	-9.81
1.547	2644.8	-1.02	-9.89

Depth	Age	$\delta^{13}C$	$\delta^{18}O$
cm	yr BP	VPDB	VPDB
1.548	2647.7	-0.92	-9.76
1.549	2650.7	-0.92	-10.08
1.55	2653.6	-0.89	-10.27
1.551	2656.6	-0.42	-9.98
1.552	2659.5	0.05	-10.00
1.553	2662.4	-0.68	-10.33
1.554	2665.4	-0.88	-9.86
1.555	2668.3	-0.50	-9.91
1.556	2671.2	-0.68	-9.71
1.557	2674.2	-0.74	-9.86
1.558	2677.1	-1.08	-9.76
1.559	2680.0	-0.79	-9.76
1.56	2683.0	-0.65	-9.72
1.561	2685.9	-0.81	-9.68
1.562	2688.8	-0.64	-9.96
1.563	2691.8	0.01	-9.98
1.564	2694.7	-0.44	-9.63
1.565	2697.6	-0.61	-9.66
1.566	2700.6	-0.57	-9.76
1.567	2703.5	-0.84	-9.89
1.568	2706.5	-0.89	-9.89
1.569	2709.4	-0.44	-10.13
1.57	2712.3	-0.63	-10.22
1.571	2715.3	-0.42	-10.15
1.572	2718.2	-0.73	-10.21
1.573	2721.1	-1.20	-9.68
1.574	2724.1	-0.88	-10.25
1.575	2727.0	-1.03	-10.03
1.576	2729.9	-0.78	-9.88
1.577	2732.9	-1.23	-10.18
1.578	2735.8	-0.37	-9.82
1.579	2738.7	-1.08	-9.80
1.58	2741.7	-0.76	-10.16
1.581	2744.6	-0.81	-10.21
1.582	2747.5	-0.50	-10.11
1.583	2750.5	-0.43	-10.24
1.584	2753.4	-0.65	-10.46
1.585	2756.4	-0.55	-10.27
1.586	2759.3	-0.63	-10.11

Depth	Age	$\delta^{13}C$	$\delta^{18}O$
cm	yr BP	VPDB	VPDB
1.587	2762.2	-1.90	-10.68
1.588	2765.2	-1.27	-10.24
1.589	2768.1	-0.92	-10.10
1.59	2771.0	-1.27	-10.37
1.593	2779.8	-1.53	-10.15
1.594	2782.8	-1.36	-10.63
1.595	2785.7	-1.35	-10.69
1.599	2797.4	-1.72	-10.97
1.601	2803.3	-1.86	-11.00
1.602	2806.3	-1.90	-10.97
1.603	2809.2	-1.71	-11.40
1.604	2812.1	-1.72	-11.54
1.606	2818.0	-1.57	-11.41
1.607	2820.9	-2.44	-11.52
1.609	2826.8	-2.70	-11.38
1.61	2829.7	-2.94	-11.59
1.611	2832.7	-2.81	-11.43
1.612	2835.6	-2.62	-11.57
1.613	2838.5	-2.39	-11.44
1.614	2841.5	-2.85	-11.69
1.615	2844.4	-2.60	-11.54
1.616	2847.3	-2.31	-11.56
1.617	2850.3	-2.36	-11.61
1.618	2853.2	-2.31	-11.45
1.619	2856.2	-1.89	-11.35
1.625	2873.8	-2.14	-11.63
1.628	2882.6	-1.94	-11.31
1.629	2885.5	-1.85	-11.22
1.63	2888.4	-1.82	-11.54
1.631	2891.4	-1.28	-11.34
1.632	2894.3	-1.25	-10.81
1.633	2897.2	-1.47	-11.25
1.634	2900.2	-1.23	-11.23
1.635	2903.1	-1.32	-11.21
1.636	2906.1	-1.34	-11.32
1.637	2909.0	-1.77	-11.11
1.638	2911.9	-1.74	-11.49
1.639	2914.9	-1.48	-11.37
1.64	2917.8	-0.50	-11.37

Depth	Age	$\delta^{13}C$	$\delta^{18}O$
cm	yr BP	VPDB	VPDB
1.641	2920.7	-0.88	-10.87
1.642	2923.7	-0.79	-10.78
1.643	2926.6	-1.03	-10.94
1.644	2929.5	-0.75	-10.50
1.645	2932.5	-0.67	-11.18
1.646	2935.4	-0.77	-10.90
1.647	2938.3	-1.10	-10.80
1.648	2941.3	-0.74	-10.70
1.649	2944.2	-1.39	-10.88
1.65	2947.1	-1.31	-11.05
1.651	2950.1	-1.39	-11.04
1.652	2953.0	-0.95	-10.71
1.653	2956.0	-0.58	-10.63
1.654	2958.9	-0.89	-10.78
1.655	2961.8	-0.82	-10.58
1.656	2964.8	-0.99	-10.74
1.657	2967.7	-1.18	-10.73
1.658	2970.6	-1.02	-10.67
1.659	2973.6	-0.73	-10.20
1.66	2976.5	-1.20	-11.25
1.661	2979.4	-1.90	-11.04
1.662	2982.4	-1.66	-10.98
1.663	2985.3	-1.80	-11.33
1.664	2988.2	-1.22	-10.98
1.665	2991.2	-1.79	-10.87
1.666	2994.1	-1.95	-11.14
1.667	2997.0	-1.09	-11.47
1.668	3000.0	-1.72	-10.79
1.669	3002.9	-1.55	-10.81
1.67	3005.9	-1.66	-10.63
1.671	3008.8	-1.33	-11.03
1.672	3011.7	-1.43	-10.90
1.673	3014.7	-1.53	-10.83
1.674	3017.6	-1.58	-10.92
1.675	3020.5	-0.81	-11.13
1.676	3023.5	-1.04	-10.56
1.677	3026.4	-0.83	-10.60
1.678	3029.3	-1.84	-10.84
1.679	3032.3	-1.63	-10.85

Depth	Age	$\delta^{13}C$	$\delta^{18}O$
cm	yr BP	VPDB	VPDB
1.68	3035.2	-1.31	-10.91
1.681	3038.1	-1.39	-10.68
1.682	3041.1	-1.27	-10.69
1.683	3044.0	-1.25	-10.36
1.684	3046.9	-1.14	-10.41
1.685	3049.9	-1.12	-10.52
1.686	3052.8	-0.70	-10.51
1.687	3055.8	-0.78	-10.32
1.688	3058.7	-1.11	-10.57
1.689	3061.6	-0.91	-10.36
1.69	3064.6	-1.11	-10.51
1.691	3067.5	-0.87	-10.40
1.692	3070.4	-0.64	-10.33
1.693	3073.4	-0.68	-10.45
1.694	3076.3	-0.16	-10.34
1.695	3079.2	-0.59	-10.83
1.696	3082.2	-1.04	-10.64
1.697	3085.1	-1.70	-10.85
1.698	3088.0	-1.17	-10.41
1.699	3091.0	-2.07	-10.93
1.7	3093.9	-1.50	-10.84
1.701	3096.8	-1.06	-10.40
1.702	3099.8	-0.68	-10.79
1.703	3102.7	-1.17	-10.53
1.704	3105.7	-1.21	-10.51
1.705	3108.6	-0.76	-10.48
1.706	3111.5	-1.20	-10.46
1.707	3114.5	-0.93	-10.33
1.708	3117.4	-0.96	-10.30
1.709	3120.3	-1.16	-10.61
1.71	3123.3	-1.21	-10.55
1.711	3126.2	-0.87	-10.48
1.712	3129.1	-0.83	-10.39
1.713	3132.1	-0.94	-10.40
1.714	3135.0	-0.12	-10.81
1.715	3137.9	-1.29	-10.57
1.716	3140.9	-1.38	-10.38
1.717	3143.8	-1.03	-10.77
1.718	3146.7	-0.88	-10.46

Depth	Age	$\delta^{13}C$	$\delta^{18}O$
cm	yr BP	VPDB	VPDB
1.719	3149.7	-0.64	-10.35
1.72	3152.6	-1.41	-10.71
1.721	3155.6	-1.40	-10.48
1.722	3158.5	-1.39	-10.60
1.723	3161.4	-1.91	-10.84
1.724	3164.4	-1.45	-10.78
1.725	3167.3	-1.31	-10.64
1.726	3170.2	-1.12	-10.22
1.727	3173.2	-1.30	-10.50
1.728	3176.1	-1.26	-10.48
1.729	3179.0	-1.00	-10.27
1.73	3182.0	-1.22	-10.42
1.731	3184.9	-1.13	-10.50
1.732	3187.8	-0.71	-10.35
1.733	3190.8	-0.78	-10.46
1.734	3193.7	-1.12	-10.35
1.735	3196.6	-1.10	-10.38
1.736	3199.6	-1.49	-10.51
1.737	3202.5	-1.25	-10.62
1.738	3205.5	-0.84	-10.42
1.739	3208.4	-1.12	-10.60
1.74	3211.3	-1.01	-10.68
1.741	3214.3	-1.18	-10.95
1.742	3217.2	-1.46	-10.46
1.743	3220.1	-1.15	-10.73
1.744	3223.1	-1.31	-10.45
1.745	3226.0	-0.65	-10.36
1.746	3228.9	-1.03	-10.45
1.747	3231.9	-0.49	-10.22
1.748	3234.8	-0.86	-10.06
1.749	3237.7	-0.98	-10.42
1.75	3240.7	-0.95	-10.41
1.751	3243.6	-0.26	-10.21
1.752	3246.5	-0.68	-10.18
1.753	3249.5	-0.71	-10.18
1.754	3252.4	-0.64	-10.03
1.755	3255.4	-0.78	-10.27
1.756	3258.3	-0.82	-10.05
1.757	3261.2	-0.78	-10.01

Depth	Age	$\delta^{13}C$	$\delta^{18}O$
cm	yr BP	VPDB	VPDB
1.758	3264.2	-0.89	-10.04
1.759	3267.1	-0.92	-10.40
1.76	3270.0	-1.01	-10.62
1.761	3273.0	-0.67	-10.30
1.762	3275.9	-0.88	-10.39
1.763	3278.8	-0.82	-10.31
1.764	3281.8	-0.69	-10.26
1.765	3284.7	-0.59	-10.15
1.766	3287.6	-0.33	-10.34
1.767	3290.6	-0.44	-9.91
1.768	3293.5	-0.38	-10.13
1.769	3296.4	-0.50	-10.11
1.77	3299.4	-0.45	-9.90
1.771	3302.3	-0.93	-9.94
1.772	3305.3	-0.56	-10.12
1.773	3308.2	-1.00	-10.13
1.774	3311.1	-1.09	-9.97
1.775	3314.1	0.13	-10.01
1.776	3317.0	-0.88	-10.19
1.777	3319.9	-0.44	-10.15
1.778	3322.9	-0.65	-10.35
1.779	3325.8	-0.05	-9.98
1.78	3328.7	-0.33	-10.46
1.781	3331.7	-0.47	-10.11
1.782	3334.6	-0.15	-10.30
1.783	3337.5	-0.87	-9.96
1.784	3340.5	-0.45	-9.85
1.785	3343.4	-0.90	-10.30
1.786	3346.3	-1.43	-10.29
1.787	3349.3	-0.81	-10.27
1.788	3352.2	-0.61	-10.40
1.789	3355.2	-0.36	-10.05
1.79	3358.1	-0.60	-9.88
1.791	3361.0	-1.00	-9.99
1.792	3364.0	-0.89	-9.79
1.793	3366.9	-0.79	-9.87
1.794	3369.8	-0.83	-10.18
1.795	3372.8	-0.64	-10.13
1.796	3375.7	-0.48	-10.24

Depth	Age	$\delta^{13}C$	$\delta^{18}O$
cm	yr BP	VPDB	VPDB
1.797	3378.6	-0.41	-9.91
1.798	3381.6	-0.35	-10.14
1.799	3384.5	-0.77	-10.14
1.8	3387.4	-0.32	-10.25
1.801	3390.4	-0.17	-9.95
1.802	3393.3	-0.17	-9.99
1.803	3396.2	-0.12	-9.94
1.804	3399.2	-0.70	-9.87
1.805	3402.1	-0.55	-9.80
1.806	3405.1	-0.45	-10.20
1.807	3408.0	-0.34	-9.99
1.808	3410.9	-0.21	-9.95
1.809	3413.9	-0.50	-10.38
1.81	3416.8	-0.87	-10.25
1.811	3419.7	-0.54	-10.24
1.812	3422.7	-0.49	-10.07
1.813	3425.6	-0.68	-10.16
1.814	3428.5	-0.45	-9.97
1.815	3431.5	-0.65	-10.10
1.816	3434.4	-0.60	-9.83
1.817	3437.3	-0.55	-10.07
1.818	3440.3	-0.23	-10.03
1.819	3443.2	-0.29	-10.17
1.82	3446.1	-0.46	-10.15
1.821	3449.1	-0.27	-10.50
1.822	3452.0	-0.75	-10.48
1.823	3455.0	-1.16	-10.18
1.824	3457.9	-0.86	-10.38
1.825	3460.8	-0.52	-10.28
1.826	3463.8	-0.80	-10.44
1.827	3466.7	-1.05	-10.58
1.828	3469.6	-0.64	-10.55
1.829	3472.6	-0.47	-10.14
1.83	3475.5	-0.28	-10.16
1.831	3478.4	-0.45	-10.14
1.833	3484.3	-0.80	-10.20
1.834	3487.2	-0.73	-10.39
1.835	3490.2	-0.89	-10.40
1.836	3493.1	-1.00	-10.40

Depth	Age	$\delta^{13}C$	$\delta^{18}O$
cm	yr BP	VPDB	VPDB
1.837	3496.0	-0.94	-10.47
1.838	3499.0	-1.03	-10.09
1.839	3501.9	-0.65	-10.11
1.841	3507.8	-0.93	-10.33
1.842	3510.7	-0.52	-10.26
1.843	3513.7	-0.76	-10.31
1.844	3516.6	-0.83	-10.06
1.845	3519.5	-1.04	-10.13
1.846	3522.5	-0.61	-10.14
1.847	3525.4	-0.39	-10.28
1.848	3528.3	-0.67	-10.35
1.849	3531.3	-0.57	-10.28
1.85	3534.2	-0.28	-9.92
1.851	3537.1	-0.62	-10.15
1.852	3540.1	-0.98	-10.19
1.853	3543.0	-0.63	-10.13
1.854	3545.9	-0.87	-10.11
1.855	3548.9	-0.83	-10.11
1.856	3551.8	-0.73	-10.00
1.857	3554.8	-0.62	-10.33
1.858	3557.7	-1.02	-10.42
1.859	3560.6	-0.31	-10.43
1.86	3563.6	-0.45	-10.25
1.861	3566.5	-0.50	-10.31
1.862	3569.4	-0.93	-10.22
1.863	3572.4	-0.63	-10.17
1.864	3575.3	-0.92	-10.29
1.865	3578.2	-0.87	-10.27
1.866	3581.2	-0.78	-10.15
1.867	3584.1	-0.96	-10.25
1.868	3587.0	-1.08	-10.26
1.869	3590.0	-1.04	-10.38
1.87	3592.9	-0.82	-10.49
1.871	3595.8	-1.04	-10.17
1.872	3598.8	-0.76	-10.13
1.873	3601.7	-0.98	-10.01
1.874	3604.7	-0.92	-10.33
1.875	3607.6	-0.86	-10.33
1.876	3610.5	-0.89	-10.14

Depth	Age	$\delta^{13}C$	$\delta^{18}O$
cm	yr BP	VPDB	VPDB
1.877	3613.5	-0.83	-10.29
1.878	3616.4	-1.12	-10.48
1.879	3619.3	-0.82	-10.61
1.88	3622.3	-1.16	-10.56
1.881	3625.2	-1.18	-10.43
1.882	3628.1	-1.05	-10.48
1.883	3631.1	-0.81	-10.21
1.884	3634.0	-1.27	-10.40
1.885	3636.9	-0.50	-10.05
1.886	3639.9	-0.68	-10.20
1.887	3642.8	-1.06	-10.39
1.888	3645.7	-1.34	-10.35
1.889	3648.7	-1.56	-10.53
1.89	3651.6	-0.69	-10.62
1.891	3654.6	-1.05	-10.45
1.892	3657.5	-1.09	-10.22
1.893	3660.4	-1.16	-10.27
1.894	3663.4	-1.05	-10.47
1.895	3666.3	-0.81	-10.63
1.896	3669.2	-0.64	-10.81
1.897	3672.2	-1.74	-11.07
1.898	3675.1	-0.83	-10.79
1.899	3678.0	-1.27	-10.97
1.9	3681.0	-0.84	-11.22
1.901	3683.9	-1.32	-10.87
1.902	3686.8	-1.28	-10.79
1.903	3689.8	-1.03	-10.56
1.904	3692.7	-1.27	-10.71
1.905	3695.6	-0.86	-10.79
1.906	3698.6	-0.80	-11.06
1.907	3701.5	-1.41	-10.81
1.908	3704.5	-0.85	-10.53
1.909	3707.4	-0.79	-10.84
1.91	3710.3	-1.49	-10.76
1.911	3713.3	-0.67	-10.46
1.912	3716.2	-0.58	-10.57
1.913	3719.1	-0.90	-10.41
1.914	3722.1	-0.86	-10.45
1.915	3725.0	-1.04	-10.34

Depth	Age	$\delta^{13}C$	$\delta^{18}O$
cm	yr BP	VPDB	VPDB
1.916	3727.9	-0.53	-10.56
1.917	3730.9	-0.52	-10.45
1.918	3733.8	-0.67	-10.86
1.92	3739.7	-0.82	-10.49
1.921	3742.6	-0.88	-10.27
1.922	3745.5	-0.82	-10.27
1.923	3748.5	-0.62	-10.28
1.924	3751.4	-1.10	-10.25
1.925	3754.4	-1.62	-10.51
1.926	3757.3	-1.19	-10.26
1.927	3760.2	-1.14	-10.33
1.928	3763.2	-1.12	-10.37
1.929	3766.1	-1.20	-10.17
1.93	3769.0	-1.33	-10.21
1.931	3772.0	-1.47	-10.61
1.932	3774.9	-1.26	-10.55
1.933	3777.8	-1.22	-10.66
1.934	3780.8	-1.47	-10.61
1.935	3783.7	-1.22	-10.70
1.936	3786.6	-1.20	-10.93
1.937	3789.6	-1.39	-10.68
1.938	3792.5	-1.05	-10.64
1.939	3795.4	-1.44	-10.75
1.94	3798.4	-1.42	-10.87
1.941	3801.3	-1.33	-10.80
1.942	3804.3	-1.40	-10.76
1.943	3807.2	-1.44	-10.95
1.944	3810.1	-1.53	-10.93
1.945	3813.1	-0.93	-11.38
1.946	3816.0	-1.16	-10.76
1.947	3818.9	-1.60	-11.18
1.948	3821.9	-1.52	-11.02
1.949	3824.8	-1.43	-11.02
1.949	3824.8	-1.63	-11.08
1.95	3827.7	-1.35	-10.78
1.951	3830.7	-1.32	-10.71
1.952	3833.6	-1.37	-10.94
1.953	3836.5	-1.31	-10.86
1.954	3839.5	-1.43	-10.86

Depth	Age	$\delta^{13}C$	$\delta^{18}O$
cm	yr BP	VPDB	VPDB
1.955	3842.4	-1.20	-10.71
1.956	3845.3	-1.79	-10.97
1.957	3848.3	-1.39	-11.07
1.959	3854.2	-1.81	-11.17
1.96	3857.1	-0.95	-10.97
1.961	3860.0	-1.72	-11.14
1.962	3863.0	-1.41	-11.01
1.963	3865.9	-1.42	-11.24
1.964	3868.8	-0.95	-10.68
1.965	3871.8	-1.73	-11.23
1.966	3874.7	-1.41	-11.12
1.967	3877.6	-1.43	-11.20
1.968	3880.6	-1.09	-11.04
1.969	3883.5	-1.41	-11.05
1.97	3886.4	-0.71	-10.68
1.971	3889.4	-1.36	-11.07
1.972	3892.3	-1.62	-11.04
1.973	3895.2	-1.42	-11.22
1.974	3898.2	-1.83	-11.07
1.975	3901.1	-1.47	-11.07
1.976	3904.1	-1.53	-11.08
1.977	3907.0	-1.90	-11.30
1.978	3909.9	-1.65	-11.46
1.979	3912.9	-1.57	-11.19
1.98	3915.8	-1.49	-11.28
1.981	3918.7	-1.63	-11.27
1.982	3921.7	-1.72	-11.66
1.983	3924.6	-1.03	-11.00
1.984	3927.5	-1.48	-11.26
1.985	3930.5	-1.78	-11.44
1.986	3933.4	-1.72	-11.44
1.987	3936.3	-1.58	-11.45
1.988	3939.3	-1.49	-10.96
1.99	3945.1	-0.85	-10.70
1.991	3948.1	0.15	-10.04
1.992	3951.0	-0.93	-10.87
1.993	3954.0	-1.19	-10.30
1.994	3956.9	-0.34	-10.89
1.995	3959.8	-1.08	-11.01

Depth	Age	$\delta^{13}C$	$\delta^{18}O$
cm	yr BP	VPDB	VPDB
1.996	3962.8	-1.87	-11.80
1.997	3965.7	-1.82	-11.95
1.998	3968.6	-2.30	-12.18
1.999	3971.6	-2.35	-12.10
2	3974.5	-2.11	-12.17
2.001	3977.4	-1.79	-11.56
2.002	3980.4	-1.57	-11.49
2.003	3983.3	-1.67	-12.12
2.004	3986.2	-2.48	-12.00
2.005	3989.2	-1.95	-12.01
2.006	3992.1	-2.04	-11.78
2.007	3995.0	-2.14	-11.71
2.008	3998.0	-2.08	-11.79
2.009	4000.9	-2.20	-12.20
2.01	4003.9	-1.38	-12.03
2.011	4006.8	-1.64	-11.96
2.012	4009.7	-1.63	-11.66
2.013	4012.7	-2.51	-12.17
2.014	4015.6	-1.92	-12.03
2.015	4018.5	-2.66	-12.15
2.016	4021.5	-2.55	-12.28
2.017	4024.4	-2.25	-12.24
2.018	4027.3	-1.92	-12.09
2.019	4030.3	-2.15	-12.23
2.02	4033.2	-1.92	-11.91
2.021	4036.1	-2.59	-12.15
2.022	4039.1	-2.17	-12.12
2.023	4042.0	-1.90	-12.31
2.025	4047.9	-2.44	-12.06
2.026	4050.8	-2.00	-11.99
2.027	4053.8	-1.96	-12.14
2.028	4056.7	-2.11	-12.05
2.029	4059.6	-2.47	-12.22
2.03	4062.6	-2.13	-11.92
2.031	4065.5	-2.42	-12.08
2.032	4068.4	-2.06	-11.99
2.033	4071.4	-2.22	-12.07
2.034	4074.3	-1.91	-11.76
2.035	4077.2	-1.57	-11.88

Depth	Age	$\delta^{13}C$	$\delta^{18}O$
cm	yr BP	VPDB	VPDB
2.036	4080.2	-1.09	-11.29
2.037	4083.1	-1.23	-11.04
2.038	4086.0	-1.71	-11.03
2.039	4089.0	-1.72	-11.32
2.04	4091.9	-1.49	-11.36
2.041	4094.8	-1.03	-11.24
2.042	4097.8	-1.14	-11.03
2.043	4100.7	-1.30	-10.74
2.044	4103.7	-1.12	-10.85
2.045	4106.6	-1.19	-10.62
2.046	4109.5	-1.33	-10.68
2.047	4112.5	-1.12	-11.02
2.048	4115.4	-1.28	-11.10
2.049	4118.3	-1.64	-11.00
2.05	4121.3	-1.28	-11.01
2.051	4124.2	-1.35	-10.77
2.052	4127.1	-2.02	-11.19
2.053	4130.1	-1.68	-10.73
2.054	4133.0	-1.82	-11.12
2.055	4135.9	-1.72	-11.11
2.056	4138.9	-1.84	-11.31
2.057	4141.8	-1.70	-11.39
2.058	4144.7	-1.87	-11.53
2.059	4147.7	-1.82	-11.16
2.06	4150.6	-1.99	-11.29
2.061	4153.6	-2.15	-11.49
2.062	4156.5	-2.28	-11.63
2.063	4159.4	-2.12	-11.68
2.064	4162.4	-2.20	-11.58
2.065	4165.3	-2.24	-11.70
2.066	4168.2	-2.31	-11.59
2.067	4171.2	-2.39	-11.62
2.068	4174.1	-2.39	-11.54
2.069	4177.0	-2.49	-11.64
2.07	4180.0	-2.40	-11.48
2.071	4182.9	-2.34	-11.46
2.072	4185.8	-1.95	-11.51
2.073	4188.8	-2.25	-11.49
2.074	4191.7	-2.54	-11.56

Depth	Age	$\delta^{13}C$	$\delta^{18}O$
cm	yr BP	VPDB	VPDB
2.075	4194.6	-2.56	-11.55
2.076	4197.6	-2.37	-11.44
2.077	4200.5	-2.59	-11.25
2.078	4203.5	-2.41	-11.37
2.079	4206.4	-1.79	-11.20
2.08	4209.3	-2.02	-11.06
2.081	4212.3	-1.93	-11.25
2.082	4215.2	-1.85	-11.16
2.084	4221.1	-1.68	-11.47
2.085	4224.0	-1.68	-11.37
2.086	4226.9	-1.71	-11.19
2.087	4229.9	-1.69	-11.41
2.088	4232.8	-1.81	-11.21
2.089	4235.7	-1.71	-11.23
2.09	4238.7	-1.78	-11.20
2.091	4241.6	-1.85	-11.21
2.092	4244.5	-1.62	-11.28
2.093	4247.5	-1.44	-11.16
2.094	4250.4	-2.00	-11.06
2.095	4253.4	-0.67	-10.39
2.096	4256.3	-1.05	-10.05
2.097	4259.2	-0.87	-10.02
2.098	4262.2	-0.79	-9.98
2.099	4265.1	-1.11	-9.67
2.1	4268.0	-0.75	-9.85
2.101	4271.0	-0.66	-10.01
2.102	4273.9	-0.67	-10.16
2.103	4276.8	-0.56	-10.56
2.104	4279.8	-0.32	-9.71
2.105	4282.7	-0.37	-9.52
2.106	4285.6	0.07	-9.55
2.107	4288.6	0.02	-9.74
2.108	4291.5	-0.07	-9.45
2.11	4297.4	0.02	-9.40
2.111	4300.3	0.19	-9.42
2.112	4303.3	-0.34	-9.14
2.113	4306.2	0.36	-9.39
2.114	4309.1	0.35	-9.02
2.115	4312.1	0.13	-9.53

Depth	Age	$\delta^{13}C$	$\delta^{18}O$
cm	yr BP	VPDB	VPDB
2.116	4315.0	0.69	-9.62
2.117	4317.9	0.55	-9.78
2.118	4320.9	0.32	-9.74
2.119	4323.8	-0.21	-9.39
2.12	4326.7	0.05	-9.01
2.121	4329.7	-0.07	-9.22
2.122	4332.6	-0.18	-10.03
2.123	4335.5	0.07	-9.28
2.124	4338.5	0.23	-9.68
2.125	4341.4	0.50	-9.26
2.126	4344.3	-0.29	-9.46
2.127	4347.3	-0.09	-9.48
2.128	4350.2	0.28	-9.25
2.129	4353.2	0.72	-10.39
2.13	4356.1	-0.30	-9.98
2.131	4359.0	-0.25	-9.01
2.132	4362.0	0.06	-9.65
2.133	4364.9	0.02	-9.42
2.134	4367.8	0.30	-10.10
2.137	4376.6	0.06	-9.63
2.138	4379.6	-0.02	-9.59
2.139	4382.5	-0.36	-9.32
2.14	4385.4	-0.09	-9.56
2.141	4388.4	-0.21	-9.82
2.142	4391.3	-0.05	-10.09
2.143	4394.2	-0.04	-9.98
2.144	4397.2	-0.02	-10.29
2.145	4400.1	-0.47	-9.96
2.146	4403.1	-0.07	-9.90
2.147	4406.0	-0.10	-9.87
2.148	4408.9	-0.81	-10.18
2.149	4411.9	-0.31	-9.95
2.15	4414.8	-0.40	-9.93
2.151	4417.7	-2.89	-10.66
2.152	4420.7	-0.22	-10.62
2.153	4423.6	-0.32	-9.83
2.154	4426.5	-0.13	-9.87
2.155	4429.5	-0.48	-9.84
2.156	4432.4	-0.29	-10.07

Depth	Age	$\delta^{13}C$	$\delta^{18}O$
cm	yr BP	VPDB	VPDB
2.157	4435.3	-0.04	-9.75
2.158	4438.3	-0.12	-10.30
2.159	4441.2	-1.57	-10.65
2.16	4444.1	-0.39	-9.96
2.161	4447.1	-0.13	-9.89
2.162	4450.0	-0.59	-9.99
2.163	4453.0	-0.13	-9.96
2.164	4455.9	-0.95	-10.58
2.165	4458.8	-0.34	-10.03
2.166	4461.8	-0.62	-9.81
2.167	4464.7	-0.03	-9.90
2.168	4467.6	0.06	-10.09
2.169	4470.6	-0.83	-9.92
2.17	4473.5	-0.35	-9.93
2.171	4476.4	-0.61	-9.84
2.172	4479.4	-0.43	-9.64
2.173	4482.3	-0.07	-9.65
2.174	4485.2	-0.41	-9.59
2.175	4488.2	-0.28	-9.68
2.176	4491.1	-0.34	-9.61
2.177	4494.0	-0.34	-9.66
2.178	4497.0	-0.44	-9.55
2.179	4499.9	-0.37	-9.60
2.18	4502.9	-0.39	-9.65
2.181	4505.8	-0.74	-9.52
2.182	4508.7	-0.66	-9.57
2.183	4511.7	-0.45	-9.80
2.184	4514.6	-0.25	-9.64
2.185	4517.5	-0.21	-9.66
2.186	4520.5	-0.33	-9.58
2.187	4523.4	0.04	-9.93
2.188	4526.3	-0.18	-9.62
2.189	4529.3	-0.41	-9.87
2.19	4532.2	-0.36	-9.73
2.191	4535.1	0.11	-10.36
2.192	4538.1	-0.10	-9.62
2.193	4541.0	-0.16	-9.59
2.194	4543.9	-0.11	-9.97
2.195	4546.9	-0.47	-9.99

Depth	Age	$\delta^{13}C$	$\delta^{18}O$
cm	yr BP	VPDB	VPDB
2.196	4549.8	-0.48	-10.00
2.197	4552.8	-0.01	-9.96
2.198	4555.7	-0.33	-9.71
2.199	4558.6	-0.38	-9.66
2.2	4561.6	-0.06	-9.71
2.201	4564.5	-0.24	-9.50
2.202	4567.4	-0.50	-9.52
2.203	4570.4	-0.71	-9.36
2.204	4573.3	-0.70	-9.27
2.205	4576.2	-0.76	-9.38
2.206	4579.2	-0.20	-9.73
2.207	4582.1	-0.52	-9.82
2.208	4585.0	-0.20	-9.69
2.209	4588.0	-0.59	-9.46
2.21	4590.9	-0.28	-9.45
2.211	4593.8	-0.40	-9.47
2.212	4596.8	-0.20	-9.41
2.213	4599.7	-0.47	-9.34
2.214	4602.7	-0.58	-9.50
2.215	4605.6	-0.11	-8.68
2.216	4608.5	-0.46	-8.23
2.217	4611.5	-1.10	-9.18
2.218	4614.4	-0.45	-9.00
2.219	4617.3	-0.02	-8.94
2.22	4620.3	-0.10	-8.66
2.221	4623.2	-0.16	-9.00
2.222	4626.1	-0.37	-9.23
2.223	4629.1	-0.71	-9.20
2.224	4632.0	-0.89	-9.38
2.225	4634.9	-0.53	-9.76
2.226	4637.9	-0.99	-8.91
2.227	4640.8	-0.82	-9.50
2.228	4643.7	-0.48	-9.75
2.229	4646.7	-0.79	-9.56
2.23	4649.6	-0.41	-9.29
2.231	4652.6	-0.45	-9.40
2.232	4655.5	0.13	-9.68
2.233	4658.4	-0.39	-9.85
2.234	4661.4	-0.19	-9.85

Depth	Age	$\delta^{13}C$	$\delta^{18}O$
cm	yr BP	VPDB	VPDB
2.235	4664.3	-0.28	-9.89
2.236	4667.2	-0.42	-9.79
2.237	4670.2	-0.36	-9.58
2.238	4673.1	-0.25	-9.31
2.239	4676.0	-0.24	-9.38
2.24	4679.0	-0.22	-9.25
2.241	4681.9	-1.53	-8.82
2.242	4684.8	-0.22	-9.48
2.243	4687.8	-0.08	-9.41
2.244	4690.7	-0.49	-9.91
2.245	4693.6	-0.43	-10.07
2.246	4696.6	-1.43	-10.75
2.247	4699.5	-0.15	-9.36
2.248	4702.5	0.11	-9.70
2.249	4705.4	-0.52	-10.22
2.25	4708.3	-0.24	-9.70
2.251	4711.3	-0.26	-9.68
2.252	4714.2	-0.13	-9.57
2.253	4717.1	0.08	-9.39
2.254	4720.1	-0.26	-9.21
2.255	4723.0	-0.52	-9.86
2.256	4725.9	-0.90	-9.52
2.257	4728.9	-0.27	-9.48
2.258	4731.8	-0.88	-9.40
2.259	4734.7	-2.40	-9.34
2.26	4737.7	-0.99	-10.03
2.261	4740.6	-0.69	-9.77
2.262	4743.5	-1.30	-10.02
2.263	4746.5	-0.63	-9.79
2.264	4749.4	-0.59	-9.39
2.265	4752.4	-0.94	-10.12
2.266	4755.3	-0.69	-9.55
2.267	4758.2	-0.87	-10.13
2.268	4761.2	-0.74	-10.28
2.269	4764.1	-1.41	-9.47
2.27	4767.0	-0.79	-10.10
2.271	4770.0	-0.94	-9.57
2.272	4772.9	-1.37	-10.09
2.273	4775.8	-0.61	-9.78

Depth	Age	$\delta^{13}C$	$\delta^{18}O$
cm	yr BP	VPDB	VPDB
2.274	4778.8	-0.86	-9.46
2.275	4781.7	-0.66	-10.01
2.276	4784.6	-1.31	-10.50
2.277	4787.6	-1.41	-10.62
2.278	4790.5	-0.35	-9.88
2.279	4793.4	-0.49	-10.01
2.28	4796.4	-1.31	-10.29
2.281	4799.3	-1.67	-9.95
2.282	4802.3	-1.43	-10.54
2.283	4805.2	-0.98	-10.61
2.284	4808.1	-1.48	-9.97
2.285	4811.1	-2.30	-10.27
2.286	4814.0	-0.58	-9.83
2.287	4816.9	-1.52	-10.19
2.288	4819.9	-0.74	-9.84
2.289	4822.8	-1.07	-10.01
2.29	4825.7	-0.69	-9.39
2.291	4828.7	0.03	-9.13
2.292	4831.6	-0.67	-9.30
2.293	4834.5	-1.93	-9.70
2.294	4837.5	-2.35	-9.93
2.295	4840.4	-1.27	-9.85
2.296	4843.3	-0.34	-8.94
2.297	4846.3	-0.14	-9.02
2.298	4849.2	-0.33	-9.03
2.299	4852.2	-0.13	-9.39
2.301	4858.0	0.18	-8.96
2.302	4861.0	-1.50	-10.12
2.303	4863.9	-1.00	-9.74
2.304	4866.8	-0.36	-9.11
2.305	4869.8	0.04	-8.95
2.306	4872.7	0.46	-9.58
2.307	4875.6	0.14	-8.85
2.308	4878.6	-0.06	-9.38
2.309	4881.5	0.01	-9.04
2.31	4884.4	-0.07	-8.67
2.311	4887.4	0.33	-8.85
2.312	4890.3	0.36	-8.77
2.313	4893.2	0.57	-8.96

Depth	Age	$\delta^{13}C$	$\delta^{18}O$
cm	yr BP	VPDB	VPDB
2.314	4896.2	0.34	-8.58
2.315	4899.1	0.29	-8.86
2.316	4902.1	0.33	-8.73
2.317	4905.0	0.79	-9.09
2.318	4907.9	0.60	-8.81
2.319	4910.9	0.28	-8.59
2.32	4913.8	0.29	-8.75
2.321	4916.7	0.00	-8.89
2.322	4919.7	0.51	-8.81
2.323	4922.6	0.20	-8.97
2.324	4925.5	-0.29	-9.56
2.325	4928.5	-1.21	-8.61
2.326	4931.4	-0.08	-8.99
2.327	4934.3	-0.29	-9.13
2.328	4937.3	-0.16	-9.25
2.329	4940.2	-0.04	-9.29
2.33	4943.1	-0.87	-9.54
2.331	4946.1	-0.33	-9.28
2.332	4949.0	-0.34	-9.21
2.333	4952.0	-0.45	-9.29
2.334	4954.9	-0.30	-9.33
2.335	4957.8	-0.39	-9.25
2.336	4960.8	-0.59	-9.75
2.337	4963.7	-0.39	-9.56
2.338	4966.6	-0.44	-9.51
2.34	4972.5	-0.73	-9.56
2.341	4975.4	-0.28	-9.75
2.342	4978.4	-0.54	-9.51
2.343	4981.3	-0.59	-9.58
2.344	4984.2	-0.37	-9.66
2.345	4987.2	-0.49	-9.50
2.346	4990.1	-0.63	-9.48
2.347	4993.0	-0.76	-9.51
2.348	4996.0	-0.54	-9.80
2.349	4998.9	-0.46	-9.88
2.35	5001.9	-0.60	-9.88
2.351	5004.8	-0.26	-10.02
2.352	5007.7	-0.44	-9.81
2.353	5010.7	-0.37	-9.63

Depth	Age	$\delta^{13}C$	$\delta^{18}O$
cm	yr BP	VPDB	VPDB
2.354	5013.6	-0.57	-9.67
2.355	5016.5	-0.52	-9.87
2.356	5019.5	-0.75	-9.70
2.357	5022.4	-0.57	-9.87
2.358	5025.3	-0.73	-10.04
2.359	5028.3	-0.52	-9.94
2.36	5031.2	-0.38	-9.72
2.361	5034.1	-0.50	-9.66
2.362	5037.1	-0.71	-10.06
2.363	5040.0	-0.34	-9.79
2.364	5042.9	-0.33	-9.19
2.365	5045.9	-0.37	-9.13
2.366	5048.8	-0.21	-8.94
2.367	5051.8	-0.25	-9.02
2.368	5054.7	-0.39	-9.15
2.369	5057.6	-0.39	-9.13
2.37	5060.6	-1.02	-9.08
2.371	5063.5	-0.63	-9.10
2.372	5066.4	-0.29	-9.19
2.373	5069.4	-0.61	-9.35
2.374	5072.3	-0.60	-9.15
2.375	5075.2	-0.74	-9.47
2.376	5078.2	-0.03	-9.17
2.377	5081.1	-0.15	-10.10
2.378	5084.0	-0.83	-9.84
2.379	5087.0	-1.12	-9.94
2.38	5089.9	-0.65	-9.78
2.381	5092.8	-1.05	-9.84
2.382	5095.8	-0.84	-10.03
2.383	5098.7	-0.60	-9.77
2.384	5101.7	-0.43	-9.93
2.385	5104.6	-1.14	-10.18
2.386	5107.5	-0.52	-9.73
2.387	5110.5	-0.36	-9.81
2.388	5113.4	-0.38	-9.82
2.389	5116.3	-1.02	-9.76
2.39	5119.3	-0.37	-9.66
2.391	5122.2	-0.62	-9.71
2.392	5125.1	-0.42	-9.80

Depth	Age	$\delta^{13}C$	$\delta^{18}O$
cm	yr BP	VPDB	VPDB
2.393	5128.1	-0.76	-10.03
2.394	5131.0	-0.01	-10.06
2.395	5133.9	-0.20	-10.19
2.396	5136.9	-0.38	-10.49
2.397	5139.8	-0.11	-9.83
2.398	5142.7	-0.07	-10.28
2.399	5145.7	-0.22	-10.10
2.4	5148.6	-0.43	-10.08
2.401	5151.6	-0.09	-9.58
2.402	5154.5	-0.25	-10.09
2.403	5157.4	-0.64	-9.93
2.404	5160.4	-0.33	-9.94
2.405	5163.3	-0.48	-9.69
2.406	5166.2	-0.34	-9.70
2.407	5169.2	0.01	-9.70
2.408	5172.1	-0.50	-9.83
2.409	5175.0	-0.47	-9.99
2.41	5178.0	-0.51	-9.92
2.411	5180.9	-0.48	-9.76
2.412	5183.8	-0.49	-9.92
2.413	5186.8	-0.77	-9.61
2.414	5189.7	-0.53	-9.92
2.415	5192.6	-0.36	-9.83
2.416	5195.6	-0.58	-10.04
2.417	5198.5	-0.48	-9.97
2.418	5201.5	-0.59	-9.61
2.419	5204.4	-0.66	-9.85
2.42	5207.3	-0.15	-9.96
2.421	5210.3	-0.11	-9.93
2.422	5213.2	-0.08	-10.06
2.423	5216.1	-0.45	-9.86
2.424	5219.1	-0.55	-9.85
2.425	5222.0	-0.49	-9.69
2.426	5224.9	-0.62	-9.68
2.427	5227.9	-0.56	-9.58
2.428	5230.8	-0.54	-9.64
2.429	5233.7	-1.54	-10.45
2.43	5236.7	-0.41	-9.88
2.431	5239.6	-0.58	-9.76

Depth	Age	$\delta^{13}C$	$\delta^{18}O$
cm	yr BP	VPDB	VPDB
2.432	5242.5	-0.58	-9.84
2.433	5245.5	-0.43	-10.09
2.434	5248.4	-0.57	-9.93
2.436	5254.3	-0.46	-10.25
2.437	5257.2	-0.38	-9.93
2.438	5260.2	-0.72	-9.74
2.439	5263.1	-0.60	-9.80
2.44	5266.0	-0.65	-9.55
2.441	5269.0	-0.17	-9.53
2.442	5271.9	-0.21	-9.88
2.443	5274.8	-0.04	-9.92
2.444	5277.8	-0.09	-9.67
2.445	5280.7	-0.22	-9.97
2.446	5283.6	-0.40	-10.30
2.447	5286.6	-0.17	-10.04
2.448	5289.5	-0.06	-10.01
2.449	5292.4	-0.40	-9.87
2.45	5295.4	-0.31	-9.85
2.451	5298.3	-0.24	-9.94
2.452	5301.3	-0.09	-9.74
2.453	5304.2	-0.38	-9.71
2.454	5307.1	-0.69	-9.84
2.455	5310.1	-0.15	-9.88
2.456	5313.0	-0.41	-9.66
2.457	5315.9	-0.58	-9.87
2.458	5318.9	-0.35	-9.79
2.459	5321.8	-0.51	-9.73
2.46	5324.7	-0.43	-9.79
2.461	5327.7	-0.92	-9.54
2.462	5330.6	-0.69	-9.64
2.463	5333.5	-0.65	-9.64
2.464	5336.5	-0.59	-9.69
2.465	5339.4	-0.50	-9.78
2.466	5342.3	-0.40	-9.58
2.467	5345.3	-0.71	-9.68
2.468	5348.2	-0.78	-10.00
2.469	5351.2	-0.29	-9.81
2.47	5354.1	-0.45	-10.02
2.471	5357.0	-0.40	-10.20

Depth	Age	$\delta^{13}C$	$\delta^{18}O$
cm	yr BP	VPDB	VPDB
2.472	5360.0	-0.07	-9.64
2.473	5362.9	-0.50	-9.87
2.474	5365.8	-0.34	-9.89
2.475	5368.8	-0.43	-9.49
2.476	5371.7	-0.40	-9.68
2.477	5374.6	-0.38	-9.49
2.478	5377.6	-0.61	-9.61
2.479	5380.5	0.02	-9.27
2.48	5383.4	-0.14	-9.16
2.481	5386.4	-0.26	-9.64
2.482	5389.3	-0.43	-9.58
2.483	5392.2	-0.42	-9.61
2.484	5395.2	-0.20	-9.52
2.485	5395.6	-0.01	-9.57
2.486	5396.7	-2.27	-9.43
2.487	5397.7	-1.84	-10.12
2.488	5398.7	-0.74	-9.73
2.489	5399.8	-1.13	-8.91
2.49	5400.8	-1.15	-9.89
2.491	5401.8	-1.34	-9.60
2.492	5402.8	0.04	-10.14
2.493	5403.9	-0.57	-9.72
2.494	5404.9	-0.55	-9.37
2.495	5405.9	-0.77	-9.85
2.496	5407.0	-0.37	-9.62
2.497	5408.0	-0.15	-9.88
2.498	5409.0	-0.22	-9.54
2.499	5410.1	-0.25	-9.33
2.5	5411.1	-0.24	-9.53
2.501	5412.1	-0.22	-9.47
2.502	5413.2	-0.28	-9.93
2.503	5414.2	-0.54	-9.69
2.504	5415.2	-0.50	-9.65
2.505	5416.3	-0.70	-9.91
2.506	5417.3	-0.27	-9.58
2.507	5418.3	-0.28	-9.68
2.507	5418.3	-0.54	-9.64
2.508	5419.4	-0.61	-9.27
2.509	5420.4	-0.73	-9.61

Depth	Age	$\delta^{13}C$	$\delta^{18}O$
cm	yr BP	VPDB	VPDB
2.51	5421.4	-0.60	-9.23
2.511	5422.4	-0.80	-9.83
2.512	5423.5	-0.53	-9.45
2.513	5424.5	-0.30	-9.29
2.514	5425.5	-0.44	-9.66
2.515	5426.6	-0.08	-9.30
2.516	5427.6	0.03	-9.37
2.517	5428.6	-0.56	-9.66
2.518	5429.7	-0.28	-9.60
2.519	5430.7	-0.34	-9.60
2.52	5431.7	-0.10	-9.31
2.521	5432.8	-0.03	-9.12
2.522	5433.8	0.12	-9.30
2.523	5434.8	0.12	-9.66
2.524	5435.9	-0.11	-9.41
2.525	5436.9	-0.14	-9.44
2.526	5437.9	-0.01	-9.59
2.527	5439.0	-0.43	-9.46
2.528	5440.0	-0.31	-9.76
2.529	5441.0	-0.22	-9.96
2.53	5442.1	-0.27	-10.03
2.531	5443.1	-0.40	-9.93
2.532	5444.1	-0.27	-9.73
2.533	5445.1	-0.26	-9.86
2.534	5446.2	-0.45	-9.85
2.535	5447.2	-0.71	-9.96
2.536	5448.2	-0.49	-10.07
2.537	5449.3	-0.49	-9.59
2.538	5450.3	-0.75	-9.81
2.539	5451.3	-0.66	-9.69
2.54	5452.4	-0.33	-9.70
2.541	5453.4	-0.62	-9.82
2.542	5454.4	-0.77	-9.49
2.543	5455.5	-0.49	-9.77
2.544	5456.5	-0.16	-9.36
2.545	5457.5	0.03	-9.61
2.546	5458.6	-0.17	-9.34
2.547	5459.6	-0.23	-9.32
2.548	5460.6	-0.32	-9.96

Depth	Age	$\delta^{13}C$	$\delta^{18}O$
cm	yr BP	VPDB	VPDB
2.549	5461.7	-0.05	-9.66
2.55	5462.7	-0.18	-9.61
2.551	5463.7	0.37	-10.14
2.552	5464.8	-0.48	-9.81
2.553	5465.8	-0.70	-9.80
2.554	5466.8	0.13	-9.90
2.555	5467.8	-0.09	-9.50
2.556	5468.9	-0.43	-9.90
2.557	5469.9	-0.36	-9.60
2.558	5470.9	-0.35	-9.63
2.559	5472.0	-0.25	-9.79
2.56	5473.0	-0.26	-9.56
2.561	5474.0	-0.12	-9.47
2.562	5475.1	-0.04	-9.42
2.563	5476.1	0.33	-8.72
2.564	5477.1	-0.05	-9.31
2.565	5478.2	-0.36	-9.30
2.566	5479.2	-0.04	-9.26
2.567	5480.2	-0.06	-9.27
2.568	5481.3	0.06	-9.06
2.569	5482.3	0.55	-8.38
2.57	5483.3	-0.13	-9.26
2.571	5484.4	-0.02	-9.62
2.572	5485.4	-0.03	-9.11
2.573	5486.4	-0.17	-9.10
2.574	5487.5	0.35	-8.89
2.575	5488.5	0.98	-8.22
2.576	5489.5	0.41	-9.23
2.577	5490.5	0.01	-9.11
2.578	5491.6	-0.44	-9.46
2.579	5492.6	-0.21	-9.26
2.58	5493.6	-0.20	-9.60
2.581	5494.7	-0.42	-9.33
2.582	5495.7	-0.56	-9.61
2.583	5496.7	-0.44	-9.70
2.584	5497.8	-0.33	-9.63
2.585	5498.8	-2.21	-8.84
2.586	5499.8	-0.83	-10.23
2.587	5500.9	-0.65	-9.71

Depth	Age	$\delta^{13}C$	$\delta^{18}O$
cm	yr BP	VPDB	VPDB
2.588	5501.9	-1.11	-10.05
2.589	5502.9	-1.29	-10.20
2.59	5504.0	-0.86	-10.42
2.591	5505.0	-1.21	-10.18
2.592	5506.0	-1.43	-10.46
2.593	5507.1	-0.85	-9.67
2.594	5508.1	-0.69	-10.23
2.595	5509.1	-2.07	-11.30
2.596	5510.2	-0.71	-10.05
2.597	5511.2	-0.78	-10.08
2.598	5512.2	-0.90	-10.15
2.599	5513.2	-0.96	-10.26
2.6	5514.3	-0.57	-10.11
2.601	5515.3	-0.77	-9.76
2.602	5516.3	-0.71	-10.23
2.603	5517.4	-0.71	-10.13
2.604	5518.4	-0.71	-10.13
2.605	5519.4	0.12	-10.07
2.606	5520.5	0.04	-9.82
2.608	5522.5	-0.97	-9.91
2.609	5523.6	-1.03	-10.13
2.61	5524.6	-0.57	-9.93
2.611	5525.6	-0.92	-9.77
2.612	5526.7	-0.62	-9.94
2.613	5527.7	-0.87	-9.99
2.614	5528.7	-0.44	-9.76
2.615	5529.8	-0.44	-9.92
2.616	5530.8	-0.30	-9.88
2.617	5531.8	-0.30	-9.97
2.618	5532.9	-0.19	-9.84
2.619	5533.9	-0.07	-10.06
2.62	5534.9	-0.17	-9.89
2.621	5535.9	-0.43	-9.78
2.622	5537.0	-0.09	-9.93
2.623	5538.0	-0.13	-9.87
2.624	5539.0	-0.21	-9.57
2.625	5540.1	-0.20	-9.95
2.626	5541.1	-0.29	-9.85
2.627	5542.1	-0.27	-9.60

Depth	Age	$\delta^{13}C$	$\delta^{18}O$
cm	yr BP	VPDB	VPDB
2.628	5543.2	-0.41	-9.74
2.629	5544.2	-0.36	-9.78
2.63	5545.2	-0.34	-9.67
2.631	5546.3	-0.44	-9.80
2.632	5547.3	-0.19	-9.76
2.633	5548.3	-0.16	-9.94
2.634	5549.4	-0.33	-9.82
2.635	5550.4	-0.52	-9.88
2.636	5551.4	-0.42	-9.68
2.637	5552.5	-1.35	-9.58
2.638	5553.5	-0.08	-10.18
2.639	5554.5	-0.52	-10.09
2.64	5555.6	-0.46	-9.99
2.641	5556.6	-0.35	-9.81
2.642	5557.6	-0.18	-9.85
2.643	5558.6	-0.78	-9.72
2.644	5559.7	-0.70	-9.93
2.645	5560.7	-0.43	-10.04
2.646	5561.7	-0.39	-9.99
2.647	5562.8	-0.39	-9.96
2.648	5563.8	-0.61	-9.95
2.649	5564.8	-0.79	-9.98
2.65	5565.9	-1.22	-10.30
2.651	5566.9	-1.11	-10.21
2.652	5567.9	-0.93	-9.92
2.653	5569.0	-0.99	-10.19
2.654	5570.0	-0.64	-10.05
2.655	5571.0	-1.20	-10.10
2.656	5572.1	-0.81	-10.25
2.657	5573.1	-0.96	-10.34
2.658	5574.1	-1.10	-10.41
2.659	5575.2	-1.47	-10.38
2.66	5576.2	-1.45	-10.37
2.661	5577.2	-1.60	-10.50
2.662	5578.3	-1.09	-10.12
2.663	5579.3	-0.59	-9.98
2.664	5580.3	-0.71	-9.74
2.665	5581.3	-0.41	-9.80
2.666	5582.4	-0.37	-9.83

Depth	Age	$\delta^{13}C$	$\delta^{18}O$
cm	yr BP	VPDB	VPDB
2.667	5583.4	-0.01	-10.03
2.668	5584.4	-0.10	-9.96
2.669	5585.5	-0.51	-9.70
2.67	5586.5	-0.37	-9.57
2.671	5587.5	-0.35	-9.61
2.672	5588.6	-0.42	-9.72
2.673	5589.6	-0.41	-9.89
2.674	5590.6	-0.79	-9.85
2.675	5591.7	-0.59	-9.81
2.676	5592.7	-0.78	-9.71
2.677	5593.7	-0.56	-9.74
2.678	5594.8	-0.61	-9.51
2.679	5595.8	-0.52	-10.05
2.68	5596.8	-0.60	-9.88
2.681	5597.9	-0.63	-9.94
2.682	5598.9	-0.92	-10.18
2.683	5599.9	-0.62	-9.85
2.684	5601.0	-0.76	-10.15
2.685	5602.0	-0.73	-9.97
2.686	5603.0	-0.67	-9.75
2.687	5604.0	-0.72	-9.93
2.688	5605.1	-0.37	-10.20
2.689	5606.1	-0.36	-9.77
2.69	5607.1	-0.75	-9.99
2.691	5608.2	-0.70	-10.11
2.692	5609.2	-0.92	-10.16
2.693	5610.2	-0.77	-10.04
2.694	5611.3	-0.32	-9.92
2.695	5612.3	-0.65	-9.83
2.696	5613.3	-0.55	-9.71
2.697	5614.4	-0.43	-9.75
2.698	5615.4	-0.68	-9.83
2.699	5616.4	-0.55	-9.90
2.7	5617.5	-0.06	-9.53
2.701	5618.5	-0.48	-9.41
2.702	5619.5	-0.38	-9.63
2.703	5620.6	-0.65	-9.85
2.704	5621.6	-0.60	-9.98
2.705	5622.6	-0.36	-9.55

Depth	Age	$\delta^{13}C$	$\delta^{18}O$
cm	yr BP	VPDB	VPDB
2.706	5623.7	-0.58	-9.81
2.707	5624.7	-0.58	-9.70
2.708	5625.7	-0.47	-9.48
2.709	5626.7	-0.59	-9.68
2.71	5627.8	-0.20	-9.76
2.711	5628.8	-0.53	-9.97
2.712	5629.8	-0.84	-9.87
2.713	5630.9	-0.99	-9.78
2.714	5631.9	-0.53	-10.15
2.715	5632.9	-0.38	-9.91
2.716	5634.0	-0.29	-10.32
2.717	5635.0	-0.60	-10.56
2.718	5636.0	-0.16	-9.94
2.719	5637.1	-0.28	-9.98
2.72	5638.1	-0.09	-9.99
2.721	5639.1	-0.36	-9.78
2.722	5640.2	-0.78	-9.73
2.723	5641.2	-0.63	-9.90
2.724	5642.2	-0.80	-9.98
2.725	5643.3	-0.64	-9.81
2.726	5644.3	-0.75	-9.96
2.727	5645.3	-0.93	-10.00
2.728	5646.4	-0.75	-9.66
2.729	5647.4	-0.65	-9.96
2.73	5648.4	-0.75	-9.88
2.731	5649.4	-0.67	-10.19
2.732	5650.5	-0.87	-10.04
2.733	5651.5	-0.78	-9.96
2.734	5652.5	-1.36	-10.13
2.735	5653.6	-1.31	-10.17
2.736	5654.6	-1.19	-10.37
2.737	5655.6	-0.98	-10.42
2.738	5656.7	-1.35	-10.43
2.739	5657.7	-1.19	-10.37
2.74	5658.7	-1.21	-10.42
2.741	5659.8	-1.32	-10.34
2.742	5660.8	-1.71	-10.60
2.743	5661.8	-1.55	-10.81
2.744	5662.9	-1.46	-10.73

Depth	Age	$\delta^{13}C$	$\delta^{18}O$
cm	yr BP	VPDB	VPDB
2.745	5663.9	-1.33	-10.75
2.746	5664.9	-1.14	-10.89
2.747	5666.0	-1.30	-11.45
2.748	5667.0	-1.68	-10.84
2.749	5668.0	-1.78	-10.91
2.75	5669.1	-2.21	-11.03
2.751	5670.1	-1.72	-10.90
2.752	5671.1	-1.72	-10.93
2.753	5672.1	-1.64	-10.90
2.754	5673.2	-1.85	-11.16
2.755	5674.2	-1.91	-10.94
2.756	5675.2	-1.90	-11.00
2.757	5676.3	-1.77	-11.00
2.758	5677.3	-1.73	-11.01
2.759	5678.3	-1.47	-10.89
2.76	5679.4	-1.54	-10.90
2.761	5680.4	-1.88	-10.96
2.762	5681.4	-1.57	-11.00
2.763	5682.5	-1.56	-11.09
2.764	5683.5	-1.74	-10.90
2.765	5684.5	-1.48	-10.99
2.766	5685.6	-1.67	-11.13
2.767	5686.6	-1.69	-10.90
2.768	5687.6	-1.75	-11.01
2.769	5688.7	-2.12	-11.10
2.77	5689.7	-1.89	-11.19
2.771	5690.7	-2.18	-11.12
2.772	5691.7	-1.97	-11.12
2.773	5692.8	-2.19	-11.72
2.774	5693.8	-2.04	-11.28
2.779	5699.0	-2.35	-11.45
2.78	5700.0	-1.38	-10.98
2.781	5701.0	-0.94	-10.95
2.782	5702.1	-1.82	-10.45
2.783	5703.1	-1.71	-10.02
2.784	5704.1	-0.91	-10.18
2.785	5705.2	-1.32	-10.58
2.786	5706.2	-1.07	-10.04
2.787	5707.2	-1.27	-10.42

Depth	Age	$\delta^{13}C$	$\delta^{18}O$
cm	yr BP	VPDB	VPDB
2.788	5708.3	-0.66	-10.17
2.789	5709.3	-1.52	-9.82
2.79	5710.3	-0.93	-10.07
2.791	5711.4	-0.76	-9.98
2.792	5712.4	-0.43	-9.38
2.793	5713.4	-0.53	-10.08
2.794	5714.4	-1.34	-9.62
2.795	5715.5	-0.36	-9.39
2.796	5716.5	-0.67	-9.70
2.797	5717.5	-0.33	-9.38
2.798	5718.6	-0.45	-9.68
2.799	5719.6	-1.01	-10.06
2.8	5720.6	-0.80	-10.39
2.801	5721.7	-1.27	-9.95
2.802	5722.7	-0.83	-9.68
2.803	5723.7	0.17	-9.29
2.804	5724.8	-0.28	-9.08
2.805	5725.8	-0.59	-9.18
2.806	5726.8	-0.12	-8.99
2.807	5727.9	-0.13	-9.06
2.808	5728.9	-0.07	-9.09
2.809	5729.9	-0.08	-9.37
2.81	5731.0	-0.67	-9.21
2.811	5732.0	-0.06	-9.11
2.812	5733.0	-0.03	-9.22
2.813	5734.1	-0.23	-9.07
2.814	5735.1	-0.62	-9.67
2.815	5736.1	-0.10	-8.98
2.815	5736.1	-0.10	-8.98
2.816	5737.1	-0.03	-9.32
2.816	5737.1	-0.03	-9.32
2.817	5738.2	-0.15	-8.95
2.817	5738.2	-0.15	-8.95
2.818	5739.2	-0.44	-9.03
2.818	5739.2	-0.44	-9.03
2.819	5740.2	-0.22	-8.98
2.819	5740.2	-0.22	-8.98
2.82	5741.3	-0.06	-9.05
2.82	5741.3	-0.06	-9.05

Depth	Age	$\delta^{13}C$	$\delta^{18}O$
cm	yr BP	VPDB	VPDB
2.821	5742.3	-0.75	-9.42
2.821	5742.3	-0.75	-9.42
2.822	5743.3	-0.49	-9.05
2.822	5743.3	-0.49	-9.05
2.823	5744.4	-0.04	-8.97
2.823	5744.4	-0.04	-8.97
2.824	5745.4	-0.08	-8.78
2.824	5745.4	-0.08	-8.78
2.825	5746.4	-0.18	-8.78
2.825	5746.4	-0.18	-8.78
2.826	5747.5	-0.10	-9.03
2.826	5747.5	-0.10	-9.03
2.827	5748.5	0.36	-8.32
2.827	5748.5	0.36	-8.32
2.828	5749.5	-0.40	-9.28
2.828	5749.5	-0.40	-9.28
2.829	5750.6	-0.29	-8.95
2.829	5750.6	-0.29	-8.95
2.83	5751.6	-0.20	-8.83
2.83	5751.6	-0.20	-8.83
2.831	5752.6	-0.27	-8.62
2.831	5752.6	-0.27	-8.62
2.832	5753.7	-0.76	-8.30
2.832	5753.7	-0.76	-8.30
2.833	5754.7	-0.31	-8.66
2.833	5754.7	-0.31	-8.66
2.834	5755.7	0.09	-9.04
2.834	5755.7	0.09	-9.04
2.835	5756.8	-0.34	-9.21
2.836	5757.8	-0.56	-9.03
2.837	5758.8	-0.16	-9.09
2.838	5759.8	-0.44	-9.24
2.839	5760.9	-0.01	-9.48
2.84	5761.9	-0.72	-9.24
2.841	5762.9	0.27	-9.35
2.842	5764.0	0.11	-9.33
2.843	5765.0	0.07	-9.16
2.844	5766.0	-0.11	-9.11
2.845	5767.1	0.64	-9.28

Depth	Age	$\delta^{13}C$	$\delta^{18}O$
cm	yr BP	VPDB	VPDB
2.846	5768.1	-0.03	-9.35
2.847	5769.1	-0.84	-9.41
2.848	5770.2	-0.89	-9.10
2.849	5771.2	0.00	-9.08
2.85	5772.2	-0.20	-9.05
2.851	5773.3	0.16	-8.67
2.852	5774.3	0.05	-9.06
2.853	5775.3	-0.28	-8.79
2.854	5776.4	0.07	-8.99
2.855	5777.4	-0.51	-9.29
2.856	5778.4	-0.29	-9.42
2.857	5779.5	-0.25	-9.51
2.858	5780.5	-0.35	-9.40
2.859	5781.5	-0.34	-9.35
2.86	5782.5	-0.57	-9.31
2.861	5783.6	-0.59	-9.39
2.862	5784.6	-0.41	-9.60
2.863	5785.6	-0.45	-9.35
2.864	5786.7	-0.09	-9.59
2.865	5787.7	-0.49	-9.27
2.866	5788.7	-0.33	-9.19
2.867	5789.8	-0.53	-9.27
2.868	5790.8	-0.94	-9.30
2.869	5791.8	-0.65	-9.50
2.87	5792.9	-1.08	-9.60
2.871	5793.9	-1.01	-9.45
2.872	5794.9	-1.03	-9.56
2.873	5796.0	-0.87	-9.52
2.874	5797.0	-0.83	-9.62
2.875	5798.0	-1.42	-9.62
2.876	5799.1	-1.79	-8.60
2.877	5800.1	-1.00	-9.88
2.878	5801.1	-1.19	-9.86
2.879	5802.2	-0.39	-9.88
2.88	5803.2	-0.90	-9.47
2.881	5804.2	-0.85	-9.64
2.882	5805.2	-0.62	-9.58
2.883	5806.3	-0.04	-9.09
2.884	5807.3	-0.57	-9.26

Depth	Age	$\delta^{13}C$	$\delta^{18}O$
cm	yr BP	VPDB	VPDB
2.885	5808.3	-0.89	-9.36
2.886	5809.4	-0.11	-9.39
2.887	5810.4	-0.85	-9.69
2.888	5811.4	-0.68	-9.50
2.889	5812.5	-0.50	-9.49
2.89	5813.5	-0.58	-9.70
2.891	5814.5	-0.70	-9.65
2.892	5815.6	-0.44	-9.25
2.893	5816.6	-0.86	-9.29
2.894	5817.6	-0.90	-9.09
2.895	5818.7	-0.55	-9.89
2.896	5819.7	-0.76	-9.76
2.897	5820.7	-0.30	-10.03
2.898	5821.8	-0.25	-9.39
2.899	5822.8	-0.44	-9.72
2.9	5823.8	0.14	-9.42
2.901	5824.9	-0.37	-9.21
2.902	5825.9	-0.03	-9.78
2.903	5826.9	-0.20	-9.37
2.904	5827.9	-0.15	-9.49
2.905	5829.0	0.23	-8.98
2.906	5830.0	-0.38	-9.41
2.907	5831.0	-0.52	-9.63
2.908	5832.1	-0.13	-9.36
2.909	5833.1	-0.01	-9.18
2.91	5834.1	0.04	-9.06
2.911	5835.2	-0.08	-8.90
2.912	5836.2	-0.04	-9.07
2.913	5837.2	-0.04	-9.12
2.914	5838.3	-0.24	-9.05
2.915	5839.3	-0.09	-9.15
2.916	5840.3	-0.06	-9.23
2.917	5841.4	0.02	-9.23
2.918	5842.4	-0.08	-9.17
2.919	5843.4	-0.15	-9.34
2.92	5844.5	-0.33	-9.41
2.921	5845.5	-0.16	-9.25
2.922	5846.5	-0.27	-9.44
2.923	5847.6	-0.30	-9.55

Depth	Age	$\delta^{13}C$	$\delta^{18}O$
cm	yr BP	VPDB	VPDB
2.924	5848.6	-0.27	-9.69
2.925	5849.6	-0.38	-9.60
2.926	5850.6	-0.38	-9.64
2.927	5851.7	-0.33	-9.57
2.928	5852.7	-0.14	-10.10
2.929	5853.7	-0.29	-10.13
2.93	5854.8	-0.53	-10.35
2.931	5855.8	-0.67	-10.39
2.932	5856.8	-0.42	-10.34
2.933	5857.9	-1.16	-10.76
2.934	5858.9	-1.00	-11.06
2.935	5859.9	-1.08	-10.90
2.936	5861.0	-1.33	-10.93
2.9365	5861.5	-1.29	-11.31
2.937	5862.0	-1.13	-11.41
2.938	5863.0	-1.35	-10.95
2.939	5864.1	-1.11	-10.94
2.94	5865.1	-1.14	-10.78
2.941	5866.1	-1.11	-10.93
2.942	5867.2	-0.86	-11.11
2.943	5868.2	-1.49	-10.56
2.944	5869.2	-1.22	-10.37
2.945	5870.3	-0.83	-10.12
2.946	5871.3	-1.08	-9.93
2.947	5872.3	-1.28	-10.16
2.948	5873.3	-1.34	-10.21
2.949	5874.4	-1.25	-10.21
2.951	5876.4	-1.68	-10.71
2.951	5876.4	-1.68	-10.71
2.952	5877.5	-1.71	-10.59
2.952	5877.5	-1.71	-10.59
2.953	5878.5	-1.84	-10.70
2.953	5878.5	-1.84	-10.70
2.954	5879.5	-1.61	-10.54
2.955	5880.6	-1.48	-10.34
2.956	5881.6	-1.27	-9.97
2.957	5882.6	-1.13	-9.81
2.958	5883.7	-0.97	-10.05
2.959	5884.7	-1.36	-10.21

Depth	Age	$\delta^{13}C$	$\delta^{18}O$
cm	yr BP	VPDB	VPDB
2.96	5885.7	-0.68	-9.97
2.961	5886.8	-1.16	-9.93
2.962	5887.8	-1.14	-10.23
2.963	5888.8	-1.32	-10.32
2.964	5889.9	-1.43	-10.61
2.965	5890.9	-1.66	-10.66
2.966	5891.9	-2.15	-10.70
2.967	5893.0	-1.75	-10.48
2.968	5894.0	-2.14	-10.57
2.969	5895.0	-2.01	-10.62
2.97	5896.0	-2.05	-10.67
2.971	5897.1	-1.83	-10.56
2.972	5898.1	-1.35	-10.01
2.973	5899.1	-1.04	-10.42
2.974	5900.2	-1.29	-10.49
2.975	5901.2	-1.14	-10.50
2.976	5902.2	-1.16	-10.75
2.977	5903.3	-1.08	-10.53
2.978	5904.3	-1.13	-10.49
2.979	5905.3	-1.31	-10.51
2.98	5906.4	-1.17	-10.57
2.981	5907.4	-1.31	-10.62
2.982	5908.4	-1.34	-10.48
2.983	5909.5	-1.47	-10.58
2.984	5910.5	-1.16	-10.58
2.985	5911.5	-1.25	-10.49
2.986	5912.6	-1.26	-10.48
2.987	5913.6	-1.00	-10.52
2.988	5914.6	-1.17	-10.72
2.989	5915.7	-1.35	-10.39
2.99	5916.7	-1.09	-10.85
2.991	5917.7	-1.24	-10.64
2.992	5918.7	-1.04	-10.56
2.993	5919.8	-1.22	-10.49
2.994	5920.8	-1.05	-10.35
2.995	5921.8	-1.70	-10.42
2.996	5922.9	-1.38	-10.50
2.997	5923.9	-1.45	-10.60
2.998	5924.9	-1.40	-10.47

Depth	Age	$\delta^{13}C$	$\delta^{18}O$
cm	yr BP	VPDB	VPDB
2.999	5926.0	-1.20	-10.37
3.012	5939.4	-1.03	-10.74
3.013	5940.4	-0.94	-10.62
3.014	5941.4	-1.10	-10.45
3.015	5942.5	-0.66	-10.45
3.016	5943.5	-0.71	-10.68
3.017	5944.5	-0.61	-10.61
3.018	5945.6	-1.13	-10.52
3.019	5946.6	-0.95	-10.54
3.02	5947.6	-1.16	-10.55
3.021	5948.7	-0.79	-10.48
3.022	5949.7	-1.13	-10.51
3.023	5950.7	-0.60	-10.73
3.024	5951.8	-1.46	-10.75
3.025	5952.8	-1.41	-10.73
3.026	5953.8	-1.27	-10.84
3.027	5954.9	-0.99	-10.62
3.028	5955.9	-1.33	-10.76
3.029	5956.9	-1.11	-10.66
3.03	5958.0	-1.34	-10.84
3.031	5959.0	-1.12	-10.36
3.034	5962.1	-1.27	-10.77
3.035	5963.1	-1.61	-10.91
3.036	5964.1	-1.24	-11.07
3.037	5965.2	-1.34	-10.76
3.038	5966.2	-0.32	-10.69
3.039	5967.2	-1.41	-10.61
3.04	5968.3	-0.79	-10.95
3.041	5969.3	-0.73	-10.21
3.042	5970.3	-0.66	-10.86
3.043	5971.4	-0.91	-10.66
3.045	5973.4	-0.41	-9.92
3.046	5974.5	-0.33	-9.85
3.047	5975.5	-0.10	-9.90
3.048	5976.5	0.16	-9.49
3.049	5977.6	-0.42	-9.89
3.05	5978.6	-0.36	-10.03
3.051	5979.6	0.23	-10.20
3.052	5980.7	-0.34	-9.92

Depth	Age	$\delta^{13}C$	$\delta^{18}O$
cm	yr BP	VPDB	VPDB
3.053	5981.7	-0.15	-10.15
3.054	5982.7	-0.71	-10.03
3.055	5983.7	-0.68	-9.99
3.056	5984.8	-0.51	-9.93
3.057	5985.8	-0.19	-9.91
3.058	5986.8	-0.13	-9.96
3.059	5987.9	-0.43	-10.43
3.06	5988.9	-1.04	-10.36
3.061	5989.9	-0.83	-10.53
3.062	5991.0	-0.87	-10.60
3.063	5992.0	-1.26	-10.40
3.064	5993.0	-0.51	-10.29
3.065	5994.1	-0.90	-10.22
3.066	5995.1	-0.86	-10.62
3.067	5996.1	-0.58	-10.56
3.068	5997.2	-0.96	-10.37
3.069	5998.2	-0.34	-10.52
3.07	5999.2	-0.29	-10.62
3.071	6000.3	-0.27	-10.57
3.072	6001.3	-0.43	-10.76
3.073	6002.3	-0.59	-10.52
3.074	6003.4	-0.33	-10.47
3.075	6004.4	-0.29	-11.01
3.076	6005.4	0.17	-10.99
3.077	6006.4	0.70	-11.05
3.078	6007.5	-0.25	-10.43
3.079	6008.5	-0.38	-10.52
3.08	6009.5	0.62	-11.54
3.081	6010.6	-0.07	-10.58
3.082	6011.6	-0.35	-10.25
3.083	6012.6	-0.34	-10.17
3.084	6013.7	-0.40	-10.09
3.085	6014.7	-0.38	-10.05
3.086	6015.7	-0.45	-10.12
3.087	6016.8	-0.27	-10.27
3.088	6017.8	-0.41	-9.84
3.089	6018.8	-0.25	-9.56
3.09	6019.9	0.70	-9.46
3.09	6019.9	-0.08	-9.34

Depth	Age	$\delta^{13}C$	$\delta^{18}O$
cm	yr BP	VPDB	VPDB
3.091	6020.9	0.75	-8.94
3.091	6020.9	0.07	-9.17
3.092	6021.9	0.78	-7.29
3.093	6023.0	0.54	-8.69
3.094	6024.0	0.34	-8.96
3.095	6025.0	0.40	-8.92
3.096	6026.1	0.66	-8.60
3.097	6027.1	0.55	-8.55
3.098	6028.1	0.46	-8.77
3.099	6029.1	0.35	-8.61
3.1	6030.2	0.11	-8.94
3.101	6031.2	0.23	-9.16
3.102	6032.2	-0.01	-9.12
3.103	6033.3	0.12	-9.35
3.104	6034.3	0.46	-9.54
3.105	6035.3	-0.11	-9.52
3.106	6036.4	0.16	-9.21
3.107	6037.4	-0.13	-9.25
3.108	6038.4	0.05	-9.64
3.109	6039.5	-0.09	-9.48
3.11	6040.5	-0.40	-9.96
3.111	6041.5	-0.58	-9.42
3.112	6042.6	-0.68	-9.77
3.113	6043.6	-0.70	-9.65
3.114	6044.6	-1.07	-9.80
3.115	6045.7	-0.66	-10.05
3.116	6046.7	-0.48	-9.87
3.117	6047.7	-1.80	-10.40
3.118	6048.8	-0.08	-7.80
3.119	6049.8	-0.32	-9.69
3.12	6050.8	-0.97	-10.57
3.121	6051.8	-0.93	-9.88
3.122	6052.9	-0.81	-10.18
3.123	6053.9	-0.76	-10.72
3.124	6054.9	-1.12	-9.82
3.125	6056.0	0.25	-7.40
3.126	6057.0	-1.07	-10.21
3.127	6058.0	-0.63	-10.07
3.128	6059.1	-2.29	-9.38

Depth	Age	$\delta^{13}C$	$\delta^{18}O$
cm	yr BP	VPDB	VPDB
3.129	6060.1	-0.48	-10.18
3.145	6076.6	-0.35	-10.16
3.146	6077.6	0.15	-9.78
3.147	6078.7	-0.28	-9.68
3.148	6079.7	-0.12	-9.52
3.149	6080.7	-0.11	-9.48
3.15	6081.8	-0.41	-10.12
3.151	6082.8	-0.51	-9.97
3.152	6083.8	-0.45	-9.97
3.153	6084.9	-0.50	-10.13
3.154	6085.9	-0.59	-9.74
3.155	6086.9	-1.00	-9.48
3.156	6088.0	-0.41	-9.70
3.157	6089.0	-0.57	-9.93
3.158	6090.0	-0.50	-10.04
3.159	6091.1	-0.84	-10.09
3.16	6092.1	-1.82	-9.86
3.161	6093.1	-0.59	-9.99
3.162	6094.2	-1.47	-9.97
3.163	6095.2	-1.26	-9.77
3.164	6096.2	-1.06	-10.18
3.165	6097.2	-1.76	-10.44
3.166	6098.3	-0.91	-10.17
3.167	6099.3	-1.21	-10.08
3.168	6100.3	-1.11	-10.01
3.169	6101.4	-1.11	-10.11
3.17	6102.4	-1.12	-9.97
3.171	6103.4	-1.15	-10.11
3.172	6104.5	-0.98	-10.17
3.173	6105.5	-1.01	-9.96
3.175	6107.6	-1.09	-9.65
3.176	6108.6	-1.19	-9.67
3.177	6109.6	-1.34	-9.80
3.179	6111.7	-0.92	-9.77
3.18	6112.7	-1.10	-9.76
3.181	6113.8	-1.10	-9.87
3.182	6114.8	-1.11	-9.69
3.183	6115.8	-1.15	-9.85
3.184	6116.9	-1.52	-9.89

Depth	Age	$\delta^{13}C$	$\delta^{18}O$
cm	yr BP	VPDB	VPDB
3.185	6117.9	-1.28	-10.16
3.186	6118.9	-1.13	-9.31
3.187	6119.9	-1.06	-10.03
3.188	6121.0	-1.41	-10.00
3.189	6122.0	-1.15	-9.90
3.19	6123.0	-1.67	-10.04
3.191	6124.1	-0.97	-9.92
3.192	6125.1	-1.59	-10.01
3.193	6126.1	-1.13	-10.01
3.194	6127.2	-0.84	-10.33
3.195	6128.2	-0.98	-10.29
3.196	6129.2	-1.02	-9.95
3.197	6130.3	-1.23	-10.24
3.198	6131.3	-1.33	-10.18
3.2	6133.4	-1.07	-10.39
3.201	6134.4	-1.13	-10.27
3.202	6135.4	-0.97	-10.44
3.203	6136.5	-1.42	-10.44
3.204	6137.5	-0.97	-10.08
3.205	6138.5	-1.26	-10.59
3.206	6139.6	-1.42	-10.59
3.207	6140.6	-0.71	-10.71
3.208	6141.6	-0.86	-10.49
3.209	6142.6	-0.97	-10.41
3.21	6143.7	-1.12	-10.81
3.211	6144.7	-1.27	-10.85
3.212	6145.7	-1.24	-10.80
3.213	6146.8	-1.14	-10.77
3.214	6147.8	-1.45	-10.75
3.215	6148.8	-1.41	-10.76
3.216	6149.9	-1.43	-11.16
3.217	6150.9	-1.39	-11.04
3.218	6151.9	-1.42	-10.84
3.219	6153.0	-1.32	-10.83
3.22	6154.0	-1.36	-10.95
3.221	6155.0	-1.21	-11.09
3.222	6156.1	-1.42	-10.71
3.223	6157.1	-1.27	-11.20
3.225	6159.2	-1.52	-10.82

Depth	Age	$\delta^{13}C$	$\delta^{18}O$
cm	yr BP	VPDB	VPDB
3.226	6160.2	-1.48	-10.60
3.227	6161.2	-1.73	-11.02
3.228	6162.3	-1.68	-10.91
3.229	6163.3	-1.72	-10.71
3.23	6164.3	-1.60	-10.84
3.231	6165.3	-1.95	-11.22
3.232	6166.4	-1.60	-11.25
3.233	6167.4	-2.16	-10.98
3.234	6168.4	-1.36	-10.80
3.235	6169.5	-1.80	-10.84
3.236	6170.5	-1.64	-11.08
3.237	6171.5	-1.88	-10.89
3.238	6172.6	-2.00	-11.21
3.239	6173.6	-2.52	-11.01
3.24	6174.6	-2.68	-10.94
3.241	6175.7	-1.85	-11.09
3.242	6176.7	-1.72	-11.14
3.243	6177.7	-1.92	-11.12
3.244	6178.8	-2.12	-11.12
3.245	6179.8	-2.06	-11.00
3.246	6180.8	-2.28	-10.93
3.247	6181.9	-1.92	-10.91
3.248	6182.9	-2.01	-11.14
3.249	6183.9	-1.77	-10.98
3.25	6185.0	-1.77	-10.85
3.251	6186.0	-1.40	-10.64
3.252	6187.0	-1.52	-10.40
3.253	6188.0	-1.46	-10.39
3.254	6189.1	-1.78	-10.35
3.255	6190.1	-1.47	-10.60
3.256	6191.1	-1.40	-10.64
3.257	6192.2	-1.60	-10.46
3.258	6193.2	-1.39	-10.91
3.259	6194.2	-1.63	-10.73
3.26	6195.3	-1.41	-10.24
3.261	6196.3	-1.84	-10.55
3.262	6197.3	-1.70	-10.52
3.263	6198.4	-1.01	-10.26
3.264	6199.4	-1.30	-10.27

Depth	Age	$\delta^{13}C$	$\delta^{18}O$
cm	yr BP	VPDB	VPDB
3.265	6200.4	-1.19	-10.37
3.267	6202.5	-0.66	-10.34
3.268	6203.5	-0.83	-10.03
3.269	6204.6	-1.11	-10.40
3.27	6205.6	-0.99	-10.09
3.271	6206.6	-1.17	-10.38
3.272	6207.6	-1.36	-10.37
3.273	6208.7	-1.10	-10.35
3.274	6209.7	-1.07	-10.48
3.275	6210.7	-0.97	-10.34
3.276	6211.8	-0.94	-10.36
3.277	6212.8	-1.82	-10.78
3.278	6213.8	-1.10	-10.79
3.279	6214.9	-1.10	-10.57
3.28	6215.9	-0.82	-10.39
3.281	6216.9	-0.99	-10.66
3.282	6218.0	-0.88	-10.61
3.283	6219.0	-0.88	-10.57
3.284	6220.0	-0.76	-10.73
3.285	6221.1	-1.23	-10.19
3.286	6222.1	-1.23	-11.15
3.287	6223.1	-0.77	-10.44
3.288	6224.2	-0.62	-10.56
3.289	6225.2	-0.70	-9.98
3.29	6226.2	-0.46	-10.06
3.291	6227.3	-0.24	-9.69
3.292	6228.3	-0.21	-9.86
3.293	6229.3	-0.37	-9.72
3.294	6230.3	-0.63	-9.66
3.295	6231.4	-0.31	-9.75
3.296	6232.4	-1.01	-9.84
3.297	6233.4	0.02	-9.48
3.298	6234.5	-0.62	-9.55
3.299	6235.5	-0.29	-9.63
3.3	6236.5	-0.26	-9.52
3.301	6237.6	-0.20	-9.42
3.302	6238.6	-0.25	-9.54
3.303	6239.6	0.13	-8.89
3.304	6240.7	-0.27	-9.12
3.305	6241.7	-0.42	-9.77
3.306	6242.7	-0.22	-9.65
3.307	6243.8	-0.56	-9.60
3.308	6244.8	-0.16	-9.98
3.31	6246.9	-0.27	-9.69
3.311	6247.9	-0.23	-9.80
3.312	6248.9	-0.37	-9.66
3.313	6250.0	-0.17	-9.54
3.314	6251.0	-0.02	-9.82
3.315	6252.0	-0.19	-9.64
3.316	6253.0	-0.19	-9.87
3.317	6254.1	-0.12	-9.76
3.318	6255.1	0.17	-9.66
3.319	6256.1	-0.47	-9.46
3.32	6257.2	-0.12	-9.56
3.321	6258.2	-0.29	-9.78
3.322	6259.2	-0.41	-9.67
3.323	6260.3	-0.22	-9.84
3.324	6261.3	-0.26	-9.76
3.325	6262.3	-0.11	-9.98
3.327	6264.4	-0.20	-9.91
3.328	6265.4	-0.42	-10.17
3.329	6266.5	-0.27	-9.82
3.33	6267.5	-0.12	-9.88
3.331	6268.5	-0.66	-9.52
3.332	6269.6	0.29	-9.89
3.333	6270.6	-0.08	-9.97
3.334	6271.6	-0.20	-10.16
3.335	6272.7	0.34	-9.57
3.336	6273.7	0.56	-9.88
3.337	6274.7	-0.09	-9.86
3.338	6275.7	0.18	-9.85
3.339	6276.8	0.25	-10.21
3.34	6277.8	0.05	-9.69
3.341	6278.8	0.16	-9.87
3.342	6279.9	0.06	-9.69
3.343	6280.9	-0.13	-10.00
3.344	6281.9	0.08	-10.58
3.345	6283.0	0.08	-10.25

Depth	Age	$\delta^{13}C$	$\delta^{18}O$
cm	yr BP	VPDB	VPDB
3.346	6284.0	-0.16	-9.67
3.347	6285.0	-0.22	-10.13
3.348	6286.1	0.02	-9.96
3.349	6287.1	0.03	-9.89
3.35	6288.1	-0.61	-10.19
3.351	6289.2	-0.37	-10.24
3.352	6290.2	0.17	-9.98
3.353	6291.2	-0.17	-9.61
3.353	6291.2	0.21	-9.04
3.354	6292.3	-0.24	-10.01
3.355	6293.3	-0.39	-9.83
3.356	6294.3	-0.07	-10.05
3.357	6295.4	-0.12	-10.30
3.358	6296.4	0.02	-10.50
3.359	6297.4	-0.08	-10.33
3.36	6298.4	0.23	-10.07
3.361	6299.5	0.21	-10.44
3.362	6300.5	0.24	-10.33
3.363	6301.5	-0.26	-9.96
3.364	6302.6	-0.23	-9.93
3.365	6303.6	-0.52	-10.03
3.366	6304.6	0.00	-9.95
3.367	6305.7	-0.06	-10.05
3.368	6306.7	0.15	-10.04
3.369	6307.7	-0.34	-9.75
3.37	6308.8	-0.01	-9.83
3.371	6309.8	-0.17	-9.92
3.372	6310.8	-0.45	-10.14
3.373	6311.9	-0.33	-9.85
3.374	6312.9	-0.06	-10.22
3.375	6313.9	-0.28	-9.88
3.376	6315.0	-0.26	-9.88
3.377	6316.0	-0.39	-9.95
3.378	6317.0	-0.26	-9.67
3.379	6318.1	0.02	-9.96
3.38	6319.1	-0.24	-9.77
3.381	6320.1	-0.39	-9.85
3.382	6321.1	-0.41	-9.69
3.383	6322.2	-0.14	-9.91

Depth	Age	$\delta^{13}C$	$\delta^{18}O$
cm	yr BP	VPDB	VPDB
3.384	6323.2	-0.42	-9.80
3.385	6324.2	-0.03	-9.75
3.385	6324.2	-0.03	-9.75
3.386	6325.3	-0.09	-9.71
3.386	6325.3	-0.09	-9.71
3.387	6326.3	-0.33	-9.69
3.388	6327.3	-0.15	-9.70
3.389	6328.4	-0.02	-9.59
3.39	6329.4	-0.34	-9.89
3.391	6330.4	-0.13	-9.64
3.392	6331.5	-0.32	-9.76
3.393	6332.5	-0.13	-9.73
3.394	6333.5	0.45	-9.84
3.395	6334.6	0.76	-10.17
3.396	6335.6	0.06	-10.06
3.397	6336.6	0.06	-9.75
3.398	6337.7	-0.06	-9.52
3.399	6338.7	-0.21	-9.65
3.4	6339.7	-0.19	-9.72
3.401	6340.8	-0.03	-9.69
3.402	6341.8	0.30	-9.44
3.403	6342.8	0.69	-9.81
3.404	6343.8	0.17	-9.82
3.405	6344.9	-0.17	-9.45
3.406	6345.9	0.04	-9.48
3.407	6346.9	0.61	-9.35
3.408	6348.0	0.43	-9.52
3.409	6349.0	0.40	-9.57
3.41	6350.0	0.64	-9.83
3.411	6351.1	0.61	-9.49
3.412	6352.1	0.34	-9.35
3.413	6353.1	0.41	-9.44
3.415	6355.2	0.69	-9.50
3.416	6356.2	0.46	-9.25
3.417	6357.3	-0.06	-9.25
3.418	6358.3	0.10	-9.18
3.419	6359.3	0.94	-9.53
3.42	6360.4	0.32	-9.30
3.421	6361.4	0.31	-9.46

Depth	Age	$\delta^{13}C$	$\delta^{18}O$
cm	yr BP	VPDB	VPDB
3.422	6362.4	0.46	-9.09
3.423	6363.5	0.38	-9.27
3.424	6364.5	0.53	-9.34
3.425	6365.5	0.35	-9.20
3.426	6366.5	0.14	-9.20
3.427	6367.6	0.58	-9.27
3.428	6368.6	0.24	-9.28
3.429	6369.6	0.25	-9.02
3.43	6370.7	0.34	-9.22
3.431	6371.7	0.21	-9.38
3.432	6372.7	0.29	-9.22
3.433	6373.8	-0.16	-8.91
3.434	6374.8	0.31	-9.21
3.435	6375.8	0.10	-9.29
3.436	6376.9	0.20	-9.09
3.437	6377.9	0.00	-9.45
3.438	6378.9	0.41	-9.26
3.439	6380.0	-0.23	-9.39
3.44	6381.0	0.41	-9.40
3.441	6382.0	0.17	-9.16
3.442	6383.1	-0.43	-9.83
3.443	6384.1	0.20	-9.37
3.444	6385.1	0.36	-9.20
3.445	6386.2	0.20	-9.23
3.446	6387.2	0.31	-9.16
3.447	6388.2	0.25	-9.07
3.448	6389.2	0.38	-9.27
3.449	6390.3	0.17	-9.38
3.45	6391.3	0.53	-9.02
3.451	6392.3	0.27	-9.33
3.452	6393.4	0.45	-9.02
3.453	6394.4	0.59	-8.85
3.454	6395.4	0.30	-9.08
3.455	6396.5	0.04	-9.16
3.456	6397.5	0.16	-9.44
3.457	6398.5	0.11	-9.48
3.458	6399.6	0.25	-9.69
3.459	6400.6	-0.34	-9.73
3.46	6401.6	0.12	-9.71

Depth	Age	$\delta^{13}C$	$\delta^{18}O$
cm	yr BP	VPDB	VPDB
3.461	6402.7	-0.13	-9.84
3.462	6403.7	0.12	-9.84
3.463	6404.7	-0.48	-10.19
3.464	6405.8	-0.26	-10.54
3.465	6406.8	-0.64	-10.30
3.466	6407.8	-0.48	-10.31
3.467	6408.9	-0.75	-10.18
3.468	6409.9	-0.47	-10.31
3.469	6410.9	-0.38	-10.10
3.47	6411.9	-1.53	-9.37
3.471	6413.0	-0.26	-9.99
3.472	6414.0	-0.40	-10.13
3.473	6415.0	-0.42	-10.16
3.474	6416.1	-0.30	-10.18
3.475	6417.1	-0.61	-10.03
3.476	6418.1	-0.58	-10.21
3.477	6419.2	-0.15	-10.04
3.478	6420.2	-0.43	-10.14
3.479	6421.2	-0.13	-10.32
3.48	6422.3	-0.33	-10.45
3.481	6423.3	-0.26	-10.13
3.482	6424.3	-0.11	-10.31
3.483	6425.4	-0.40	-10.27
3.484	6426.4	-0.41	-10.37
3.485	6427.4	-0.12	-10.41
3.486	6428.5	-0.42	-10.45
3.487	6429.5	-0.21	-10.27
3.488	6430.5	-0.32	-10.35
3.489	6431.6	-0.35	-10.24
3.49	6432.6	-0.14	-10.24
3.491	6433.6	-0.03	-10.38
3.492	6434.6	-0.53	-10.55
3.493	6435.7	-0.46	-10.44
3.494	6436.7	-0.38	-10.41
3.495	6437.7	-0.57	-10.95
3.496	6438.8	-0.87	-10.86
3.497	6439.8	-0.83	-10.63
3.498	6440.8	-0.97	-10.74
3.499	6441.9	-0.73	-10.85

Depth	Age	$\delta^{13}C$	$\delta^{18}O$
cm	yr BP	VPDB	VPDB
3.5	6442.9	-0.93	-10.68
3.501	6443.9	-0.76	-10.64
3.502	6445.0	-0.93	-10.86
3.503	6446.0	-0.77	-10.77
3.504	6447.0	-0.87	-10.73
3.505	6448.1	-0.74	-10.84
3.506	6449.1	-1.04	-10.85
3.507	6450.1	-0.58	-10.81
3.508	6451.2	-0.68	-11.18
3.509	6452.2	-0.95	-11.01
3.51	6453.2	-0.67	-11.00
3.511	6454.2	-0.56	-11.06
3.512	6455.3	-1.33	-10.64
3.513	6456.3	-0.93	-10.80
3.514	6457.3	-0.87	-10.98
3.515	6458.4	-0.85	-10.92
3.516	6459.4	-0.79	-10.77
3.517	6460.4	-1.22	-10.78
3.518	6461.5	-1.22	-10.91
3.519	6462.5	-1.16	-10.85
3.52	6463.5	-0.75	-10.74
3.522	6465.6	-1.02	-11.09
3.523	6466.6	-1.27	-10.73
3.524	6467.7	-1.07	-11.12
3.525	6468.7	-1.22	-10.80
3.526	6469.7	-0.98	-11.09
3.527	6470.8	-1.12	-10.82
3.528	6471.8	-1.50	-10.95
3.529	6472.8	-1.24	-11.03
3.53	6473.9	-1.08	-10.99
3.531	6474.9	-1.11	-10.91
3.532	6475.9	-1.48	-11.10
3.533	6476.9	-1.21	-10.98
3.534	6478.0	-1.26	-11.17
3.535	6479.0	-1.18	-11.11
3.536	6480.0	-1.23	-11.03
3.537	6481.1	-1.39	-11.41
3.538	6482.1	-1.44	-11.49
3.539	6483.1	-1.32	-10.94

Depth	Age	$\delta^{13}C$	$\delta^{18}O$
cm	yr BP	VPDB	VPDB
3.54	6484.2	-1.61	-11.43
3.541	6485.2	-1.10	-11.01
3.542	6486.2	-0.81	-10.50
3.543	6487.3	-0.51	-10.09
3.544	6488.3	-0.53	-10.53
3.545	6489.3	-0.64	-10.66
3.546	6490.4	-1.02	-10.62
3.547	6491.4	-0.77	-10.51
3.548	6492.4	-0.51	-10.44
3.549	6493.5	-0.74	-10.48
3.55	6494.5	-0.98	-10.57
3.551	6495.5	-0.86	-10.11
3.553	6497.6	-1.36	-9.89
3.553	6497.6	-0.84	-9.88
3.554	6498.6	-0.08	-9.93
3.555	6499.6	-0.25	-10.04
3.556	6500.7	-0.65	-10.24
3.557	6501.7	-0.98	-10.16
3.558	6502.7	-0.86	-10.20
3.559	6503.8	-0.94	-10.20
3.56	6504.8	-0.63	-10.40
3.561	6505.8	-0.86	-9.71
3.562	6506.9	-0.35	-9.96
3.563	6507.9	-0.69	-9.73
3.564	6508.9	-0.70	-10.26
3.565	6510.0	-0.24	-10.06
3.566	6511.0	-0.89	-10.01
3.567	6512.0	-0.51	-9.81
3.568	6513.1	-0.14	-9.97
3.569	6514.1	-0.31	-10.34
3.57	6515.1	-0.05	-9.92
3.571	6516.2	0.08	-9.92
3.572	6517.2	-0.13	-9.95
3.573	6518.2	-0.16	-10.00
3.574	6519.3	0.12	-10.10
3.575	6520.3	-0.06	-10.23
3.576	6521.3	-0.07	-10.27
3.577	6522.3	-0.28	-10.22
3.578	6523.4	0.28	-10.20

Depth	Age	$\delta^{13}C$	$\delta^{18}O$
cm	yr BP	VPDB	VPDB
3.579	6524.4	-0.14	-10.32
3.58	6525.4	-0.05	-10.24
3.581	6526.5	0.06	-10.37
3.582	6527.5	-0.20	-9.93
3.583	6528.5	-0.19	-10.08
3.584	6529.6	0.00	-10.30
3.585	6530.6	-0.22	-9.96
3.586	6531.6	-0.05	-10.36
3.587	6532.7	-0.21	-10.31
3.588	6533.7	0.22	-10.28
3.589	6534.7	-0.13	-9.89
3.59	6535.8	-0.36	-10.21
3.591	6536.8	-0.26	-10.12
3.592	6537.8	-0.40	-10.28
3.593	6538.9	-0.10	-10.36
3.594	6539.9	-0.52	-9.95
3.595	6540.9	0.00	-10.07
3.596	6542.0	-2.43	-11.34
3.597	6543.0	-0.22	-10.27
3.598	6544.0	-0.51	-10.11
3.599	6545.0	0.11	-10.24
3.6	6546.1	-0.48	-10.33
3.601	6547.1	-0.07	-10.22
3.602	6548.1	-0.25	-10.03
3.603	6549.2	-0.41	-10.29
3.604	6550.2	0.00	-10.28
3.605	6551.2	-0.09	-10.11
3.606	6552.3	-1.08	-10.39
3.607	6553.3	-0.20	-10.06
3.608	6554.3	0.08	-10.17
3.609	6555.4	0.14	-10.05
3.61	6556.4	-0.05	-9.91
3.611	6557.4	-0.09	-9.79
3.612	6558.5	0.34	-9.80
3.613	6559.5	0.21	-9.86
3.614	6560.5	0.05	-9.83
3.615	6561.6	0.68	-9.86
3.616	6562.6	0.12	-9.55
3.617	6563.6	0.43	-9.76

Depth	Age	$\delta^{13}C$	$\delta^{18}O$
cm	yr BP	VPDB	VPDB
3.618	6564.7	0.31	-9.83
3.619	6565.7	0.58	-9.92
3.62	6566.7	0.18	-9.67
3.621	6567.7	0.13	-9.54
3.622	6568.8	0.47	-9.61
3.623	6569.8	0.26	-9.69
3.624	6570.8	0.48	-9.54
3.625	6571.9	0.65	-9.62
3.626	6572.9	0.42	-9.31
3.627	6573.9	0.42	-9.51
3.628	6575.0	0.59	-9.47
3.629	6576.0	0.23	-9.54
3.63	6577.0	0.07	-9.38
3.631	6578.1	0.03	-9.33
3.632	6579.1	-0.02	-9.50
3.633	6580.1	0.04	-9.53
3.634	6581.2	0.30	-9.28
3.635	6582.2	0.21	-9.08
3.636	6583.2	0.72	-9.17
3.637	6584.3	0.73	-9.30
3.638	6585.3	0.88	-9.97
3.639	6586.3	1.07	-9.36
3.64	6587.4	0.48	-9.00
3.641	6588.4	0.35	-9.18
3.644	6591.5	0.44	-8.79
3.645	6592.5	0.53	-9.02
3.646	6593.5	0.42	-9.03
3.647	6594.6	0.36	-9.05
3.648	6595.6	0.50	-9.24
3.649	6596.6	0.32	-9.24
3.65	6597.7	0.27	-9.64
3.651	6598.7	0.26	-9.25
3.652	6599.7	0.42	-9.34
3.654	6601.8	0.28	-8.72
3.655	6602.8	-0.21	-8.89
3.656	6603.9	0.64	-8.23
3.657	6604.9	0.31	-9.23
3.658	6605.9	0.43	-8.89
3.659	6607.0	0.37	-8.92

Depth	Age	$\delta^{13}C$	$\delta^{18}O$
cm	yr BP	VPDB	VPDB
3.66	6608.0	0.71	-8.71
3.661	6609.0	0.66	-8.59
3.662	6610.1	0.59	-8.62
3.663	6611.1	0.62	-8.73
3.664	6612.1	0.45	-8.78
3.665	6613.1	0.47	-8.86
3.666	6614.2	0.37	-8.61
3.667	6615.2	0.38	-8.62
3.668	6616.2	0.16	-9.34
3.669	6617.3	0.52	-9.08
3.67	6618.3	0.69	-9.12
3.671	6619.3	0.46	-9.28
3.672	6620.4	0.18	-9.09
3.673	6621.4	0.78	-8.80
3.674	6622.4	0.08	-9.31
3.675	6623.5	0.48	-9.29
3.676	6624.5	0.55	-9.12
3.677	6625.5	0.67	-9.09
3.678	6626.6	0.48	-8.99
3.679	6627.6	0.55	-9.42
3.681	6629.7	0.49	-9.01
3.682	6630.7	0.23	-9.10
3.683	6631.7	0.57	-8.93
3.684	6632.8	0.59	-9.21
3.685	6633.8	0.61	-9.03
3.686	6634.8	0.73	-9.22
3.687	6635.8	0.70	-9.26
3.688	6636.9	0.54	-9.19
3.689	6637.9	0.79	-9.25
3.69	6638.9	0.59	-9.03
3.691	6640.0	0.67	-9.04
3.692	6641.0	0.88	-9.17
3.693	6642.0	0.26	-9.01
3.694	6643.1	0.33	-9.12
3.695	6644.1	0.50	-9.00
3.696	6645.1	0.68	-9.00
3.697	6646.2	0.82	-9.02
3.698	6647.2	0.24	-9.07
3.699	6648.2	0.45	-9.12

Depth	Age	$\delta^{13}C$	$\delta^{18}O$
cm	yr BP	VPDB	VPDB
3.7	6649.3	0.54	-9.10
3.701	6650.3	0.80	-9.21
3.702	6651.3	0.67	-9.04
3.703	6652.4	0.59	-9.10
3.704	6653.4	0.83	-9.25
3.705	6654.4	0.70	-9.15
3.706	6655.5	0.85	-9.17
3.707	6656.5	0.78	-9.12
3.708	6657.5	1.12	-9.08
3.709	6658.5	0.78	-9.00
3.71	6659.6	1.04	-9.21
3.711	6660.6	0.76	-9.19
3.712	6661.6	0.50	-9.07
3.713	6662.7	0.63	-9.11
3.714	6663.7	0.62	-9.21
3.715	6664.7	0.78	-9.33
3.716	6665.8	0.14	-9.42
3.717	6666.8	0.26	-8.89
3.718	6667.8	0.49	-8.81
3.719	6668.9	0.75	-9.08
3.72	6669.9	0.42	-8.99
3.721	6670.9	0.63	-9.03
3.722	6672.0	0.48	-8.80
3.723	6673.0	0.89	-9.00
3.724	6674.0	0.17	-8.74
3.725	6675.1	0.30	-8.99
3.726	6676.1	0.29	-8.72
3.727	6677.1	0.51	-9.10
3.728	6678.2	0.32	-8.74
3.729	6679.2	0.52	-8.76
3.73	6680.2	0.45	-8.72
3.731	6681.2	0.35	-9.00
3.732	6682.3	0.34	-9.08
3.733	6683.3	0.17	-9.05
3.734	6684.3	0.60	-9.19
3.735	6685.4	0.45	-8.91
3.736	6686.4	0.38	-9.12
3.737	6687.4	0.31	-8.96
3.738	6688.5	0.64	-8.88

Depth	Age	$\delta^{13}C$	$\delta^{18}O$
cm	yr BP	VPDB	VPDB
3.739	6689.5	-2.47	-7.60
3.741	6691.6	0.45	-9.04
3.742	6692.6	0.23	-8.67
3.743	6693.6	0.56	-9.21
3.744	6694.7	0.30	-8.76
3.745	6695.7	-0.12	-9.53
3.746	6696.7	-0.52	-10.03
3.747	6697.8	-0.51	-10.23
3.748	6698.8	-0.59	-10.48
3.749	6699.8	-0.77	-10.04
3.75	6700.9	-0.52	-10.37
3.752	6702.9	-0.44	-10.20
3.753	6703.9	-0.18	-10.20
3.754	6705.0	-0.59	-10.64
3.755	6706.0	-0.95	-11.15
3.756	6707.0	-0.83	-10.58
3.757	6708.1	-0.96	-10.58
3.758	6709.1	-1.08	-10.78
3.759	6710.1	-1.07	-10.64
3.76	6711.2	-0.93	-10.84
3.761	6712.2	-0.95	-10.72
3.762	6713.2	-0.88	-10.81
3.763	6714.3	-0.86	-10.67
3.764	6715.3	-0.57	-10.72
3.765	6716.3	-0.85	-10.84
3.766	6717.4	-0.81	-10.85
3.767	6718.4	-0.67	-11.00
3.768	6719.4	-0.86	-11.00
3.769	6720.5	-0.80	-10.64
3.77	6721.5	-1.09	-11.27
3.771	6722.5	-0.99	-10.97
3.772	6723.5	-0.83	-11.18
3.773	6724.6	-0.82	-11.19
3.774	6725.6	-1.18	-11.33
3.775	6726.6	-1.01	-11.12
3.776	6727.7	-0.95	-11.16
3.777	6728.7	-2.83	-10.32
3.778	6729.7	-0.70	-10.80
3.779	6730.8	-0.63	-10.76

Depth	Age	$\delta^{13}C$	$\delta^{18}O$
cm	yr BP	VPDB	VPDB
3.78	6731.8	-0.72	-10.67
3.781	6732.8	-0.67	-10.71
3.782	6733.9	-0.81	-10.66
3.783	6734.9	-0.65	-10.83
3.784	6735.9	-0.89	-10.62
3.785	6737.0	-0.62	-10.62
3.786	6738.0	-0.58	-10.73
3.787	6739.0	-0.62	-10.84
3.788	6740.1	-1.09	-10.80
3.789	6741.1	-1.52	-10.57
3.79	6742.1	-0.82	-10.77
3.791	6743.2	-0.97	-10.64
3.792	6744.2	-1.31	-10.79
3.793	6745.2	-0.89	-11.27
3.794	6746.2	-1.32	-11.04
3.795	6747.3	-1.05	-10.54
3.796	6748.3	-1.34	-10.80
3.797	6749.3	-1.32	-11.04
3.798	6750.4	-2.32	-11.66
3.799	6751.4	-1.73	-10.67
3.8	6752.4	-1.13	-10.49
3.801	6753.5	-0.54	-10.08
3.802	6754.5	-0.39	-10.43
3.803	6755.5	-0.80	-10.36
3.804	6756.6	-0.70	-10.31
3.805	6757.6	-0.52	-10.21
3.806	6758.6	-0.70	-10.47
3.807	6759.7	-0.51	-10.13
3.808	6760.7	-0.49	-10.14
3.809	6761.7	-0.66	-10.21
3.81	6762.8	-0.42	-10.09
3.811	6763.8	-0.61	-10.67
3.812	6764.8	-0.59	-9.76
3.814	6766.9	-0.70	-10.24
3.815	6767.9	-0.56	-9.63
3.816	6768.9	-0.36	-9.55
3.817	6770.0	-1.47	-9.42
3.818	6771.0	-0.59	-9.69
3.819	6772.0	-2.30	-9.96

Depth	Age	$\delta^{13}C$	$\delta^{18}O$
cm	yr BP	VPDB	VPDB
3.82	6773.1	-0.76	-9.75
3.821	6774.1	-0.09	-9.91
3.822	6775.1	-0.34	-9.93
3.823	6776.2	0.05	-9.28
3.824	6777.2	-0.09	-9.56
3.825	6778.2	-0.29	-10.06
3.826	6779.3	-0.44	-9.68
3.827	6780.3	0.41	-9.27
3.828	6781.3	0.47	-8.59
3.829	6782.4	0.39	-8.90
3.83	6783.4	0.26	-9.07
3.831	6784.4	-0.08	-9.54
3.833	6786.5	0.31	-9.45
3.834	6787.5	0.03	-9.42
3.835	6788.6	0.28	-9.26
3.836	6789.6	0.37	-9.40
3.837	6790.6	0.06	-9.53
3.838	6791.6	0.09	-9.48
3.839	6792.7	0.28	-9.48
3.84	6793.7	0.37	-9.29
3.841	6794.7	0.25	-9.25
3.842	6795.8	0.45	-9.48
3.843	6796.8	0.43	-9.35
3.844	6797.8	0.50	-9.67
3.845	6798.9	0.31	-9.23
3.846	6799.9	0.36	-9.36
3.847	6800.9	-0.09	-9.59
3.848	6802.0	0.25	-8.99
3.85	6804.0	0.09	-9.33
3.851	6805.1	0.21	-9.30
3.852	6806.1	0.28	-9.23
3.853	6807.1	0.43	-9.00
3.854	6808.2	0.25	-8.89
3.855	6809.2	0.36	-8.94
3.856	6810.2	0.23	-9.22
3.857	6811.3	0.39	-8.74
3.858	6812.3	0.50	-8.74
3.861	6815.4	0.31	-9.22
3.862	6816.4	0.32	-8.99

Depth	Age	$\delta^{13}C$	$\delta^{18}O$
cm	yr BP	VPDB	VPDB
3.863	6817.4	0.44	-9.16
3.865	6819.5	0.27	-9.20
3.866	6820.5	0.54	-9.59
3.868	6822.6	0.76	-8.92
3.869	6823.6	0.69	-8.79
3.872	6826.7	0.58	-9.05
3.873	6827.8	0.42	-8.98
3.874	6828.8	0.43	-8.76
3.875	6829.8	0.35	-8.86
3.877	6831.9	0.54	-9.09
3.878	6832.9	0.35	-8.81
3.879	6834.0	0.14	-8.92
3.88	6835.0	0.85	-9.16
3.881	6836.0	0.07	-8.58
3.882	6837.0	0.68	-9.13
3.883	6838.1	0.39	-8.89
3.885	6840.1	0.86	-9.00
3.886	6841.2	0.39	-8.75
3.888	6843.2	0.58	-9.06
3.889	6844.3	0.59	-8.82
3.89	6845.3	0.81	-8.38
3.891	6846.3	0.82	-8.57
3.892	6847.4	0.90	-8.58
3.893	6848.4	0.69	-8.70
3.894	6849.4	0.99	-8.94
3.895	6850.5	0.78	-8.66
3.896	6851.5	0.76	-8.78
3.897	6852.5	1.01	-8.62
3.898	6853.6	0.91	-8.61
3.899	6854.6	0.77	-8.38
3.9	6855.6	0.91	-8.31
3.901	6856.7	0.91	-8.43
3.902	6857.7	0.62	-8.63
3.903	6858.7	0.85	-8.47
3.904	6859.7	0.55	-8.50
3.905	6860.8	0.77	-8.64
3.906	6861.8	1.06	-8.63
3.907	6862.8	1.10	-8.58
3.91	6865.9	0.31	-8.55

Depth	Age	$\delta^{13}C$	$\delta^{18}O$
cm	yr BP	VPDB	VPDB
3.911	6867.0	0.93	-8.43
3.912	6868.0	-0.35	-7.06
3.913	6869.0	0.97	-8.56
3.914	6870.1	1.11	-8.37
3.915	6871.1	0.92	-8.40
3.916	6872.1	0.86	-8.36
3.922	6878.3	0.28	-8.37
3.927	6883.5	-1.94	-11.10
3.928	6884.5	-1.05	-10.65
3.947	6904.1	0.17	-8.75
3.947	6904.1	0.17	-8.75
3.948	6905.1	0.05	-8.88
3.949	6906.2	-0.02	-8.66
3.95	6907.2	0.30	-8.84
3.951	6908.2	0.17	-8.94
3.952	6909.3	0.14	-8.86
3.953	6910.3	-0.05	-8.88
3.954	6911.3	0.17	-8.93
3.955	6912.4	0.15	-8.96
3.956	6913.4	0.14	-8.87
3.957	6914.4	0.13	-8.98
3.958	6915.5	0.09	-9.30
3.959	6916.5	0.33	-8.96
3.96	6917.5	0.24	-9.05
3.961	6918.6	0.32	-9.13
3.962	6919.6	0.32	-9.04
3.963	6920.6	0.14	-9.06
3.964	6921.7	-0.07	-9.22
3.965	6922.7	-1.38	-8.99
3.966	6923.7	0.05	-9.28
3.967	6924.8	0.08	-9.04
3.968	6925.8	-0.04	-9.00
3.969	6926.8	-0.02	-9.17
3.97	6927.8	0.00	-9.15
3.971	6928.9	0.31	-9.07
3.972	6929.9	0.03	-9.00
3.973	6930.9	0.09	-9.16
3.974	6932.0	0.06	-9.29
3.975	6933.0	-0.04	-8.88

Depth	Age	$\delta^{13}C$	$\delta^{18}O$
cm	yr BP	VPDB	VPDB
3.976	6934.0	0.10	-9.38
3.977	6935.1	-0.02	-9.33
3.978	6936.1	0.39	-9.19
3.979	6937.1	-0.05	-9.44
3.98	6938.2	-0.01	-9.23
3.981	6939.2	-0.03	-9.41
3.982	6940.2	0.04	-9.42
3.983	6941.3	0.07	-9.31
3.984	6942.3	-0.03	-9.38
3.985	6943.3	0.04	-9.31
3.986	6944.4	-0.14	-9.28
3.987	6945.4	0.23	-9.27
3.988	6946.4	-0.11	-9.36
3.989	6947.5	0.07	-9.24
3.99	6948.5	-0.07	-9.33
3.991	6949.5	-0.25	-9.43
3.992	6950.5	-0.05	-9.41
3.993	6951.6	0.07	-9.48
3.994	6952.6	0.01	-9.49
3.995	6953.6	-0.08	-9.32
3.996	6954.7	-0.14	-8.72
3.997	6955.7	-0.27	-9.32
3.998	6956.7	-0.29	-9.47
3.999	6957.8	-0.09	-9.46
4	6958.8	-0.24	-9.15
4.001	6959.8	-0.34	-9.41
4.002	6960.9	-0.18	-9.46
4.003	6961.9	-0.07	-9.47
4.004	6962.9	-0.30	-9.45
4.005	6964.0	-0.24	-9.37
4.006	6965.0	-0.44	-9.56
4.007	6966.0	-0.34	-9.42
4.008	6967.1	-0.38	-9.59
4.009	6968.1	-0.64	-9.22
4.01	6969.1	-0.31	-9.28
4.011	6970.1	-0.33	-8.84
4.012	6971.2	-0.02	-8.78
4.013	6972.2	-0.12	-8.65
4.014	6973.2	-0.18	-9.06

Depth	Age	$\delta^{13}C$	$\delta^{18}O$
cm	yr BP	VPDB	VPDB
4.015	6974.3	-0.06	-9.12
4.016	6975.3	-0.47	-8.90
4.017	6976.3	0.16	-8.99
4.018	6977.4	-0.22	-8.56
4.019	6978.4	-0.01	-9.00
4.02	6979.4	-0.07	-8.97
4.021	6980.5	-0.17	-8.64
4.022	6981.5	-1.22	-8.52
4.023	6982.5	0.26	-8.26
4.024	6983.6	0.51	-8.05
4.025	6984.6	0.65	-8.26
4.026	6985.6	0.51	-8.36
4.027	6986.7	-0.40	-8.01
4.028	6987.7	0.13	-8.49
4.029	6988.7	0.40	-8.35
4.03	6989.8	0.01	-8.27
4.031	6990.8	0.40	-8.39
4.032	6991.8	0.11	-8.16
4.033	6992.8	0.11	-8.51
4.034	6993.9	0.00	-8.61
4.035	6994.9	0.02	-8.68
4.036	6995.9	0.02	-8.59
4.037	6997.0	-0.02	-8.20
4.038	6998.0	0.59	-8.59
4.039	6999.0	0.25	-8.48
4.04	7000.1	0.09	-8.58
4.041	7001.1	0.11	-8.72
4.042	7002.1	0.40	-9.07
4.043	7003.2	0.40	-8.69
4.044	7004.2	0.37	-8.65
4.045	7005.2	-0.01	-8.91
4.046	7006.3	0.30	-8.67
4.047	7007.3	0.13	-9.14
4.048	7008.3	0.28	-8.37
4.049	7009.4	0.11	-8.54
4.05	7010.4	0.83	-8.93
4.051	7011.4	0.21	-8.72
4.052	7012.5	-0.44	-9.01
4.053	7013.5	-0.11	-9.04

Depth	Age	$\delta^{13}C$	$\delta^{18}O$
cm	yr BP	VPDB	VPDB
4.054	7014.5	-0.05	-9.04
4.055	7015.5	-0.27	-8.99
4.056	7016.6	-0.01	-9.04
4.057	7017.6	0.02	-8.76
4.058	7018.6	-0.05	-8.86
4.059	7019.7	-0.05	-8.85
4.06	7020.7	-0.10	-8.76
4.061	7021.7	-0.13	-8.91
4.062	7022.8	-0.08	-8.89
4.063	7023.8	-0.08	-8.96
4.064	7024.8	-0.15	-9.04
4.065	7025.9	0.02	-8.88
4.066	7026.9	0.11	-8.83
4.067	7027.9	-0.04	-8.82
4.068	7029.0	-0.08	-8.70
4.069	7030.0	-0.08	-8.82
4.07	7031.0	-0.04	-8.89
4.071	7032.1	-0.03	-9.37
4.072	7033.1	-0.14	-8.80
4.073	7034.1	-0.08	-8.71
4.074	7035.2	-0.28	-8.65
4.075	7036.2	-0.13	-8.95
4.076	7037.2	-0.19	-8.76
4.077	7038.2	-0.55	-8.89
4.078	7039.3	-0.55	-8.80
4.079	7040.3	-0.51	-9.24
4.08	7041.3	0.01	-8.66
4.081	7042.4	0.15	-8.89
4.082	7043.4	-0.82	-8.47
4.083	7044.4	0.42	-8.84
4.084	7045.5	0.15	-8.78
4.085	7046.5	0.07	-8.83
4.086	7047.5	0.24	-8.78
4.087	7048.6	-0.01	-9.01
4.088	7049.6	0.15	-9.06
4.089	7050.6	0.13	-8.87
4.09	7051.7	0.40	-8.56
4.091	7052.7	0.12	-8.95
4.092	7053.7	0.22	-9.02

Depth	Age	$\delta^{13}C$	$\delta^{18}O$
cm	yr BP	VPDB	VPDB
4.093	7054.8	-0.12	-8.89
4.094	7055.8	0.27	-9.21
4.095	7056.8	0.02	-8.94
4.096	7057.9	0.52	-8.97
4.097	7058.9	0.03	-8.93
4.098	7059.9	0.10	-8.79
4.099	7060.9	0.32	-8.56
4.1	7062.0	-0.16	-9.09
4.101	7063.0	0.04	-9.19
4.102	7064.0	-0.30	-8.51
4.103	7065.1	0.18	-8.56
4.104	7066.1	0.27	-8.74
4.105	7067.1	0.09	-8.80
4.106	7068.2	0.12	-8.75
4.107	7069.2	0.03	-8.82
4.108	7070.2	-0.04	-8.99
4.109	7071.3	-0.05	-9.02
4.11	7072.3	-0.01	-8.83
4.111	7073.3	-0.05	-8.99
4.112	7074.4	-0.07	-8.99
4.113	7075.4	-0.04	-8.92
4.114	7076.4	-0.13	-9.04
4.115	7077.5	-0.12	-8.88
4.116	7078.5	-0.07	-9.00
4.117	7079.5	-0.19	-9.08
4.118	7080.6	-0.22	-8.99
4.119	7081.6	-0.18	-9.17
4.12	7082.6	-0.05	-8.93
4.121	7083.6	-0.03	-9.35
4.122	7084.7	0.04	-9.22
4.123	7085.7	-0.14	-8.98
4.124	7086.7	0.06	-8.92
4.125	7087.8	-0.06	-8.93
4.126	7088.8	-0.16	-8.74
4.127	7089.8	-0.27	-9.05
4.128	7090.9	-0.63	-8.84
4.129	7091.9	-0.51	-8.78
4.13	7092.9	-0.33	-8.75
4.131	7094.0	-0.13	-8.96

Depth	Age	$\delta^{13}C$	$\delta^{18}O$
cm	yr BP	VPDB	VPDB
4.132	7095.0	-0.17	-8.90
4.133	7096.0	-0.15	-8.89
4.134	7097.1	-0.11	-8.79
4.135	7098.1	-0.30	-8.80
4.136	7099.1	-0.15	-8.78
4.137	7100.2	-0.31	-8.96
4.138	7101.2	-0.45	-8.87
4.139	7102.2	-0.43	-8.85
4.14	7103.3	-0.47	-8.83
4.141	7104.3	-0.50	-8.84
4.142	7105.3	-0.37	-8.94
4.143	7106.3	-0.80	-8.76
4.144	7107.4	-0.80	-8.35
4.145	7108.4	-0.80	-8.59
4.146	7109.4	-0.78	-8.30
4.147	7110.5	-0.92	-8.42
4.148	7111.5	-0.78	-8.43
4.149	7112.5	-1.45	-8.27
4.15	7113.6	-1.06	-8.51
4.151	7114.6	-1.10	-8.11
4.152	7115.6	-1.06	-7.95
4.153	7116.7	-1.15	-8.55
4.154	7117.7	-1.32	-7.92
4.155	7118.7	-1.42	-8.15
4.156	7119.8	-1.22	-7.79
4.157	7120.8	-1.43	-7.31
4.158	7121.8	-1.53	-7.09
4.159	7122.9	-1.31	-7.55
4.16	7123.9	-1.75	-6.92
4.161	7124.9	-1.33	-7.91
4.162	7126.0	-1.55	-7.25
4.163	7127.0	-1.37	-7.64
4.164	7128.0	-1.36	-8.08
4.165	7129.0	-1.39	-7.47
4.166	7130.1	-1.57	-7.02
4.167	7131.1	-1.67	-7.27
4.168	7132.1	-1.56	-7.99
4.169	7133.2	-1.62	-8.06
4.17	7134.2	-1.08	-8.45

Depth	Age	$\delta^{13}C$	$\delta^{18}O$
cm	yr BP	VPDB	VPDB
4.171	7135.2	-0.93	-9.04
4.172	7136.3	-1.19	-8.91
4.173	7137.3	-0.90	-9.00
4.174	7138.3	-0.90	-9.07
4.175	7139.4	-0.73	-8.93
4.176	7140.4	-1.24	-8.87
4.177	7141.4	-1.38	-7.99
4.178	7142.5	-2.53	-7.95
4.179	7143.5	-2.08	-7.97
4.18	7144.5	-2.25	-7.74
4.181	7145.6	-2.10	-7.15
4.182	7146.6	-2.22	-7.45
4.183	7147.6	-2.29	-8.61
4.184	7148.7	-2.95	-8.41
4.185	7149.7	-2.34	-8.72
4.186	7150.7	-2.31	-8.70
4.187	7151.7	-2.58	-8.60
4.188	7152.8	-2.71	-8.84
4.189	7153.8	-1.99	-9.03
4.19	7154.8	-2.09	-9.42
4.191	7155.9	-1.60	-8.95
4.192	7156.9	-0.60	-9.28
4.193	7157.9	-0.37	-9.10
4.194	7159.0	-0.39	-9.47
4.195	7160.0	-0.30	-9.13
4.196	7161.0	0.16	-9.06
4.197	7162.1	0.14	-9.14
4.198	7163.1	-0.05	-8.86
4.199	7164.1	-0.59	-8.95
4.2	7165.2	0.14	-8.85
4.201	7166.2	0.16	-8.68
4.202	7167.2	0.20	-8.62
4.203	7168.3	0.27	-8.57
4.204	7169.3	0.09	-8.95
4.205	7170.3	0.33	-8.73
4.206	7171.4	0.35	-8.80
4.207	7172.4	0.25	-8.83
4.208	7173.4	0.37	-8.73
4.209	7174.4	0.20	-8.67

Depth	Age	$\delta^{13}C$	$\delta^{18}O$
cm	yr BP	VPDB	VPDB
4.21	7175.5	0.16	-8.86
4.211	7176.5	0.31	-8.76
4.212	7177.5	0.35	-8.64
4.213	7178.6	0.28	-8.70
4.214	7179.6	0.14	-8.45
4.215	7180.6	0.16	-8.57
4.216	7181.7	0.23	-8.99
4.217	7182.7	0.11	-8.91
4.218	7183.7	0.25	-8.91
4.219	7184.8	0.19	-8.56
4.22	7185.8	-0.03	-8.91
4.223	7188.9	0.06	-8.84
4.224	7189.9	0.08	-8.70
4.225	7191.0	-0.02	-8.63
4.226	7192.0	-0.07	-8.75
4.228	7194.1	-0.05	-8.60
4.229	7195.1	-0.12	-8.73
4.23	7196.1	0.21	-8.88
4.231	7197.1	-0.02	-8.65
4.232	7198.2	0.03	-8.65
4.233	7199.2	-0.08	-8.77
4.234	7200.2	-0.02	-8.42
4.235	7201.3	0.01	-8.55
4.236	7202.3	-0.19	-8.60
4.237	7203.3	-0.14	-8.48
4.238	7204.4	-0.36	-8.70
4.24	7206.4	-0.11	-8.69
4.241	7207.5	-0.06	-8.93
4.242	7208.5	0.06	-8.50
4.243	7209.5	0.06	-8.77
4.244	7210.6	0.01	-8.85
4.245	7211.6	-0.17	-8.75
4.246	7212.6	0.03	-8.57
4.247	7213.7	-0.05	-8.63
4.248	7214.7	-0.25	-8.68
4.249	7215.7	-0.23	-8.62
4.25	7216.8	-0.24	-8.49
4.251	7217.8	-0.17	-8.68
4.252	7218.8	0.14	-8.91

Depth	Age	$\delta^{13}C$	$\delta^{18}O$
cm	yr BP	VPDB	VPDB
4.253	7219.8	0.37	-8.63
4.254	7220.9	0.05	-9.07
4.255	7221.9	0.07	-8.61
4.256	7222.9	0.18	-8.72
4.257	7224.0	0.01	-8.78
4.258	7225.0	-0.07	-8.92
4.259	7226.0	-0.03	-8.91
4.26	7227.1	0.11	-8.58
4.261	7228.1	0.04	-8.30
4.262	7229.1	0.01	-8.18
4.263	7230.2	0.03	-8.10
4.264	7231.2	-0.01	-8.12
4.265	7232.2	0.02	-8.15
4.266	7233.3	0.63	-7.45
4.267	7234.3	0.05	-8.10
4.268	7235.3	0.13	-8.00
4.269	7236.4	0.16	-7.99
4.27	7237.4	0.03	-7.69
4.271	7238.4	0.08	-7.96
4.272	7239.4	0.00	-8.05
4.273	7240.5	0.25	-7.95
4.274	7241.5	0.10	-7.85
4.275	7242.5	0.28	-7.71
4.276	7243.6	0.27	-7.92
4.277	7244.6	0.36	-7.97
4.278	7245.6	0.33	-7.96
4.279	7246.7	-0.17	-8.68
4.281	7248.7	0.24	-7.82
4.282	7249.8	0.23	-8.03
4.283	7250.8	0.17	-8.12
4.284	7251.8	-0.14	-8.09
4.285	7252.9	-0.05	-8.11
4.286	7253.9	-0.03	-8.15
4.287	7254.9	0.17	-8.10
4.288	7256.0	0.15	-8.04
4.289	7257.0	0.07	-8.10
4.29	7258.0	0.08	-7.98
4.291	7259.1	-0.01	-8.27
4.292	7260.1	0.03	-8.43

Depth	Age	$\delta^{13}C$	$\delta^{18}O$
cm	yr BP	VPDB	VPDB
4.293	7261.1	-0.30	-8.20
4.294	7262.1	-0.21	-8.24
4.295	7263.2	-0.11	-8.21
4.296	7264.2	0.08	-8.19
4.297	7265.2	-0.07	-8.00
4.298	7266.3	-0.01	-8.01
4.299	7267.3	-0.31	-7.02
4.3	7268.3	-0.34	-8.11
4.301	7269.4	0.05	-7.97
4.302	7270.4	-0.12	-8.17
4.303	7271.4	-0.18	-8.14
4.304	7272.5	-0.17	-8.17
4.305	7273.5	-0.16	-8.26
4.306	7274.5	-0.40	-8.13
4.307	7275.6	-0.21	-8.34
4.308	7276.6	-0.25	-8.37
4.309	7277.6	-0.14	-8.37
4.31	7278.7	-0.13	-7.84
4.311	7279.7	0.18	-8.15
4.312	7280.7	0.13	-8.24
4.313	7281.8	0.19	-8.33
4.314	7282.8	0.18	-8.30
4.315	7283.8	-0.02	-8.41
4.316	7284.8	-0.09	-8.54
4.317	7285.9	0.00	-8.50
4.318	7286.9	-0.11	-8.50
4.319	7287.9	-0.12	-8.33
4.32	7289.0	-0.06	-8.50
4.321	7290.0	0.05	-8.27
4.322	7291.0	-0.03	-8.38
4.323	7292.1	-0.21	-8.37
4.324	7293.1	-0.19	-8.27
4.325	7294.1	-0.20	-8.22
4.326	7295.2	-0.25	-8.31
4.327	7296.2	-0.04	-8.46
4.328	7297.2	-0.18	-8.39
4.329	7298.3	-0.16	-8.37
4.33	7299.3	-0.19	-8.58
4.331	7300.3	-0.24	-8.42

Depth	Age	$\delta^{13}C$	$\delta^{18}O$
cm	yr BP	VPDB	VPDB
4.332	7301.4	-0.03	-8.71
4.333	7302.4	-0.01	-8.76
4.334	7303.4	-0.75	-8.43
4.335	7304.5	-0.42	-8.30
4.337	7306.5	-0.19	-8.66
4.338	7307.5	-0.04	-9.07
4.339	7308.6	-0.11	-8.89
4.34	7309.6	-0.29	-8.73
4.341	7310.6	-0.29	-9.03
4.342	7311.7	-0.13	-8.99
4.343	7312.7	-0.19	-8.83
4.345	7314.8	-0.31	-8.89
4.346	7315.8	-0.27	-8.83
4.347	7316.8	-0.16	-8.80
4.348	7317.9	-0.16	-8.57
4.349	7318.9	-0.26	-8.59
4.356	7326.1	-0.47	-8.71
4.357	7327.2	-0.49	-8.76
4.358	7328.2	-0.42	-8.72
4.359	7329.2	-0.31	-8.95
4.36	7330.2	0.17	-9.97
4.36	7330.2	-0.37	-8.73
4.361	7331.3	-0.26	-8.78
4.362	7332.3	-0.34	-8.82
4.363	7333.3	-0.42	-8.91
4.364	7334.4	-0.42	-8.69
4.365	7335.4	-0.37	-8.87
4.366	7336.4	-0.16	-8.96
4.367	7337.5	-0.39	-8.91
4.369	7339.5	-0.33	-8.62
4.37	7340.6	-0.34	-8.81
4.371	7341.6	-0.24	-6.75
4.372	7342.6	-0.72	-7.40
4.373	7343.7	-0.85	-7.14
4.374	7344.7	-0.17	-8.92
4.375	7345.7	-0.28	-8.84
4.376	7346.8	-0.47	-8.97
4.377	7347.8	-0.44	-9.08
4.378	7348.8	-0.54	-8.97

Depth	Age	$\delta^{13}C$	$\delta^{18}O$
cm	yr BP	VPDB	VPDB
4.379	7349.9	-0.29	-9.01
4.38	7350.9	-0.49	-9.17
4.381	7351.9	-0.29	-9.05
4.382	7352.9	-0.42	-9.13
4.383	7354.0	-0.44	-8.96
4.384	7355.0	-0.35	-9.25
4.385	7356.0	-0.70	-9.13
4.386	7357.1	-0.39	-9.06
4.387	7358.1	-0.36	-8.91
4.388	7359.1	-0.49	-9.19
4.389	7360.2	-0.36	-8.70
4.39	7361.2	-0.37	-8.80
4.391	7362.2	-0.47	-9.11
4.392	7363.3	-0.40	-8.92
4.393	7364.3	-1.01	-8.92
4.394	7365.3	-0.69	-9.06
4.395	7366.4	-0.57	-9.20
4.396	7367.4	-0.36	-9.42
4.397	7368.4	-0.39	-9.36
4.398	7369.5	-0.41	-9.17
4.399	7370.5	-0.52	-8.87
4.4	7371.5	-0.40	-9.17
4.401	7372.6	-0.53	-9.00
4.402	7373.6	-0.39	-8.98
4.403	7374.6	-0.31	-8.72
4.404	7375.6	-0.25	-8.77
4.405	7376.7	-0.06	-8.75
4.406	7377.7	-0.12	-8.78
4.407	7378.7	0.00	-8.86
4.408	7379.8	-0.09	-8.95
4.409	7380.8	-0.13	-8.88
4.41	7381.8	0.03	-8.81
4.411	7382.9	-0.11	-8.88
4.412	7383.9	-0.02	-8.71
4.413	7384.9	-0.05	-8.73
4.413	7384.9	-0.19	-8.56
4.414	7386.0	0.09	-8.74
4.415	7387.0	-0.01	-8.65
4.416	7388.0	-0.09	-8.70

Depth	Age	$\delta^{13}C$	$\delta^{18}O$
cm	yr BP	VPDB	VPDB
4.417	7389.1	-0.17	-8.70
4.418	7390.1	-0.32	-8.50
4.419	7391.1	-0.16	-8.58
4.42	7392.2	0.00	-8.59
4.421	7393.2	-0.04	-8.76
4.422	7394.2	-0.26	-8.69
4.423	7395.3	-0.28	-8.66
4.424	7396.3	-0.23	-8.68
4.425	7397.3	-0.06	-8.82
4.426	7398.3	0.12	-8.62
4.427	7399.4	-0.21	-8.60
4.428	7400.4	-0.22	-8.78
4.429	7401.4	-0.19	-8.80
4.43	7402.5	-0.16	-8.86
4.431	7403.5	-0.22	-8.71
4.432	7404.5	-0.17	-8.76
4.433	7405.6	-0.16	-8.84
4.434	7406.6	-0.30	-8.81
4.435	7407.6	-0.58	-8.82
4.436	7408.7	-1.89	-8.56
4.437	7409.7	-0.26	-8.59
4.438	7410.7	-0.32	-8.61
4.439	7411.8	-0.20	-8.33
4.44	7412.8	-0.41	-8.80
4.441	7413.8	-0.22	-8.96
4.442	7414.9	-0.08	-9.09
4.443	7415.9	-0.42	-9.23
4.444	7416.9	-1.03	-9.47
4.445	7418.0	-0.62	-9.10
4.446	7419.0	-0.11	-9.39
4.447	7420.0	-0.19	-9.19
4.448	7421.0	-0.20	-8.98
4.449	7422.1	-0.40	-9.13
4.45	7423.1	-0.18	-9.06
4.451	7424.1	-0.27	-8.93
4.452	7425.2	-0.73	-9.25
4.453	7426.2	-0.69	-9.15
4.454	7427.2	-0.57	-9.45
4.455	7428.3	-0.36	-9.08
4.456	7429.3	-0.37	-9.11
4.457	7430.3	-0.25	-9.07
4.458	7431.4	-0.34	-9.29
4.459	7432.4	-0.27	-9.31
4.46	7433.4	-0.72	-9.43
4.461	7434.5	-0.28	-9.13
4.462	7435.5	-0.23	-9.33
4.463	7436.5	-0.34	-9.21
4.464	7437.6	-0.24	-9.48
4.465	7438.6	-0.42	-9.57
4.466	7439.6	-0.34	-9.49
4.467	7440.7	-1.10	-9.63
4.468	7441.7	-1.02	-9.29
4.469	7442.7	-0.93	-8.94
4.47	7443.7	-0.46	-9.01
4.471	7444.8	-0.52	-9.31
4.472	7445.8	-0.67	-9.05
4.473	7446.8	-0.67	-9.42
4.474	7447.9	-0.75	-8.71
4.475	7448.9	-0.58	-9.09
4.476	7449.9	-1.15	-9.55
4.477	7451.0	-0.57	-9.46
4.478	7452.0	-0.59	-9.36
4.479	7453.0	-0.70	-9.49
4.48	7454.1	-0.52	-9.67
4.481	7455.1	-0.94	-9.70
4.482	7456.1	-0.47	-9.23
4.483	7457.2	-1.50	-9.74
4.484	7458.2	-1.73	-9.60
4.485	7459.2	-1.61	-9.47
4.486	7460.3	-1.34	-9.42
4.487	7461.3	-1.34	-9.49
4.488	7462.3	-1.26	-9.51
4.489	7463.4	-1.35	-9.53
4.49	7464.4	-1.16	-9.62
4.491	7465.4	-1.86	-9.87
4.492	7466.4	-1.28	-9.30
4.493	7467.5	-1.08	-9.13
4.494	7468.5	-1.15	-9.80

Depth	Age	$\delta^{13}C$	$\delta^{18}O$
cm	yr BP	VPDB	VPDB
4.495	7469.5	-1.34	-8.93
4.496	7470.6	-1.08	-9.83
4.497	7471.6	-1.06	-9.24
4.498	7472.6	-0.92	-9.60
4.499	7473.7	-1.90	-9.83
4.5	7474.7	-1.24	-9.16
4.501	7475.7	-1.03	-9.76
4.503	7477.8	-1.40	-9.10
4.504	7478.8	-1.13	-9.12
4.505	7479.9	-1.20	-9.26
4.506	7480.9	-1.24	-9.20
4.507	7481.9	-0.96	-9.15
4.508	7483.0	-0.79	-8.96
4.51	7485.0	-1.06	-9.58
4.511	7486.0	-0.83	-9.13
4.512	7487.1	-1.14	-9.30
4.513	7488.1	-1.17	-9.27
4.514	7489.1	-1.01	-9.61
4.515	7490.2	-1.03	-8.96
4.516	7491.2	-1.15	-9.43
4.517	7492.2	-1.15	-9.36
4.518	7493.3	-1.18	-9.14
4.519	7494.3	-1.61	-8.78
4.52	7495.3	-1.53	-8.74
4.521	7496.4	-1.46	-8.60
4.522	7497.4	-1.72	-8.90
4.523	7498.4	-1.86	-8.85
4.524	7499.5	-1.87	-9.02
4.525	7500.5	-1.54	-8.58
4.526	7501.5	-1.88	-8.49
4.527	7502.6	-1.65	-8.84
4.528	7503.6	-2.00	-8.77
4.529	7504.6	-2.31	-8.79
4.53	7505.7	-1.84	-8.77
4.531	7506.7	-1.35	-8.70
4.532	7507.7	-1.79	-8.87
4.533	7508.7	-1.79	-8.87
4.534	7509.8	-1.75	-8.75
4.535	7510.8	-1.52	-8.91

Depth	Age	$\delta^{13}C$	$\delta^{18}O$
cm	yr BP	VPDB	VPDB
4.536	7511.8	-1.59	-8.73
4.537	7512.9	-0.76	-8.10
4.538	7513.9	-1.20	-8.37
4.539	7514.9	-0.97	-8.16
4.54	7516.0	-1.10	-7.99
4.541	7517.0	-0.61	-7.98
4.542	7518.0	-1.08	-8.39
4.543	7519.1	-0.95	-8.14
4.544	7520.1	-1.29	-8.20
4.545	7521.1	-1.15	-8.11
4.546	7522.2	-0.96	-7.61
4.547	7523.2	-0.77	-7.64
4.548	7524.2	-1.07	-8.27
4.549	7525.3	-0.49	-7.96
4.55	7526.3	-0.60	-7.97
4.551	7527.3	-0.75	-7.85
4.552	7528.4	-0.75	-8.15
4.553	7529.4	-0.76	-7.98
4.554	7530.4	-0.56	-8.17
4.555	7531.4	-0.62	-8.25
4.556	7532.5	-0.67	-8.42
4.557	7533.5	-0.61	-8.34
4.558	7534.5	-1.00	-8.91
4.559	7535.6	-0.73	-8.41
4.56	7536.6	-1.33	-8.82
4.561	7537.6	-1.18	-8.58
4.562	7538.7	-1.25	-8.29
4.563	7539.7	-1.11	-8.41
4.564	7540.7	-1.13	-8.53
4.565	7541.8	-1.36	-8.83
4.566	7542.8	-1.25	-8.79
4.567	7543.8	-1.34	-8.77
4.568	7544.9	-1.08	-8.53
4.569	7545.9	-1.58	-8.22
4.57	7546.9	-0.89	-8.37
4.571	7548.0	-1.06	-8.35
4.572	7549.0	-1.35	-8.62
4.573	7550.0	-1.27	-8.78
4.574	7551.1	-1.03	-8.94

Depth	Age	$\delta^{13}C$	$\delta^{18}O$
cm	yr BP	VPDB	VPDB
4.575	7552.1	-1.13	-8.72
4.576	7553.1	-1.19	-8.52
4.577	7554.1	-1.56	-8.26
4.578	7555.2	-1.78	-8.48
4.579	7556.2	-1.96	-8.25
4.58	7557.2	-2.24	-8.59
4.582	7559.3	-1.06	-8.15
4.583	7560.3	-2.23	-8.52
4.584	7561.4	-1.73	-7.46
4.585	7562.4	-1.51	-7.86
4.586	7563.4	-1.32	-8.59
4.587	7564.5	-0.91	-7.49
4.588	7565.5	-0.66	-7.90
4.589	7566.5	-1.78	-6.92
4.59	7567.6	-2.34	-8.04
4.592	7569.6	-1.66	-7.83
4.593	7570.7	-2.09	-8.86
4.594	7571.7	-1.80	-8.30
4.595	7572.7	-1.68	-8.69
4.596	7573.8	-2.22	-8.48
4.597	7574.8	-2.68	-9.08
4.598	7575.8	-2.41	-8.81
4.599	7576.8	-2.98	-9.11
4.6	7577.9	-2.77	-9.16
4.601	7578.9	-2.29	-8.62
4.602	7579.9	-2.02	-8.48
4.603	7581.0	-2.32	-8.52
4.604	7582.0	-1.88	-8.36
4.605	7583.0	-1.48	-8.90
4.607	7585.1	-2.95	-9.56
4.609	7587.2	-2.17	-9.33
4.61	7588.2	-2.65	-8.98
4.611	7589.2	-2.34	-8.99
4.612	7590.3	-2.74	-8.99
4.613	7591.3	-2.02	-8.75
4.614	7592.3	-1.44	-8.59
4.616	7594.4	-1.54	-8.79
4.617	7595.4	-1.27	-8.66
4.618	7596.5	-1.28	-8.62

Depth	Age	$\delta^{13}C$	$\delta^{18}O$
cm	yr BP	VPDB	VPDB
4.619	7597.5	-1.52	-8.19
4.62	7598.5	-0.79	-8.41
4.621	7599.5	-1.12	-8.25
4.622	7600.6	-0.98	-8.21
4.623	7601.6	-1.91	-9.28
4.624	7602.6	-2.06	-10.02
4.626	7604.7	-2.06	-8.79
4.627	7605.7	-1.88	-9.21
4.628	7606.8	-1.66	-8.32
4.629	7607.8	-0.55	-8.55
4.63	7608.8	-1.20	-8.85
4.631	7609.9	-0.53	-8.24
4.632	7610.9	-0.77	-8.36
4.633	7611.9	-0.78	-8.87
4.634	7613.0	-0.52	-7.95
4.635	7614.0	-1.06	-7.82
4.637	7616.1	-0.86	-7.97
4.638	7617.1	-0.50	-8.39
4.639	7618.1	-1.49	-8.23
4.64	7619.2	-0.87	-8.08
4.642	7621.2	-0.10	-8.48
4.643	7622.2	-0.99	-8.28
4.644	7623.3	-0.40	-7.73
4.645	7624.3	-1.17	-8.44
4.646	7625.3	-1.68	-6.51
4.647	7626.4	0.38	-7.37
4.648	7627.4	-1.33	-8.32
4.65	7629.5	-1.57	-8.30
4.651	7630.5	-1.28	-8.46
4.652	7631.5	-1.32	-9.28
4.654	7633.6	-0.80	-8.43
4.655	7634.6	-1.30	-8.50
4.657	7636.7	-1.40	-8.68
4.658	7637.7	-1.10	-8.53
4.659	7638.8	-1.52	-8.82
4.66	7639.8	-1.64	-8.85
4.661	7640.8	-1.47	-8.99
4.662	7641.9	-1.57	-8.81
4.663	7642.9	-2.09	-8.57

Depth	Age	$\delta^{13}C$	$\delta^{18}O$
cm	yr BP	VPDB	VPDB
4.664	7643.9	-2.45	-10.96
4.665	7644.9	-1.54	-8.42
4.666	7646.0	-2.24	-8.66
4.668	7648.0	-1.78	-8.84
4.67	7650.1	-2.67	-8.24
4.671	7651.1	-2.96	-9.04
4.672	7652.2	-2.31	-8.74
4.674	7654.2	-2.23	-8.49
4.675	7655.3	-2.93	-8.70
4.676	7656.3	-2.96	-9.10
4.681	7661.5	-2.71	-8.16
4.682	7662.5	-1.68	-8.50
4.683	7663.5	-2.13	-9.59
4.684	7664.6	-1.51	-8.72
4.685	7665.6	-1.60	-8.63
4.686	7666.6	-1.21	-8.45
4.687	7667.6	-1.74	-8.77
4.688	7668.7	-1.82	-8.61
4.689	7669.7	-2.05	-9.25
4.69	7670.7	-0.48	-7.46
4.692	7672.8	-2.49	-8.42
4.693	7673.8	-1.80	-8.81
4.694	7674.9	-2.07	-8.92
4.695	7675.9	-2.30	-8.89
4.696	7676.9	-2.22	-8.79
4.697	7678.0	-2.53	-8.75
4.698	7679.0	-1.39	-8.25
4.699	7680.0	-1.59	-8.14
4.7	7681.1	-1.79	-8.48
4.702	7683.1	-1.12	-7.95
4.703	7684.2	-0.15	-8.71
4.704	7685.2	-0.65	-7.98
4.705	7686.2	-0.52	-7.88
4.706	7687.3	-0.58	-8.08
4.707	7688.3	-0.57	-8.06
4.708	7689.3	-0.77	-7.91
4.709	7690.3	-0.53	-7.94
4.71	7691.4	0.11	-7.39
4.711	7692.4	0.02	-7.81

Depth	Age	$\delta^{13}C$	$\delta^{18}O$
cm	yr BP	VPDB	VPDB
4.712	7693.4	-0.68	-8.11
4.714	7695.5	-0.49	-8.44
4.715	7696.5	-0.34	-7.79
4.716	7697.6	-0.83	-8.65
4.717	7698.6	-0.38	-8.00
4.718	7699.6	-0.57	-8.16
4.72	7701.7	-0.27	-8.24
4.721	7702.7	-0.09	-8.21
4.722	7703.8	0.48	-8.23
4.724	7705.8	-0.74	-8.44
4.725	7706.9	-0.62	-8.58
4.726	7707.9	-0.42	-8.38
4.727	7708.9	-1.16	-8.85
4.728	7710.0	-1.15	-8.94
4.729	7711.0	0.68	-8.16
4.73	7712.0	-0.59	-8.55
4.731	7713.0	-0.17	-8.30
4.732	7714.1	-0.80	-8.33
4.733	7715.1	-0.97	-8.41
4.734	7716.1	-0.58	-8.50
4.735	7717.2	-0.54	-8.31
4.736	7718.2	-0.60	-8.67
4.737	7719.2	-0.70	-8.43
4.738	7720.3	-0.67	-8.31
4.739	7721.3	-0.62	-8.40
4.74	7722.3	-0.15	-7.90
4.742	7724.4	-0.40	-8.03
4.743	7725.4	-0.46	-8.00
4.744	7726.5	-0.50	-7.80
4.745	7727.5	-0.28	-7.80
4.746	7728.5	-0.56	-8.01
4.747	7729.6	-0.27	-7.82
4.748	7730.6	-0.49	-7.83
4.749	7731.6	-1.39	-8.06
4.75	7732.7	-0.37	-7.71
4.751	7733.7	-0.93	-7.95
4.752	7734.7	-0.61	-7.49
4.753	7735.7	-0.09	-7.67
4.754	7736.8	-0.40	-7.60

Depth	Age	$\delta^{13}C$	$\delta^{18}O$
cm	yr BP	VPDB	VPDB
4.755	7737.8	-0.15	-7.78
4.756	7738.8	-0.55	-7.89
4.757	7739.9	-0.27	-7.78
4.759	7741.9	-0.27	-8.07
4.76	7743.0	-0.53	-8.32
4.761	7744.0	-0.41	-7.85
4.762	7745.0	-2.12	-8.56
4.763	7746.1	-0.68	-7.99
4.764	7747.1	-0.63	-8.19
4.765	7748.1	-0.55	-7.94
4.766	7749.2	-0.80	-7.86
4.767	7750.2	-0.53	-7.84
4.768	7751.2	-0.47	-7.88
4.769	7752.3	-0.95	-8.16
4.77	7753.3	-1.14	-8.72
4.771	7754.3	-0.90	-8.09
4.772	7755.3	-1.23	-8.14
4.773	7756.4	-0.96	-8.59
4.774	7757.4	-0.48	-8.06
4.775	7758.4	-0.50	-8.20
4.776	7759.5	-0.28	-7.91
4.78	7763.6	-0.34	-8.03
4.782	7765.7	-0.25	-7.87
4.783	7766.7	-0.21	-8.10
4.784	7767.7	-0.41	-7.92
4.785	7768.8	-0.83	-8.27
4.786	7769.8	-0.62	-7.99
4.787	7770.8	-0.67	-8.19
4.788	7771.9	-0.90	-7.81
4.789	7772.9	-0.71	-8.07
4.79	7773.9	-0.80	-8.15
4.791	7775.0	-0.81	-8.21
4.792	7776.0	-1.32	-8.49
4.793	7777.0	-1.00	-8.19
4.794	7778.0	-0.90	-8.01
4.795	7779.1	-0.65	-8.08
4.796	7780.1	-0.66	-7.83
4.797	7781.1	-0.52	-7.66
4.798	7782.2	-0.48	-7.59

Depth	Age	$\delta^{13}C$	$\delta^{18}O$
cm	yr BP	VPDB	VPDB
4.799	7783.2	-0.66	-7.84
4.8	7784.2	-0.46	-7.83
4.801	7785.3	-0.34	-7.76
4.802	7786.3	-0.48	-7.69
4.803	7787.3	-0.44	-7.74
4.804	7788.4	-0.43	-7.80
4.805	7789.4	-0.47	-7.70
4.806	7790.4	-0.75	-7.44
4.807	7791.5	-0.69	-7.74
4.808	7792.5	-0.69	-7.73
4.809	7793.5	-0.62	-7.85
4.81	7794.6	-0.48	-7.70
4.811	7795.6	-1.02	-8.03
4.812	7796.6	-0.92	-8.03
4.813	7797.7	-0.76	-7.97
4.814	7798.7	-0.22	-7.62
4.815	7799.7	-0.43	-7.75
4.816	7800.7	-0.36	-7.98
4.817	7801.8	-0.55	-7.94
4.818	7802.8	-0.67	-7.91
4.819	7803.8	-0.62	-7.97
4.82	7804.9	-0.70	-8.07
4.821	7805.9	-0.98	-7.95
4.822	7806.9	-1.18	-7.32
4.823	7808.0	-1.01	-8.05
4.824	7809.0	-0.70	-8.52
4.825	7810.0	-0.62	-8.38
4.826	7811.1	-0.37	-7.88
4.827	7812.1	-0.72	-8.30
4.828	7813.1	-0.80	-8.15
4.829	7814.2	-0.64	-7.93
4.83	7815.2	-0.57	-7.81
4.831	7816.2	-0.43	-8.04
4.832	7817.3	-0.90	-8.15
4.833	7818.3	-1.25	-7.80
4.834	7819.3	-0.86	-8.01
4.835	7820.4	-0.92	-7.93
4.836	7821.4	-1.03	-7.90
4.837	7822.4	-0.95	-7.95

Depth	Age	$\delta^{13}C$	$\delta^{18}O$
cm	yr BP	VPDB	VPDB
4.838	7823.4	-1.06	-8.15
4.839	7824.5	-0.93	-7.81
4.84	7825.5	-1.25	-7.96
4.841	7826.5	-0.97	-7.76
4.842	7827.6	-1.30	-7.76
4.843	7828.6	-1.10	-7.60
4.844	7829.6	-0.81	-7.62
4.845	7830.7	-0.62	-8.01
4.846	7831.7	-1.12	-7.43
4.847	7832.7	-0.74	-7.54
4.848	7833.8	-0.63	-7.58
4.849	7834.8	-1.15	-7.49
4.85	7835.8	-0.99	-7.77
4.851	7836.9	-0.71	-7.50
4.852	7837.9	-1.33	-7.91
4.853	7838.9	-1.21	-7.84
4.854	7840.0	-1.70	-8.22
4.855	7841.0	-1.44	-7.95
4.856	7842.0	-1.95	-8.71
4.857	7843.1	-2.11	-8.92
4.858	7844.1	-1.95	-8.83
4.859	7845.1	-1.93	-8.68
4.86	7846.1	-1.95	-8.70
4.861	7847.2	-1.92	-8.63
4.862	7848.2	-1.69	-8.62
4.863	7849.2	-1.53	-8.52
4.864	7850.3	-1.84	-8.58
4.865	7851.3	-1.71	-8.58
4.866	7852.3	-1.50	-8.61
4.867	7853.4	-1.50	-8.38
4.868	7854.4	-1.40	-8.51
4.869	7855.4	-1.01	-8.10
4.87	7856.5	-0.86	-7.92
4.871	7857.5	-0.92	-7.56
4.872	7858.5	-1.17	-8.09
4.873	7859.6	-0.98	-8.07
4.874	7860.6	-0.85	-7.71
4.875	7861.6	-1.01	-7.93
4.876	7862.7	-0.98	-8.16

Depth	Age	$\delta^{13}C$	$\delta^{18}O$
cm	yr BP	VPDB	VPDB
4.877	7863.7	-1.31	-8.06
4.878	7864.7	-0.91	-7.32
4.879	7865.8	-0.93	-7.68
4.881	7867.8	-0.89	-7.52
4.882	7868.8	-1.56	-7.71
4.883	7869.9	-1.09	-7.41
4.884	7870.9	-1.07	-7.24
4.885	7871.9	-0.81	-7.41
4.886	7873.0	-0.74	-7.50
4.887	7874.0	-1.22	-7.56
4.888	7875.0	-0.90	-7.56
4.889	7876.1	-1.21	-7.62
4.89	7877.1	-1.25	-7.85
4.891	7878.1	-1.54	-8.12
4.892	7879.2	-1.33	-8.26
4.893	7880.2	-1.07	-7.92
4.894	7881.2	-1.13	-7.73
4.895	7882.3	-1.27	-7.92
4.896	7883.3	-1.10	-7.82
4.897	7884.3	-0.97	-7.91
4.898	7885.4	-1.30	-7.76
4.899	7886.4	-0.98	-7.54
4.9	7887.4	-1.38	-8.09
4.901	7888.5	-0.97	-8.11
4.902	7889.5	-1.21	-8.24
4.903	7890.5	-0.99	-8.38
4.904	7891.5	-1.20	-8.31
4.905	7892.6	-1.49	-8.22
4.906	7893.6	-1.43	-8.23
4.907	7894.6	-0.93	-8.40
4.908	7895.7	-1.02	-7.54
4.909	7896.7	-1.34	-8.44
4.91	7897.7	-0.88	-8.41
4.911	7898.8	-0.99	-8.44
4.912	7899.8	-0.90	-8.37
4.913	7900.8	-0.77	-7.95
4.914	7901.9	-1.10	-8.24
4.915	7902.9	-0.93	-8.17
4.916	7903.9	-0.73	-7.68

Depth	Age	$\delta^{13}C$	$\delta^{18}O$
cm	yr BP	VPDB	VPDB
4.917	7905.0	-0.94	-8.00
4.918	7906.0	-0.71	-7.79
4.919	7907.0	-0.65	-8.23
4.92	7908.1	-1.08	-8.14
4.921	7909.1	-0.88	-8.23
4.922	7910.1	-0.78	-8.14
4.923	7911.2	-0.70	-8.02
4.924	7912.2	-0.81	-8.35
4.925	7913.2	-0.83	-8.40
4.926	7914.2	-0.76	-8.08
4.927	7915.3	-0.64	-8.16
4.928	7916.3	-0.76	-7.73
4.929	7917.3	-0.66	-7.82
4.93	7918.4	-0.73	-7.91
4.931	7919.4	-0.87	-8.02
4.932	7920.4	-1.29	-7.81
4.933	7921.5	-1.00	-8.01
4.934	7922.5	-1.57	-8.48
4.935	7923.5	-0.90	-8.35
4.936	7924.6	-1.25	-7.97
4.937	7925.6	-1.11	-8.19
4.938	7926.6	-1.24	-8.13
4.939	7927.7	-1.07	-7.94
4.94	7928.7	-1.69	-8.23
4.941	7929.7	-1.27	-8.42
4.942	7930.8	-0.85	-8.25
4.943	7931.8	-1.28	-8.05
4.944	7932.8	-1.08	-8.73
4.945	7933.9	-1.31	-8.64
4.946	7934.9	-1.01	-8.31
4.947	7935.9	-1.02	-8.40
4.948	7936.9	-1.19	-8.80
4.949	7938.0	-1.46	-8.75
4.95	7939.0	-1.08	-8.78
4.951	7940.0	-1.09	-8.42
4.952	7941.1	-1.14	-8.48
4.953	7942.1	-1.30	-8.77
4.954	7943.1	-1.15	-8.63
4.955	7944.2	-1.07	-8.76
4.956	7945.2	-1.09	-8.43
4.957	7946.2	-1.11	-8.86
4.958	7947.3	-1.21	-8.80
4.959	7948.3	-1.69	-9.63